INSTITUTO POTOSINO DE INVESTIGACIÓN CIENTÍFICA Y TECNOLÓGICA, A.C.

POSGRADO EN CIENCIAS APLICADAS

Production of Activated Carbon from *Agave salmiana* Bagasse and its Modification to Remove Arsenic from Water

Tesis que presenta

César Nieto Delgado

Para obtener el grado de

Doctor en Ciencias Aplicadas

En la opción de

Ciencias Ambientales

Directores:

Dr. José René Rangel Méndez

Dr. Mauricio Terrones Maldonado (7/07 – 12/09)

San Luis Potosí, S.L.P. Diciembre 2010.

IPICYT
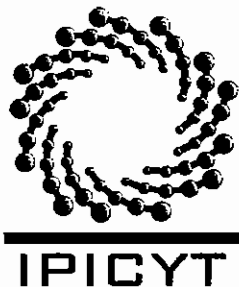
Constancia de aprobación de la tesis

La tesis "**Production of Activated Carbon from *Agave salmiana* Bagasse and its Modification to Remove Arsenic from Water**" presentada para obtener el Grado de de Doctor en Ciencias Aplicadas en la opción de Ciencias Ambientales fue elaborada por **César Nieto Delgado** y aprobada el **10 de diciembre del 2010** por los suscritos, designados por el Colegio de Profesores de la División de Biología Molecular del Instituto Potosino de Investigación Científica y Tecnológica, A.C.
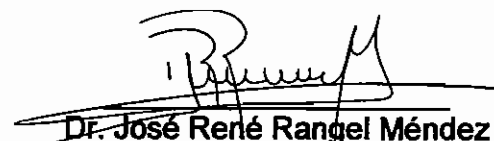
Dr. José René Rangel Méndez
(Director de la tesis)

Dr. Felipe Alatriste Mondragón
(Asesor de la tesis)

IPICYT

Institutional Credits

This thesis was elaborated in the Environmental Science Division at the Instituto Potosino de Investigación Científica y Tecnológica A.C., under the supervision of Dr. José René Rangel Méndez.

Instituto Potosino de Investigación Científica y Tecnológica, A.C.

Acta de Examen de Grado

El Secretario Académico del Instituto Potosino de Investigación Científica y Tecnológica, A.C., certifica que en el Acta 010 del Libro Primero de Actas de Exámenes de Grado del Programa de Doctorado en Ciencias Aplicadas en la opción de Ciencias Ambientales está asentado lo siguiente:

En la ciudad de San Luis Potosí a los 10 días del mes de diciembre del año 2010, se reunió a las 09:00 horas en las instalaciones del Instituto Potosino de Investigación Científica y Tecnológica, A.C., el Jurado integrado por:

Dr. Felipe Alatriste Mondragón	**Presidente**	**IPICYT**
Dr. Roberto Leyva Ramos	**Secretario**	**UASLP**
Dr. Alejandro López Valdivieso	**Sinodal externo**	**UASLP**
Dr. José René Rangel Méndez	**Sinodal**	**IPICYT**

a fin de efectuar el examen, que para obtener el Grado de:

DOCTOR EN CIENCIAS APLICADAS EN LA OPCION DE CIENCIAS AMBIENTALES

sustentó el C.

César Nieto Delgado

sobre la Tesis intitulada:

Producción de carbón activado a partir de bagazo de agave salmiana y su modificación para la remoción de arsénico en agua

que se desarrolló bajo la dirección de

Dr. José René Rangel Méndez

y de la codirección del Dr. Mauricio Terrones Maldonado, hasta el 17 de diciembre de 2009.

El Jurado, después de deliberar, determinó

APROBARLO

Dándose por terminado el acto a las 12:00 horas, procediendo a la firma del Acta los integrantes del Jurado. Dando fe el Secretario Académico del Instituto.

A petición del interesado y para los fines que al mismo convengan, se extiende el presente documento en la ciudad de San Luis Potosí, S.L.P., México, a los 10 días del mes de diciembre de 2010.

Dr. Marcial Bonilla María
Secretario Académico
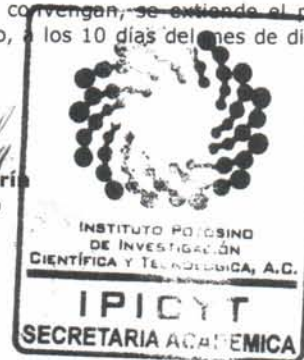
Mtra. Ivonne Lizette Cuevas Vélez
Jefa del Departamento de Asuntos Escolares

DEDICATORIA

En este trabajo se plasma sólo una parte de todo lo que he aprendido dentro de mis estudios doctorales. Entre las cosas que he omitido están las relaciones con mis compañeros, el trato con mi asesor, un criterio más analítico, la manera de entretener a mi hija mientras terminaba un experimento y lo práctico que es regresar a casa todos los días en busca de inspiración.

Para lograr este trabajo he requerido de fe, confianza en mí mismo, determinación, dedicación y por supuesto... trabajo duro. Este trabajo es de gran importancia para mí, por lo que lo dedico a las personas más importantes en mi vida...

Isabel y Fernanda

AGRADECIMIENTOS

CONTENTS

━━━━━● (Chapter 1) ●━━━━━

INTRODUCTION

(Chapter 2)

AGAVE *salmiana* BAGASSE AS A PRECURSOR TO PRODUCE HIGHLY MICROPOROUS ACTIVATED CARBONS

──────────● (Chapter **3**) ●──────────

PRODUCTION OF ACTIVATED CARBON FROM AGAVE *salmiana* BAGASSE: SURFACE AREA AND HARDNESS OPTIMIZATION BY USING THE RESPONSE SURFACE METHODOLOGY

(Chapter 4)

MODIFICATION OF ACTIVATED CARBON WITH IRON OXIDE PARTICLES FOR THE REMOVAL OF ARSENIC FROM WATER

$$(\text{Chapter } 5)$$

GENERAL DISCUSSION

$$(\text{Chapter } 6)$$

GENERAL CONCLUSIONS

$$(\text{Appendix } A)$$

IN SITU TRANSFORMATION OF AGAVE BAGASSE INTO ACTIVATED CARBON BY USING AN ENVIRONMENTAL SCANNING ELECTRON MICROSCOPE

LIST OF TABLES

CHAPTER 4

LIST OF FIGURES

CHAPTER 1

the different oxygenated groups of the sugar monomers. After that hydrogen elimination promotes double bond formation (B), cleavage of the glycosidic linkage between polysaccharides (C) and the degradation of sugar monomers (D).

CHAPTER 2

promote the H_2O formation in the early stages of the activation. Zinc chloride acts as Lewis acid, making chemical complexes with oxygen of the biopolymer to eliminate hydroxyl groups (A) or promoting the bond cleavage of the biopolymer (B).

CHAPTER 3

of 95%.

CHAPTER 4

the reaction are independent of the temperatures (constant specific heat, Cp)

APPENDIX A

ABSTRACT

Production of activated carbon from Agave *salmiana* bagasse and its modification to remove arsenic from water

Activated carbon is a well known adsorbent material, its porosity, large surface area, physical and chemical stability, and diverse chemical functionality make this suitable for the adsorption of both polar and no polar compounds in liquid and gas environments. Commercial activated carbons are mainly produced from anthracite, bituminous carbon, lignite, peat and lignocellulosic materials, such as wood and coconut shells. However, the relatively high cost of these raw materials increases the price of activated carbon and difficult its practical applications in the treatment of liquid and gaseous streams.

Previous studies have reported that agricultural and industrial wastes are promising activated carbon precursors due their large availability and low cost. The use of these residues also helps to deal with the treatment and disposal of these wastes. Taking into account the commercial importance of activated carbon, this thesis explored the feasibility to produce activated carbon from Agave *salmiana* bagasse which is a waste from the mescal industry in San Luis Potosí.

The chemical activation process (by $ZnCl_2$ and H_3PO_4) was studied by thermogravimetric analyses and scanning electron microscopy. The produced activated carbons were characterized by nitrogen adsorption at -196 °C, elemental analyses, hardness and pH_{PZC}. The response surface methodology was employed to determine the effect of the production conditions (concentration of activating agent, activation temperature and time) on the surface area and hardness of the resulting activated carbons. We also determined the production conditions to obtain the carbons with an adequate balance between surface area and hardness, needed in packed columns. The generated activated carbons are mainly microporous, with pore volumes between 0.24 and 1.20 cm^3/g. Also, the pore's size can be increased by modifying the amount of activating agent and temperature. The hardness and surface area of H_3PO_4 activated carbons ranged from 75.9 to 95.5 % and from 235 to 1327 m^2/g, respectively. On the other hand, $ZnCl_2$ activated carbons exhibited higher surface area when compared to H_3PO_4 activated carbons (from 2 to 2109 m^2/g) and hardness from 60.7 to 95.4 %. The optimal synthesis conditions of H_3PO_4 activated carbons were 392 °C, 1.02 g/g and 23.8 min for the temperature, activating agent per gram of bagasse and time. For the case of $ZnCl_2$ activated carbons, the optimum conditions were and 456 °C, 1.08 g activating agent/g bagasse and 23.8 min. Our activated carbons show similar surface area and hardness to those reported for commercial activated carbons (surface area > 800 m^2/g and hardness > 85 %).

Elemental analyses of agave bagasse based activated carbons showed that these materials have a considerable amount of oxygen 9.9–30.5 %. It was also observed when using H_3PO_4 during the production of activated carbon, some trace of phosphorus was incorporated into the carbon structure, thus generating carbons with 1.7 to 6.8 % of phosphorus content. According with the low pH_{pzc} of the

generated carbons, (1.9-3.4) it is expected that the activated carbons based on agave bagasse will be efficient materials for the removal of cations from aqueous solution.

The second part of this research involved the modification of activated carbons with iron oxide nanoparticles, aiming materials with high arsenic adsorption capacity. The anchorage methodology of iron oxides on activated carbons was based on the thermal hydrolysis of iron solution. The surface response methodology was used to evaluate the experimental variables during the hydrolysis process. The studied parameters were: hydrolysis temperature (T: 60-120 °C), hydrolysis time (Ht: 4-16 hours), and the $FeCl_3$ concentration in the hydrolysis solution (C_{Fe}: 0.4-3 M). The arsenic adsorption capacity and the iron content of the modified carbons were the analyzed responses. We compared three activated carbons: Filtrasorb-400 (F400, from Calgon), and two agave bagasse based activated carbons (chemically activated with $ZnCl_2$, ACZ, or with H_3PO_4, ACP) to evaluate the effect of the surface chemistry on the anchorage of iron oxide nanoparticles process. The iron content and the size of the attached iron oxide nanoparticles are hardly influenced by the reactivity of the surface on the activated carbons. The iron content of the modified activated carbons was found from 0.73 to 5.27 %, being higher on activated carbons with high oxygen content. The analysis of representative samples demonstrated that modified activated carbons with iron oxide nanoparticles (average diameter of 8 nm) exhibited the highest arsenic adsorption capacity. The production parameters for the better materials for arsenic adsorption were C_{Fe} = 3.05 mol Fe/L, T = 96 °C and Ht = 56 hours for F400 activated carbon; C_{Fe} = 1.16 mol Fe/L, T = 110 °C and Ht = 6.8 hours for ACZ activated carbon; and C_{Fe} = 0.56 mol Fe/L, T = 58 °C and Ht = 6.8 hours for ACP activated carbon. The optimal materials reported an arsenic adsorption capacity (calculated at an arsenic concentration of 1.5 ppm at equilibrium) of 4.56 mg As/g (F400), 1.18 mg As/g (ACZ) and 0.96 mg As/g (ACP). The adsorption capacity of these materials is similar and in some cases superior to previously reported iron modified activated carbons in the literature, and have the advantage of being generated by a simple methodology, without a significant modification of the pore structure and surface area.

Keywords: Chemical activation, $ZnCl_2$, H_3PO_4, arsenic removal, iron oxides, response surface methodology.

RESUMEN

Producción de carbón activado a partir de bagazo de Agave *salmiana* y su modificación para remover arsénico de agua

El carbón activado (CA) es conocido como uno de los mejores adsorbentes debido a su gran área específica, estabilidad química, y diversas funcionalidades químicas, haciéndolo un material apto para la adsorción de compuestos polares y no polares en fase líquida y gaseosa. Comercialmente, el CA se produce a partir de antracita, hulla, lignito, turba y materiales lignocelulósicos, como cáscaras de coco y madera. Sin embargo, el costo relativamente alto de éstas materias primas incrementa el precio del CA, haciendo incosteable su aplicación. Estudios previos han demostrado que los desechos agrícolas son una prometedora opción para ser utilizados como precursores de CA debido a su gran disponibilidad y bajo costo. Teniendo en cuenta la importancia comercial del carbón activo, ésta tesis explora la posibilidad de producir CA a partir del bagazo de Agave *salmiana,* que es un desperdicio de la industria del mezcal en San Luis Potosí.

El proceso de activación química (con $ZnCl_2$ y H_3PO_4) fue estudiado por análisis termogravimétrico y microscopía electrónica de barrido. A los materiales obtenidos se les determinó el área específica, distribución de tamaño de poro, composición elemental, dureza y pH_{PZC}. La metodología de superficie de respuesta se utilizó para determinar el efecto de las condiciones de producción (concentración de agente activante, temperatura de activación y tiempo de activación), sobre el área superficial y la dureza de los carbones activados resultantes. Se determinaron las condiciones de producción para obtener CA con características físicas adecuadas para ser utilizados en columnas empacadas. Los poros presentes en el carbón activado están dentro del rango de los microporos (diámetro<2nm). La dureza y el área específica de los materiales generados con H_3PO_4 variaron desde 75.9 hasta 95.5% y de 235 a 1327 m^2/g, respectivamente. Por otra parte, los carbones activados con $ZnCl_2$ exhibieron una mayor área específica en comparación con los materiales activados con H_3PO_4 (de 2 a 2109 m^2/g), pero menor dureza (de 60.7 a 95.4%).

Al utilizar H_3PO_4 como agente activante, las condiciones de producción para generar CA con un balance adecuado entre área y dureza fueron 392 °C, 1,02 g/g y 23.8 minutos para la temperatura de activación, la cantidad de agente activado utilizado (g agente activante / g bagazo) y el tiempo de activación, respectivamente. Para el caso de los carbones activados con $ZnCl_2$, las condiciones de producción óptimas fueron: 456 °C, 1,08 g agente activante/g de bagazo y 23.8 minutos. Los carbones activado generados mostraron un área específica y dureza similar a los reportados para carbones activados comerciales (superficie>800 m^2/g y dureza>85%). La composición elemental de los carbones demostró que estos materiales tienen una cantidad considerable de oxígeno 9.9-30.5 %, observando que en las muestras activadas con H_3PO_4 parte del fosforo queda remanente en la estructura carbonosa (2.8 – 3.2 % de P). De acuerdo a el bajo pH_{PCZ} presentado por los materiales generados (1.9-3.4), se espera que

xxiii

estos carbones sean materiales eficientes para la remoción de cationes en solución acuosa.

La segunda parte de esta tesis abordó la modificación de carbones activados con nanopartículas de óxidos de hierro, con el objetivo de generar un material con alta capacidad de adsorción de arsénico. La metodología de anclaje de los óxidos de hierro sobre el CA se basó en una hidrólisis térmica de hierro en solución acuosa. La metodología de superficie de respuesta se utilizó para evaluar las variables experimentales durante el proceso de hidrólisis. Los parámetros estudiados fueron: temperatura de hidrólisis (T: 60-120 °C), tiempo de hidrólisis (Ht: 4-16 horas), y la concentración de $FeCl_3$ en la solución de hidrólisis (C_{Fe}: 0.4-3 M). La capacidad de adsorción de arsénico y el contenido de hierro en los carbones activados fueron las propiedades analizadas. Se compararon tres carbones activados: Filtrasorb-400 (F400, de Calgon), y dos carbones activados sintetizados a partir bagazo de agave (ACZ: activado con $ZnCl_2$ y ACP: activado con H_3PO_4) para evaluar el efecto de la química superficial en el anclaje de las nanopartículas. Los resultados demostraron que existe una gran influencia de la química superficial de los carbones activados en la cantidad de hierro anclado y el tamaño de las nanopartículas de óxido de hierro ancladas. El contenido de hierro en los carbones activados modificados fue de 0.73 a 5.27 %, siendo mayor en los carbones activados con alto contenido de oxígeno. Mediante microscopía electrónica de barrido fue posible encontrar que los materiales que contenían las nanopartículas de óxidos de hierro con el menor tamaño de partícula (diámetro promedio de 8 nm) exhiben la más alta capacidad de adsorción de arsénico. Los parámetros óptimos para generar los materiales con mayor capacidad de adsorción de arsénico para cada CA fueron: C_{Fe} = 3.05 mol Fe/L, T = 96 °C y Ht = 56 horas para el carbón F400; C_{Fe} = 1.16 mol Fe/L, T = 110 °C y Ht = 6.8 horas para el carbón ACZ y C_{Fe} = 0.56 mol Fe/L, T = 58 °C y Ht = 6.8 horas para el carbón ACP. Los materiales óptimos presentaron una capacidad de adsorción de arsénico (calculada a una concentración de arsénico de 1.5 ppm en el equilibrio) de 4.56 mg As/g (F400), 1.18 mg As/g (ACZ) y 0.96 mg As/g (ACP). La capacidad de adsorción de éstos materiales es similar y en algunos casos superior a los carbones activados modificados con partículas de óxidos de hierro reportados previamente, con la ventaja de ser generados por una metodología sencilla, sin una modificación significativa de su estructura porosa y su área específica.

Palabras clave: activación química, $ZnCl_2$, H_3PO_4, remoción de arsénico, óxidos de hierro, metodología de superficie de respuesta.

"From small beginnings come great things"
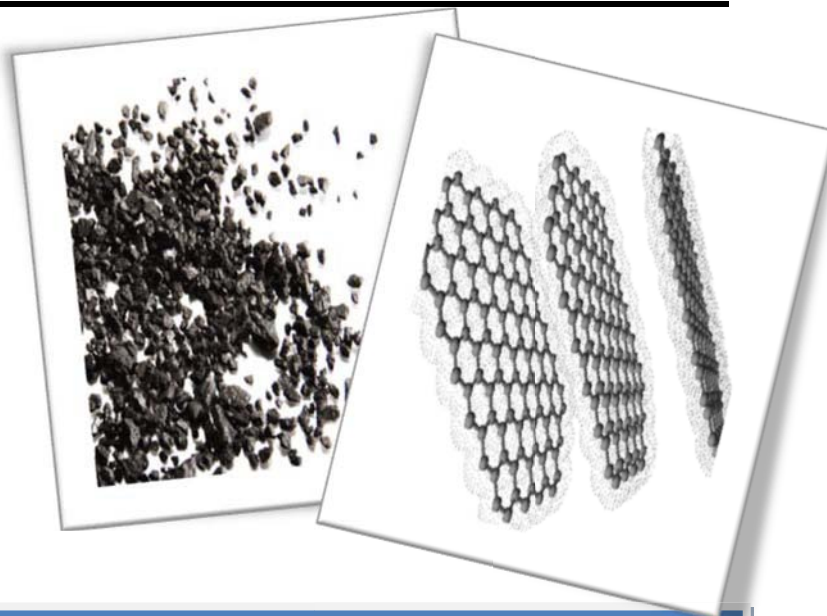
CHAPTER 1

INTRODUCTION

A ctivated carbon is one of the most versatile materials. One of its main applications is in adsorption processes in both aqueous and gas phase. However it has applications in very diverse areas such as catalysis, molecular sieves, electrochemistry, as capacitors, gas storage, among others. The success of activated carbon among these areas is mainly due to its extensive surface area and diverse chemical functionalities that can be modified both during and after the production process. In recent decades, millions of tons of activated carbon has been produced by the carbon industry, consuming tons of precursors such as mineral carbon and wood. Nowadays the production of activated carbon from waste biomass is preferred because it offers the treatment of wastes and the generation of products of high commercial value. In the following section a brief review of the most important aspects related to the production, characterization and modification of activated carbon is presented.

1.1. ACTIVATED CARBON

Activated carbon (AC) is the employed name to a group of solid materials that are mainly composed of carbon, characterized by their highly developed surface areas and porosities. One of the main applications of AC is related to adsorption process: water purification, solvents and precious metal recovery, purification of effluents, removal of taste and odor from water among others, being this material the most commonly used adsorbent around the world. AC has found applications in areas different to adsorption, such as catalyst, biocatalyst, gas storage, molecular sieves and recently on electronic devices [1-7]. The use of carbon materials by human kind is reported to be so far back in time that its origin is impossible to determine exactly. Prior to the use of activated carbon as we know, (which has a highly developed porous structure), either wood char, charcoal or simply a partially devolatilized carbonaceous material was employed as an adsorbent. For instance, Hippocrates (around 400 BC) recommended that water should be filtered with woodchar prior to consumption, in order to eliminate bad taste and odor and to prevent several diseases. Also, on Phoenician ships (450 BC), drinking water was stored in charred wooden barrels, a practice which continued until the 18th century as a means of prolonging the supply of drinking water on transatlantic voyages [8].

On the other hand, the first reported application of AC in the industrial sector was in England in 1794, when it was used as a decolorizing agent in the sugar production industry. The first large scale gas-phase application took place in 1854, the Mayor of London ordered the installation of wood char filters in all the sewer ventilation systems to remove nasty odours; also in 1872 gas masks with carbon filters were used in chemical industries. Despite all these previously applications, was until 1901 when R. von Ostrejko discovered the activated carbon as it is known nowadays. He patented two different methods of producing activated carbons: carbonization of lignocellulosic materials with metal chlorides (the basis of

chemical activation), and the gasification of chars with steam or carbon dioxide at high temperatures (thermal or physical activation) [8]. Activated carbon was initially employed in the sugar industry to remove impurities and undesired color. Later, during the First World War AC was employed as adsorbent by the allies on gas masks against the poisonous gases of the German army. After that, the production and application of activated carbon was stimulated togheter with an intensive research program mainly in USA [8]. The rapid development of society over the 20th century, promoted by the industrial revolution of the previous century, has also augmented the use of activated carbon. Indeed the production and utilization of activated carbon has increased mainly by the stricter environmental regulations regarding both water resources and gas application [9].
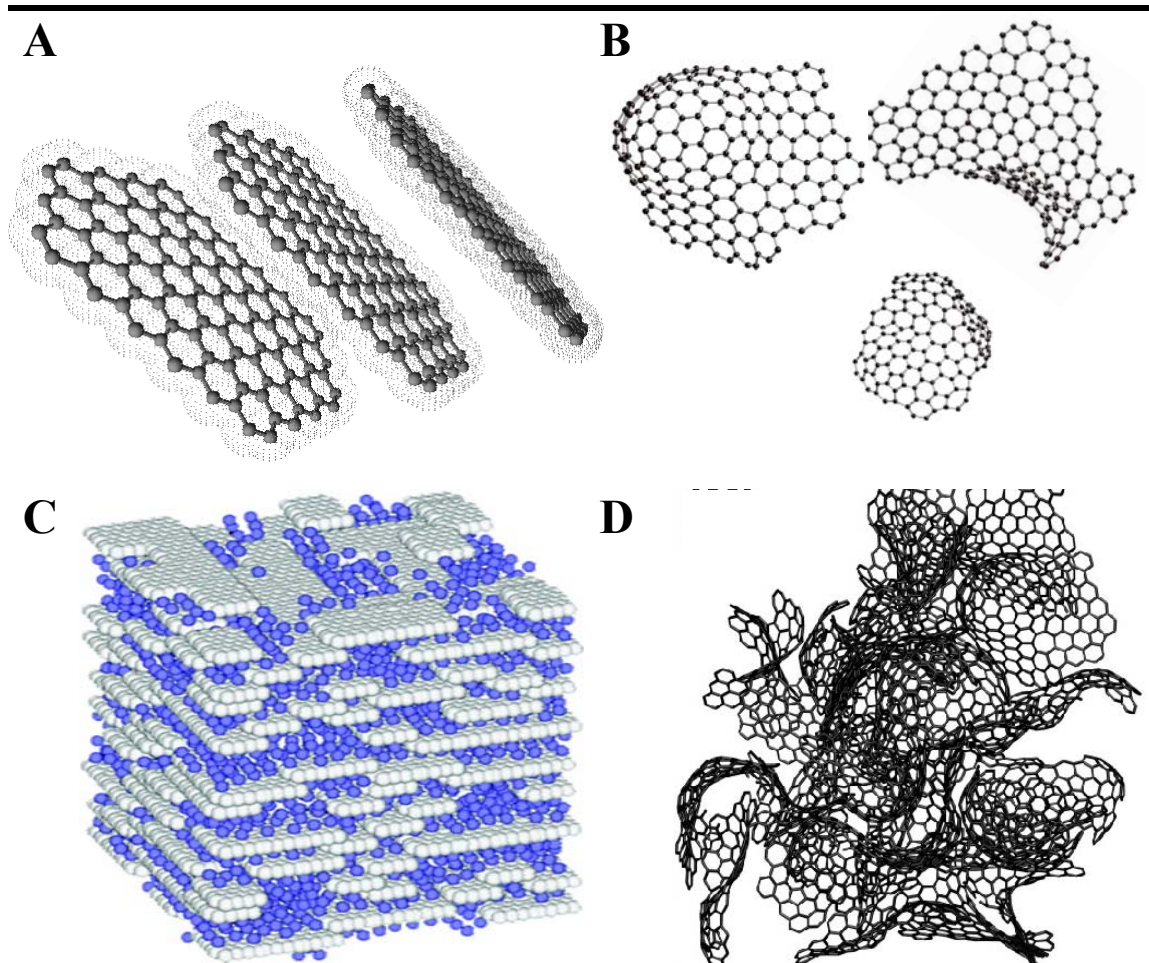
Figure 1.1. Illustration of carbon fragments (A and B [11]) and their corresponding activated carbon structures that could perform (C [10] and D [12]).

A

B

C

D
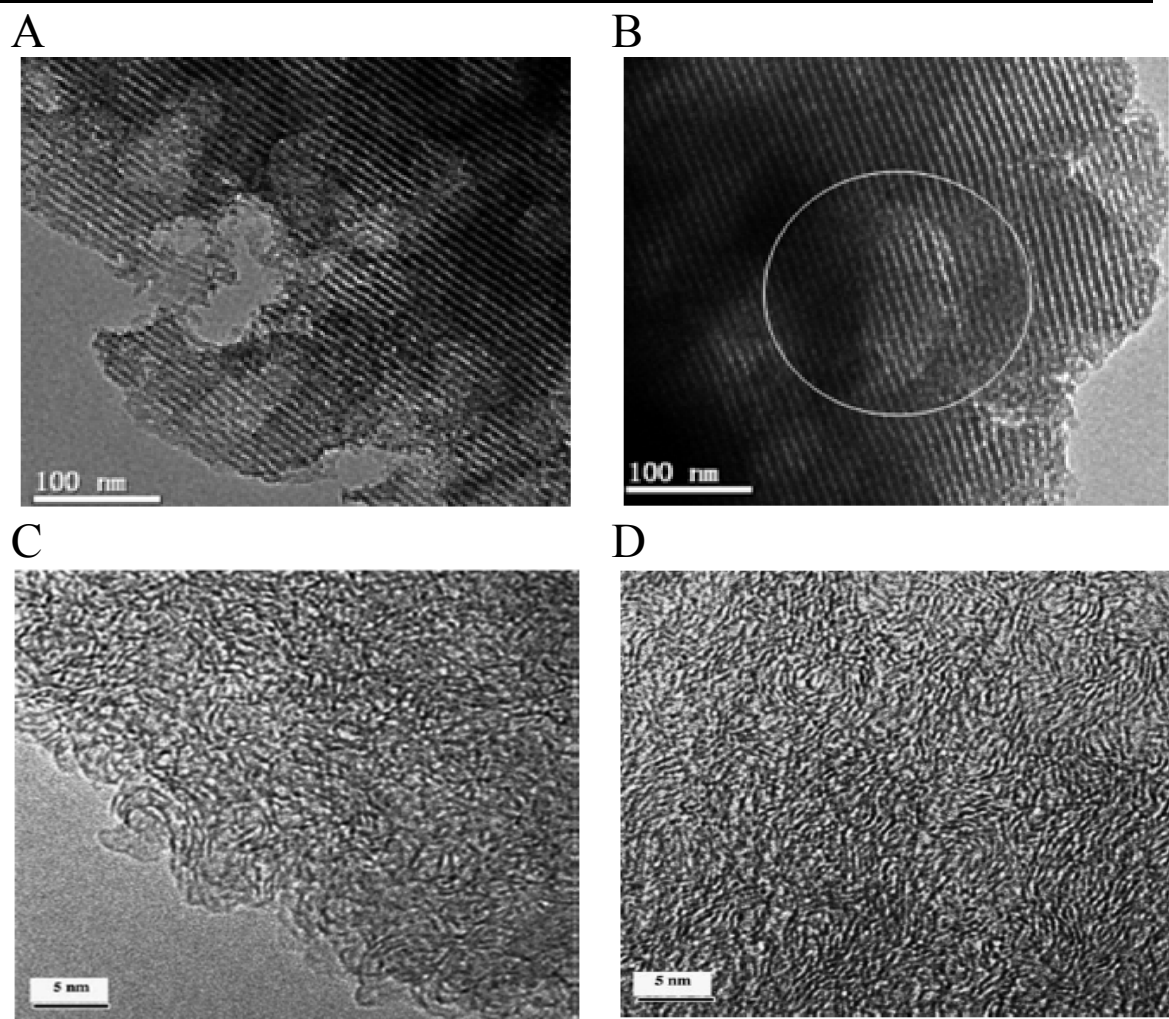
Figure 1.2. HRTEM images of activated carbon. A and B activated carbon formed by high ordered graphite sheets [13]. C and D activated carbon formed by aleatory carbon fragments [14].

About its structure, AC consists in different arrangements of sp^2 carbon atoms that can perform two kinds of structures: graphite, which is composed by hexagonal carbon rings (Figure 1.1A); and non graphitizing carbon that has a structure consisting of curved fragments containing pentagons, hexagons and other carbon rings, as illustrated in Figure 1.1B. These layers of graphitized and / or non graphitized carbons are randomly oriented, leaving empty spaces between each

fragment, generating the pore structure of activated carbon, as illustrated in Figure 1.1C and Figure 1.1D. In the last years with the development of high resolution microscopes it was possible to identify the atomic structure of several activated carbons, supporting the previously exposed structures (Figure 1.2).

1.2. ACTIVATED CARBON PRODUCTION

Once the adsorption process was developed for separation and purification purposes, the development of porous materials has been an area of great study. Among the adsorbents, AC was the first material to be developed [8]. During the production process the precursor is "activated" by means of a thermal treatment which gasifies part of the precursor, generating a new pore structure that provide to the activated carbon their high surface area. The characteristics of the AC will depend of the precursor properties and the activation methodology employed. In these sense by controlling the activation process it is possible to improve the performance of AC in typical applications and to prepare better adsorbents to satisfy emerging applications. AC can be produced from a large variety of raw materials, mainly by two methods: physical and chemical activation. The physical activation involves the carbonization of the raw material under inert atmosphere and the subsequent activation at higher temperatures in the presence of oxidizing gases. On the other hand, in chemical activation the carbonization and activation are carried out simultaneously by means of a catalyst (activating agent) that promotes diverse reactions. Also, the combination of both methodologies has been successfully applied. In the following section, details of the activated carbon production will be presented.

1.2.1. Precursors

Carbon, hydrogen, oxygen and other minor components such as sulfur, nitrogen and inorganic salts are the elements that constitute the materials often used as

precursor of activated carbon. Therefore, almost any organic product can by used as a precursor of AC. However, there are some desired characteristics on the raw material to be an AC precursor: availability, cost, workability, minimum presence of inorganic salts, density (from 0.4 to 1.45 g /cm^3),and high carbon content (from 40 to 90 %) [15, 16].

Table 1.1. **Alternative feedstocks proposed for the production of activated carbon [16, 18].**

Agricultural wastes	Industrial Wastes
Fruit Stones	Acrylic fabric waste
Apricot	Buffing dust
Cherry	Cotton refuse
Date	Fly ash
Olive	Furfural residue
Peach	Olive refuse
Plum	PET scrap
Shells	PVC scrap
Almond	Rubber
Ground nut	Scrap tires
Hazelnut	Sewage sludge
Macadamia	
Nut	**Woody materials**
Palm	Cedar wood shavings
Peanut	Chesnut shaving
Pecan	Cotton stalks
Pistachio nut	Fir wood
Sunflowers	Palm tree cobs
Wallnut	Pine sawdust
Hulls	Tear sawdust
Coton seeds	Vineyard shoot
Oat	Walnut chavings
Peanut	
Rice	
Others	**Other**
Casava peel	News paper
Coffee beans	Bones
Coffee bean husk	
Corn cobs	
Grape seeds	
Sugar cane bagasse	
Wheat straw	

The estimated world production of AC in 2007 was 890,000 ton/year which represents a rise of two times the level of production in less than 10 years [17].

Around the world, the most common feedstock for the commercial production of activated carbon are wood (24 %), coal (31 %), and coconut shell (34 %). However, the raw materials used per world region shows a very different picture. In Europe, the most used raw material was peat (36 %), whereas the production of coconut shell based carbon occupied the fourth place with only 12 % of the share. On the other hand, coconut based carbons led in Asia with over 60 % of the share [8].

A

B

C

D

Figure 1.3. Pictures that illustrate the mescal production. A: agave plant field. B: agave plant head after harvest. C: sliced agave piñas that are cooked in a traditional oven. D: cooked agave heads are milled to extract their sugars, the remaing solids are known as agave bagasse. Images

availables   from: http://www.galenfrysinger.com/tequila_agave.htm;   and
http://www.rsfotografia.com/Reportaje/Mezcal/MZEspanol.html

The increased use of activated carbon has encouraged many researchers to explore new alternative feedstock to produce activated carbon, empathizing on locally available materials which present significantly economical advantages in comparison with traditional precursors. Table 1.1 shows some of the tested precursors.

Only some of the materials that have been previously evaluated as activated carbon precursor are available in Mexico. Therefore, the study of the agro wastes generated in Mexico as activated carbon precursors can be an interesting alternative for activated carbon production locally. This thesis focuses on studing the agave bagasse as an alternative precursor of activated carbon due to its high availability and low cost. The agave bagasse is a lignocellulosic material that is generated on both tequila and mescal distilleries. To produce tequila and mescal, the leaves of agave plants are cut out and the plant heads are sliced to cook them in furnaces to convert the complex carbohydrates stored in the agave head into simple sugar. Once the agave heads are cooked, these are mechanically milled, to extract all the juices. The solid waste from the agave plant is usually known as agave bagasse; Figure 1.3 illustrates this. The national production of tequila and mescal in 2006 was about 285 [19] and 16 [20] millions of litters, respectively. The quantity of agave bagasse generated varies for each distillery, depending on the machinery used to process the agave and to the agaves specie used. In general, according with the national production of tequila and mescal in 2006, the generated agave bagasse was about 350,000 tons [19-21] on a dry basis, being this waste an important source of low-cost lignocelluloses material. Recently, other uses for this waste have been proved including paper precursor [22], as raw material for animal feeding and also in the production of oyster mushroom (*Pleurotus ostreatus*) [23]. However most of this waste is burned or used like a low quality food for livestock [24].

1.2.2. Chemical activation

The production of activated carbon by chemical activation implies the carbonization of the precursor in the presence of chemicals also called activating agents. Generally, activating agents acts as catalyst, promoting reactions that avoid the gasification of carbon. Also, promote the formation of the pore structure by means of the elimination of elements different to carbon (H, O, N, S). Chemical activation offers several advantages since it is carried out in a single thermal step at lower temperatures than physical activation and generally resulting in the development of a better porous structure. The main concern about chemical activation is the environmental implications that could generate the spent activating agent. However, recent investigations have demonstrated that part of the added chemicals (such as zinc salts and phosphoric acid), can be easily recovered and reuse in the production of AC [25, 26].

The production of activated carbon by chemical activation involves the following steps: first, the precursor is impregnated with an adequate amount of the activating agent, often by mixing of the required volume of concentrated solution of the activating agent; after the activating agent is incorporated to the raw material, the mixture is dried; subsequently, the product is submitted to a thermal treatment, generally under inert atmosphere, where the activating agent catalyzes reactions to convert the precursor into activated carbon; finally, the pyrolyzed samples are rinsed with water in order to remove the residual catalyst which can be recovered for subsequent reuse.

Numerous chemicals have been proved as activating agent, the most widely used are $ZnCl_2$, $AlCl_3$, $MgCl_2$, H_3PO_4, H_2SO_4, HNO_3, KOH, NaOH, K_2CO_3 and Na_2CO_3. In the case of chemical activation with metal chlorides or acids, lignocellulosic materials are preferred as precursor. Moreover high rank coals (carbon content > 90%), devolatilized chars or petroleum coke are the preferred precursor when alkyl

hydroxides or carbonates are used as activating agent. There are several studies that attempted to explain the mechanism by which activating agents influence the formation of pore structure. The following section gives a brief description of the promoted reactions by the activating agents often used in chemical activation: zinc chloride, phosphoric acid and potassium hydroxide.

1.2.2.1. Zinc chloride activation

Zinc chloride is an activating agent widely used to produce activated carbon from lignocelluloses materials being wood the most common precursor. The major components of wood and other lignocelulosic materials are three biopolymers: cellulose, hemicelluloses and lignin (Figure 1.4).

The proportion of these components in lignocellulosic materials varies according with the source of the material. As previously mentioned, the first step on chemical activation is the impregnation of the precursor with activating agent. In this first step, the precursor is mixed with the chemical in an aqueous solution which is later evaporated. During the evaporation, the structure of the lignocellulosic precursor begin to be degraded by the hydrolysis reactions promoted by the activating agent [27]. Chemically, $ZnCl_2$ can be considered as Lewis acid, it means that Zn can form complexes with the nonbonding electrons of an atom. Analyzing the chemical structure of the biopolymers that form the lignocellulosic materials, oxygen is the element that contains nonbonding electrons and hence is expected that the $ZnCl_2$ reacts directly with this element. Most of the oxygen in the biopolymers is found as OH groups attached to the main chain of the biopolymer or as part of the bond between sugar monomers. These functional groups can react with the activating agent as follows: first $ZnCl_2$ accepts an electron pair of the nonbonding electrons of the oxygen, forming a complex as appears in Figure 1.5.

A

B

xylose   mannose   galactose

rhammose   arabinose
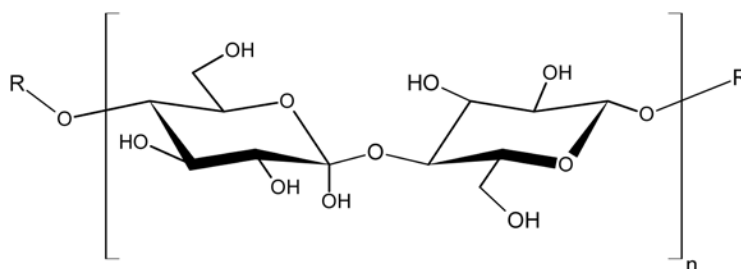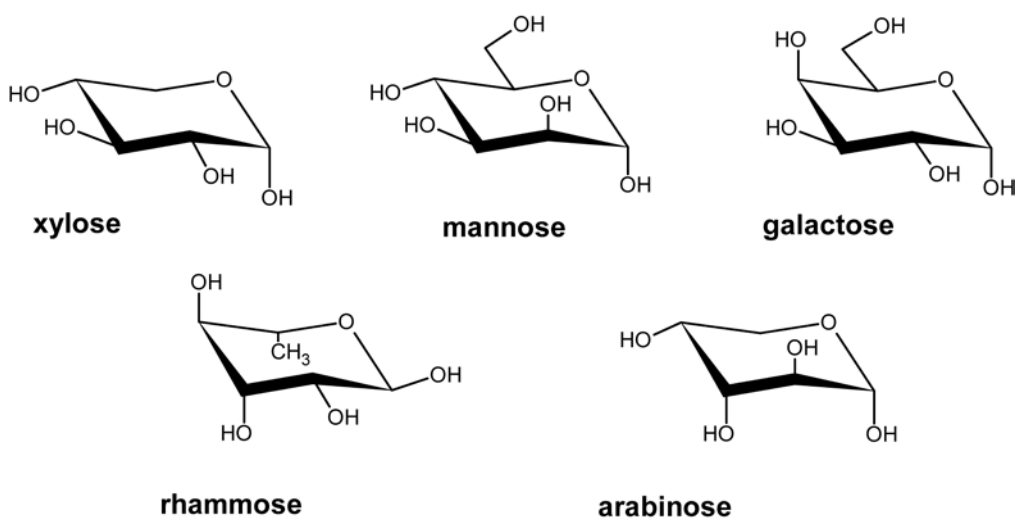
C
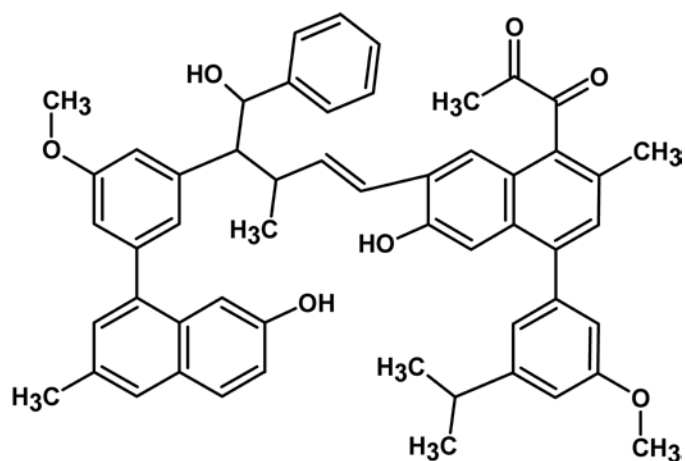
Figure 1.4. Major components of lignocellulosic materials: A) cellulose, composed by glucose

monomers; B) different sugar monomers that constitute hemicellulose; C) heterogeneous structure of lignin.
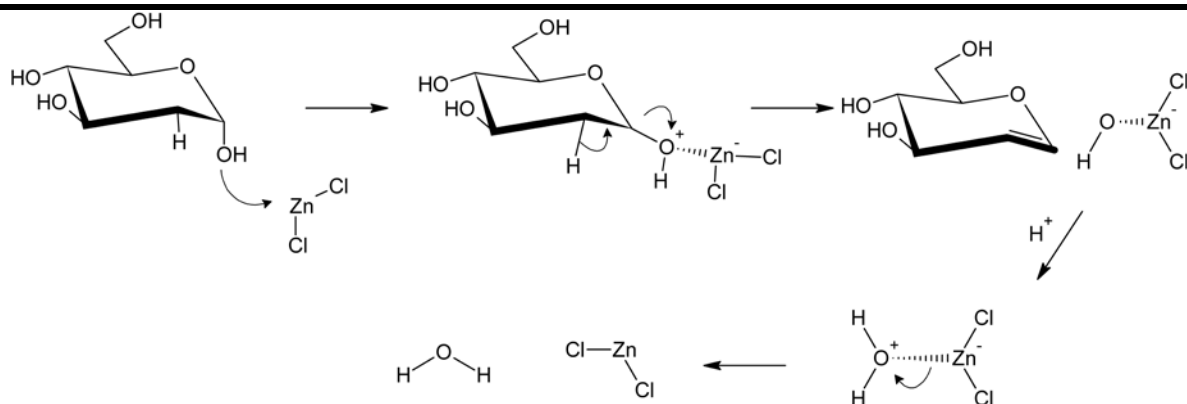
Figure 1.5. Dehydration mechanism of $ZnCl_2$ with a fragment of the biopolymer.

Once the $ZnCl_2$-OH complex has being formed, the C-O bond is weakened. This bond is finally broken by the elimination of the hydrogen from the neighboring carbon atom. Finally, the catalyst is regenerated, releasing water to the media. Similar reaction mechanism can occur with the oxygen of the ether group (Figure 1.6). In this case, the reaction promote the cleavage of the biopolymer chains by means of a nucleophilic attack (Figure 1.6B) or by hydrogen elimination (Figure 1.6C). After that, $ZnCl_2$ can be regenerated by a similar mechanism as appears in Figure1.5. It is expected that other reactions can occur during the activation, however according whit the $ZnCl_2$ chemistry and the rapid evolution of water reported previously when using $ZnCl_2$ as activating agent [27-30], these could be the main reactions.

After these reactions, the biopolimers contained in the lignocellulosic material are transformed into randomly oriented carbon structures. These randomly oriented structures generate cavities that increase the surface area of the generated carbon. Also, some authors have suggested that the porosity created by the $ZnCl_2$ is due to the spaces left by the activating agent after the corresponding washing [31, 32].
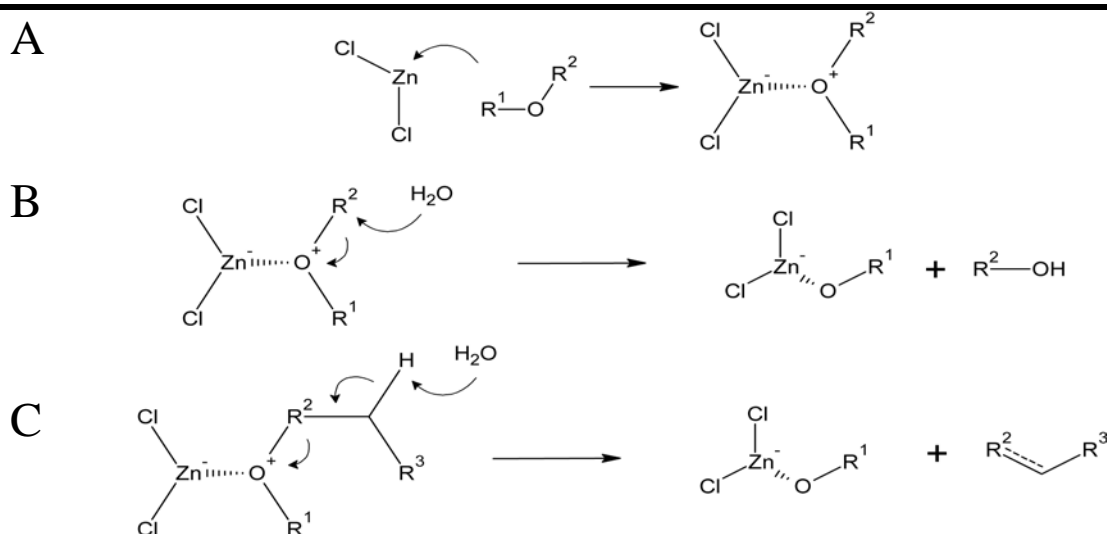
Figure 1.6. Lewis acid reactions between $ZnCl_2$ and ether functional groups of the biopolymers. R^1 and R^2 can be any fragment of carbon corresponding to biopolymers.

1.2.2.2. Phosphoric acid activation

Phosporic acid has been used as activating agent of lignocellulosic materials such as wood and some agricultural by-products (such as almond shells and olive stones) as well as carbonaceous materials with a high volatile content [18]. Lignocellulosic based activated carbons with H_3PO_4 can reach surface areas of 1500 m^2/g, however, when mineral carbon is employed as precursor, the surface area do not reach this surface area values [33]. This effect is related to the activation mechanism promoted by phosphoric acid. Marit Jagtoyen, Frank Derbyshire and coworkers have carried out extensive studies of H_3PO_4 activation of different raw materials and proposed an activation mechanism that can be summarized as follows [34-37]: the reaction of lignocellulosic materials with phosphoric acid begins as soon as the components are mixed. The generation of large amounts of tar and the morphological changes of the precursor during the impregnation step confirm these reactions.
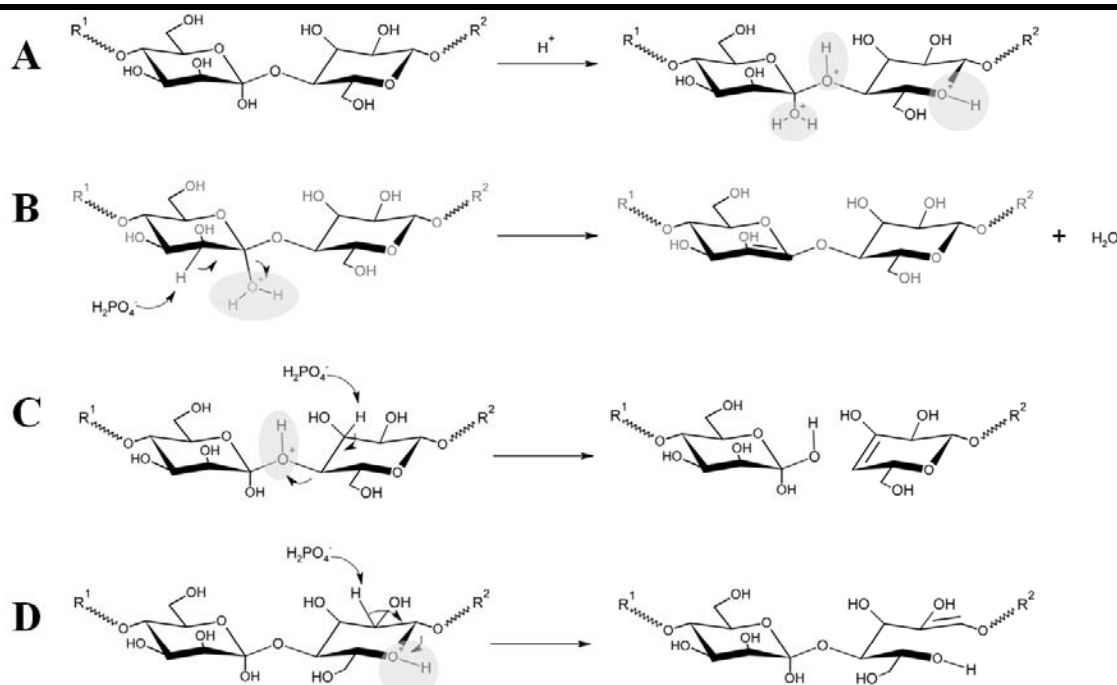
Figure 1.7. Chemical reactions acid catalyzed by H_3PO_4: A) protonation of the different oxygenated groups of the sugar monomers. After that hydrogen elimination promotes double bond formation (B), cleavage of the glycosidic linkage between polysaccharides (C) and the degradation of sugar monomers (D).

The acid media lead the protonation of the different oxygenated groups on the polysaccharides (Figure 1.7A). Once the oxygen is protonated, diverse reactions can occur. The main reactions are dehydration (Figure 1.7B), the hydrolysis of glycosidic linkages in polysaccharides (Figure 1.7C) and the degradation of the sugar monomers (Figure 1.7D). Also during this stage, the acid attacks the lignin cleaving the aril ether bonds of the lignin. These reactions also depends on the activation temperature: during the activation at low temperatures (100–200 °C), an accelerated weight loss and volumetric contraction is observed, due to the removal of the volatile products of low molecular weight formed by depolymerization. At higher temperatures the rate of weight loss considerably slows, this because H_3PO_4 inhibits the formation of volatile cellulose products as appears in Figure 1.8A.
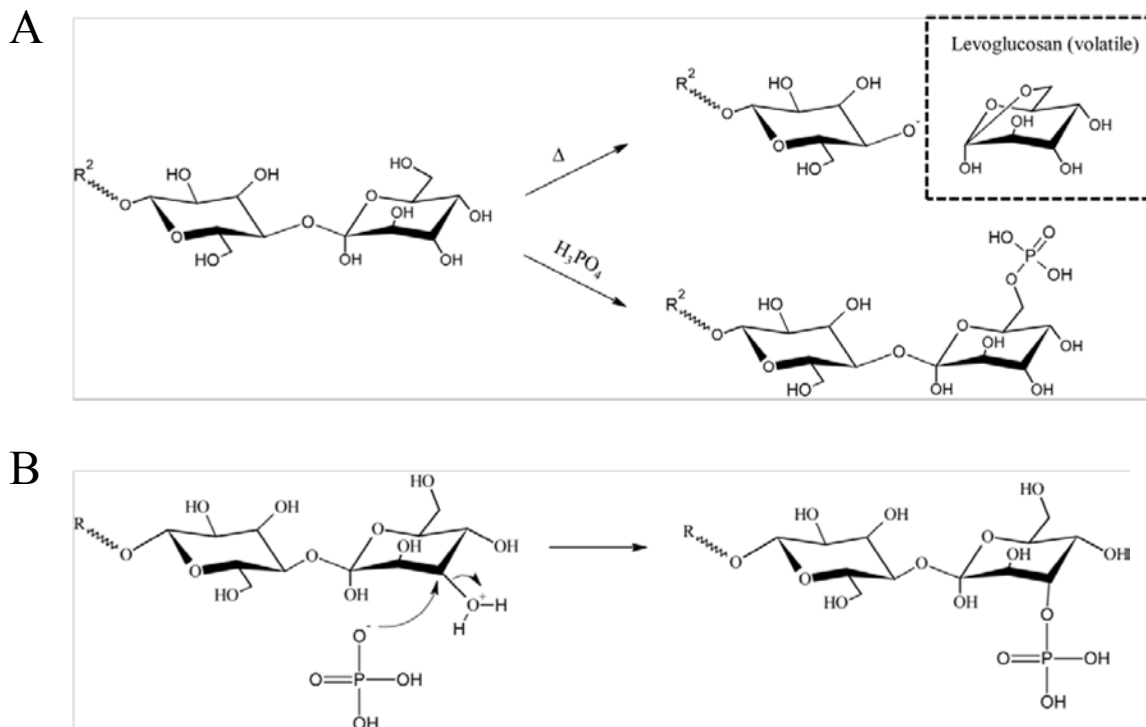
Figure 1.8. A: reaction mechanism by which esterification of phosphoric acid would block the formation of cyclic levoglucosan; B: formation of ester linkages between phosphoric acid and OH groups of biopolymers.

It was observed that at an activation temperature around 400 °C, the dilation of the precursor structure begins. This dilation is related to crosslinking reactions between the polymer chains by the formation of ester linkages between phosphoric acid and OH groups (see Figure 1.8B). As the temperature is increased, cyclization and condensation reactions lead to an increase in aromaticity and in the size of the polyaromatic units, enabled by the scission of P-O-C bonds. After removal of the acid on the washing step, the matrix remains expanded by the polyphosphates bridges promoted by the activating agent, leaving an accessible pore structure.

1.2.2.3. Potassium hydroxide activation

In the 1970s, researchers from the AMOCO Corporation, USA, developed a process that produced extremely high surface area carbons (super activated carbons, with surface area over 3000 m^2/g) by chemical activation with alkaline hydroxides, especially KOH [8]. As previously mentioned lignocelulosic materials or carbon with high volatile content are the desired precursor when chemical activation with $ZnCl_2$ or H_3PO_4 is carried out. In contrast, the most appropriate raw materials for chemical activation with KOH are those with a low volatiles content and high quantity of carbon such as high rank coals, devolatilized chars and petroleum coke.

In the KOH activation, the precursor (as powder or granular) is mixed with the activating agent either by impregnation with aqueous solution or just physically, generating mixtures with weight ratio between 2 and 4 (KOH/precursor). The activation temperatures must be superior to the melting point of KOH (360 °C), being 700-900 °C the activation temperature often used. Linares Solano, Lillo Rodenas and coworkers have been studing carbon activation by alkaline hydroxides during the last 18 years, and have analised the generated porosity and the reactions taking place during the activation process [38]. According with their publications [39, 40], the activation mechanism of carbon with KOH can be summarized as follows: during the thermal treatment H_2, CO, and CO_2 are the main components of the releasing gases. Hydrogen evolution starts at about 550 °C and increases at higher temperatures. From FTIR and XRD it was observed that K_2CO_3 appears also at about this temperature (550 °C) and K_2O and metallic potassium at higher temperatures. These results suggest that activation takes place when carbon reacts with the melted KOH producing H_2 and carbonate by means of a redox reaction as appears in equation 1. Further potassium carbonate decomposes to form K_2O and CO_2 (equation 2). The *in situ* generation of CO_2 by the thermal decomposition of K_2CO_3 acts as an activating agent promoting similar reactions to those on the physical activation.

$$6KOH + 2C \rightarrow 2K_2CO_3 + 3H_2 + 2K \qquad (1)$$

$$K_2CO_3 \rightarrow K_2O + CO_2 \qquad (2)$$
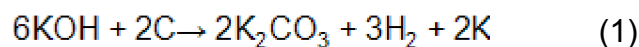
Equation 1 is a redox reaction in which the carbon is oxidized to carbonate and the hydroxide is reduced, giving metallic potassium and hydrogen. Of course, in both reactions not all the carbon is converted to carbonate; the residual carbon perform the activated carbon structure. Also the elimination of metallic potassium, potassium oxide, potassium carbonate and the remaining potassium hydroxide generate the well developed porous structure that characterizes these activated carbons. Something to remark is that according to the stoichiometry of equation 1, in most of the published studies a reasonably lower hydroxide amount than that needed for 100% carbon conversion was used since hydroxide/carbon ratios as high as 14/1 for KOH would be needed.

1.2.3. Physical activation

Physical activation, also called thermal activation, is the processes that consist in diverse thermal treatments by which the carbon precursor develops porosity and hence extensive surface areas. The employed precursor to produce activated carbon by thermal activation includes either lignocellulosic materials or mineral carbons. However, the preferred materials are mineral carbons, wood and lignocellulosic materials such as fruit stones and hard shells. The raw material needs some pretreatments prior to its activation: the required particle size must first be prepared by crushing and sieving. Also, sometimes a washing step is applied with water or acid in order to remove any undesired material and to reduce the inorganic content.

Generally, physical activation consists of two consecutive steps. The first step is thermal carbonization of the raw material, carried out at moderate temperatures, to produce a char rich in carbon. The second step is the activation, where the remaining char is partially gasified with an oxidizing agent, usually CO_2 or steam.
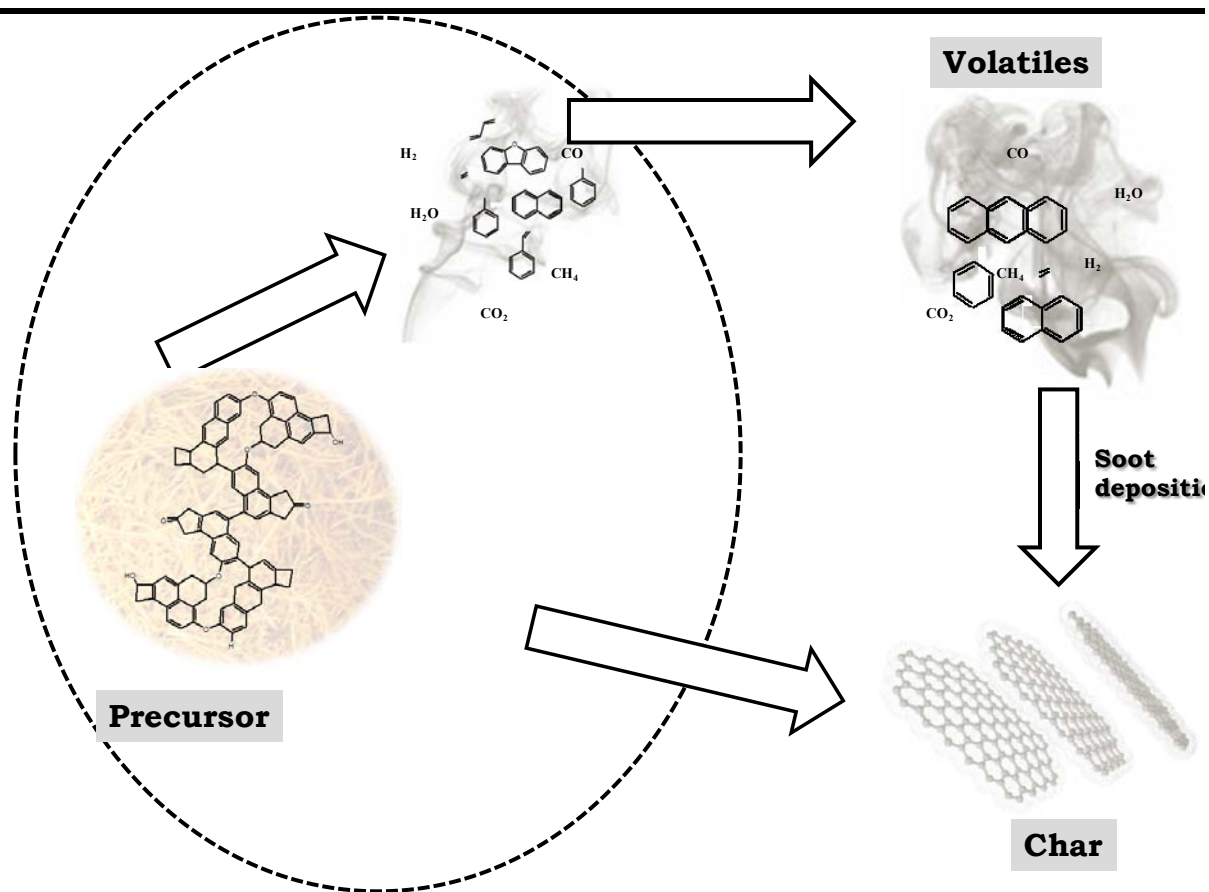
Figure 1.9. Carbonization scheme of a carbonaceous precursor.

1.2.3.1. Carbonization

During this step the starting material, which major content is organic and/or inorganic carbon decomposes to generate a gaseous fraction and the remained solid. The chemical composition of the gas phase varies regarding the precursor, heating rates and the carbonization temperature. In general, the gases that first evolve are those coming from labile carbon presented in the precursor in the form of radical species. These fractions can react among themselves in the gas phase to yield cracking products.

At temperatures above 1000 °C these reactions become more important and the formation of stabilized polyaromatics compounds is confirmed by the presence of

soot in the carbonization furnace. Also, olefins, methane, hydrogen, water and carbon oxides can appear in the gas phase. Regarding the solid phase, enrichment in both carbon content and aromaticity is observed. At this point the char is composed of a group of disordered short graphitic crystals. Between the crystals there is little void space on the micropore range, which often is not accessible from the external surface because the meso and macroporous structure is blocked by soot deposition. A scheme of the carbonization of a carbonaceous precursor is shown in Figure 1.9. The starting material, based on an organic macromolecular structure, decomposes during the thermal treatment to yield two main fractions: a gaseous fraction, rich in hydrogen, light hydrocarbons and tar; and a solid fraction, rich in carbon, called char.

1.2.3.2. Activation

The objective of the activation process is to enlarge and open the incipient pore structure developed in the carbonization. Also, during this process oxygenated groups are incorporated to the carbon structure, generating a more "active" carbon for specific applications. To carry out this task the reaction atmosphere is changed from inert to oxidant. This is accomplished by the introduction of gases such as oxygen, steam and carbon dioxide. Depending on the activating agent employed, different reactions can be performed with carbon:

$$
\begin{array}{lll}
O_2 & 2C + O_2 \rightarrow 2CO & \Delta H = -387 \text{ kJ/mol} \quad (3) \\
 & C + O_2 \rightarrow CO_2 & \Delta H = -226 \text{ kJ/mol} \quad (4) \\
H_2O & C + H_2O \rightarrow CO + H_2 & \Delta H = 132 \text{ kJ/mol} \quad (5) \\
CO_2 & C + CO_2 \rightarrow 2CO & \Delta H = 159 \text{ kJ/mol} \quad (6)
\end{array}
$$
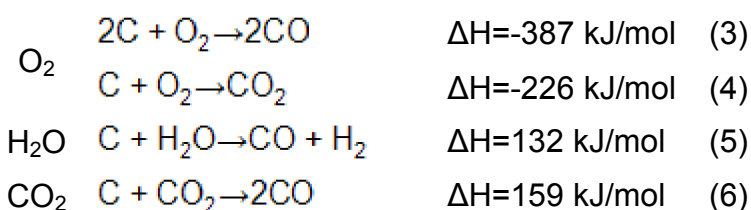
According with the reaction enthalpy, O_2 is the most reactive oxidant and CO_2 the least reactive. Due to the highly exothermic enthalpy of oxygen reactions, the temperature of the reaction is extremely difficult to control, usually generating the consumption of the precursor due to the burn of only the external surface of the particle and not to the inner surface. Consequently oxygen activation is scarcely

applied. On the other hand CO_2 and H_2O are an option to activate carbon under moderate oxidation, since the promoted reactions by both activating agents are endothermic, requiring external heating for maintaining the reactions [41-43]. Therefore controlling activation temperature and residence time, carbon oxidation can be controlled. Finally, other factor that influences the characteristics of the generated carbon by thermal activation is the presence of inorganic impurities because these can catalyze or inhibit the gasification reactions [44-46].

1.3. ACTIVATED CARBON CHARACTERISTICS

As state above, activated carbon can be produced from a wide variety of precursors by means of chemical or physical activation. Production conditions and the chemical composition of the precursor determine the characteristics of the activated carbon developed. In these sense we can produce activated carbons with different properties, for diverse applications. The tests commonly used to characterize activated carbons are summarized in Table 1.2, also the typical value for these tests are included. A comprehensive discussion of the main physical and chemical properties of activated carbons has been included in this section.

Table 1.2. **Major test for activated carbons and their typical values [8, 47].**

Test	Typical value	Purpose
Physical		
Bulk density [a]	0.5-0.6 (g/mL) coal carbons	For estimation of the filter packing volume
	0.24–0.3 (g/mL) wood carbons	
Real density [b]	2.1–2.2 (g/mL)	Important for flow characteristics of the activated carbon bed
Surface area	800–1200 m^2/g	
Particle size (n/m) [c]	Granular:	Factor influencing the adsorption kinetics, and flow characteristics
	2.36/0.83, 1.65/0.83, 0.83/0.295	
	Powder: from 0.150 to 0.043 mm	
Mechanical strength	70–75(%) [d]	For estimation of resistance to abrasion and attrition during operation
Adsorptive		
Iodine number	800–1000 (mg/g) [e]	Gives an indication of internal surface area
Methylene blue number	200-400 (mg/g)	Indicates adsorption capacity for large molecules
Phenol adsorption	100-200 (mg/g)	Indicates applicability of activated carbon to drinking water treatment
Molasses number	200-230	Informs about usefulness of activated carbon in sugar industry
Butane adsorption	7–8 g/100mL	Indicates applicability of activated carbon to gas phase applications
Chemical and physico-chemical		
Moisture	3–7%	Provides information about the purity of AC
Ash content	3–10%	
Water soluble content	0.5–10%	
pH value	2-10	Indicates the presence of inorganics and the surface groups that may influence the pH of treated liquids

[a] *Weight per unit volume of dry carbon in a packed bed*
[b] *Weight per unit volume of the solid carbonaceous material alone*
[c] *Carbon that passes through a sieve with open size of n mm but is retained by a sieve of m mm open size*
[d] *According with the ASTM D3802 standard test*
[e] *According with the ASTM D4607 standard test*

1.3.1. Physical properties

1.3.1.1. Surface area

As adsorption is a surface phenomena, the majority of the adsorbents show an extensive surface area at which some molecules can be retained. The internal surface area of porous materials such as activated carbon is determined generally by using the so called BET equation [48]. This equation describes multilayers of condensed gas which occurs when an adsorbable gas such as nitrogen is contacted with the porous solid. In such a test N_2 is normally used at a temperature corresponding to its boiling point (-196 °C at 760 mmHg of pressure). The BET equation was derived making the following assumptions: 1) in the first layer, the rate of condensation of molecules on bare sites is equal to the rate of evaporation of molecules from sites covered by only one molecule. 2) the heat of adsorption beyond this layer is constant and is equal to the heat of liquefaction. These assumptions are only approximately correct. The linearize form of the BET equation is:

$$\frac{P}{q(Ps-P)} = \frac{1}{bq_m} + \left(\frac{1}{bq_m}\right)(b-1)\left(\frac{P}{Ps}\right) \qquad (7)$$

where Ps is the saturation vapor pressure at the temperature used in the test, q is the amount of gas adsorbed at any given pressure P, q_m is the amount of substance adsorbed when one complete monolayer of gas coverage is attained, and b is a constant that depends on the isotherm shape. From an adsorption experiment, we can take the data of the amount of gas adsorbed (q) at the different pressures (P) used, and compute values of P/q(Ps-P). These values are then plotted vs the corresponding P/Ps value, and data taken over the range of 0.05 to 0.3 P/Ps values are fitted to the best straight line using the linear least squares procedure. From the regression we can get the intercept at P/Ps=0 that is equal to

$1/bq_m$ and the slope of the line that is equal to $(1/bq_m)(b-1)$. Getting the regression values, b and q_m can be determined. As previously mention q_m represents the amount (moles) of nitrogen corresponding to the exactly one complete monolayer of the surface. If the area that covers a single molecule of N_2 is 16.2 Å^2 , and taking the Avogadro number, the surface area of the analyzed material can be determined [47, 49]. Regarding the BET model, it is an approximation of the surface area of the porous material, all researchers agree to use the BET method as standard to measure the surface area of porous materials. The typical surface areas of activated carbons are in the range of 800 to 1200 m^2/g.

1.3.1.2. Pore structure

The resulting channels after activating the precursor, make up the porous structure which form the large surface area of activated carbons. The recommended classification of pore size by IUPAC is as follows: micropores, pore diameter <2 nm; mesopores, pore diameter from 2 to 50 nm; and macropores, pore diameter >50 nm. This classification is arbitrary and was developed based on the adsorption of nitrogen at its normal boiling point on a wide range of porous solids. Depending on the size of the adsorbate molecules, especially in the case of some organic molecules of a large size, molecular sieve effects may occur either because the pore width is narrower than the molecules of the adsorbate or because the shape of the pores does not allow the molecules of the adsorbate to penetrate into the micropores. Thus, slit-shaped micropores are not accessible to molecules of a spherical geometry, which have a diameter larger than the pore width. This is why the specific surface area of a carbon is not necessarily proportional to the adsorption capacity of the activated carbon. Pore size distribution, therefore, is a factor that cannot be ignored. The suitability of a given activated carbon for a given application depends on the proportion of pores of a particular size. Generally highly microporous activated carbons are preferred for the adsorption of gases and vapours and for the separation of gas molecules of different dimensions if the carbon possesses a suitable distribution of narrow size pores (molecular sieves)

while well developed meso- and macroporosity is necessary for the adsorption of solutes from solutions [8].
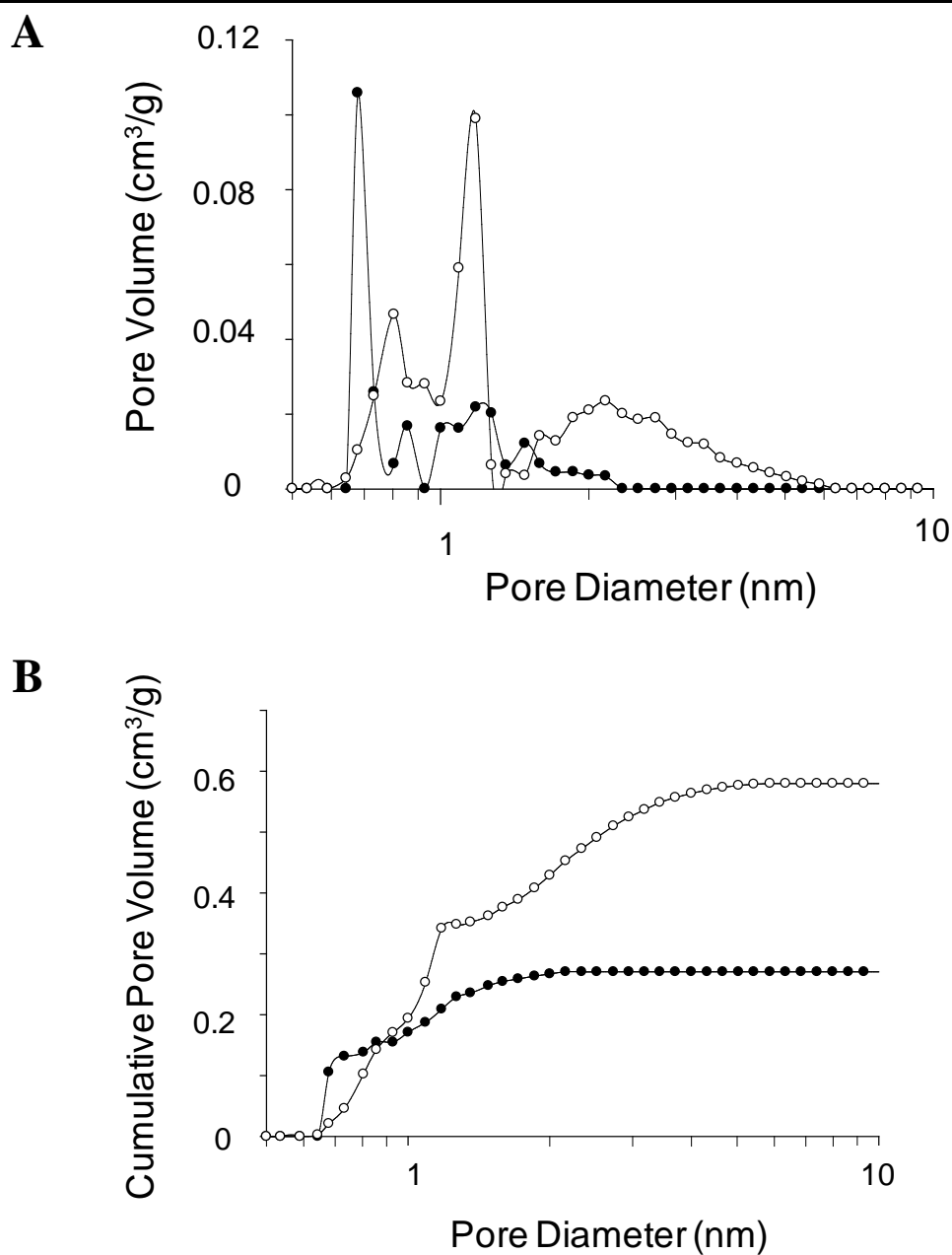
Figure 1.10. Pore size distribution of agave bagasse based activated carbons expressed as pore volume (A) and cumulative pore volume (B) as a function of pore diameter.

To evaluate the pore size distribution, various procedures have been employed by using data from nitrogen adsorption at -196 °C. The most common methods are the Dubinin-Radushkevich (DR) plot, Barrett-Joyner-Halenda (BJH) method, Horvath-Kawazoe (HK) method, t plot, alpha plot, density functional theory (DFT) and the theoretical calculations based on the Grand Canonical Monte-Carlo (GCMC) method [8].

The information of these analyses is usually expressed as a plot of pore volume vs pore width (Figure 1.10A). Also the pore volume is often changed by the "cumulative pore volume" that represents the total pore volume contained in pores of any given pore diameter or less (Figure 1.10B). By means of these graphs we can determine the pore diameter range with which most of the pore volume is associated, and hence stablish a criteria about the components that can be removed from gas or liquid streams.

1.3.1.3. Hardness

The most common method to employ activated carbon in adsorption processes is by means of a packed column system where a fluid crosses the column and some diluted compounds (often called adsorbate) are removed by the stationary fixed carbon bed. The pass of the stream through the carbon bed implies attrition forces that can fraction the carbon, generating dust that can block the column. Also this results in a loss of valuable material and in a undesirable increase on the column pressure. In these sense the ability of activated carbon to resist the attrition forces during the stream flow in packed column systems is needed in order to apply activated carbon in real systems. The ASTM D3802 is a standard test to evaluate the attrition resistance of an activated carbon. The procedure consists in placing a screened and weighed sample of carbon in a special pan with a certain number of stainless steel balls. The pan is shaken on a mechanical sieve shaker for 30 minutes. The sample is then sieved with a sieve having openings of one half the size of the original carbon. The weight percentage of the carbon retained on this

sieve is known as the "ball pan hardness number". The common ball pan hardness values for activated carbons are from 65 to 80%.

1.3.2. Chemical properties

1.3.2.1. Carbon surface groups

As stated above, a high surface area and an adequate pore size distribution of activated carbon are necessary to succeed in a particular application. However, the analysis of an activated carbon quality based only on its surface area is obviously incomplete. For instance, if we compare the adsorption capacity of two activate carbons from different raw materials and/or activated by different methods, but having similar surface area, their performance as adsorbents could be different. Part of such differences would be explained by the different pore size distribution of each carbon; for example, narrow pores can restrict the diffusion of a certain compound to the entire carbon surface. However, another part of the differences can be attributed to the nature and amount of the surface groups that may be present on the carbon surfaces. The unsaturated carbon atoms located mainly at the edges of the graphite layers possess unpaired electrons that can be easily bonded to heteroatoms (e.g. O, N, S, P), generating the so called surface groups. Oxygen containing groups are the most common surface species in carbons and are the responsible of the acid behavior of the carbon. On the other hand, ammonia or urea can introduce nitrogenated functionalities into the carbon surface, being such surface groups responsible of the basic behavior of the AC. Also, functionalities like pyrones, chromenes, ethers, carbonyls and electron rich regions (carbon π electrons) can interact as basic species. Figure 1.11 summarizes the most important types of surface groups that can be present on carbon surfaces.

Carbon surface groups have two principal effects: the modification of the hydrophobic character of the carbon and the generation of localized electric charges where polar molecules can be retained by electrostatic interaction. Activated carbon is in general hydrophobic; however, the presence of polar atoms

such as oxygen, sulfur and nitrogen promote an increase in hydrophilicity, since water molecules can form hydrogen bonds with the polar atoms of the carbon surface. This effect is of particular importance to the treatment of water streams, since a good interaction between water and carbon allows the pollutant to reach the entire carbon surface. In contrast, for adsorption of compounds in a gas stream, the presence of polar functionalities can be unfavorable since it causes the adsorption of water molecules, which may block the access of the adsorbate to some pores of the activated carbon.
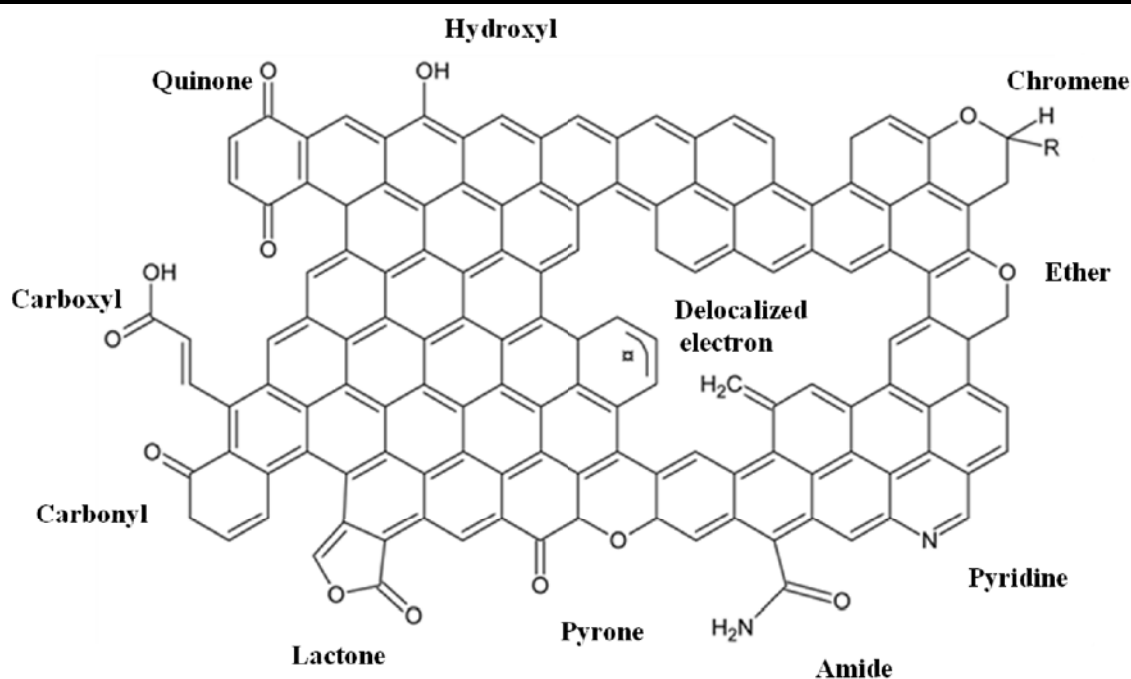
Figure 1.11. Schematic representation of the most important types of surface groups that may be found on a carbon surface.

The other important effect of the surface groups is related to the generation of localized electric charges all over the carbon surface. Most of the oxygenated surface groups that can be found on activated carbon can establish acid-base equilibrium when these are in contact with aqueous solutions. On one hand, the functional groups can release a proton to the media, leaving in the carbon surface

a negative electric charge that can interact with some cations in solution. This reactivity can be exhibited by carboxyl, hydroxyl and lactones groups as appears in Figure 1.12A. On the other hand, atoms with unpaired electrons such as pyrone, pyridine, and carbonyl groups can accept protons from the media, generating in this way a positively electric charged group on the carbon surface (Figure 1.12B). Also, functional groups (e.g. chromene) stabilize carbocations on the carbon surface (Figure 1.12C) leaving a positive electric charge on the carbon surface. The occurrence of these acid-base equilibriums depends on the solution pH and the surface groups acid strength (i.e. their pKa).
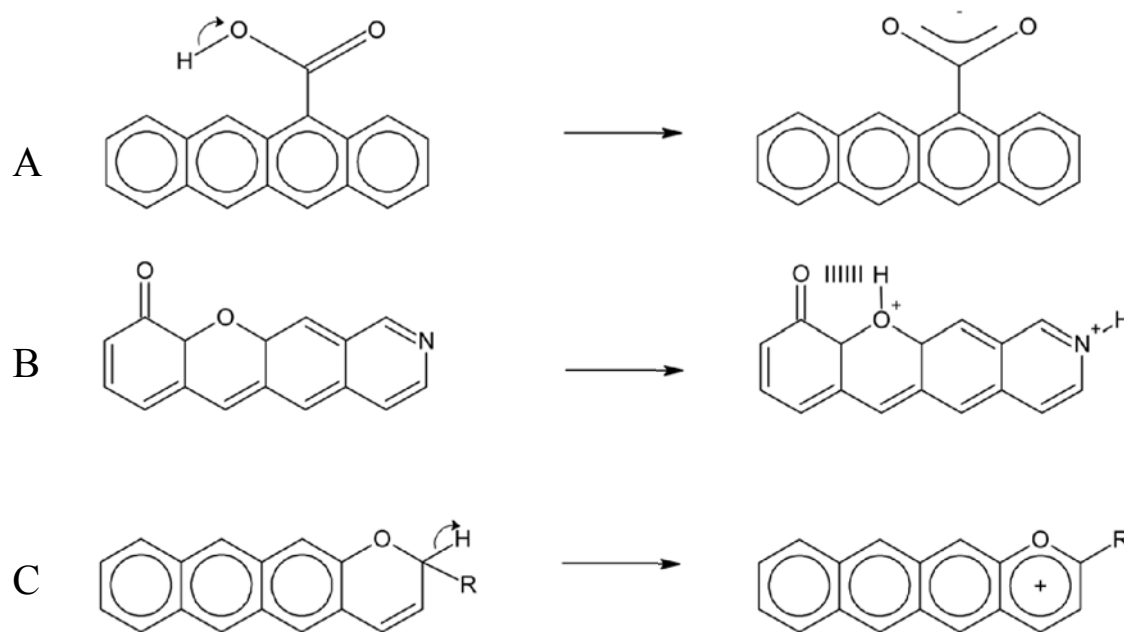
Figure 1.12. Acid – base equilibrium of carbon surface group to generate localize electric charges on the activated carbon surface. A: carboxylic group. B: pyrone group. C: chromene group.

Hence, all these localized electric charges on the carbon surface greatly influence the adsorption capacity of carbon. Two interactions dominate the adsorption process: those related to dispersion forces (i.e. London and van der Waals forces) and those related to electrostatic forces. The dispersion forces arise from the rapid fluctuation in electron density within each atom, which induces an electric moment

in a near neighbor and thus leads to attraction between such two atoms; this interaction is the responsible of the adsorption of a non polar compound onto the surface of the adsorbent. The electrostatic forces exist as a result of the permanent electric dipole or electric charge on a molecule or surface group, which promotes the adsorption of ionic species onto the surface functional groups of opposite electric charge [49].

1.3.2.2. Point of zero charge

As previously mentioned, activated carbon have acidic and basic sites that coexist on their surface. These groups can be protonated or deprotonated according to the pH of the solution that is in contact with them. The pH at which each surface group establishes this acid-base equilibrium depends of both the acid strength (pKa) of the functional group and the chemical environment. For instance, at pH below the pKa of an acid group (i.e. carboxyl), the protonated specie may predominate, and hence the carbon surface remains electrically neutral. However if the solution pH is higher than their pKa, the proton is released to the media, generating a negative electric charge in the carbon surface. Similarly, basic surface groups can generate a positive electric charge if the solution pH is lower than their pKa. Due to the great diversity of functional groups that can coexist on the activated carbon, it is difficult to establish a constant equilibrium which describes in general terms the acid–base reactions. In these sense, the so called point of zero electric charge (pH_{PZC}) which is defined as the pH value at which the net surface electric charge of the material is zero, is a useful parameter that allows estimating the overall electric charge of the activated carbon regarding the solution pH. Thus, at $pH > pH_{PZC}$, acidic functionalities dissociate, releasing protons into the medium and leaving a negatively electric charged surface on the carbon. On the other hand, at $pH < pH_{PZC}$, basic sites combine with protons from the medium to leave a positively electric charged surface. This behavior is schematically represented in Figure 1.13.

Considering that the surface electric charge of activated carbon depends on the solution pH, the interactions and the adsorption capacity of the activated carbons

can be optimized by modifying the surface chemistry of the carbon (and/or the pH of the medium, when this is possible). Thus, basic carbons are prefer for adsorbing acidic molecules while acidic carbons will perform better for the adsorption of basic compounds. Moreover, the adsorption of cations will be favored (by electrostatic forces) if the carbon surface is negatively electric charged, while the adsorption of anions will be enhanced on a positively electric charged surface.
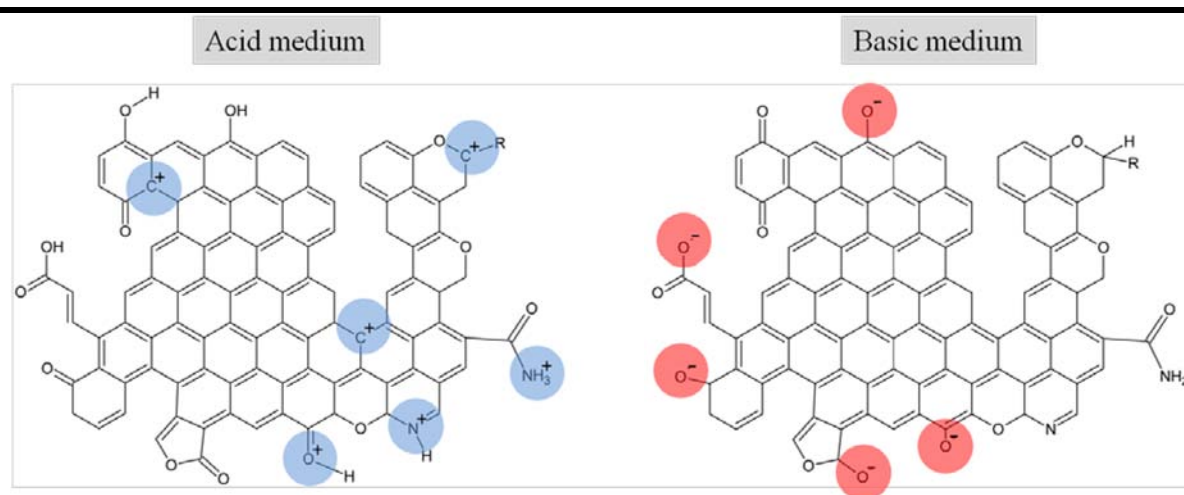
Figure 1.13. Schematic representation of the acidic and basic behavior of the surface groups and delocalized π electrons of basal planes.

1.4. MODIFICATION OF ACTIVATED CARBON

Activated carbon has proven to be an effective adsorbent for the removal of a wide variety of organic and inorganic pollutants dissolved in aqueous medium, or from gaseous environment. Recent research has emphasized on modifying the physical and chemical attributes of AC to enhance their affinities toward different molecules present in aqueous solutions [50]. Also, the modification of AC has been proposed to induce the adsorption of diverse molecules that carbon usually cannot remove. The proposed modifications can be classified in two groups: the modification of their atomic structure by means of chemical treatments with oxidizing or reducing

compounds or thermal treatments with gases such as ammonia and hydrogen. And the modifications based on the incorporation of molecules or metal clusters onto the carbon surface. A brief discussion of both modifications is presented on the following section.

1.4.1. Chemical modification

Chemical modification of AC has the purpose of changing the chemical groups present on the carbon surface. As previously mentioned, AC has diverse functional groups that can be classified as acid and basic groups. The predominant type of AC surface functional groups are those conformed by oxygen complexes such as carbonyl groups. The surface oxygen complexes of AC can be created via two major oxidation methods: dry and wet oxidations. Dry oxidation is a method involving contact of the AC with oxidizing gases (such as steam, CO_2, etc.) at high temperatures (>700 °C); wet oxidation involves reactions between AC surfaces and oxidizing solutions (such as aqueous solutions of HNO_3, H_2O_2, $NaClO$ and $(NH_4)_2S_2O_8$) under relatively mild reaction conditions (20–100 °C) [50-52]. These treatments generate a beneficial effect on adsorption of metal ions; however, produce a decrease in the adsorption of organic compounds. It is widely recognized that the presence of acid oxygen-containing groups on the AC surface decreases the adsorption of organic compounds in aqueous solution, while their absence favors the adsorption of such compounds, independently of their polarity [50]. The general strategy to eliminate oxygenated surface groups consists on thermal treatment under inert atmosphere at high temperatures. This promotes the arrangement of graphite layer by means of heteroatoms elimination [53]. Also, the thermal treatment has the function of modifing the surface area, the pH_{PZC} and the pore structure of an activated carbon. These kind of modification has been employed to increase the adsorption of organic molecules such as dyes, herbicides, and carbohydrates onto AC [50].

1.4.2. Impregnation with foreign materials

The impregnation of activated carbon with foreign materials is an alternative to produce carbons that adsorb molecules with low affinity toward carbon surface or their functional groups. The incorporated materials to the carbon surface are specific compounds that have proven affinity for the molecule to be adsorbed. The materials often used on this kind of modifications are organic molecules and metal oxides. It is well known that AC is able to effectively adsorb organic molecules. This chemical behavior leads to immobilization of organic compounds on the carbon surface. The organic molecules attached to the AC surface acts as chelating agents to adsorb some specific adsorbates. It has been reported the adsorption of copper(II), zinc(II), chromium(VI) and cyanide (CN^-) ions onto the surface of AC immobilized with tetrabutyl ammonium (TBA) and sodium diethyl dithiocarbamate (SDDC) [54]. Also, Oxine (8-hydroxyquinoline) has been used to modify activated carbon, founding that oxine-impregnated activated carbon had an increased adsorption of cadmium, lead and zinc [55]. An advantage of the carbon modification with organic molecules is the generation of materials with a selective removal capacity of metal ions, due to their different affinities for the surface functional groups of AC. For instance, it has been reported that citric acid has a superior binding affinity to copper [56] and, hence, the materials modified with this organic molecule significantly improve its copper ion adsorption capacity [57].

On the other hand, metal oxides are employed to modify AC to take advantage of its capacity to attract dissolved species such as metal cations, anions, neutral molecules and polymers [58]. In aqueous solutions, metal oxides can ionize as appears in Equation 8. The electric charge on surface groups can be negative, positive or zero depending on the nature of the oxide, and give to the surface a basic, acidic or neutral character, respectively. These characteristics are related to the solution pH; Table 1.3 shows the pH_{PZC} of some metal oxides.

$$M\text{-}O^- + H_3O^+ \leftrightarrow M\text{-}OH + H_2O \leftrightarrow M\text{-}OH_2^+ + OH^- \qquad (8)$$
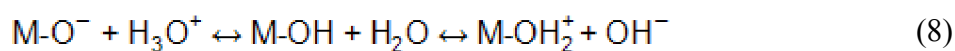
These hydroxylated groups may also act as coordination sites for dissolved cations, or be substituted by anions (surface coordination). These may also act as nucleation sites in the case of surface precipitation. Therefore, several possible mechanisms should be considered in the overall phenomena of adsorption, and most of them can be described in terms of the classical concepts of coordination chemistry. An application of these modifications to AC is to enhance ammonia adsorption. Usually, activated carbon is not a good adsorbent of ammonia; however, the ammonia is easily adsorbed by metal oxides. In these sense the coating of activated carbon with metal oxides of molybdenum, tungsten, aluminum, zirconium, and vanadium, has generated composite materials that remove ammonia from both aqueous and gas phase [59-63]. Also, the metal oxide coated activated carbon has been used to remove anionic species of arsenic and fluorine, as well as dissolved organic mater [64-69].

Table 1.3. **Point of zero electric charge of some metal oxides [58].**

Valence	Oxide Formula	pH_{PZC}
+II	MgO	12.5
	ZnO	9 – 10
+III	α-Fe_2O_3	5.5 – 9
	α-Al_2O_3	6.5 – 10
+IV	TiO_2	3.5 – 6.5
	SiO_2	2 – 4
+V	Sb_2O_5	0.5
+VI	WO_3	0.4

Besides, it is well known that oxides of polyvalent metals such as Al(III), Fe(III), Ti(IV), and Zr(IV), exhibit ligand sorption properties through formation of inner-sphere complexes [70-73]. Among such compounds, iron oxide is particularly

advantageous because their low cost, availability and chemical stability over a wide pH range. Previous studies have shown that Fe(III) oxides have high sorption affinity toward both As(V) and As(III) oxoanions. Their selective sorption onto iron oxide-hydroxide particles results from ligand exchange in the coordination spheres of structural iron atoms. Recent investigations using extended X-ray absorption fine structure spectroscopy (EXAFS) confirmed that As(III) and As(V) oxoanions are selectively bound to the iron oxide surface through coordinate bonding [74]. Taking into account the high affinity of iron oxides toward arsenic, this thesis propose the modification of AC including agave bagasse based activated carbon with iron oxide-hydroxide nanoparticles in order to generate a composite material with competitive arsenic adsorption capacity.

1.4.3. Iron oxide impregnated activated carbon

Since the effectiveness of iron oxides for arsenic removal from water has been proven, numerous attempts to employ iron oxides in packed column system have been done. Granular ferric hydroxide was prepared by diverse techniques generating materials with capacity of 30 000 to 40 000 bed volumes before the breakthrough concentration (10 μg/L) was reached [64]. However, some disadvantages were found: (i) the mechanical strength of the granular iron oxides need to be improved; (ii) an important pressure drop through the adsorbent bed is quickly produced and becomes more significant after backwashing, probably because of the material weakening that produces fine particles; (iii) when large particles are used (1.0 to 2.0 mm), the arsenic adsorption capacity is reduced by 50 %. Taking into account such disadvantages of the iron oxides, an alternative recently proposed is to modify granular materials often used in adsorption systems with iron oxides. Researchers have proposed the modification of activated carbon with iron oxide-hydroxide particles, with the aim to generate a composite material with suitable properties for packed-bed adsorption column applications, and arsenic adsorption capacity that allows a feasible potable water treatment. Table 1.4 summarizes the studies related to this issue. In order to compare the arsenic

adsorption capacity of the modified carbons, the values reported in Table 1.4 were calculated with the isotherm parameters reported in each publication, at an As concentration of 1 ppm at equilibrium. As can be observed in Table 1.4, the modified carbons developed high arsenic removal efficiency, getting values from 0.028 to 11.85 mg As/g AC. However, some of these reports mention that during the adsorption tests, part of the iron loaded onto the activated carbon is released to the stream, which is an undesirable situation. On the other hand, something to remark is that the material that has the maximum arsenic adsorption capacity (11.85 mg As/g AC) is the activated carbon modified with zero valent iron at nanometric size by Zhu et al [78]. It is worth noticing that the main reason of this superior arsenic adsorption capacity is related to the size of the anchored iron particles. However, the consumption of expensive reagents to generate iron nanoparticles is a disadvantage of this procedure.

Table 1.4. Previously proposed modification of activated carbon with iron species for arsenic removal in aqueous solutions.

Fe loaded	Methodology	Fe loaded (%)	As uptake mg As / g AC	Reference
Amorphous	10.0 g of the AC was placed into Erlenmeyer flasks, containing 150.0 mL solution of increasing $FeCl_2$ concentration (0.002, - 0.10 M). Each series was then treated under different oxidation conditions. Sodium hypochlorite (oxidant that generates the best material) was added four times during the mixing, with a 6-h interval, according to a ratio of 10 g $FeCl_2$ $4H_2O$/20 mL NaClO (10-13 %). pH was controlled at 4.5-5.0	1-7	Q^a=3.47 pH=4.7; 25 °C	64
Fe_3O_4 α-Fe_2O_3 γ-Fe_2O_3 α-FeO(OH)	FeO/AC adsorbent was prepared by mixing $FeCl_3$/$FeSO_4$ (molar ratio 2:1) and 5 mol NaOH, remaining for 10 min at the temperature of 70 °C and pH value of 9.5, along with the gentle stirring (60 rpm). The mixture was impregnated into the AC. The obtained materials were dried in an oven at 100 °C for 3 h.	8	Q^a=1.94 pH=5; 30 °C	66
Fe_3O_4	2 g of sawdust, 20 mL of 1.0 mol/L $FeCl_3$ and 10 mL 50 % H_2SO_4 were mixed. The resulting mixture was ultrasonicated for 2 h and aged at 60°C for 12 h. The solids were pyrolyzed at 600 °C under 30 mL/min nitrogen gas and held at 600°C for 60 min.	39	Q^a=1.90 pH=8; 30 °C	75
α-Fe_2O_3	5 g of oxidized carbon were introduced into 150 mL of a 0.05 M $FeCl_3$ solution in acidic media (3M HCl) for 2 h. Forced hydrolysis was next carried out at 100 °C for different times: 1, 3, 6 and 24 h. The samples were washed to reach neutral pH and then dried at 80 °C overnight.	1.5-9.4	0.028 mg As/gAC (calculated from kinetic study, C_0=300 ppb As)	76
NR	2 g of oxidized AC was added to 200 mL solution with 2 g of $Fe(NO)_3$ $9H_2O$. The mixture was heated to 100 °C until dry, cooled at room temperature, washed with distilled water, dried and sieved	2.28-33.6	Q^a =5.68 pH=8; 20 °C	65

Table 1.4. (Continue)

NR	$KMnO_4$ pretreated activated carbon was subsequently mixed with a 1 M solution of $FeSO_4 \cdot 7H_2O$ for 6 h to oxidize the Fe(II) and precipitate the iron (hydr)oxide nanoparticles.	0.5 – 16	Q^a=1.74 pH=6.4; 20 °C	77
Akaganéite Ferrihydrite	1.0–1.5 mL of ferric nitrate solution at concentrations of 0.5–1 g/mL was dispersed over 1 g of dried GAC and mixed thoroughly for 24 hours. Mixture was then dried in a rotary evaporator at temperatures of 60, 80, or 90 °C for 12 h. After that AC was then washed thoroughly with deionized water.	11.7	26 mg As/g from a column test C_0=300 ppb As	*67*
Zero valent iron (nano)	One gram of dry based carbon was equilibrated with 30 mL 1.0 M Fe_2SO_4 N_2-purged solution for 3 h. The slurry was diluted by five times using a mixture of ethanol and deionized water (v/v 1:1). 100 mL of 0.2 M $NaBH_4$ was then added in a dropwise at 25 °C with magnetic stirring and N_2 bubbling. The carbon was washed with acetone for three times.	8.2	Q^a=11.85 pH=6.5 25 °C	78
NR	Mesoporous carbon were syntetyzed by using silica templates. The porous carbon were covered with iron by the methodology proposed by Gu et al [64]	3.85	Q^a=6.42 pH=6.5; 20°C	79

Q^a: Arsenic adsorption capacity calculated from the isotherm data exposed by the authors at an As concentration of 1ppm

NR No Reported

C_0: initial concentration

1.5. THE NATURE OF ADSORPTION ON ACTIVATED CARBON

Activated carbon has capacity to adsorb organic and inorganic compounds, by means of specific interaction between the adsorbed molecules and the carbon surface. There are several studies that attempt to explain the carbon adsorption mechanisms of diverse molecules dissolved in both liquid an gas phase. Due to the complexity of the activated carbon structure, it is difficult to establish a general process by which any molecule is adsorbed on the activated carbon. In the following section, the possible mechanism to adsorb organic and inorganic molecules on activated carbon from aqueous solutions is discussed.

1.5.1. Adsorption on a solid surface

At the surface of a solid, the forces that hold the molecules of the solid together are unsaturated. These unbalanced forces generate the tendency of a solid to attract and retain on its surface some molecules coming from any substance that is in contact with the solid. In this phenomenon, named adsorption, the substance attached to the surface is called adsorbate, and the substance to which it is attached is known as the adsorbent.

Depending of the nature of the forces involved in the adsorption process, the adsorption can be classified in a simplistic way in two types: physisorption, which is driven by van der Waals forces, and chemisorption, that involves a chemical reaction (exchange or share of electrons). Table 1.5 summarizes the main differences between these two types of adsorption. The word sorption is a more general term which groups the occurrence (proven or not) of some simultaneous surface phenomena as physisorption, chemisorption, surface precipitation, surface complexation and ion exchange. Hence, the term sorption is usually employed when there is not certainty about the occurring of one or more of the mentioned surface phenomena.

Adsorption equilibrium is very important to understand an adsorption process, since provides information about how much of the adsorbate can be attached to the solid surface. The adsorption phenomenon is a dynamic process where desorption (the inverse process) happens simultaneously with the adsorption. The moment at which the rate of both process are equal is known as adsorption equilibrium.

Table 1.5. **Main difference between physical and chemical adsorption [8,15].**

	Physisorption	Chemisorption
Forces involved	Weak - van der Waals	Strong – Chemical
Heat of adsorption	10–20 kJ/mole	40–400 kJ/mole
Specificity	Nonspecific	Site specific
Saturation uptake	Multilayer	Limited to one monolayer
Kinetics	Fast (active process)	Very variable

Because adsorption is strongly influenced by temperature, pH and adsorbate concentration, the common way to study the adsorption equilibrium is by obtaining adsorption isotherms. The adsorption isotherms represent the adsorption capacity of an adsorbent for some specific molecule measured as to the concentration of the adsorbate at equilibrium. Usually, mathematical models are used to fit experimental data; each model implies empirical or theoretical assumptions to explain the adsorption phenomena. Table 1.6 resumes the main adsorption isotherm models and its assumptions.

Table 1.6. Adsorption isotherm models often used for activated carbon experiments (modified from [80]).

Isotherm	Mathematical model		Assumption
Langmuir	$q_e = \dfrac{q_m b C_e}{1 + b C_e}$	**b** : constant related to the free energy of adsorption.	Assumes uniform energies of adsorption onto the surface and no transmigration of adsorbate in the plane of the surface.
Freundlich	$q_e = K_F C_e^{1/n}$	**K_F** : constant indicative of the relative adsorption capacity of the adsorbent. **n** :constant indicative of the intensity of the adsorption.	Assumes that as the adsorbate concentration increases, the concentration of adsorbate on the adsorbent surface also increases.
Elovich	$\dfrac{q_e}{q_m} = K_E C_e \exp\left(-\dfrac{q_e}{q_m}\right)$	**K_E** :Elovich equilibrium constant.	Based on a kinetic principle assuming that the adsorption sites increase exponentially with adsorption, which implies a multilayer adsorption.
Temkin	$\theta = \dfrac{RT}{\Delta Q} \ln K_0 C_e$	**ΔQ** = (−ΔH) the variation of adsorption energy. **K_0** is the Temkin equilibrium constant.	Assumes that the heat of adsorption of all the molecules in the layer decreases linearly with coverage due to adsorbent–adsorbate interactions, and that the adsorption is characterized by a uniform distribution of the binding energies, up to some maximum binding energy.
Fowler–Guggenheim	$K_{FG} C_e = \dfrac{\theta}{1-\theta} \exp\left(\dfrac{2\theta W}{RT}\right)$	**K_{FG}** : Fowler–Guggenheim equilibrium constant. **W**: is the interaction energy.	Take into account the lateral interaction of the adsorbed molecules.
Hill–de Boer	$K_1 C_e = \dfrac{\theta}{1-\theta} \exp\left(\dfrac{\theta}{1-\theta} - \dfrac{K_2 \theta}{RT}\right)$	**K_1**: Hill–de Boer constant. **K_2**: energetic constant of the interaction between adsorbed molecules.	Describes the case where we have mobile adsorption and lateral interaction among adsorbed molecules.

Table 1.6. (Continuation)

Redlich–Peterson	$q_e = \dfrac{A C_e}{1 + B C_e^{\beta}}$	**A** and **B**: Redlich–Peterson isotherm constants. **β** is an exponent that lies between 0 and 1.	Empirical isotherm incorporating three parameters. It combines elements from both the Langmuir and Freundlich equations, and the mechanism of adsorption is a hybrid and does not follow ideal monolayer adsorption.
Sips	$q_e = \dfrac{q_{m_S} K_S C_e^{m_S}}{1 + K_S C_e^{m_S}}$	**q$_{ms}$**: Sipss maximum adsorption capacity. **K$_S$**: Sips equilibrium constant. **m$_S$** is the Sips model exponent.	Recognizing the problem of the continuing increase in the adsorbed amount with an increase in concentration in the Freundlich equation Sips equeation is proposed with a finite limit when the concentration is sufficiently high.
Jossens	$C_e = \dfrac{q_e}{H} exp\left(F q_e^{P}\right)$	**H**, **F**, and **p**: parameters of the equation of Jossen that depend only of temperature.	Based on a distribution of the energy of interactions adsorbate–adsorbent on adsorption sites. It considers that the activated carbon surface is heterogeneous, with respect to the interactions which it engages with the adsorbate.

q_e : amount of solute adsorbed per unit weight of adsorbent at equilibrium (mg g^{-1})
C_e : equilibrium concentration of the solute in the bulk solution (mg L^{-1}),
q_m : the maximum adsorption capacity (mg g^{-1})

θ: Fractional coverage
R: universal gas constant (kJ mol^{-1} K^{-1})
T: Temperature (K)

1.5.2. Adsorption of inorganic molecules

The major concern in the tertiary process of water treatment is the elimination of metal ions, mainly due to their toxicity and the potential threat to human life and to the environment. Adsorption onto activated carbon, together with ion exchange and reverse osmosis, are the most common processes to remove low concentrations of metals from wastewater or drinking water. Several phenomena are involved in this process: adsorption (physisorption or chemisorption), surface precipitation, ion exchange, and surface complexation. The mechanisms involved and their degree of importance depend on the materials used and the operating conditions [81].

Different studies have shown that during metal ions removal by activated carbon, a decrease in pH is observed as the metal ion concentration decreases. This fact implies the release of hydrogen ions (H^+), indicating that the adsorption is carried out by an ion exchange mechanism, expressed by the following reaction:

$$M^{n+} + R\text{-}OH \rightarrow R\text{-}OM^{n-1} + H^+ \tag{9}$$
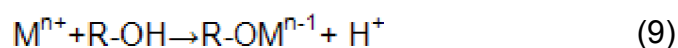
Ion exchange consists of the replacement of an initially adsorbed readily exchangeable ion by another. The involvement of oxygen surface groups in the sorption mechanism by ion exchange was confirmed by an improvement of adsorption metal ions onto oxidized adsorbents [56, 82]. The formation of surface complexes may also happen, depending on the stability of the complex that could be formed between the metal ion and the carbon surface groups [56]. If the cation concentration is high, the surface sites become saturated and the metal begins to precipitate (see Figure 1.14), which involves the formation of a new solid or gel metal hydroxide at the surface. Finally, it is already reported that adsorption by electrostatic attraction may also occurs by interaction between cation (M^{n+}) and the negatively electric charged surface of the activated carbon, without exchange of ions or electrons.
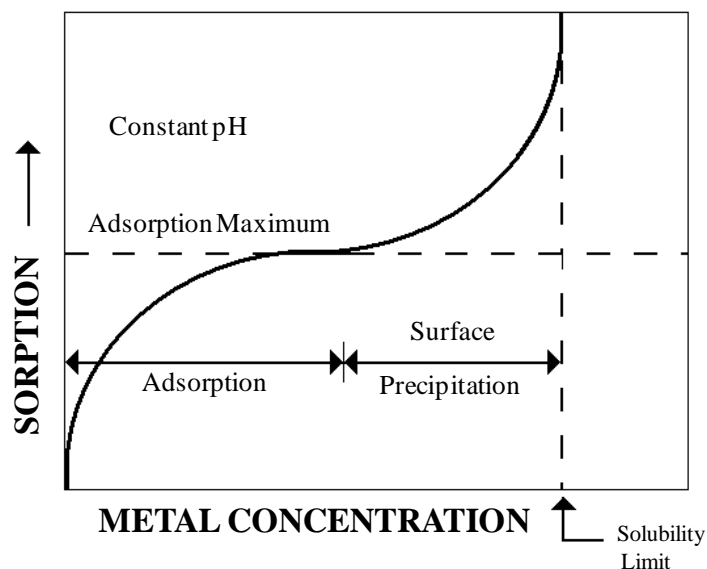
Figure 1.14. Sorption process of metal ions in aqueous solution according to their concentration.

1.5.3. Adsorption of non polar molecules

Organic pollutants are characterized by their hydrophobic character, caused by their lack of dipole that could allow their solvation. As previously mentioned, ionic compounds can be adsorbed by the carbon surface by electrostatic interaction between the ion molecule and the carbon surface groups. However, as organic compounds (non polar) do not exhibit a surface electric charge, their adsorption on carbons is related to hydrophobic / hydrophilic interaction of the adsorbate and carbon surface. Carbonaceous materials can be considered as a combination of basal planes (non polar sites) and unsaturated carbons at the edges of the graphene layers that are frequently combined with other heteroatom-based functional groups (polar sites). As stated in the previous section, the polar surface groups are the responsible of the adsorption of ionic species by electrostatic interactions. On the other hand, the basal planes generate affinity for non polar compounds by hydrophobic interactions. These interactions are based on the incompatibility of the hydrophobic substance to water, that cause the association of

organic molecules with nonpolar environments such as the basal planes of the activated carbon [56]. Two mechanisms have been proposed to explain this behavior [81]: the π-π dispersion interaction mechanism, proposed by Coughlin and Ezra in 1968 [83] and the electron donor-acceptor complexation mechanism proposed by Mattson and coworkers in 1969 [84]. These mechanisms were based on experimental adsorption of different organic compounds such as phenol, benzene and nitrobenzene; however, these mechanisms have been employed to explain the adsorption of other organic molecules.

The π-π interactions are the result of two attraction forces: on one hand, the overlapping of the electron clouds that provides stability to the unpaired electrons of the aromatic systems and, on the other hand, the electrostatic interaction between the negative π electrons and the positive atoms connected by sigma bonds [85]. Coughlin and Ezra studied the adsorption of phenol and nitrobenzene on previously modified carbon, finding that the presence of acidic surface oxygen groups on activated carbon inhibited the adsorption of both organic molecules from aqueous solution. Based on different adsorption experiments, they considered that carboxylic surface groups removed electrons from the π electron systems of the carbon. Since the electrons were removed from the basal plane, π-π interactions became weaker and therefore interfered with the adsorption of organic compounds. These considerations appeared consistent with the concept of dispersion forces between the phenol π electron system and the π band of the graphitic planes of the carbon as responsible for adsorption. Further investigations have confirmed the existence of π-π electron interactions [85-89], and the generation of positive electric charges in the basal plane of the carbon sheets by means of electron delocalization [90, 91], supporting the adsorption mechanism proposed by Coughlin and Ezra.

On the other hand, Mattson and coworkers complemented this mechanism establishing that aromatic compounds can adsorb on carbons by a donor-acceptor complexation mechanism, being the carbonyl group the electron donor and the

aromatic ring of the organic compound the electron acceptor. Once the carbonyl groups are exhausted, the aromatic compounds can be adsorbed on the basal plane of the graphite sheets. This mechanism is restricted by the presence of carboxyl groups since these cannot perform an electron donor complex. Both mechanisms have been confirmed by other researchers under different conditions and also have suggested complementary mechanisms, and it is hoped that future research will totally clarify the adsorption interactions between organic compounds and activated carbon.

1.6. MOTIVATION OF THIS RESEARCH

San Luis Potosi is one of the Mexican states that are certified to produce mescal and significantly contributes to the national production of this alcoholic beverage. Agave bagasse is the main waste produced at mescal distilleries, which causes environmental problems by its inappropriate disposal. Also, due to the absence of specific applications of this residue, most of the agave bagasse is burned under uncontrolled conditions, generating large amounts of ashes and particulate matter that are released to the environment. On the other hand, activated carbon is the most used adsorbent around the world and its production has considerably increased due to more rigorous environmental regulations in the last years. Previous researchers have analyzed the use of lignocellulosic materials as activated carbon precursor, finding that agro-wastes are a promising alternative. Taking into account the commercial significance of activated carbon and in order to take advantage of the organic wastes from the mescal industry in Mexico and more specifically in San Luis Potosi, this project evaluates the production of activated carbon from agave bagasse (Agave *salmiana*), generating therefore a viable alternative for the treatment of this waste and at the same time producing a material of high commercial value.

On the other hand, because activated carbon does not exhibit a high affinity for anionic species in aqueous solution, as a second part of this project, the modification of the previously generated activated carbon is proposed in order to increase their adsorption of anions, particularly arsenic. This contaminant is of high priority around the world due to its high toxicity for human beings. The modification is based on the anchorage of iron oxide nanoparticles onto the activated carbon surface, due to the high affinity between arsenic anions and iron oxides.

1.7. MAIN OBJECTIVE

The purpose of this research is to establish the production conditions to generate activated carbon from agave bagasse by means of chemical activation, characterizing the activation process and determining the influence of the production parameters on the characteristics of the activated carbons generated. Also, this research focuses on developing an easy and inexpensive method to anchor iron oxide nanoparticles onto activated carbon in order to generate an adsorbent with high arsenic adsorption capacity.

1.8. SPECIFIC OBJECTIVES

a) To determine the physical and chemical properties of the agave bagasse.

b) To elucidate the effects of chemical additives on the carbonization process of agave bagasse.

c) To implement a chemical activation process for agave bagasse by using $ZnCl_2$ and H_3PO_4, and to characterize the generated products.

d) To determine the recovery of activating agent after the activation process.

e) To determine the effect of the production conditions onto the surface area and hardness of the generated activated carbons, and to select the production conditions that favor these activated carbon characteristics.

f) To find the production conditions to anchor iron oxide / hydroxide nanoparticles onto three activated carbons with different surface chemistry, by means of the thermal hydrolysis of $FeCl_3$.

g) To elucidate the effect of the anchorage procedure (iron concentration, hydrolysis time and hydrolysis temperature) in the iron content and the arsenic adsorption capacity of the iron modified activated carbons.

h) To determine the physical and chemical properties of the iron modified activated carbon and to evaluate their performance on the arsenic adsorption.

1.9. HYPOTHESIS

It is possible to produce activated carbon with similar characteristics to commercially available activate carbons employing agave bagasse as a precursor. Also, the *in situ* precipitation of iron oxides by thermal hydrolysis is a methodology that allows the anchorage of iron nanoparticles onto graphite layers, without the blockage of their pore structure.

1.10. THESIS STRUCTURE

Chapter 1 of this thesis contains a general review about the production and main characteristics of activated carbon. A brief description of the previous modifications of activated carbons is also included. Finally, a general revision about the adsorption of diverse compounds on activated carbons is presented.

Chapter 2 includes the characterization of agave bagasse and its chemical activation with $ZnCl_2$ and H_3PO_4. Also, the conditions to produce activated carbons with surface area similar to commercial activated carbons are established. Starting from this initial study, the activated carbon production optimization is carried out.

Chapter 3 reports the results of this optimization, including statistical analyses, carbon characterization and the effect of the production parameters on the surface area and hardness of the activated carbons.

Chapter 4 contains the results concerning the modification of activated carbons with iron oxide nanoparticles. This chapter includes a detailed study of the effect of anchoring conditions (hydrolysis time, hydrolysis temperature and iron concentration in the hydrolysis solution) on the iron content and arsenic adsorption capacity, establishing the experimental conditions that favor the removal of arsenic.

The discussion and conclusions of the main results of this work are presented in Chapter 5 and Chapter 6, respectively. Finally, Appendix A contain the results of the in situ characterization of the activation of agave bagasse with $ZnCl_2$ employing an Environmental Scanning Electron Microscope (ESEM). This characterization was carried out with the aim to clarify the processes occurring during this step.

1.11. REFERENCES

[1]   Sircar S, Golden TC, Rao MB. Activated carbon for gas separation and storage. Carbon 1996;34:1-12.

[2]   Mezohegyi G, Gonçalves F, Órfão JJM, Fabregat A, Fortuny A, Font J, Bengoa C, Stuber F. Tailored activated carbons as catalysts in biodecolourisation of textile azo dyes. Applied Catalysis B: Environmental 2010;94:179-85.

[3]   Mezohegyi G, Kolodkin A, Castro UI, Bengoa C, Stuber F, Font J, Fabregat A, Fortuny A. Effective Anaerobic Decolorization of Azo Dye Acid Orange 7 in Continuous Upflow Packed-Bed Reactor Using Biological Activated Carbon System. Ind Eng Chem Res 2007;46:6788-92.

[4]   Carrott PJM. Molecular sieve behaviour of activated carbons. Carbon 1995;33:1307-12.

[5]   Suarez-Ojeda ME, Stüber F, Fortuny A, Fabregat A, Carrera J, Font J. Catalytic wet air oxidation of substituted phenols using activated carbon as catalyst. Applied Catalysis B: Environmental 2005;58:105-14.

[6]   Frackowiak E, Béguin F. Carbon materials for the electrochemical storage of energy in capacitors. Carbon 2001;39:937-50.

[7]   Endo M, Maeda T, Takeda T, Kim YJ, Koshiba K, Hara H, Dresselhaus MS. Capacitance and Pore-Size Distribution in Aqueous and Nonaqueous Electrolytes Using Various Activated Carbon Electrodes. Journal of The Electrochemical Society 2001;148:A910-A4.

[8]   Bandosz TJ, ed. Activated Carbon Surfaces in Environmental Remediation. New York: Elsevier 2006.

[9]   Thrower PA, ed. Chemistry & Physics of Carbon Volume 25 1996.

[10]   Biggs MJ, Buts A, Williamson D. Molecular Simulation Evidence for Solidlike Adsorbate in Complex Carbonaceous Micropore Structures. Langmuir 2004;20:5786-800.

[11]   Peter JFH, et al. Imaging the atomic structure of activated carbon. Journal of Physics: Condensed Matter 2008;20:362201.

[12]   Terzyk, Artur P, Furmaniak, Sylwester, Harris, Peter JF, Gauden, Piotr A, Och, Jerzy, Kowalczyk, Piotr, Rychlicki, Gerhard. How realistic is the pore size distribution calculated from adsorption isotherms if activated carbon is composed of fullerene-like fragments. Cambridge, ROYAUME-UNI: Royal Society of Chemistry 2007.

[13]   Wu Z, Webley PA, Zhao D. Comprehensive Study of Pore Evolution, Mesostructural Stability, and Simultaneous Surface Functionalization of Ordered Mesoporous Carbon (FDU-15) by Wet Oxidation as a Promising Adsorbent. Langmuir 2010;26:10277-86.

[14]   Lillo-Ródenas MA, Cazorla-Amorós D, Linares-Solano A, Béguin F, Clinard C, Rouzaud JN. HRTEM study of activated carbons prepared by alkali hydroxide activation of anthracite. Carbon 2004;42:1305-10.

[15]   Roop Chand Bansal MG. Activated Carbon Asdorption: CRC Press 2005.

[16] Pollard SJT, Fowler GD, Sollars CJ, Perry R. Low-cost adsorbents for waste and wastewater treatment: a review. Sci Total Environ 1992;116:31-52.

[17] World Activated Carbon Freedonia study #2363:Group TF;2008.

[18] Dias JM, Alvim-Ferraz MCM, Almeida MF, Rivera-Utrilla J, Sánchez-Polo M. Waste materials for activated carbon preparation and its use in aqueous-phase treatment: A review. J Environ Manage 2007;85:833-46.

[19] Tequila CRd. Producción total de tequila. 2007 [cited; Available from: http://crtnew.crt.org.mx/index.php?option=com_content&task=view&id=42&Itemid=47&PTT=aja

[20] Mescal. Comite Nacional del Sistema Producto Maguey-Mescal 2006 [cited; Available from: http://www.cnspmm.org/oaxaca.html

[21] Aguirre Rivera JR, Flores Flores JL, ed. El maguey mezcalero potosino. 1a Edición ed. San Luis Potosi, México: Editorial Universitaria Potosina 2001.

[22] Idarraga G, Ramos J, Zuniga V, Sahin T, Young RA. Pulp and Paper from Blue Agave Waste from Tequila Production. Journal of Agricultural and Food Chemistry 1999;47:4450-5.

[23] González Baena A. Aprovechamiento del Bagazo de Maguey Verde *(Agave salmiana*) de la Agroindustria del Mezcal en San Luís Potosí para la Producción de Hongo Ostra (*Pleurotus ostreatus*). M.S. Thesis San Luís Potosí: Instituto Potosino de Investigación Científica y Tecnoógica; 2005.

[24] Iniguez-Covarrubias G, Lange SE, Rowell RM. Utilization of byproducts from the tequila industry: part 1: agave bagasse as a raw material for animal feeding and fiberboard production. Bioresour Technol 2001;77:25-32.

[25] Tsai W, Chang C, Lee S, Wang S. Thermogravimetric Analysis of Corn Cob Impregnated With Zinc Chloride for Preparation of Activated Carbon. J Therm Anal Calorim 2000;63:351-7.

[26] Hussein MZB, Rahman MBBA, Yahaya AHJ, Hin T-YY, Ahmad N. Oil Palm Trunk as a Raw Material for Activated Carbon Production. J Porous Mat 2001;8:327-34.

[27] Rodriguez-Reinoso F, Molina-Sabio M. Activated carbons from lignocellulosic materials by chemical and/or physical activation: an overview. Carbon 1992;30:1111-8.

[28] Varhegyi G, Antal MJ, Szekely T, Till F, Jakab E, Szabo P. Simultaneous thermogravimetric-mass spectrometric studies of the thermal decomposition of biopolymers. 2. Sugarcane bagasse in the presence and absence of catalysts. Energy Fuels 1988;2:273-7.

[29] Varhegyi G, Antal MJ, Szekely T, Szabo P. Kinetics of the thermal decomposition of cellulose, hemicellulose, and sugarcane bagasse. Energy Fuels 1989;3:329-35.

[30] Bruice PY. Organic chemistry. 6th ed. Boston: Prentice Hall 2001.

[31] Caturla F, Molina-Sabio M, Rodríguez-Reinoso F. Preparation of activated carbon by chemical activation with $ZnCl_2$. Carbon 1991;29:999-1007.

[32] Molina-Sabio M, Rodríguez-Reinoso F. Role of chemical activation in the development of carbon porosity. Colloid Surf A-Physicochem Eng Asp 2004;241:15-25.

[33] Villar-Rodil S, Denoyel R, Rouquerol J, Martínez-Alonso A, Tascón JMD. Porous Texture Evolution in Nomex-Derived Activated Carbon Fibers. Journal of Colloid and Interface Science 2002;252:169-76.

[34] Jagtoyen M, Thwaites M, Stencel J, McEnaney B, Derbyshire F. Adsorbent carbon synthesis from coals by phosphoric acid activation. Carbon 1992;30:1089-96.

[35] Jagtoyen M, Derbyshire F. Some considerations of the origins of porosity in carbons from chemically activated wood. Carbon 1993;31:1185-92.

[36] Solum MS, Pugmire RJ, Jagtoyen M, Derbyshire F. Evolution of carbon structure in chemically activated wood. Carbon 1995;33:1247-54.

[37] Jagtoyen M, Derbyshire F. Activated carbons from yellow poplar and white oak by H_3PO_4 activation. Carbon 1998;36:1085-97.

[38] Radovic LR, ed. Chemistry and Physics of Carbon Volume 30. Pennsylvania: CRC Press, Taylor & Francis Group, 2008.

[39] Lillo-Ródenas MA, Juan-Juan J, Cazorla-Amorós D, Linares-Solano A. About reactions occurring during chemical activation with hydroxides. Carbon 2004;42:1371-5.

[40] Lillo-Rodenas MA, Cazorla-Amoros D, Linares-Solano A. Understanding chemical reactions between carbons and NaOH and KOH: An insight into the chemical activation mechanism. Carbon 2003;41:267-75.

[41] Román S, González JF, González-García CM, Zamora F. Control of pore development during CO_2 and steam activation of olive stones. Fuel Processing Technology 2008;89:715-20.

[42] Molina-Sabio M, Gonzalez MT, Rodriguez-Reinoso F, Sepúlveda-Escribano A. Effect of steam and carbon dioxide activation in the micropore size distribution of activated carbon. Carbon 1996;34:505-9.

[43] Rodríguez-Reinoso F, Molina-Sabio M, González MT. The use of steam and CO_2 as activating agents in the preparation of activated carbons. Carbon 1995;33:15-23.

[44] Samaras P, Diamadopoulos E, Sakellaropoulos GP. The effect of demineralization on lignite activation. Carbon 1991;29:1181-90.

[45] Samaras P, Diamadopoulos E, Sakellaropoulos GP. Acid treatment of lignite and its effect on activation. Carbon 1994;32:771-6.

[46] Samaras P, Diamadopoulos E, Sakellaropoulos GP. The effect of mineral matter and pyrolysis conditions on the gasification of Greek lignite by carbon dioxide. Fuel 1996;75:1108-14.

[47] Cooney DO. Adsorption design for wastewater treatment. Boca Raton, Fl: Lewis Publishers 1999.

[48] Brunauer S, Emmett PH, Teller E. Adsorption of Gases in Multimolecular Layers. J Am Chem Soc 1938;60:309-19.

[49] Gregg SJ, K.S.W. Adsorption, Surface Area and Porosity. Second Edition ed. London: Academic Press 1982.

[50] Yin CY, Aroua MK, Daud WMAW. Review of modifications of activated carbon for enhancing contaminant uptakes from aqueous solutions. Sep Purif Technol 2007;52:403-15.

[51] Moreno-castilla C, Carrasco-marín F, Maldonado-hódar FJ, Rivera-utrilla J. Effects of non-oxidant and oxidant acid treatments on the surface properties of an activated carbon with very low ash content. Carbon 1998;36:145-51.

[52] Moreno-Castilla C, Ferro-Garcia MA, Joly JP, Bautista-Toledo I, Carrasco-Marin F, Rivera-Utrilla J. Activated Carbon Surface Modifications by Nitric Acid, Hydrogen Peroxide, and Ammonium Peroxydisulfate Treatments. Langmuir 1995;11:4386-92.

[53] Radovic LR, Silva IF, Ume JI, Menéndez JA, Leon CALY, Scaroni AW. An experimental and theoretical study of the adsorption of aromatics possessing electron-withdrawing and electron-donating functional groups by chemically modified activated carbons. Carbon 1997;35:1339-48.

[54] Monser L, Adhoum N. Modified activated carbon for the removal of copper, zinc, chromium and cyanide from wastewater. Sep Purif Technol 2002;26:137-46.

[55] Varadarajan R, Mario RS, Badri NB, Massoud P. Modeling the sorption of toxic metals on chelant-impregnated adsorbent. AIChE Journal 1999;45:1135-46.

[56] Aquatic chemistry chemical equilibria and rates in natural waters.New York:Stumm W, Morgan JJ, NetLibrary Inc.;1996.

[57] Chen JP, Wu S, Chong K-H. Surface modification of a granular activated carbon by citric acid for enhancement of copper adsorption. Carbon 2003;41:1979-86.

[58] Jean-Pierre Jolivet MH, Jacques Livage, Eric Bescher. Metal Oxide Chemistry and Synthesis, From Solution to Solid State. West Sussex: John Wiley and Sons Ltd 2000.

[59] Petit C, Bandosz TJ. Role of surface heterogeneity in the removal of ammonia from air on micro/mesoporous activated carbons modified with molybdenum and tungtsen oxides. Microporous Mesoporous Mat 2009;118:61-7.

[60] Bandosz TJ, Petit C. On the reactive adsorption of ammonia on activated carbons modified by impregnation with inorganic compounds. Journal of Colloid and Interface Science 2009;338:329-45.

[61] Seredych M, Bandosz TJ. Graphite oxide/AlZr polycation composites: Surface characterization and performance as adsorbents of ammonia. Materials Chemistry and Physics 2009;117:99-106.

[62] Petit C, Bandosz TJ. Complexity of ammonia interactions on activated carbons modified with V_2O_5. Journal of Colloid and Interface Science 2008;325:301-8.

[63] Petit C, Bandosz TJ. Activated carbons modified with aluminium-zirconium polycations as adsorbents for ammonia. Microporous Mesoporous Mat 2008;114:137-47.

[64] Gu Z, Fang J, Deng B. Preparation and Evaluation of GAC-Based Iron-Containing Adsorbents for Arsenic Removal. Environmental Science & Technology 2005;39:3833-43.

[65] Chen W, Parette R, Zou J, Cannon FS, Dempsey BA. Arsenic removal by iron-modified activated carbon. Water Res 2007;41:1851-8.

[66] Zhang QL, Lin YC, Chen X, Gao NY. A method for preparing ferric activated carbon composites adsorbents to remove arsenic from drinking water. J Hazard Mater 2007;148:671-8.

[67] Jang M, Chen W, Cannon FS. Preloading Hydrous Ferric Oxide into Granular Activated Carbon for Arsenic Removal. Environmental Science & Technology 2008;42:3369-74.

[68] Ramos RL, Ovalle-Turrubiartes J, Sanchez-Castillo MA. Adsorption of fluoride from aqueous solution on aluminum-impregnated carbon. Carbon 1999;37:609-17.

[69] Dastgheib SA, Karanfil T, Cheng W. Tailoring activated carbons for enhanced removal of natural organic matter from natural waters. Carbon 2004;42:547-57.

[70] Gao Y-M, Sengupta AK, Simpson D. A new hybrid inorganic sorbent for heavy metals removal. Water Res 1995;29:2195-205.

[71] Suzuki TM, Bomani JO, Matsunaga H, Yokoyama T. Preparation of porous resin loaded with crystalline hydrous zirconium oxide and its application to the removal of arsenic. Reactive and Functional Polymers 2000;43:165-72.

[72] Dutta PK, Ray AK, Sharma VK, Millero FJ. Adsorption of arsenate and arsenite on titanium dioxide suspensions. Journal of Colloid and Interface Science 2004;278:270-5.

[73] Pierce ML, Moore CB. Adsorption of arsenite and arsenate on amorphous iron hydroxide. Water Res 1982;16:1247-53.

[74] Manning BA, Fendorf SE, Goldberg S. Surface Structures and Stability of Arsenic(III) on Goethite: Spectroscopic Evidence for Inner-Sphere Complexes. Environmental Science & Technology 1998;32:2383-8.

[75] Liu Z, Zhang F-S, Sasai R. Arsenate removal from water using Fe_3O_4-loaded activated carbon prepared from waste biomass. Chemical Engineering Journal;160:57-62.

[76] Fierro V, Muñiz G, Gonzalez-Sánchez G, Ballinas ML, Celzard A. Arsenic removal by iron-doped activated carbons prepared by ferric chloride forced hydrolysis. J Hazard Mater 2009;168:430-7.

[77] Hristovski KD, Westerhoff PK, Möller T, Sylvester P. Effect of synthesis conditions on nano-iron (hydr)oxide impregnated granulated activated carbon. Chemical Engineering Journal 2009;146:237-43.

[78] Zhu H, Jia Y, Wu X, Wang H. Removal of arsenic from water by supported nano zero-valent iron on activated carbon. J Hazard Mater 2009;172:1591-6.

[79] Gu Z, Deng B, Yang J. Synthesis and evaluation of iron-containing ordered mesoporous carbon (FeOMC) for arsenic adsorption. Microporous Mesoporous Mat 2007;102:265-73.

[80] Hamdaoui O, Naffrechoux E. Modeling of adsorption isotherms of phenol and chlorophenols onto granular activated carbon: Part II. Models with more than two parameters. J Hazard Mater 2007;147:401-11.

[81] Bottani EJ, Tascón JMD. Adsorption by carbons. Amsterdam ; London: Elsevier 2008.

[82] Jia YF, Thomas KM. Adsorption of Cadmium Ions on Oxygen Surface Sites in Activated Carbon. Langmuir 1999;16:1114-22.

[83] Coughlin RW, Ezra FS. Role of surface acidity in the adsorption of organic pollutants on the surface of carbon. Environmental Science & Technology 1968;2:291-7.

[84] Mattson JA, Mark HB, Malbin MD, Weber WJ, Crittenden JC. Surface chemistry of active carbon: Specific adsorption of phenols. Journal of Colloid and Interface Science 1969;31:116-30.

[85] Hunter CA, Sanders JKM. The nature of π-π interactions. Journal of the American Chemical Society 1990;112:5525-34.

[86] Gleiter R, Schaefer W. Interactions between nonconjugated .pi.-systems. Accounts of Chemical Research 1990;23:369-75.

[87] Lambert JB, Clikeman RR, Magyar ES. Conformational interactions of .pi. electrons. Journal of the American Chemical Society 1974;96:2265-7.

[88] Headen TF, Howard CA, Skipper NT, Wilkinson MA, Bowron DT, Soper AK. Structure of π-π Interactions in Aromatic Liquids. Journal of the American Chemical Society 2010;132:5735-42.

[89] Neusser HJ, Krause H. Binding Energy and Structure of van der Waals Complexes of Benzene. Chemical Reviews 1994;94:1829-43.

[90] Leon y Leon CA, Solar JM, Calemma V, Radovic LR. Evidence for the protonation of basal plane sites on carbon. Carbon 1992;30:797-811.

[91] Lopez-Ramon MV, Stoeckli F, Moreno-Castilla C, Carrasco-Marin F. On the characterization of acidic and basic surface sites on carbons by various techniques. Carbon 1999;37:1215-21.

"Wastes are the raw materials of the future"

CHAPTER 2

AGAVE SALMIANA BAGASSE AS A PRECURSOR TO PRODUCE HIGHLY MICROPOROUS ACTIVATED CARBONS

This work is aimed to employ agave bagasse, a waste from tequila and mescal industries, to obtain a product of high commercial value such as activated carbon. The activated carbon production methodology was based on a chemical activation, by using $ZnCl_2$ and H_3PO_4 as activating agent and agave bagasse as a natural source of carbon. The activation temperature (150–450 °C), activation time (0-60 min) and weight ratio of activating agent to precursor (0.2–4) were studied. The produced carbon materials were characterized by scanning electron microscopy (SEM), thermogravimetric analysis (TGA) and surface area and porosity measurements by nitrogen physisorption at -196 °C. In addition, the activating agent recovery was evaluated. We were able to obtain highly microporous activated carbons with micropore volumes between 0.24 and 1.20 cm^3/g and a surface area within 300 and 2139 m^2/g. These results demonstrated the feasibility to treat the industrial wastes of the tequila and mescal industries, being this wastes an excellent precursor to produce highly microporous activated carbons (pore diameter<2nm) that can be processed at low activation temperatures in short times, with the possibility of recycling the activating agent.

2.1. INTRODUCTION

One of the most traditional industries in Mexico is dedicated to the production of distilled beverages such as tequila and mescal. The raw material employed to produce these beverages is the agave plant, which is a succulent plant of a large botanical genus of the same name, belonging to the Agavaceae family. Basically the agave plant has two main parts: long spiked leaves and the "head" or also called "piña" by its similarity to a pineapple after the leaves are cut off. At the distillery, the agave heads are split and placed in a large oven made of stainless steel, brick or stone. This cooking step partially hydrolyzes the polymers present in the plant. Subsequently, the agave heads are shredded and compressed in roll mills to extract the hydrolyzed sugars, which are then fermented with assistance of selected yeast. During fermentation, the sugars are converted into alcohol. Finally, the fermented juices are concentrated and purified through the distillation process in order to obtain the alcoholic beverages known as tequila or mescal. The main difference between these two beverages is the agave plant from which they are obtained: agave *azul tequilana weber* for tequila production and agave *angustifolia haw*, agave *esperrima jacobi,* agave *weberi cela,* agave *patatorum zucc*, and *agave salmiana otto* for mescal production [1, 2].

The national production of tequila and mescal in 2008 was around 181 million litters [3, 4]. This production implies the generation of large amounts of agave bagasse in the distilleries, being this waste an environmental problem. According with the national production of tequila and mescal of 2008, the quantity of agave bagasse arise to 350,000 tons on dry basis [5].

Recently, researchers have found some uses for this waste that include paper precursor [6], as raw material for animal feeding [7] and also in the production of oyster mushroom (*Pleurotus Ostreatus*) [8]. However, these products do not have

an important demand and most of this waste is burned under uncontrolled conditions, generating large amounts of ash and particulated matter which are released into the environment.

On the other hand, activated carbon is the most widely used material in adsorption processes. Its properties such as surface area, pore size distribution and adsorption capacity make this material a unique adsorbent that can be used to treat effluents in both liquid and gas phase. The demand of activated carbon world wide was 890 500 metric tons in 2007, and it is prospected to raise about 5.2 % per year through 2012 to achieve consumption levels of 1.15 millions of metric tons [9]. In order to fulfill this demand, a variety of raw materials have been used; for example coals (lignite, bituminous and anthracites), wood, coconut shell and peat [10]. However, various investigations have concentrated on testing new raw materials to produce activated carbon, mainly agricultural byproducts such as fruit stones [11], seeds hulls (cottonseed, peanut, sunflower, soybean, faba bean, lupine) [12], straw and stalks (corn, rice, cotton, wheat) [13], wastes of wood industry [14] and other low-cost lignocelluloses materials that offer inexpensive source of carbons.

Knowing the commercial significance of activated carbon worldwide and taking into account the large quantity of agave bagasse that is generated in Mexico, this research was focused on evaluating the feasibility of using agave bagasse to produce low cost activated carbon, which in turn also contributes to solve environmental problems at distilleries.

There are a wide variety of approaches that can be used to evaluate a new material as a precursor to produce activated carbon. In general the production of activated carbon can be carried out by chemical activation or physical activation. Chemical activation is of our interest because only involves one thermal step at lower temperature when compared to the physical activation and allows better control of the pore size distribution on the carbonaceous precursors [15]. The selected activating agents to evaluate the production of activated carbon were

$ZnCl_2$ and H_3PO_4, because these chemicals can be used at low temperature, avoiding their chemical decomposition that allows their reusability during the activation process.

2.2. MATERIALS AND METHODS

The agave bagasse used in this study was collected from the distillery "Ipiña" located in San Luis Potosi, Mexico. The agave bagasse was composed of *Agave salmiana* plants. This material was sun dried previous to its storage. The inorganic content of the activated carbon samples and the raw material was determined as follow: a representative sample was burned in a furnace operating at 650 ºC for 4 h in the presence of air: the ash content was calculated from the residue. Prior to the activation, the agave bagasse was fractioned employing garden shears in order to obtain fibers of less than 1 cm long. After that, the fibers were dried at 110 ºC for 24 hours. The methodology to transform this material into activated carbon was by chemical activation; H_3PO_4 (98%, Fermont ACS grade) and $ZnCl_2$ (97%, Fermont ACS grade) were used as activating agents. Air-dried agave bagasse (10 g) was mixed in a beaker with 50 mL of H_3PO_4 or $ZnCl_2$ solution of adequate concentrations. The mixing was performed at room temperature (25 °C) for 12 hours. The mixture was then heated up to 60 ºC until the material had dried. The impregnated bagasse (200 mg) was activated using a thermo gravimetric analyzer (Thermo VersaTherm High Sensitivity) as a furnace, under a nitrogen atmosphere (min. purity 99.999%, Praxair). The heating rate was 10 ºC/min and the nitrogen flow was set to 20 cm^3/min. Different materials were obtained by varying the weight ratios (R) between activating agent and agave bagasse, from 0.2 to 4 (R=weight of activating agent/weight of dry bagasse); the activation temperature (T) ranged from 150 ºC to 450 ºC; and the activation time (t) from 0 to 60 minutes. After activation, the carbon materials were rinsed with 0.01 M HCl in order to remove the excess of the activating agent, and then distilled water was used to reach neutral pH. The recovery of the activating agent was evaluated by measuring the concentration of

Zn and P in the rinse water. Zn content was measured by atomic absorption spetrophotometry (PerkinElmer AAnalyst 400 at a wavelength of 213.86 nm). Total phosphorus was determined in the rinse water by the ascorbic acid colorimetric method [16] as follow: 10 mL of the rinse solution (pH=2) was mixed with 1.6 mL of the combined reagent. After at least 10 min but no more than 30 min, measure absorbance of each sample at 880 nm, using reagent blank as the reference solution. Calibration curve was made by dilution with distilled water of stock phosphate solution (99.0%, Fermont ACS grade). 10 mL of distilled water with 1.6 mL of combined reagent was employed as blank. 100 mL of the combined reagent solution is composed by 50 mL of 5N H_2SO_4 (98%, J.T. Baker ACS grade); 5 mL of antimony potassium tartrate solution: 2.6 g $C_8H_4K_2O_{12}Sb_2 \bullet 3H_2O$ (99.0%, Fermont ACS grade) diluted to 500-mL in distilled water; 15 mL ammonium molybdate solution: 20 g of $(NH_4)_6Mo_7O_{24} \cdot 4H_2O$ (83.0%, Fermont ACS grade) diluted to 500-mL in distilled water; and 30 mL ascorbic acid solution: 1.76 g ascorbic acid (99.0%, Fermont ACS grade) in 100 mL distilled water. The BET (Brunauer-Emmett-Teller) surface area was determined by N_2 physisorption at -196 °C by ASAP 2020 equipment (Micromeritics Instrument Corporation) and the pore volume was calculated from the DFT method. Elemental analysis of samples (carbon, hydrogen and nitrogen) was carried out by using an ECS costech analyzer model 4010. Finally, the natural and carbonized materials were characterized by Scanning Electron Microscopy (SEM, FEIXL30 field emission gun) without applying any metal coating.

2.3. RESULTS AND DISCUSSION

2.3.1. Agave bagasse characterization

In order to consider a raw material as a precursor to produce activated carbon it must possess certain characteristics, for example: low cost, availability, high carbon content, minimum presence of inorganics and the existence of natural porosity [17]. As stated above, the agave bagasse is a waste from the tequila and

mescal industry, and does not have any commercial use. Table 2.1 shows the elemental analysis of agave bagasse. Also, the chemical properties of materials often used to produce activated carbon are included.

Table 2.1. **Elemental analyses and ash content of some activated carbon precursors.**

Material	C (%)	H (%)	N (%)	Ash (%)
Agave bagasse	45	5.9	0.3	6.5
Sugar cane bagasse [18]	45.5	5.0	0.1	10.5
Coconut shell[18]	52.8	5	0.08	3.1
Coconut coir[18]	93.9	0.7	-	3.1
Pine wood[18]	48.0	6.4	0.01	0.4
Bituminous carbon [18]	80.2	6.04	1.51	11.5
Corn cobs[18]	46.3	5.6	0.57	5.3
Rice straw[18]	41.8	4.6	0.7	13.4

The ash content is an important parameter since it is related to the dissolution of these salts when the activated carbon is used, thus generating polluting problems in the stream to be treated. Therefore, low ash content in activated carbons is desired. Table 2.1 shows the ash content of agave bagasse and other activated carbon precursors. The analyses indicated that the agave bagasse had only 6.5 % of inorganic content, and the activated carbons produced from this precursor were almost ash free. This was because the washing step after the activation process removed the salts presented in the precursor. The ash content of the agave bagasse is within the same range found in other precursors. On the other hand, the carbon content of the activated carbon precursors mostly used worldwide range from 40 to 90 %. In comparison, the agave bagasse has 45 % of carbon, which is an acceptable value.
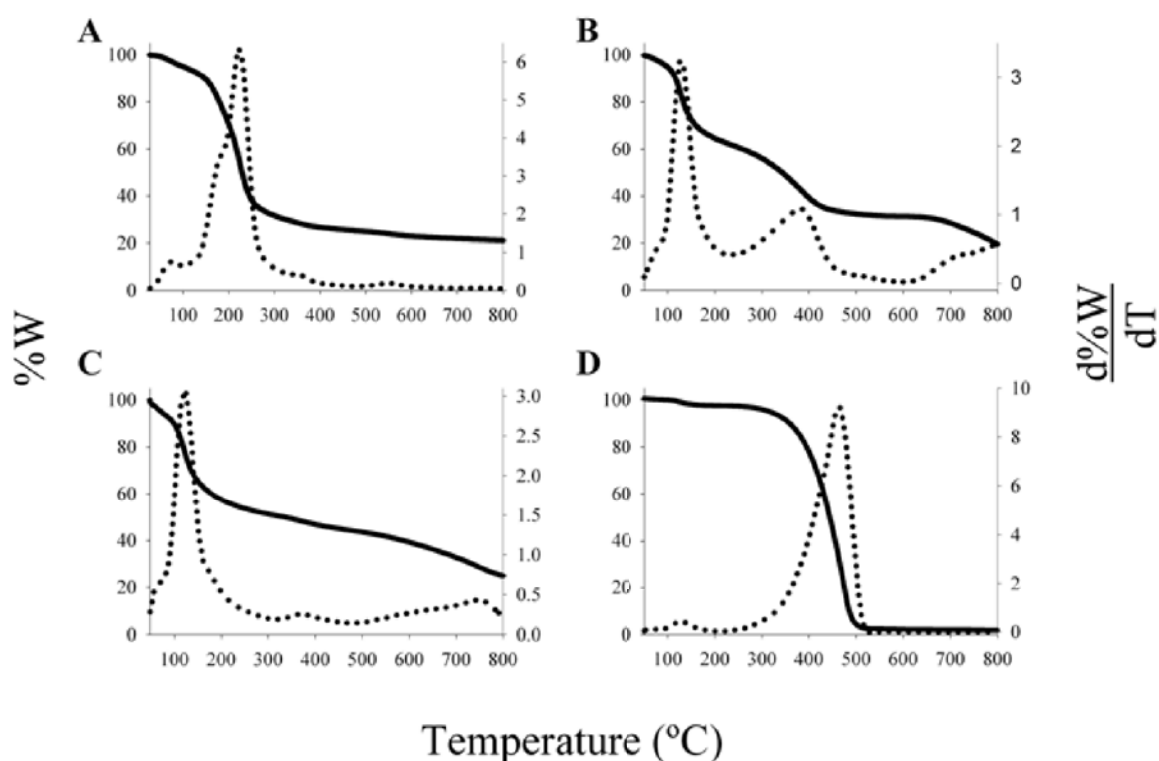
Figure 2.1. Thermogravimetric (TG, solid line) and differential thermogravimetric analysis (DTG, doted line) of raw and impregnated agave bagasse. A: natural agave bagasse. B: $ZnCl_2$ Impregnated agave bagasse (R=0.8). C: H_3PO_4 Impregnated agave bagasse (R=0.8). D: $ZnCl_2$ salt.

Thermogravimetric analysis (TGA) was used to monitor the carbonization and activation process. Figure 2.1 shows the weight loss (TG) and weight loss rate (DTG) curves of four samples: raw agave bagasse, H_3PO_4 impregnated agave bagasse, $ZnCl_2$ impregnated agave bagasse and $ZnCl_2$ salt. Figure 2.1A shows a multiple stage thermal degradation of agave bagasse. The main composition of agave bagasse is a mixture of cellulose, hemicellulose, lignin, organic extractives and inorganic minerals [10]. Previous studies of thermal degradation of lignocellulosic materials have shown that the thermal decomposition of biomass is a complex network of reactions and hence the response could include the superposition of the decomposition behavior of its individual components [10, 19]. In general, the lignin components undergoes a slow process of degradation, while

cellulose and hemicelluloses are the components that decompose in a primary stage under a complex depolymerization mechanism evolving dehydration, cyclization, condensation, and heterolytic cleavage reactions [20]. Figure 2.1A shows two stages of thermal decomposition of agave bagasse: weight loss from 70 ºC to 150 ºC that can be attributed to moisture released and to the evaporation of some volatiles; after that a significant weight loss of around 60 % of the mass from 180 ºC to 300 ºC. Above 300 ºC the weight decreased slowly, regardless of the temperature. The DTG curve (Figure 2.1A) showed two peaks, the first peak located at 85 ºC, corresponds to a moisture release process. The second peak at 231 ºC presents a shoulder around 180 ºC corresponding to the biopolymer gasification. Similar trend is reported for lignocelluloses materials, but at minor temperatures. For example, the DTG profile of sugar cane bagasse shows maximum peaks at 281 ºC and 336 ºC; corn cobs at 310 ºC and 370 ºC and coconut shell at 298 ºC and 368 ºC, all of them obtained with a heating rate of 10 ºC/min, and under nitrogen atmosphere [20-22]. According to these data, the thermal degradation of agave bagasse begins at lower temperature than similar lignocelluloses materials. This phenomenon can be attributed to the heating step of the agave head in the tequila and mescal distilleries. This thermal treatment starts to break down the biopolymers in the agave bagasse, transforming the complex arrangement into more labile structures and hence the thermal degradation of the pre-cooked bagasse can happen at lower temperatures. This property of the agave bagasse can be an advantage because if the thermal reactions start at moderate temperatures, the activation process can be conducted at lower temperatures, thus decreasing the operation cost. Figure 2.1B shows the TG-DTG curves of impregnated bagasse with $ZnCl_2$ (R=0.8). These data showed a decrease of the temperature at which the sample began to lose weight, the major peak appeared at 129 ºC, 100 ºC less than the raw agave bagasse. According to previous reports, this weight loss is mainly attributed to H_2O emission, coming from different kinds of reactions catalyzed by the activating agent [19, 20, 23].
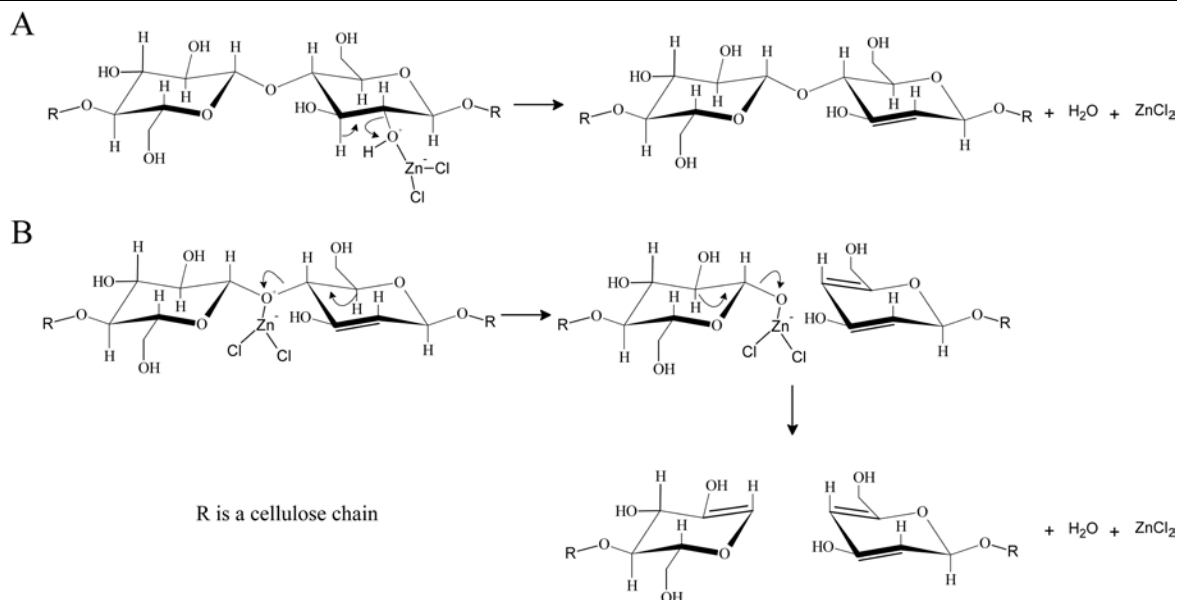
Figure 2.2. Hypothetical reactions of cellulose monomer and $ZnCl_2$ that promote the H_2O formation in the early stages of the activation. Zinc chloride acts as Lewis acid, making chemical complexes with oxygen of the biopolymer to eliminate hydroxyl groups (A) or promoting the bond cleavage of the biopolymer (B).

In the early stages of the chemical activation of lignocellulosic materials with $ZnCl_2$, the activating agent can act as a dehydrating agent, thus catalyzing the cleavage of hydroxyl groups presents in the biopolymer, promoting the formation of double bonds inside the biopolymer chain (Figure 2.2A), and also the biopolymer cleavage (Figure 2.2B), which starts to form the solid carbonaceous structure.

The second stage of the weight-loss can be attributed to carbon gasification, coming from labile carbon in the new carbonized structure. Some authors correlate this second stage, presented on the thermal treatment of $ZnCl_2$ impregnated samples, to volatilization of $ZnCl_2$ itself [21, 24]. This assumption can be confirmed with the TG results of pure $ZnCl_2$ that appear in Figure 2.1D, since it begins to lose weight around the same temperature of the second weight loss of the impregnated sample. The way in which the $ZnCl_2$ loss weight above 300 °C could be attributed to a gradually mass transfer of the molten salt by the carrier gas, since the melting point of $ZnCl_2$ is 290 ºC.

Finally, the TG-DTG responses of impregnated agave bagasse with H_3PO_4 (R=0.8), Figure 2.1C, showed also a reduction in the temperature at which the weight loss began compared with raw agave bagasse. The major peak appeared at 124 ºC, as in the $ZnCl_2$ impregnated samples; this stage consists in H_2O elimination catalyzed by H_3PO_4. Some pathways have been proposed about the reaction mechanisms that follow the phosphoric acid in the activation of biopolymers [25-27], similar to the developed reactions when $ZnCl_2$ is used (Figure 2.2).
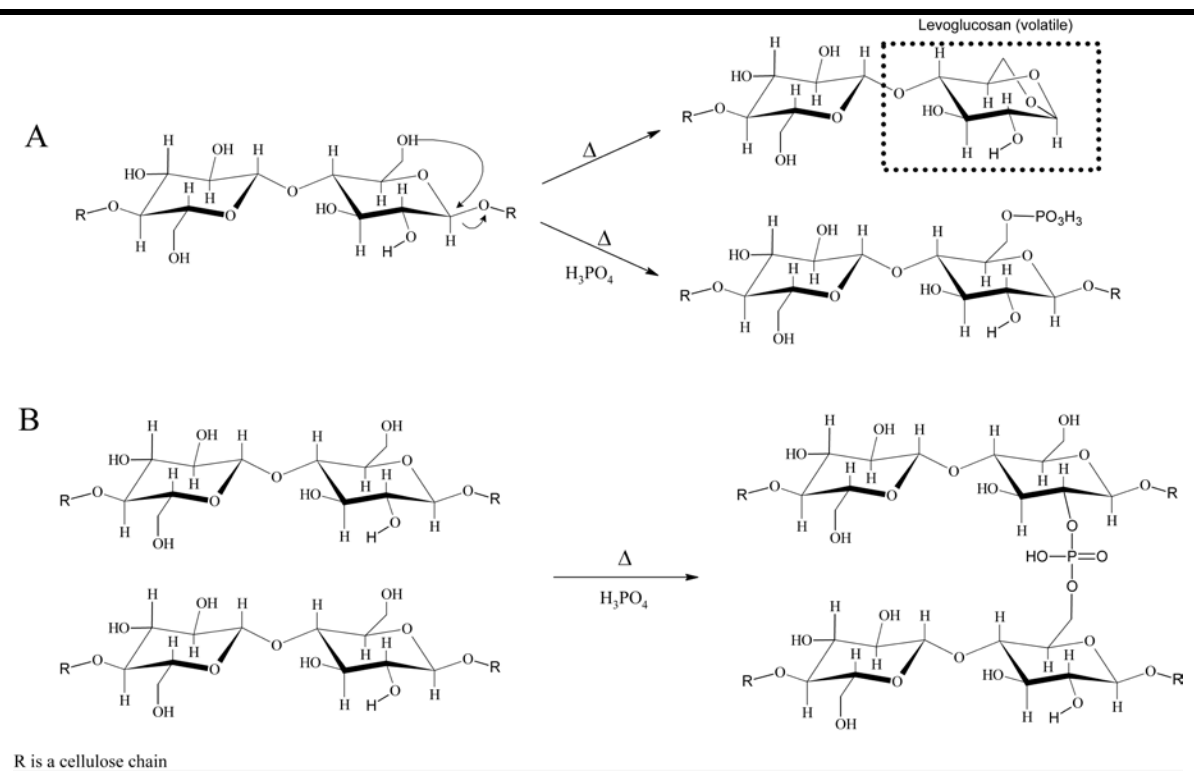
Figure 2.3. Reactions of cellulose monomer and H_3PO_4. The phosphoric acid has the capacity to form phosphate linkages between biopolymer chains (A), stables at temperatures below 450 ºC. Also the phosphoric acid can avoid the formation of volatile species such as levoglucosan, producing a slow weight loss of material (B).

However, H_3PO_4 in contrast with $ZnCl_2$, can perform phosphate linkages, such as polyphosphates esters (Figure 2.3A), that can serve to connect the biopolymer fragments. The formation of ester linkages with hydroxyl groups of the biopolymer stabilizes the structure, and also the phosphoric acid can serve as inhibitor of the formation of levoglucosan (Figure 2.3B). The levoglucosan formation is related with the route to the degradation of cellulose through its decomposition to volatile products. In this way, blocking the formation of levoglucosan by phosphoric acid, it helps to avoid the rapid gasification of the carbon structure [26, 28, 29]. This effect can be seen in Figure 2.1C, where a slowly weight loss can be observed at a temperature higher than 250 ºC. On the other hand, the formation of phosphate esters in the carbon structures can have negative consequences as far as the recovery of activating agent is concern, since this kind of structures are stable until 450 ºC [26].

Scanning electron microscope was used to obtain information about the morphology of the natural and carbonized agave bagasse. The natural bagasse does not exhibit any particular pore structure (Figure 2.4A). Samples of bagasse were carbonized in N_2 atmosphere at different temperatures (180-450 ºC) to explore the development of porosity: carbonized samples at temperature about 240 °C revealed an arrangement of parallel channels from tip to tip of the fiber (see Figure 2.4B and 2.4C). The diameter of these channels ranged between 10 and 20 μm, and the thickness of the walls from 3 to 5 μm. The formation of these structures are related to the natural physiology of the agave bagasse fiber, which are constituted by elongated cells, composed by layers with different proportions of lignin, cellulose and hemicelluloses. According with the structure formed, it is expected that the central part of the fiber were composed by labile materials such as cellulose. A deep characterization and discussion about the formation of these structures during the carbonization of agave bagasse fibers are reported in Appendix A.
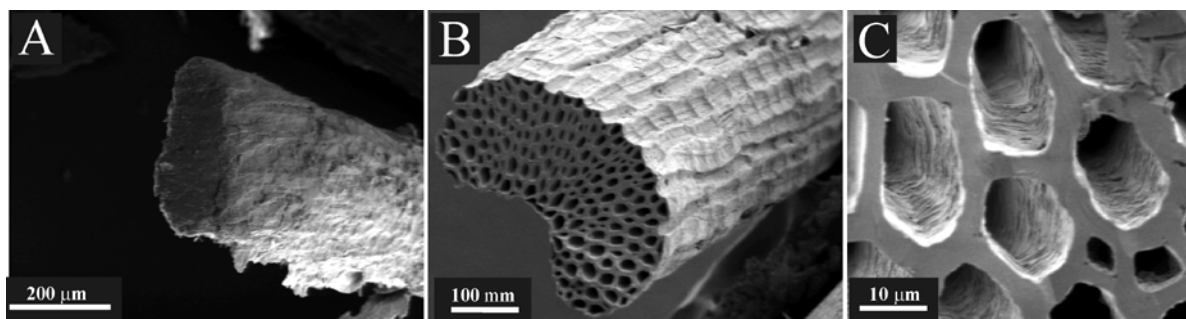
Figure 2.4. SEM images of raw (A) and carbonized (B and C) agave bagasse.

2.3.2. Activated carbon production

A large number of parameters can influence the activated carbon characteristics, being the concentration of activated agent, the activation temperature and the activation time the most influencing parameters. Activated carbon is widely used in different kind of systems, the majority of these are associated with adsorption processes. The adsorption process involves the accommodation of the adsorbate on the surface of the activated carbon. Because of this, the surface area and the number of surface groups in the activated carbon can be considered as the principal characteristics that contribute to increase the ability of carbon to adsorb some specific molecules. Taking into account the importance of the surface area in the adsorption properties of an activated carbon, the objective of the following section is to study the effect of each production parameter on surface area, in order to establish the production conditions that develop the highest surface area.
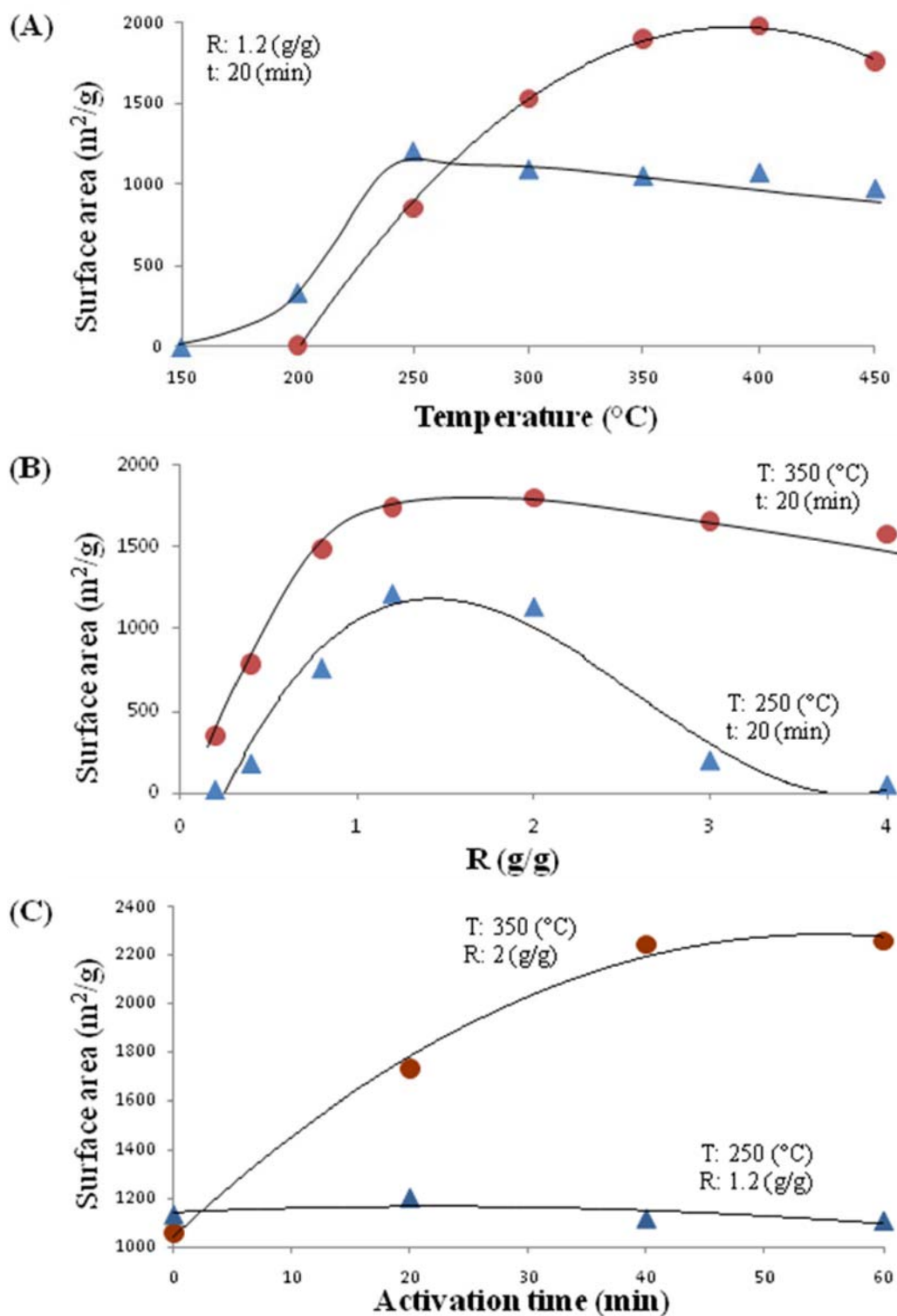
Figure 2.5. Effect of activation temperature (A), activating agent concentration (B) and activation time (C) on surface area of activated carbon developed by using $ZnCl_2$ (●) and H_3PO_4 (▲).

2.3.2.1. Activation temperature

When a precursor is impregnated with $ZnCl_2$ or H_3PO_4, its thermal degradation is accelerated. Moreover, the chemical pathways modify the carbon arrangement, thus developing a porous structure and hence a higher surface area. In this way, the activation temperature is correlated with the activation energy needed to begin the reactions, and this energy depends on the activating agent employed. This effect can be visualized in Figure 2.5A in which the developed surface area in the activated carbon is reported as function of the activation temperature for both activating agents used. In this research H_3PO_4 impregnated bagasse began to develop considerable surface area at temperatures higher than 200 ºC, in contrast, $ZnCl_2$ impregnated samples started to develop considerable surface area at 250 ºC. The surface area increased as the activation temperature rose to 400 ºC for $ZnCl_2$ impregnated samples. This phenomenon was largely due to the excessive burn-off (pore development and/or carbon conversion) of carbon constituents at this high temperature. It should be noted that at temperatures higher than 400 °C the increment in the activation temperature do not increase the surface area of the activated carbon, therefore does not make sense to explore higher activation temperatures. The temperature at which the surface area began to decrease is near to temperature at which the pure $ZnCl_2$ started to lose weight (Figure 2.1D), therefore the evaporation of $ZnCl_2$ at temperatures higher than 400 ºC could influence the decrease of surface area. On the other hand, the surface area of the H_3PO_4 impregnated samples remains constant at activation temperatures above 250 °C. As exposed previously, H_3PO_4 inhibit the gasification of the biopolymers avoiding the levoglucosan formation [26] (Figure 2.1A), hence the extensive burn off that could occur at higher temperatures do not have any appreciable effect in the activated carbon surface area.

According with these results, the activation temperature of 350 ºC and 250 °C for $ZnCl_2$ and H_3PO_4, respectively, were selected in order to explore all other production conditions.

2.3.2.2. Activating agent concentration

The zinc chloride impregnated samples presented an increase in surface area as the impregnation ratio increased (Figure 2.5B), getting a maximum at R=2. When R>2 the surface area slightly decreased, showing that high concentrations of $ZnCl_2$ did not obstruct the development of a larger surface area. When analyzing these results, one could hypothize that only part of the $ZnCl_2$ participated in the activation reactions with the precursor, and the excess not being in direct contact with the precursor, did not have any influence in the pore development. These results indicated that the use of large amounts of $ZnCl_2$ is not necessary to develop high surface area in activated carbons. The activated carbons surface area with impregnation ratio of H_3PO_4 is progressive up to 1.2, after this point it decreased. Some authors suggest that the mechanism of reaction by which the phosphoric acid promotes pore formation in the activation of lignocelluloses material consists in the dilation and stabilizing formation of cross-links in the form of phosphate esters. However, when the phosphoric acid concentration is too high, the dilation effect could be so intense causing the collapse of pores and therefore, decrease the activated carbon surface area [26]. These results are in agreement with these reported by other researches that used phosphoric acid as activating agent, finding that the optimal weight ratio is around 1.5 [30, 31]. Similarly to the activation temperatures studied, here we found that R=2 and R=1.2 for $ZnCl_2$ and H_3PO_4, respectively, were the activating agent concentrations that developed the highest surface area in agave bagasse.

2.3.2.3. Activation time

The main reason to study the activation time is to ensure that the different phases of the activation process have ended. At early stages, the moisture and most of the volatile components of the precursor are eliminated. Subsequently and depending of the activating agent, the formation of the basic pore structure proceeds. Low activation times resulted in an incomplete burn-off and excessive activation times caused enlargement of pores at the expense of surface area. In addition, the

control of the activation time is of economic interest since short times are generally desired in order to reduce energy consumption. Figure 2.5C shows the effect of activation time on the surface area of the activated carbons. Almost no effect of the activation time on the surface area developed on the phosphoric acid activated samples was found: the highest surface area developed occurred after 20 minutes of activation exhibiting surface areas of ca. 1100 m^2/g. In contrast, the $ZnCl_2$ impregnated samples increased their surface area as the activation time increased, reaching the maximum at 40 minutes of activation. Among the materials developed, we can found that the production parameters that exhibit the major surface area when H_3PO_4 was used are: R=1.2, T=250 ºC and t=20 min and R=2, T=350 ºC and t=40 min for agave bagasse activated with $ZnCl_2$. Two more samples were produced at this specific production conditions in order to test by triplicate the surface area obtained. The resulted surface area was 1073±38 m^2/g for H_3PO_4 activated samples and 2139±108 m^2/g for $ZnCl_2$ activated samples. However, to be conclusive about these results a more detailed study of the production parameters around these values is needed. It should be noted that the surface area developed with $ZnCl_2$ was always higher than the H_3PO_4 impregnated samples. The reason of this effect can be linked to the different activation mechanism of both activating agents. Some studies have correlated the pore volume to the amount of activating agent used. Thus suggesting that the created porosity by the activating agent is due to the created spaces by the chemicals after the washing step [32]. The water-soluble components are easily removed during the activated carbon washing, due to the high solubility of zinc salts ($ZnCl_2$: 4.23 g/mL). In contrast, when phosphoric acid is used as activating agent, phosphate and polyphosphate species are incorporated to the carbon matrix, through C-O-P bonds [27, 29], and therefore part of the phosphorus would not be completely removed when rising the material and as a consequence, the resulting surface area is smaller than that obtained when using $ZnCl_2$. Similar results have been found for the chemical activation of lignocelluloses materials with $ZnCl_2$ and H_3PO_4: activated carbon from oreganum stalks using an impregnation

ratio of 1 and 600 °C of carbonization temperature, had surface areas of around 1000 m^2/g and 700 m^2/g, respectively [33].

2.3.3. Pore structure

The activated carbon pores are classified based on their diameter as macropores (those greater than 500 Å), mesopores (those within 20 and 500 Å) and micropores (those smaller than 20 Å). The microporous activated carbon has commercial advantages: activated carbons with higher micropore volume have much higher capacity to adsorb small molecules, such as volatile organic chemicals.
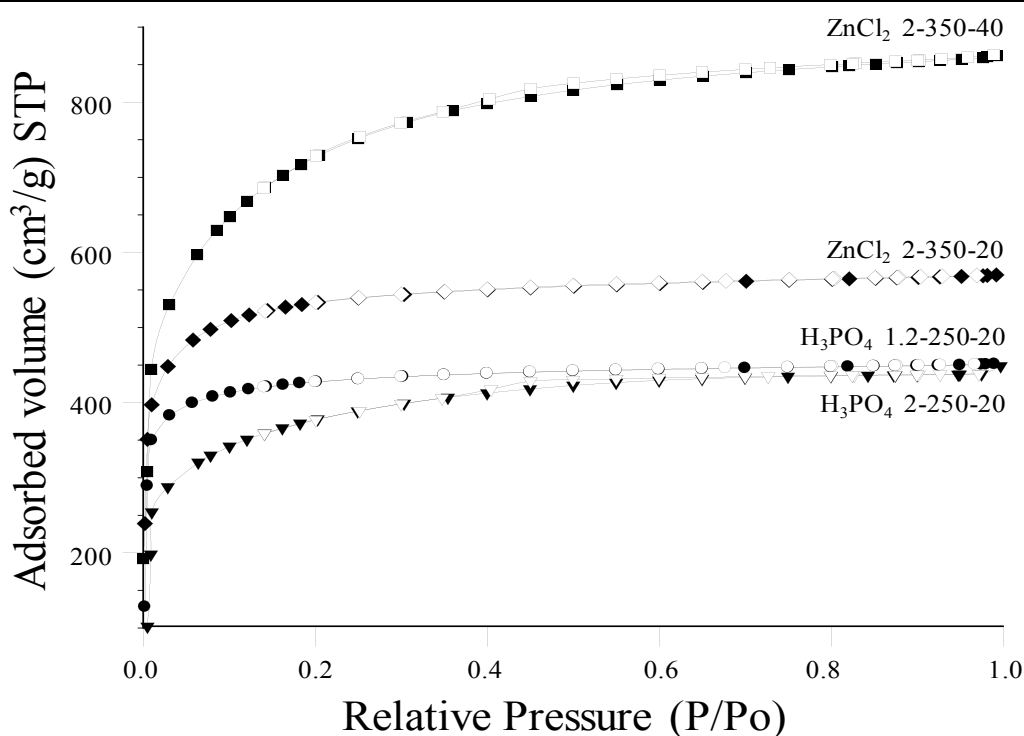
Figure 2.6. Nitrogen adsorption (close) and desorption (open) isotherms of selected samples. The employed nomenclature indicates the production conditions as follow: activating agent, weight ratio between the activating agent and the precursor (g/g), activation temperature (°C), and activation time (minutes).

Higher capacity means that the activated carbon will last longer before it needs to be replaced. Also the microporous materials are the most suitable materials for gas storage applications. In addition, the pore structure of microporous carbon can be easily modified by thermal treatments were the pore structure become wider, allowing to adsorb large molecules after modification.

Figure 2.6 shows the adsorption isotherms of selected samples. As can be observed, the shape of the isotherms showed a typical type I adsorption isotherm that are characterized of materials with narrow pore size distribution on the micropore range [34, 35]. Analizing the pore volume of these samples (Table 2.2), the activated carbons developed in this research are basically microporous because up to 70 percent of the total pore volume is contained within this range.

Table 2.2. **Porosity parameters of activated carbons calculated from nitrogen adsorption isotherms.**

Activating Agent	Production Conditions (R, g/g - T, ºC - t, min)	V_{micro} (cm^3/g)	V_{meso} (cm^3/g)	V_{tot} (cm^3/g)	V_{micro} (%)
H$_3$PO$_4$	1.2-250-20	0.764	0.095	0.894	85.5
	2-250-20	0.626	0.237	0.882	71.0
ZnCl$_2$	2-350-40	1.202	0.392	1.717	70.0
	2-350-20	1.106	0.235	1.345	82.2

V_{micro}: micropore volume V_{meso}: mesopore volume V_{tot}: total volume

It has been previously reported that some materials such as coconut shell based activated carbon and kraft lignin based activated carbon have 1.14 cm^3/g and 1.04 cm^3/g of micropore volume [24, 36]. In comparison with these materials, the agave bagasse based activated carbon showed similar micropore volumes. These results make to the agave bagasse an interesting precursor to produce versatile activated carbons.

Representative SEM micrographs of the activated carbon produced using $ZnCl_2$ and H_3PO_4 as activating agent are reported in Figure 2.7. Activated samples with $ZnCl_2$ showed different morphology than the carbonized material (see Figure 2.2) which showed a channel arrangement. It seems that the reaction of the biopolymers with high concentration of $ZnCl_2$ could lead to the formation of a "fluid phase" (Figure 2.7A and 2.7B). In order to explain this behavior, it is important to keep in mind that the agave bagasse is constituted of a complex mixture of interconnected biopolymers and therefore its chemical properties may be similar to polymers. Polymeric materials are characterized by two major types of transition temperatures: the crystalline melting temperature (Tm) and the glass transition temperature (Tg). The crystalline melting temperature is the melting temperature of the crystalline domains of a polymer sample.
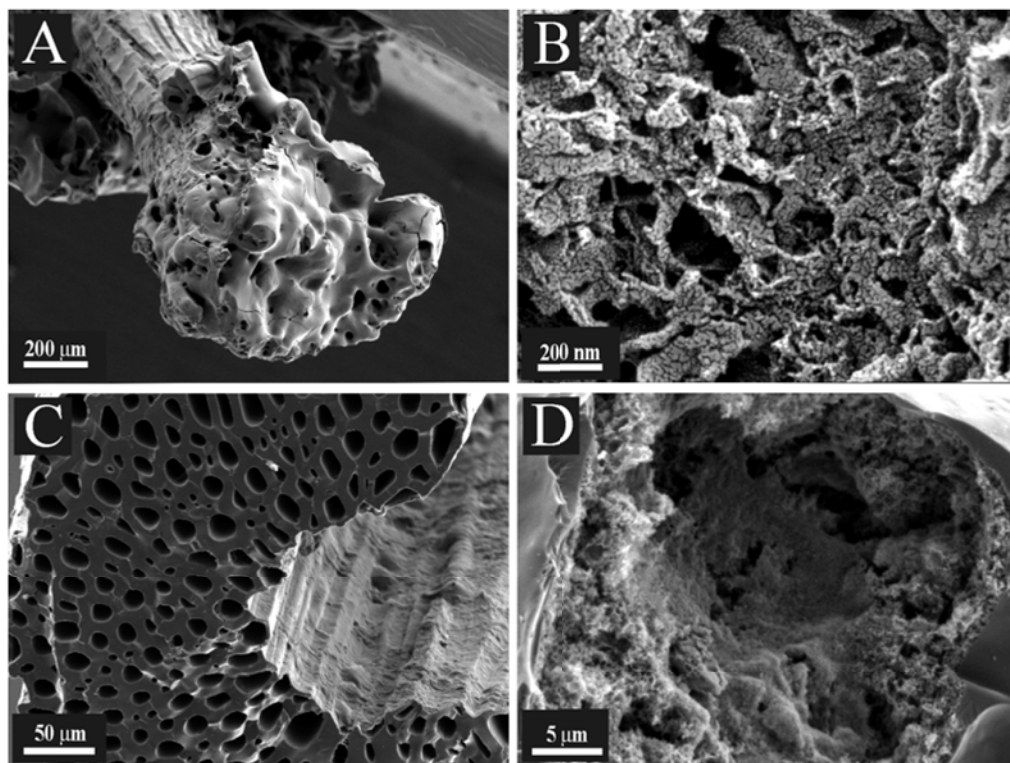
Figure 2.7. SEM images of activated carbons produced with $ZnCl_2$ (A, B) and H_3PO_4 (C, D) as activating agent.

The glass transition temperature is the temperature at which the amorphous domains of a polymer take the characteristic properties of the glassy state: brittleness, stiffness, and rigidity. This glass transition is associated with the onset of "rubbery flow" caused by slippage of the biopolymers which increase their kinetic energy when increasing temperature. These two thermal transitions depend of several parameters, including the average molecular weight [37]. As previously mentioned, the activating agent modifies the thermal degradation of the raw material, thus promoting the bond cleavage or, from the standpoint of polymers, a depolymerization reaction. Some light compounds may be released as gasses, but if the biopolymer chain generated is of a size that does not allow its volatilization, this will remain as a condensed phase. These bonds cleavage generate chains of lower molecular weight which may have lower melting temperature and hence generate the melted phase that was observed in the SEM images (Figure 2.7A and 2.7B). This effect has been previously observed, in the fast-pyrolysis of wood [19], the production of activated carbon from fruit stones, nutshells [38] and kraft lignin [24], showing that the thermal process exhibits many properties of a "molten plastic state". Something to remark is the newly created pores that can be observed in Figure 2.7B and 2.7D. Interestingly, activated samples treated with H_3PO_4 did not show a deformation of the shape of the original fiber (Figure 2.7C). This could be attributed to the lower impregnated ratio used, and to the stabilization crosslink that performed phosphate in the activation step. With the aim to clarify the reactions that occur during the activation process, *In situ* observations of the thermal activation were carried out employing an environmental scanning electron microscope (ESEM). These results are summarized in appendix A.

2.3.4. Activating agent recovery

Since the use of activating agents leads to environmental pollution, their recovery is a critical point in the production of activated carbon. For this purpose, the filtrate from the washing step of activated carbon with acid and distilled water was

analyzed to evaluate the recovery of both activating agents. Table 2.3 includes the mean recovery percentage of two replicates for the marked samples with an *.

Table 2.3. **Chemical recovery of activating agents.**

Activating agent	Activation temperature (T, ºC)	Chemical ratio (R, g/g)	Activation time (t, min)	Chemical recovery (%)
H_3PO_4	250	0.4	20	27.9*
	250	0.8	20	48.6
	250	1.0	20	45.6*
	350	0.4	20	24.6
	350	0.8	20	17.6*
	350	1.0	20	33.7
$ZnCl_2$	250	0.4	20	88.9*
	250	0.8	20	87.5*
	250	1.0	20	86.7
	350	0.4	20	88.1*
	350	0.8	20	87.4
	350	1.0	20	86.2*

mean recovery percentage of two replicates

The average deviation for the chemical recovery reported in Table 2.3 (for the marked samples with an *) was 2.8 % and 3.7 % for H_3PO_4 activated samples and $ZnCl_2$ activated samples respectively. For $ZnCl_2$, the recovery was about 89 % when the activation temperature corresponded to 250 ºC, regardless of the amount of activating agent used. When the activation temperature increased to 350 ºC, the recovery decreased slightly to 87.5 % for all the chemical ratios used. Moreover, the degrees of recovery of H_3PO_4 were between 20 and 50 % of the initial amount used. The low recovery of H_3PO_4 can be attributed to its ability to build phosphate bridges between the aromatic rings generated in the activation process [26]. These links are stable below 450 ºC, hence, unrecovered H_3PO_4 remained anchored in the activated carbon matrix. The presence of phosphate groups in the activated

carbon after the washing step was confirmed by EDX analysis; it was found to be up to 5% by weight of phosphorus. According to these results, it could be possible to reuse part of the $ZnCl_2$ recovered during the activated carbon washing, in order to avoid the generation of undesired wastes and diminish the activating agent consumption. Previous reports have successfully applied this strategy, recovering about 75% of the initial $ZnCl_2$ employed [31].

2.4. CONCLUSIONS

According with our results it is possible to take advantage of the organic wastes from the tequila and mescal industries to produce high quality activated carbons, generating therefore a viable alternative for the treatment of these residues. In agreement with the characteristics developed by the agave bagasse based activated carbons it is expected that this material can be an excellent adsorbent, which could be used in the treatment of gaseous and liquid effluents. About the production parameters that develop the highest surface area when H_3PO_4 is used are R=1.2, T=250 ºC and t=20 min, and R=2, T=350 ºC and t=40 min for agave bagasse activated with $ZnCl_2$, exhibiting surface areas of 1198 m^2/g and 2245 m^2/g, respectively. When comparing these production parameters with the typical activation temperatures (>500 ºC) and activation times (few hours) reported to produce activated carbon from other lignocelluloses precursors, agave bagasse offers important commercial and economical advantages due to the low activation times and activation temperatures required. The pores size of the activated carbons from agave bagasse is mainly within the microporous range (pore diameter < 2 nm), being the micropore volume in some samples even 80% of the total pore volume. Regarding the activating agents, $ZnCl_2$ has some advantages over H_3PO_4: $ZnCl_2$ impregnated samples display almost twice the surface area. In addition, up to 89% of $ZnCl_2$ can be recovered, which makes its use feasible at high impregnation rates. Based on these results, agave (*salmiana)* bagasse should

now be considered as a new alternative to produce highly microporous activated carbons.

2.5. REFERENCES

[1]   Norma Oficial Mexicana NOM-070-SCFI-1994. Bebidas alcohólicas -Mezcal. Especificaciones.SCFI;1994.

[2]   Norma Oficial Mexicana NOM-006-SCFI-2005,   Bebidas Alcohólicas - Tequila. Especificaciones.SCFI;2005.

[3]   CRT. Consejo Regulador del Tequila.   2007   [cited; Available from: http://crtnew.crt.org.mx

[4]   CNPMM. Consejo Nacional de Productores de Maguey Mezcal. 2009 [cited; Available from: http://www.sientemezcal.com

[5]   Aguirre-Rivera J. R. C-SH, Flores-Flores J. L., ed. El maguey mezcalero potosino. 1a ed. San Luis Potosi, México: Editorial Universitaria Potosina 2001.

[6]   Idarraga G, Ramos J, Zuniga V, Sahin T, Young RA. Pulp and Paper from Blue Agave Waste from Tequila Production. J Agric Food Chem 1999;47:4450-5.

[7]   Iniguez-Covarrubias G, Lange SE, Rowell RM. Utilization of byproducts from the tequila industry: part 1: agave bagasse as a raw material for animal feeding and fiberboard production. Bioresour Technol 2001;77:25-32.

[8]   Baena-González A. Aprovechamiento del bagazo de maguey verde (agave salmiana) de la agroindustria del mezcal en San Luis Potosí para la producción de hongo ostra (pleurotus ostreatus). [M. S. Thesis]. San Luis Potosi: Instituto Potosino de Investigacion Cientifica y Tecnologida; 2005.

[9]   World activated carbon Industry Study with forecast to 2010 & 2015.Freedonia study #2064:Freedonia;2006.

[10] Mohan D, Pittman CUJ. Activated carbons and low cost adsorbents for remediation of tri- and hexavalent chromium from water. J Hazard Mater 2006;137:762-811.

[11] Rodriguez-Reinoso F, Molina-Sabio M. Activated carbons from lignocellulosic materials by chemical and/or physical activation: an overview. Carbon 1992;30:1111-8.

[12] Omar S, Girgis B, Taha F. Carbonaceous materials from seed hulls for bleaching of vegetable oils. Food Res Int 2003;36:11-7.

[13] Ioannidou O, Zabaniotou A. Agricultural residues as precursors for activated carbon production--A review. Renew Sust Energ Rev 2007;11:1966-2005.

[14] Dias JM, Alvim-Ferraz MCM, Almeida MF, Rivera-Utrilla J, Sánchez-Polo M. Waste materials for activated carbon preparation and its use in aqueous-phase treatment: A review. J Environ Manage 2007;85:833-46.

[15] Ahmadpour A, Do DD. The preparation of active carbons from coal by chemical and physical activation. Carbon 1996;34:471-9.

[16] Clesceri LS, ed. Standard methods for the examination of water and wastewater : including bottom sediments and sludges. New York: American Public Health Association 1998.

[17] Pollard SJT, Fowler GD, Sollars CJ, Perry R. Low-cost adsorbents for waste and wastewater treatment: a review. Sci Total Environ 1992;116:31-52.

[18] Valix M, Cheung WH, McKay G. Preparation of activated carbon using low temperature carbonisation and physical activation of high ash raw bagasse for acid dye adsorption. Chemosphere 2004;56:493-501.

[19] Evans RJ, Milne TA. Molecular characterization of the pyrolysis of biomass. Energy Fuels 1987;1:123-37.

[20] Varhegyi G, Antal MJ, Szekely T, Till F, Jakab E, Szabo P. Simultaneous thermogravimetric-mass spectrometric studies of the thermal decomposition

of biopolymers. 2. Sugarcane bagasse in the presence and absence of catalysts. Energy Fuels 1988;2:273-7.

[21] Tsai W, Chang C, Lee S, Wang S. Thermogravimetric Analysis of Corn Cob Impregnated With Zinc Chloride for Preparation of Activated Carbon. J Therm Anal Calorim 2000;63:351-7.

[22] Cagnon B, Py X, Guillot A, Stoeckli F, Chambat G. Contributions of hemicellulose, cellulose and lignin to the mass and the porous properties of chars and steam activated carbons from various lignocellulosic precursors. Bioresour Technol 2009;100:292-8.

[23] Varhegyi G, Antal MJ, Szekely T, Till F, Jakab E. Simultaneous thermogravimetric-mass spectrometric studies of the thermal decomposition of biopolymers. 1. Avicel cellulose in the presence and absence of catalysts. Energy Fuels 1988;2:267-72.

[24] Gonzalez-Serrano E, Cordero T, Rodriguez-Mirasol J, Rodriguez JJ. Development of Porosity upon Chemical Activation of Kraft Lignin with $ZnCl_2$. Ind Eng Chem Res 1997;36:4832-8.

[25] Jagtoyen M, Derbyshire F. Some considerations of the origins of porosity in carbons from chemically activated wood. Carbon 1993;31:1185-92.

[26] Jagtoyen M, Derbyshire F. Activated carbons from yellow poplar and white oak by H_3PO_4 activation. Carbon 1998;36:1085-97.

[27] Solum MS, Pugmire RJ, Jagtoyen M, Derbyshire F. Evolution of carbon structure in chemically activated wood. Carbon 1995;33:1247-54.

[28] Zawadzki J, Wisniewski M. 13C NMR study of cellulose thermal treatment. J Anal Appl Pyrolysis 2002;62:111-21.

[29] Guo Y, Rockstraw DA. Physical and chemical properties of carbons synthesized from xylan, cellulose, and Kraft lignin by H_3PO_4 activation. Carbon 2006;44:1464-75.

[30] Castro JB, Bonelli PR, Cerrella EG, Cukierman AL. Phosphoric Acid Activation of Agricultural Residues and Bagasse from Sugar Cane: Influence of the Experimental Conditions on Adsorption Characteristics of Activated Carbons. Ind Eng Chem Res 2000;39:4166-72.

[31] Hussein MZB, Rahman MBBA, Yahaya AHJ, Hin T-YY, Ahmad N. Oil Palm Trunk as a Raw Material for Activated Carbon Production. J Porous Mat 2001;8:327-34.

[32] Molina-Sabio M, Rodríguez-Reinoso F. Role of chemical activation in the development of carbon porosity. Colloid Surf A-Physicochem Eng Asp 2004;241:15-25.

[33] Timur S, Kantarli IC, Ikizoglu E, Yanik J. Preparation of Activated Carbons from *Oreganum* Stalks by Chemical Activation. Energy Fuels 2006;20:2636-41.

[34] Gregg SJaS, K.S.W. Adsorption, Surface Area and Porosity. Second Edition ed. London: Academic Press 1982.

[35] Bansal RC, Goyal M. Activated Carbon Asdorption: CRC Press 2005.

[36] Hu Z, Srinivasan MP, Ni Y. Preparation of Mesoporous High-Surface-Area Activated Carbon. Advanced Materials 2000;12:62-5.

[37] Odian GG. Principles of polymerization. 4th ed. Hoboken, N.J.: Wiley 2004.

[38] Aygün A, Yenisoy-Karakas S, Duman I. Production of granular activated carbon from fruit stones and nutshells and evaluation of their physical, chemical and adsorption properties. Microporous Mesoporous Mat 2003;66:189-95.

"Statistics may be defined as a body of methods for making wise decisions in the face of uncertainty"
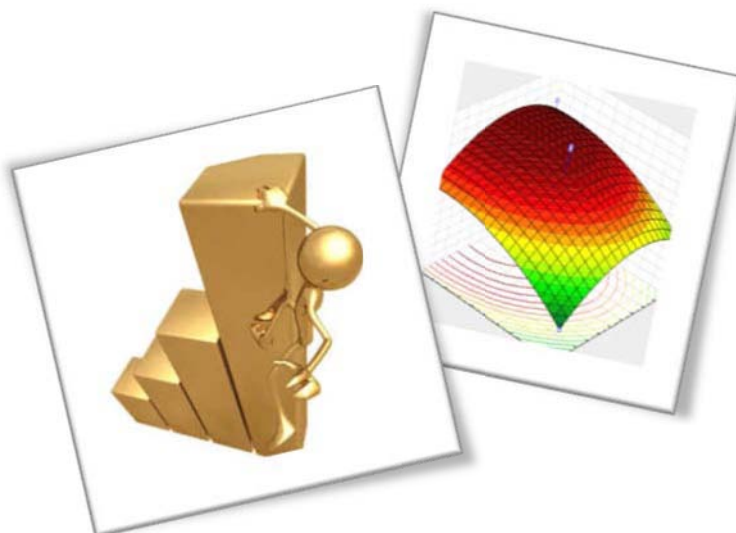
CHAPTER 3

PRODUCTION OF ACTIVATED CARBON FROM AGAVE SALMIANA BAGASSE: SURFACE AREA AND HARDNESS OPTIMIZATION BY USING THE RESPONSE SURFACE METHODOLOGY

The success of activated carbon in adsorption systems is due to its extensive surface area and diverse surface groups that allow the removal of compounds from both liquid and gas streams. However, the treatment of liquid streams on packed column systems requires granular material with mechanical strength to avoid the attrition caused by the stream flow. Therefore an appropriate balance between surface area and hardness is essential when using activated carbon in real systems. The purpose of this research is to obtain the optimal production conditions that generate activated carbon from agave bagasse with adequate mechanical properties to be used in packed column systems. Carbons were produced by chemical activation with $ZnCl_2$ or H_3PO_4. The response surface methodology (RSM) was used to evaluate the effect of the activation temperature (250-550 °C), activation time (0-50 min), and the concentration of activating agent (0.2-1.4; g activating agent/g bagasse). Both, surface area and hardness were the analyzed responses. Plus elemental composition and the point of zero electric charge were determined for selected samples. The H_3PO_4 activated carbons had hardness and a surface area that range from 75.9 to 95.5 % and from 235 to 1087

Production of activated carbon from agave salmiana bagasse: surface area and hardness optimization
César Nieto Delgado   IPICyT   2010

85

m^2/g, respectively. Carbons activated with $ZnCl_2$ showed superior surface area (2-1765m^2/g), but low mechanical properties since their hardness range from 60.7 to 95.4 %. The concentration of activating agent was the variable that most affected both responses. Increasing the concentration of activating agent, at the optimal temperature and activation time, the surface area can reach 1327 and 2109 m^2/g for H_3PO_4 and $ZnCl_2$ activated samples respectively. The production conditions that generate the material with the optimal characteristics were 392 °C, 1.02 g activating agent/g bagasse and 23.8 min for H_3PO_4 activated samples and 456 °C, 1.08 g activating agent/g bagasse and 23.8 min for $ZnCl_2$ activated samples. The surface area and hardness of the optimal materials were similar to properties of commercial activated carbons (surface area > 800 m^2/g and hardness > 85%). Finally, the low point of zero electric charge (3.0 and 2.2 for $ZnCl_2$ and H_3PO_4 activated carbons, respectively) showed that the produced activated carbons are mainly acidic.

3.1. INTRODUCTION

Activated carbon is the most widely used adsorbent around the world, which has applications on diverse areas such as in food processing, pharmaceuticals, chemical synthesis and purifications, petroleum refinery, mining processes, automotive parts, solvent recovery, odor elimination, support of catalyst, and as adsorbent of a variety of pollutants from gas and liquid phases [1]. Due to its large number of applications, the production and characterization of activated carbon is of great interest to both science and industrial applications. One of the methods to produce activated carbon involves the thermal treatment of a precursor under an inert atmosphere, step in which a porous structure is formed. When the generation of this porous structure is assisted by the addition of chemical additives such as $ZnCl_2$, KOH or H_3PO_4, the activation methodology is known as chemical activation. Instead if an oxidant gas such as air, CO_2 or steam is added during the thermal process, the activation is known as physical activation [2].

Production of activated carbon from agave salmiana bagasse: surface area and hardness optimization
César Nieto Delgado   IPICyT   2010

86

Regardless of the methodology employed to produce activated carbon, the major challenge is to produce materials with specific features to solve particular problems. To achieve this aim, it is necessary to know the influence of the production parameters on both physical and chemical characteristics of activated carbons. When chemical activation is employed to produce activated carbon, the activating agent concentration, the activation temperature and the activation time are the production parameters that most influence the properties of activated carbon [2, 3], whereas the activation time and the activation temperature are the most affecting or impacting parameters when a physical activation methodology is utilized.

Activated carbons from new precursors are traditionally obtained by studying one production parameter at a time, and evaluating key features of the activated carbon as the surface area, pore volume and/or the adsorption capacity of a model compound. This methodology can be useful to explore the feasibility of producing activated carbons from a new precursor, however, the characteristics of an activated carbon are the result of the influence of all the variables involved in the production process. Thus, by varying one condition at a time, some combinations of experimental conditions are not considered. In addition, one factor at a time analysis has generally negative implications: it is very expensive due to the number of required tests, the effect of each factor has a very limited field validity, it is not possible to detect interactions of two or more factors and finally, there is not guarantee to obtain the optimal conditions [4]. Therefore if the goal is to elucidate the influence of production parameters over some property of an activated carbon, the correct approach is to implement experimental design which explores a broad range of each production parameter, with the minor number of tests, generating useful data to predict and optimize any properties of the activated carbon produced. In this way, the response surface methodology (RSM) is a collection of mathematic and statistic techniques useful to model and analyze problems, where response variables are influenced by multiple conditions. Despite the RSM is a popular tool in processes optimization, it is rarely used in the activated carbon

production. Recently, researchers began to use the RSM to optimize the production of activated carbon from Luscar char [5], coconut shell [3], coconut husk [6], turkish lignite [7], tamarind wood [8], olive-waste cakes [9], and sewage sludge [10], demonstrating that it is an appropriate tool to optimize the activation process of carbonaceous materials.

Chapter 2 of this thesis demonstrated the possibility to produce activated carbon from agave bagasse by chemical activation using either $ZnCl_2$ or H_3PO_4 as activating agent [11]. However, carbons from soft precursors such as agave bagasse have low mechanical properties, being difficult their application in the treatment of liquid effluents on packed column systems. Taking this into account, the purpose of this research is to obtain the production conditions that generate activated carbon from agave bagasse, which is a waste from the mescal and tequila industries in Mexico, with an appropriate balance between surface area and hardness. In order to achieve this objective the effect of (1) activation temperature, (2) activating agent/precursor weight ratio and (3) the activation time on the physical characteristics (surface area and hardness) of activated carbon were evaluated employing the response surface methodology.

3.2. EXPERIMENTAL

3.2.1. Activated carbon production

Agave bagasse from *Agave salmiana* plants was collected from a distillery located in San Luis Potosi, Mexico. First, the agave bagasse was fractioned to obtain fibers no longer than 1 cm. After that the fibers were dried at 110 ºC for 24 hours. Activated carbons were produced by a chemical activation process using either H_3PO_4 or $ZnCl_2$ as activating agent. The chemicals used were ACS grade ($ZnCl_2$ 97% and H_3PO_4 98%) from Fermont Different materials, according to the experimental design (Table 3.1), were obtained varying the activating agent concentration (R, g activating agent /g bagasse), the activation temperature (T, °C),

Production of activated carbon from agave salmiana bagasse: surface area and hardness optimization
César Nieto Delgado   IPICyT   2010

88

and the activation time (AT, min): the activation time began once the activation temperature was reached. Besides, the activating agent and the agave bagasse were physically mixed in order to promote a homogeneous distribution of the activating agent into the precursor. Air-dried agave bagasse (100 g) was mixed in a beaker with 250 mL of H_3PO_4 or $ZnCl_2$ solution with the indicate concentrations. The mixing was performed at room temperature (25 °C) for 12 hours; then, the mixture was dried at 60 ºC. Afterwards, approximately 3 g of impregnated sample were placed in a stainless steel mesh capsule (10 cm long, 3 cm wide, 1 cm high), and placed in the center of a quartz tube. Then the sample was activated inside a tubular furnace under argon atmosphere (99.998 % of Ar), at a flow rate of 1.2 L/min and a heating rate of 10 ºC/min. The temperature was kept constant during the required time (AT) and the sample was cooled down outside the furnace at room temperature. The produced activated carbons were rinsed with 10 % HCl aqueous solution to remove the excess of activating agent, and then the samples were rinsed with distilled water until neutral pH.

3.2.2. Materials characterization

The BET surface area [12] was determined by N_2 adsorption at -196 °C using a Micromeritics ASAP 2020 instrument. The hardness of the activated carbon was determined by a methodology already reported [13-15]: (1) 100 mg of 20/40 US mesh (0.85–0.42 mm) activated carbon was weighed and placed in a 250 mL Erlenmeyer flask, and then 10 glass marbles (2 of 15 mm diameter and 8 of 5 mm diameter) were introduced in the flask; (2) the flask was capped and placed in an orbital incubator at 25 °C; (3) the samples were shaken at 150 RPM for 15 minutes and then sieved through a 40 US mesh screen. The retained material by the mesh was weighed and the hardness number was calculated as a percentage of the carbon retained after the milling process regarding to the initial mass. The speed and time to determine hardness as stated on step 3 were established using a commercial activated carbon (Filtrasorb 400 from Calgon). A series of experiments were developed varying the milling time and the speed of the shaker, until getting

the hardness value of 95%, which is the value reported by the manufacturer of F-400 activated carbon.

Selected materials were characterized by FTIR, elemental analysis and their point of zero electric charge. Attenuated total reflection Fourier transform infrared (ATR-FTIR) analyses (Thermo-Nicolet, Nexus 470 FT-IR E.S.P.) were used to identify the activated carbon functional groups, and their evolution regarding the production conditions. Previous to ATR-FTIR analyses, activated carbons were dried at 110 °C for 24 hours. Then, the spectra were obtained from 650 to 4000 cm^{-1} with 6 cm^{-1} resolution, taking the average of 64 scans. Elemental analysis of samples (carbon, hydrogen and nitrogen) was carried out by using an ECS costech analyzer model 4010. The inorganic content of the activated carbon samples and the raw material was determined as follow: a representative sample was burned in a furnace operating at 650 °C for 4 h in the presence of air: the ash content was calculated from the residue. Phosphorus was determined by ICP spectroscopy after microwave assisted digestion of the activated carbons, and finally, the oxygen content was determined by the following equation:

$$\%O = 100 - (\%C + \%N + \%H + \%P + \%ash)$$

The pH$_{PZC}$ of the activated carbons was determined by mixing 0.2 g of carbon with 4 mL of CO$_2$ free distilled water. The mixture was kept in a glass vial which was shaken at 120 RPM for 5 days. The supernatant pH was measured with a glass bulb electrode (semi micro electrode Orion 911600, Orion 2-Star Bench top pH Meter) taking this pH as the pH$_{PZC}$ of the solid.

3.2.3. Experimental design

The Response Surface Methodology is a statistical method that uses quantitative data from an appropriate experimental design to develop regression model equations which are useful to predict and optimize the operating conditions of some processes. This methodology assumes that a response Y also called

response variable, is a function of a set of process variables X_1, X_2, ..., X_k, which can be controlled. That function can be approximated by a polynomial model, the most commonly used are first order (equation 3.1) and second order (equation 3.2) models, where β are the constant coefficients that fit the equation [16].

$$Y = \beta_0 + \beta_1 X_1 + \cdots + \beta_k X_k \qquad (3.1)$$

$$Y = \beta_0 + \sum_{i=1}^{k} \beta_i X_i + \sum_{i=1}^{k} \beta_i X_i^2 + \sum_{\substack{i=1 \\ i<j}}^{k} \sum_{j=1}^{k} \beta_{ij} X_i X_j \qquad (3.2)$$

Production of activated carbon from agave salmiana bagasse: surface area and hardness optimization
César Nieto Delgado   IPICyT   2010

91

Table 3.1. Experimental design and the responses obtained.

Run	Production conditions (Coded levels)			H₃PO₄ based activated carbon		ZnCl₂ based activated carbon	
	T (°C)	R (g/g)	AT (minutes)	BET S.A. (m^2/g)	Hardness (%)	BET S.A. (m^2/g)	Hardness (%)
1	300 (-1)	0.4 (-1)	10 (-1)	235.1	85.1	38.1	93.5
2	500 (1)	0.4 (-1)	10 (-1)	284.2	82.4	771.9	67.9
3	300 (-1)	1.2 (1)	10 (-1)	789.4	84.1	674.2	92.6
4	500 (1)	1.2 (1)	10 (-1)	969.5	76.1	1503.3	78.2
5	300 (-1)	0.4 (-1)	40 (1)	402.8	91.9	87.4	84.0
6	500 (1)	0.4 (-1)	40 (1)	201.1	84.5	810.0	67.6
7	300 (-1)	1.2 (1)	40 (1)	406.1	83.0	184.2	88.3
8	500 (1)	1.2 (1)	40 (1)	913.5	75.9	1645.3	68.4
9	232 (-1.682)	0.8 (0)	25 (0)	388.1	83.2	2.1	92.1
10	568 (1.682)	0.8 (0)	25 (0)	521.3	80.5	1240.5	95.4
11	400 (0)	0.13 (-1.682)	25 (0)	108.1	92.8	258.4	83.3
12	400 (0)	1.47 (1.682)	25 (0)	1086.8	84.6	1765.2	60.7
13	400 (0)	0.8 (0)	0 (-1.682)	590.4	86.6	945.3	90.4
14	400 (0)	0.8 (0)	50.23 (1.682)	703.3	89.2	1430.2	86.4
15	400 (0)	0.8 (0)	25 (0)	738.4	94.7	1170.5	95.7
16	400 (0)	0.8 (0)	25 (0)	795.3	95.5	1120.4	94.9
17	400 (0)	0.8 (0)	25 (0)	754.2	92.4	1143.3	94.8

T : Temperature   R: Activating agent / agave bagasse ratio   BET S.A.: Surface area according with the BET model

AT: Activation time

The central composite experimental design was employed, with 3 center points and an α value of 1.682, considering three factors: activation temperature, concentration of activating agent, and the activation time. The studied responses were surface area and hardness. Two levels were assigned for each variable according with conditions that developed high surface area in previous studies [11], being 300 to 500 ⁰C for activation temperature, 10 to 40 min for activation time and 0.4 to 1.2 g/g for activating agent concentration. The production conditions for each experimental run are reported in Table 3.1.

3.2.4. Data analysis

STATISTICA 7.0 software was used to analyze the experimental data according the response surface methodology. Also, it was employed to evaluate the statistical significance of the surfaces generated according with the following criteria: (1) each considered variable must present a p value (probability value) lower than 0.05, which means that this term is significant at 95% of confidence level; (2) the determination coefficient (r^2) that represents how well a regression approximates to the real data points, should be close to 1; (3) the "lack of fit test" must be significant (p value < 0.05) which means that the model is adequated to describe the experimental data, and finally; (4) the generated residuals between the experimental data, those reported by the fitted model, must present a normal distribution to validate the assumptions made by the ANOVA analysis [4]. Finally, the desirability function approach was used to obtain the production conditions at which the responses exhibit the optimal value (maximum).

3.3. RESULTS AND DISCUSSION

3.3.1. Statistical analysis

The considered terms for the development of the surface response were the linear (R, T and AT), quadratic (R^2, T^2 and AT^2) and the two-factor interaction terms (R*T,

R*AT and T*AT) that had a significance superior to 95% according with the ANOVA analysis. The calculated coefficients to adjust equation 3.2 (response surface), for surface area (Y_1 in m^2/g) and for hardness (Y_2 in %), after discarding the insignificant terms, are reported in Table 3.2. These equations become a useful tool to predict the characteristics (hardness and surface area) of the produced activated carbons developed at specific production conditions. In addition, if a material with specific characteristics of surface area and hardness is needed, the experimental conditions to generate it can be easily obtained.

Table 3.2. **Final regression coefficients in terms of coded factors.**

Activating agent	H_3PO_4		$ZnCl_2$	
Term / Response	BET S.A.	Hardness	BET S.A.	Hardness
Constant	764.21	95.33	1158.09	95.39
T	55.55	-2.19	426.82	-5.17
T^2	-115.31	-5.31	-232.42	-1.37
R	263.71	-2.82	353.92	-1.73
R^2	-64.75	-2.89	-94.36	-9.07
AT	-12.08	0.88	40.62	-2.26
AT^2	-47.42	-3.17	-32.13	-3.28
T*R	105.13	-	104.13	0.98
T*AT	9.38	-	77.63	-
R*AT	-65.63	-1.27	-54.38	-

T : Temperature   AT: Activation time

R: Activating agent/agave bagasse ratio   BET S.A.: Surface area according with BET model

The accuracy of these predictions depends on how far the model represents the experimental data. The correlation coefficient (r^2) and the standard deviation are two parameters to evaluate this aspect. Table 3.3 shows the correlation coeficient and the standard deviation obtained by the models presented in Table 3.2. The correlation coefficients were found to be greater than 0.9, except for the model that describes the hardness of activated carbon generated with $ZnCl_2$ as activating agent. These values indicated that at least 90 % of the total variation in the

measured responses can be attributed to the effect of the studied variables. A possible explanation to the low value of r^2 for hardness of $ZnCl_2$ activated samples can be related to the physical properties of this material, since the generated samples with $ZnCl_2$ showed high fragility, causing problems when the samples were handled, increasing the experimental error.

The employed experimental design on this research did not include replicates of each experimental run; only the central point was replicated at least three times. These replicates were employed to estimate the variation of the experimental procedure by calculating the standard deviation. The standard deviation of the analyzed responses showed values below 5% of the mean observed response, which represent that the variation due to the experimental procedure do not interfere the variation regarding the production variables. Finally, the p value for the lack of fit test appears in Table 3.3. All the fitted models overcome this test since their p value was lower or close to 0.05.

Table 3.3. Values of the statistical test that validate the model.

Activating agent	H_3PO_4		$ZnCl_2$	
Test / Response	BET S.A.	Hardness	BET S.A.	Hardness
Lack of fit (p value)	0.05597	0.043719	0.007428	0.002428
R^2	0.94401	0.91184	0.92268	0.67293
Standard deviation	29.4	1.62	25.02	0.49

3.3.2. Production conditions effect

An advantage of this statistical analysis is that the effect of each variable on the analyzed response can be clearly identified without studying each variable individually. The common way to visualize these results is through effect plots. One of the most used effect plot is the Pareto chart: a bar graph in which each bar
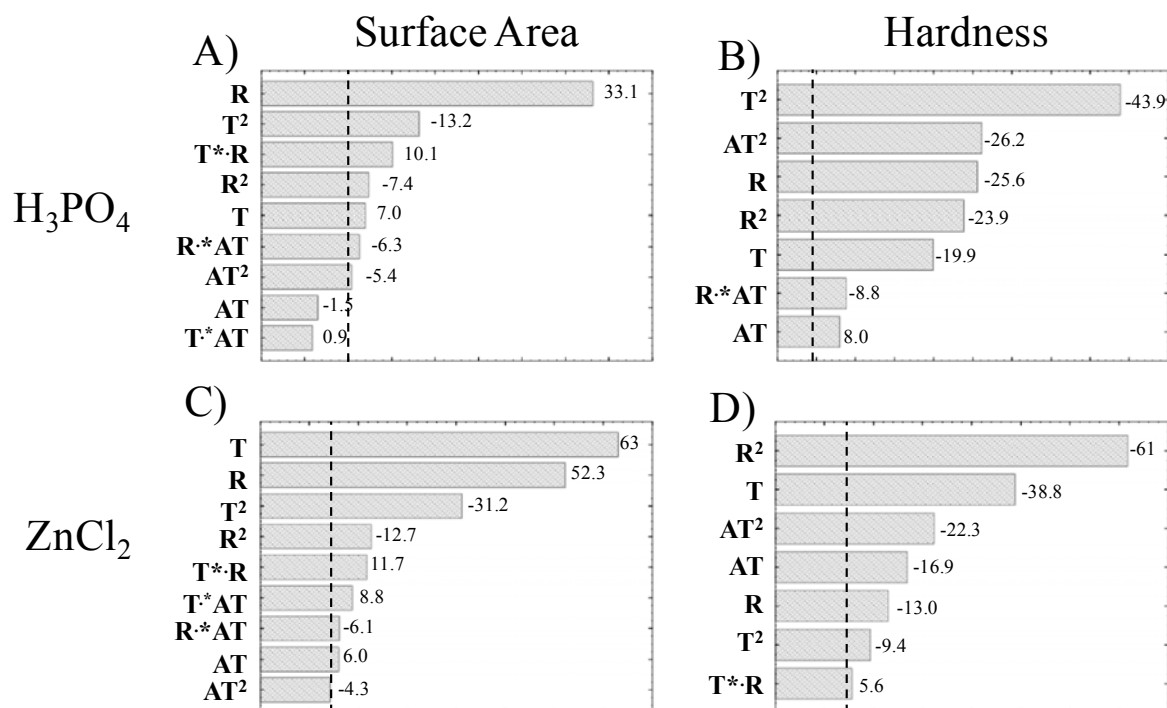
Figure 3.1. Pareto charts for H_3PO_4 (A and B) and $ZnCl_2$ (C and D) activated samples, by the follow responses: surface area A and C; hardness B and D. The values plotted appear as standardized effect estimates (absolute value). T: activation temperature; R: activating agent / bagasse weight ratio; AT: activation time. The doted line indicates a confidence limit of 95%.

represents the factor or interaction and the size of the bar represents the magnitude of the effect. Figure 3.1 shows the Pareto chart of each production variable regarding the surface area (Figure 3.1A and C) and the hardness (Figure 3.1B and D) of the carbons. The effects are plotted in decreasing order, therefore the largest effects indicate that the factor is the most important, and appear first. Although almost all the considered variables overcome the significance test, the effect of certain variables is predominant. Figure 3.1A indicates that the concentration of activating agent (R) is the variable that has most effects the surface area of H_3PO_4 activated carbons. The standardized effect has a positive value, which means that if the concentration of activating agent increases, the surface area would increase. Almost all the terms in the hardness analysis of

H_3PO_4 activated carbons have a negative effect, which means that the modification of the production parameters of values above the central point of the experimental design (see Table 3.1) could generate materials with poor mechanical properties (Figure 3.1B).

On the other hand, the activation temperature and the concentration of activating agent were the production conditions that most influenced the surface area and hardness of $ZnCl_2$ activated carbons (Figure 3.1C and D). Both production variables have a positive effect in the surface area of the activated carbon. In contrast, both production conditions have a negative effect over the hardness of the carbons. This opposite effect could be explained by assuming that the increase of surface area leads to the formation of new pores in the carbon, decreasing the mechanical strength of the material. For both activating agents, the activation time did not exhibit a significant effect for the analyzed responses, probably because the range studied was too short.

3.3.3. Response analysis and interpretation

Considering that carbons generated from soft lignocellulosic materials have poor physical properties, an adequate balance between hardness and surface area is needed. In the following section a detailed analysis of the evolution of surface area and hardness of the carbons regarding the production conditions are studied, with the aim to find the production conditions that maximize this activated carbon characteristics.

3.3.3.1. H_3PO_4 activated carbons

Figure 3.2 shows the three dimensional response surfaces and the contour plot that show the effect of both activation temperature (T) and activating agent concentration (R), on the surface area (Figure 3.2A and B) and hardness (Figure 3.2C and D) of the H_3PO_4 activated carbon. Because of its low significance for both responses (Figure 3.1), the activation time was kept constant according with the

values reported in Table 3.4, which are the production conditions that maximize the analyzed response.
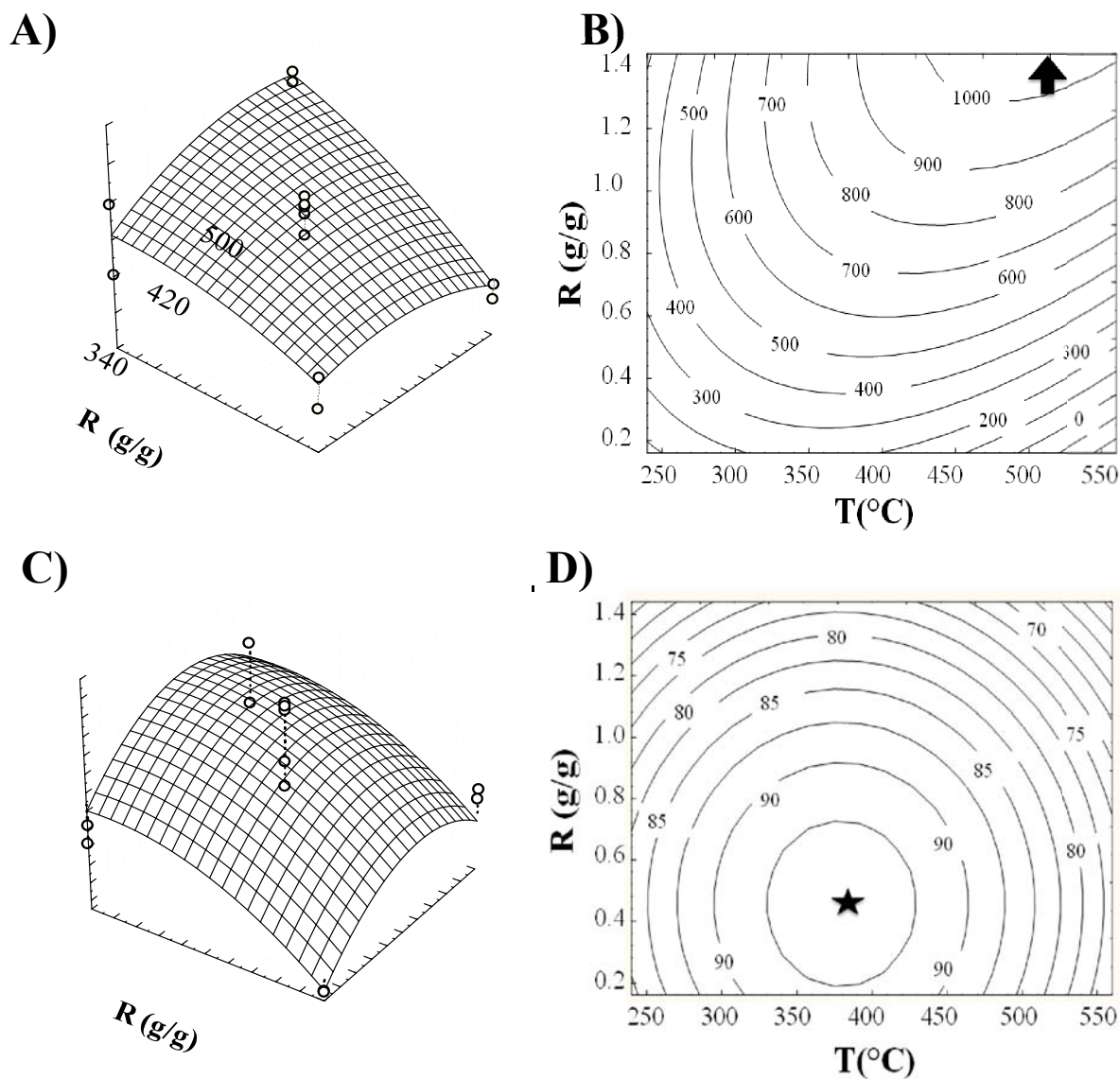
Figure 3.2. Surface response and the corresponding contour plot of H_3PO_4 activated samples. A and B for surface area; C and D for hardness. T: activation temperature; R: H_3PO_4/bagasse weight ratio.

The surface area of the H_3PO_4 activated carbon ranged from 200 to 1000 m^2/g (see Figure 3.2A). The pronounced slope corresponding to the concentration of activating agent indicated the high influence of this production variable over surface area, since this increased as the concentration of activating agent increased. The activation temperature has also a positive effect, but with a less impact than the concentration of activating agent. As can be observed in Figure 3.2B, it is expected that the surface area of H_3PO_4 activated carbons increases if the concentration of activating agent rise, since the surface response growths in this direction (marked with an arrow in Figure 3.2B). In order to confirm these speculations, five activated carbons were produced at activating agent concentrations higher than 1.47 g H_3PO_4 / g bagasse, employing the optimal values of activation time and activation temperature reported in Table 3.4.

Table 3.4. Optimum production conditions that maximize the responses.

Activating agent	H_3PO_4		$ZnCl_2$	
Factor/ Response	BET S.A.	Hardness	BET S.A.	Hardness
T (°C)	488.1	376.0	548.2	247.8
R (g/g)	1.47	0.58	1.47	0.77
AT (minutes)	7	28.6	40.6	26.2
Predicted value *	1208.5	96.4	1899.4	97.3
Measured response *	1128.4	95.2	1823.4	94.1

T : Temperature

R: Activating agent / agave bagasse ratio

AT: Activation time

*Values expressed in m^2/g and percentage by BET Surface Area and hardness respectively

The surface area and the hardness of these materials are reported in Figure 3.3A. As predicted by the model, the surface area of activated carbons increased as the activating agent concentration increased .This tendency continued until a

maximum of 1327 m^2/g at R=2.5. However, the surface area of activated carbons began to decrease at concentration values higher than 2,5 g H$_3$PO$_4$ / g bagasse.

A)
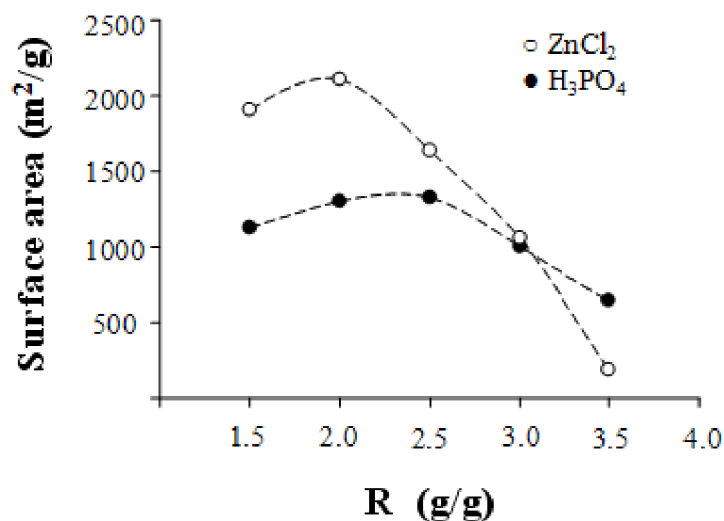
B)
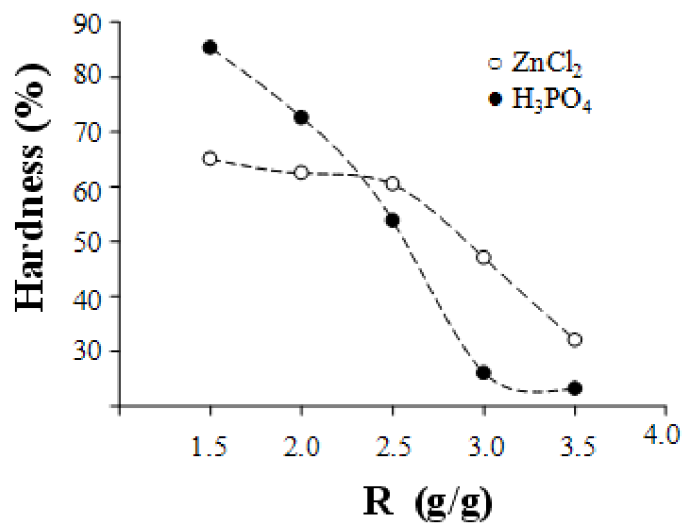
Figure 3.3. Effect of activating agent concentration on the surface area (A) and hardness (B) of activated carbons generated with H$_3$PO$_4$ and ZnCl$_2$. The reported values represent the mean of duplicate samples where the standard error did not exceed 5%.

Previous studies have reported similar behavior of the surface area of activated carbons produced by chemical activation: as the activating agent concentration increases, the surface area also increases until a maximum [17-19]. The reason why the surface area did not increase more could be related to the pore structure of the activated carbon: previous studies have demonstrated that the pore volume of samples was similar to the volume of the total amount of phosphoric acid used in the impregnation of the precursor. At low impregnation ratios carbons were essentially microporous, obtaining materials with high surface area; as the amount of impregnation agent increased, the pores in the mesoporous range became predominant [17, 19-23]. Because the meso and macropores have a less contribution to surface area, the widening of pores by increasing the concentration of activating agent decreases the surface area of activated carbons. This was confirmed by other researchers that also have reported mesoporosity development as the surface area decreases due to high acid concentration [18, 24-26].

On the other hand, the hardness indicates the percentage of activated carbon that has not been broke down to finer particles (in comparison with the initial ones), after a vigorous milling with glass marvels. A high hardness number is always preferred because the carbon will maintain its physical integrity under the attrition forces within a packed column. The evolution of the hardness of the H_3PO_4 activated carbon is reported in Figure 3.2 C and D. The hardness of the activated carbons ranged from 75.9 to 95.5%, being this values comparable with commercial carbons that have hardness between 85 and 95 % [27]. It was able to find the production conditions that generate the activated carbon with the highest hardness (start point in Figure 3.2D). The calculated surface area corresponding to these production conditions is 596 m^2/g, which is a reasonable value of surface area for an activated carbon.

It can be seen that the conditions that develop the material with high surface area are the conditions that generate carbons with low mechanical properties and vice versa. High concentrations of $ZnCl_2$ generate carbons with a surface area as high

as 2000 m^2/g, however, the hardness of these materials do not exceed 65%. Similar results were observed for H_3PO_4 activated carbons. Also, an excessive amount of activating agent causes a decrement in both surface area and hardness. This effect is clearly appreciated in Figure 3.3A, where the hardness and surface area decreased to less than 40% of hardness and 1000 m^2/g of surface area when the concentration of activated agent was higher than 3.5 g activating agent / g bagasse.

3.3.3.2. ZnCl$_2$ activated carbons

Surface responses and contour plots of hardness and surface area of $ZnCl_2$ activated carbons are reported in Figure 3.4. Similarly for H_3PO_4 activated carbons, the activation time was kept constant at the value reported in Table 3.4. The surface area of the carbons ranged from 2 to 1765 m^2/g, and it increased as both the activation temperature and the activating agent concentration increased. The long steep slope that displays the activation temperature to the surface area indicates the strong influence of this variable in the porosity of $ZnCl_2$ activated carbons. Analyzing the data reported in Table 3.2, we can see that samples activated at less than 300 °C have a negligible surface area: sample 9 activated at 232 °C has a surface area of 2 m^2/g even when the concentration of activating agent is 0.8 g $ZnCl_2$ / g bagasse. Generated samples above this activation temperature have a considerable surface area. This dependence of surface area to the activation temperature is related to the activation mechanism by which $ZnCl_2$ generates pores in the carbon precursor: $ZnCl_2$ catalyzes dehydrating reactions that begins to consolidate the carbon structure, this reactions become greater at temperatures above the melting point of the activating agent. Also, the infiltration of melted $ZnCl_2$ in the precursor generates the pore structure after the removal of the remaining activating agent. Since the melting point of $ZnCl_2$ is 290 °C, carbons activated at temperatures below 290 °C will have minimal development of surface area. It was possible to determine the optimal activation time and activation temperature that developed the activated carbon with maximum surface area (see

Table 3.4). However, the optimal concentration of activated agent coincide with the maximum value of activating agent concentration tested in the experimental design, hence it is expected that at activating agent concentrations higher than 1.47 $ZnCl_2$ / g bagasse, the surface area of the activated carbons increases.

On the other hand, hardness of the $ZnCl_2$ activated samples (Figure 3.4C and D) ranges from 60.7 to 95.7%, founding the higher values at low activation temperatures and moderate concentration of activating agent. However, as exposed previously, activation temperatures below 300 °C do not develop pore structure on the activated carbon. Particularly, activated carbons generated at an activation temperature of 500°C or higher have low mechanical properties (see Table 3.1). It could be related to the extensive burn off caused at these activation temperatures.

Similarly to what was done for H_3PO_4 activated carbons, five samples were produced at higher concentrations of $ZnCl_2$ to determine whether the activating agent concentration produces a higher surface area. The surface area and the hardness of these samples are reported in Figure 3.3B. As it can be observed, the surface area of $ZnCl_2$ activated carbons increased up to 2109 m^2/g at R=2.0. However, all the generated carbons at R>1.5 g $ZnCl_2$ / g bagasse have very low mechanical properties, since the hardness of these samples are below 70%.

Comparing the characteristics obtained in the activated carbons generated with $ZnCl_2$ with those generated with H_3PO_4, it is clear a very different effect of each activating agent: $ZnCl_2$ activated carbons develop surface areas higher than the ones activated with H_3PO_4, however, the H_3PO_4 activated carbons have better mechanical properties than the $ZnCl_2$ activated carbons. This effect can be explained according with the activation mechanism that follows both activating agents: as previously mention, the $ZnCl_2$ that remained after the thermal process was easily removed in the washing step, leaving a cavity that constitutes porous structure. The small size of $ZnCl_2$ (Zn atomic ratio: 0.134 nm) allows the generation of small and uniform micropores generating carbons with high surface area [17].
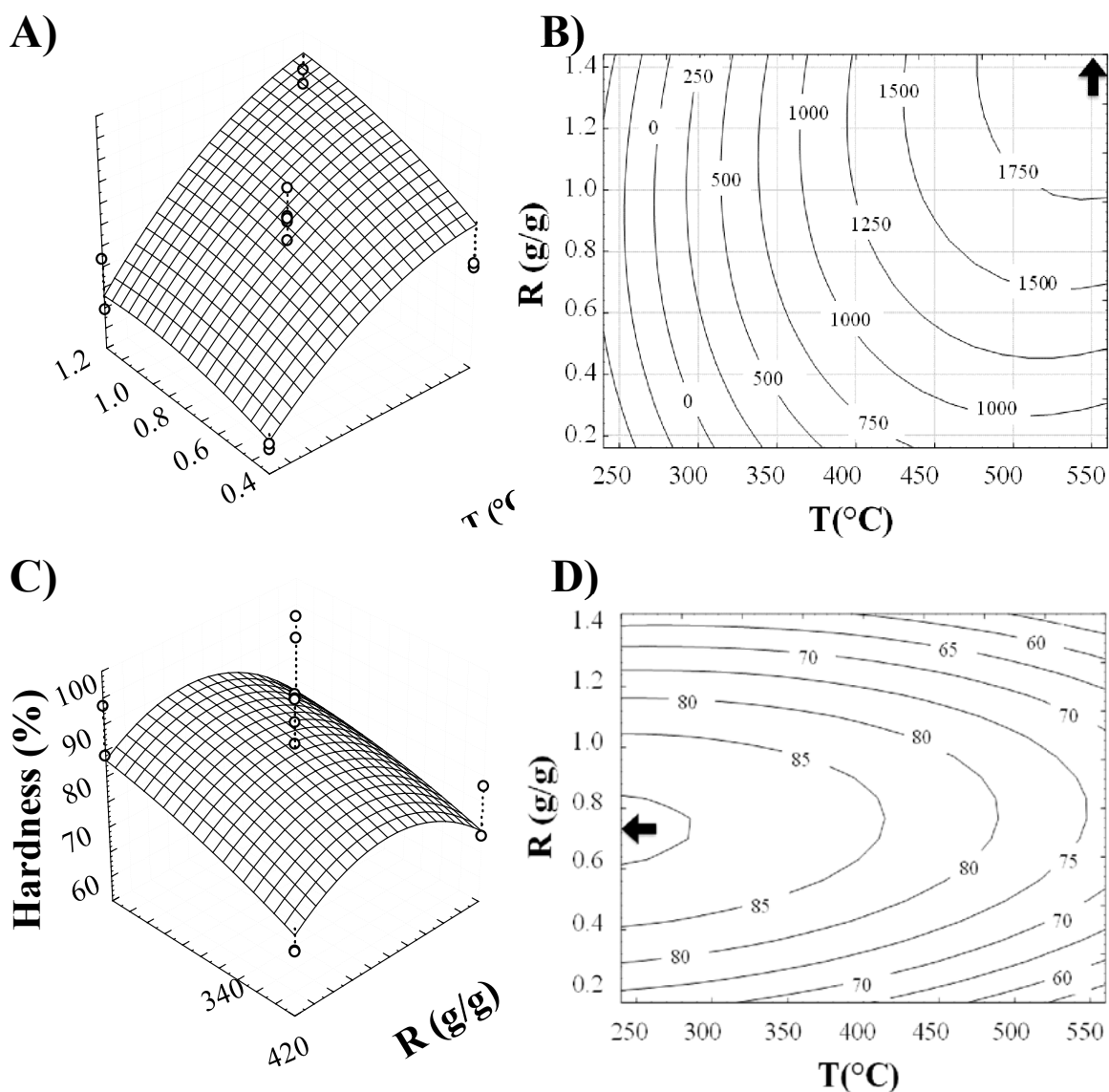
Figure 3.4. Surface response and the corresponding contour plot of $ZnCl_2$ activated samples. A and B for surface area; C and D for hardness. T: activation temperature; R: $ZnCl_2$/bagasse weight ratio.

On the other hand, during the activation process, H_3PO_4 can form polyphosphoric acids and ester bridges between the carbon sheets, generating wider pores when the remaining acid is removed from the carbon [19, 20, 26, 28, 29]. Also, it was reported that part of the phosphoric acid remains in the activated carbon and

hence can block some pores diminishing the surface area of the activated carbons. Previous studies focused on the characterization of H_3PO_4 based activated carbons, have found that an increase of the concentration of phosphate groups in the carbon, considerably decreases surface area [21, 30]. Finally, the phosphate groups anchored onto the activated carbon can acts a binder between the carbon fragments generated during the thermal treatment, increasing the mechanical properties of H_3PO_4 activated carbon.

3.3.4. Optimum operating conditions

As previously mentioned, one of the most important properties of activated carbons is surface area, since it generally leads to great adsorption capacities. However, mechanical properties are also important when activated carbon is aimed to be used in a packed column system. In this case the main objective of the optimization is to determine the experimental conditions which yield the best of both responses. According with the results of the previous section, it was possible to determine the production conditions that yield the maximum value by each response. As can be observed in the surfaces reported in Figure 3.2 and Figure 3.4, the optimal experimental conditions that maximize the responses are opposite: experimental conditions that increase the surface area, promote a decrement in the hardness of the activated carbon. It implies that we can not generate an activated carbon with the maximum value of surface area and hardness. Taking this into account, the desirability function is employed to determine the production conditions that generate an activated carbon with the best characteristics. The basic idea behind the desirability function is the transformation of a multiple response problem into a single response problem by means of mathematical analysis. This function requires the definition of acceptable results for each individual response and results which are not acceptable at all. Additionally, different degrees of importance are attributed to each experimental response depending on its importance on analytical determination [31, 32]. The desirability function was calculated with STATISTICA 7.0 software, establishing equal

importance for both responses, a surface area of 1000 m^2/g and hardness of 90% as acceptable values and a surface area below 600 m^2/g and hardness below 70% as unacceptable values.

According with this analysis the production conditions that developed the activated carbon with the best value of both responses are reported in Table 3.5. With the aim to corroborate these results, 3 samples were produced at the optimal production conditions, characterizing its surface area and hardness. As can be observed in Table 3.5, the physical characteristics developed by the generated activate carbons at optimal production conditions agree with the predicted values. The optimal activated carbon produced with H_3PO_4 showed similar properties to commercial activated carbons: surface area of about 1000 m^2/g and hardness up to 90%. On the other hand, the $ZnCl_2$ activated samples showed higher surface areas (1500 m^2/g), with a moderate hardness (86%).

Table 3.5. Production parameter and responses that maximize both responses at the same time according with the desirability function.

Activating agent	H_3PO_4		$ZnCl_2$	
Factor/ Response	BET S.A.	Hardness	BET S.A.	Hardness
Predicted value *	890.1	91.0	1522.4	88.7
Measured response*	901.3	90.2	1593.4	83.2
T (°C)	392		456.1	
R (g/g)	1.02		1.08	
AT (minutes)	23.8		23.8	

T : Temperature

R: Activating agent / agave bagasse ratio

AT: Activation time

*Values expressed in m^2/g and percentage by BET Surface Area and hardness respectively

3.3.5. Chemical properties

On adsorption at the liquid-solid interface, the electric charges of activated carbon are hardly influenced by the solution pH, for instance: basic carbons that take a positive electric charge when immersed in water by adsorbing H^+ ions on basic surface groups (amines, pyrones, ethers, carbonyls); and the acid carbons, that take a negative electric charge when immersed in water, by releasing H^+ ions from acidic groups (carboxyls, phenols, lactones) [2, 27, 33, 34]. The pH at which the surface groups adsorb or release protons depend on the type of surface groups, however, due to the complexity of the activated carbons it is hard to establish all the surface groups presented on these materials. The common way to solve this problem is determining the pH at which the carbon surface is electrically neutral, also called the point of zero electric charge (pH_{PZC}). This is a useful parameter that determines how the solid behaves in the liquid medium. At pH above the pH_{PZC}, the carbon surfaces become deprotonated and hence negatively electric charged, in contrast, at pH below the pH_{PZC} the surface groups are protonated and so positively electric charged. Hence below the pH_{PZC} carbons would adsorb anions, and at pH above their pH_{PZC}, carbon would adsorb cations both by electrostatic attraction. Table 3.6 shows the pH_{PZC} and the elemental composition of selected materials that have similar physical properties to commercial activated carbons (surface area > 800 m^2/g and hardness > 85 %).

According with the pH_{PZC}, the agave bagasse based activated carbons can be considered as acid carbons and hence it is expected that these materials are excellent adsorbents of cations in aqueous solution. According with the elemental composition, it is clear that oxygen plays an important role on the surface chemistry of these carbons, since it is the predominant heteroatom in the activated carbons. Due to the low pH_{PZC}, it is expected that most of the oxygen in the $ZnCl_2$ activated samples was parte of strong acid functional groups such as carboxylic acids, because this functional group has a pKa between 2.0 and 5.0 [35], however further characterization is needed in order to be conclusive. On the other hand,

H_3PO_4 activated samples had pH_{PZC} slightly lower (Table 3.6) than the $ZnCl_2$ activated samples. This difference could be attributed to the presence of poly phosphates that are very acidic surface groups with a pKa between 1.6 and 1.9 [30, 36].

Table 3.6. **Elemental analyses and pH_{PZC} of selected samples**

Experimental Run	pH_{PZC}	C %	O %**	P %	N %	H %	Ash %
H_3PO_4							
4	2.19	57.3	30.5	2.8	1.4	3.9	4.1
16	2.07	68.5	14.7	3.2	0.4	3.2	10.0
12	1.94	77.7	9.9	2.8	0.1	2.6	6.9
Optimal *	2.24	72.5	12.7	2.2	0.8	2.7	9.1
$ZnCl_2$							
4	3.37	67.6	27.6	<0.05	0.4	3.9	0.5
14	2.76	73.2	23.1	<0.05	0.9	2.1	0.7
15	2.47	81.4	13.8	<0.05	1.0	3.4	0.4
Optimal *	3.00	78.5	17.1	<0.05	0.8	3.1	0.5

* Activated carbon produced at optimum conditions as appear in Table 5. Value reported corresponds to the average of material developed by triplicate.

** Calculated by difference

Figure 3.5 shows the FTIR spectra of prepared activated carbons at the optimal production conditions, the FTIR of raw agave bagasse was also included. As can be observed, almost all the signals of the functional groups presented on the raw agave bagasse remain in the activated carbons. The main difference is the decrease in the wide absorption band from 3200 to 3600cm^{-1} corresponding to the O-H stretching mode of hydroxyl groups, being this decrement considerably for H_3PO_4 activated samples. It suggests the elimination of OH groups from the biopolymers that compose the agave bagasse (cellulose and hemicellulose) in the activation process. All spectra shows a broad band between 1300 and 900 cm^{-1}

with a maximum at 1100 cm^{-1}, however, the relative intensity of this band increases on the H_3PO_4 activated carbons. Within this range, there are several vibrations attributable to oxygenated functional groups: broad bands at 1300–1000 cm^{-1} have been assigned to C–O stretching in acids, alcohols, phenols, ethers and esters; also, this region is characteristic for P-O and P-C vibrations [28, 37]. Finally the absorption bands at 2850 and 2950 cm^{-1} that appear in all samples can be attributed to the C-H and –CH$_2$- stretching modes of aliphatic groups and the absorption band for carbonyl group (C=O) that appear at 1750 cm^{-1} can be attributed to carboxylic acids groups [37].
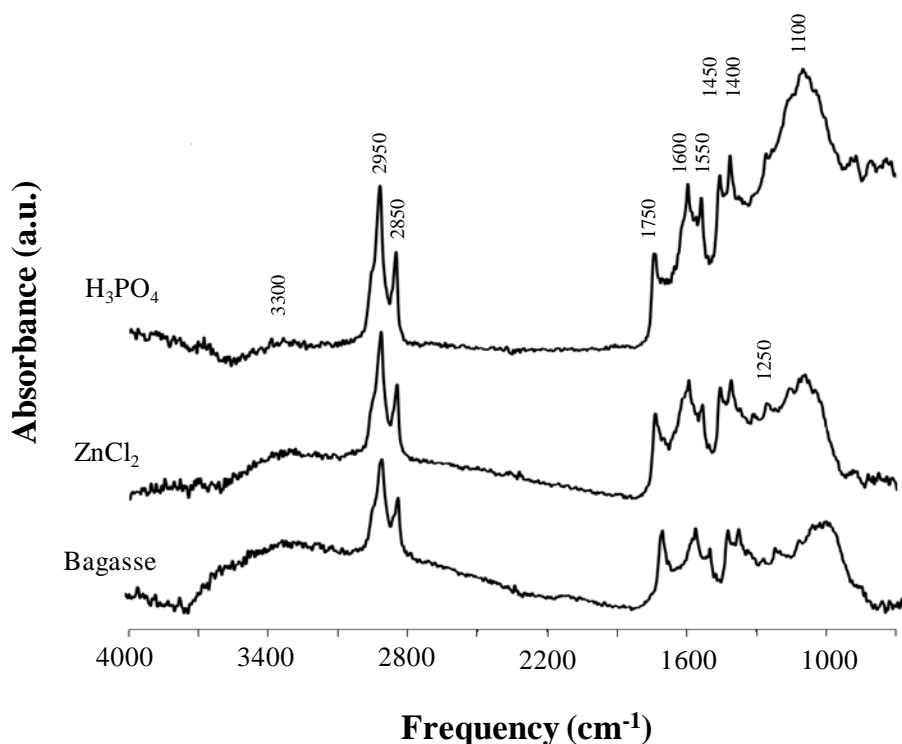
Figure 3.5. FTIR of agave bagasse and activated carbons. The employed activating agent to produce the activated carbons is located besides each spectrum.

As a second part of this work (Chapter 4), the modification of the agave bagasse based activated carbons with iron oxides of nanometric size is evaluated. The aim

of this modification is to generate a hybrid material for the removal of arsenate anions from aqueous solution. Previous studies (See Table 1.4, on Chapter 1) have attempted to modify activated carbon with iron oxides, founding a direct correlation between the oxygenated surface groups and the iron oxides loaded onto the carbon surface. Because of this, the preoxidation of activated carbon with oxidant acids or thermal treatments to increase the number of oxygenated surface groups has been carried out by different researchers [38-42]. In this study the agave bagasse based activated carbons have an advantage since these posses a large quantity of oxygenated groups and hence these are expected to be excellent supports for iron oxide nanoparticles.

3.4. CONCLUSIONS

The present work demonstrates the effect of the activation temperature, activation time and activating agent concentration on the physical properties of agave bagasse based H_3PO_4 and $ZnCl_2$ activated carbons, using the surface response methodology. After a statistical analysis, it was possible to identify the factors that mainly influence the hardness and surface area of the agave bagasse based activated carbons. The concentration of activating agent is the factor that principally affects both responses regardless of the activating agent employed. The response surfaces obtained by each experimental design can be used as a useful tool in the production of activated carbon from agave bagasse in order to predict the physical properties of the activated carbon at specific production conditions or to establish the production conditions that meet certain quality parameters. Both activating agents demonstrate to be effectives to produce activated carbon from agave bagasse, however, the developed characteristics depend hardly on the activating agent employed, since the $ZnCl_2$ impregnated samples develop higher surface area (2109 m^2/g) than those produced with H_3PO_4 (1327 m^2/g). Also, it was possible to determine the experimental conditions which yield the best of both

responses: R=1.02 g/g, T=392 °C, AT=23.8 min and R=1.08 g/g, T=456 °C, AT=23.8 min for H_3PO_4 and $ZnCl_2$ activated samples, respectively.

3.5. REFERENCES

[1]   Ioannidou O, Zabaniotou A. Agricultural residues as precursors for activated carbon production-A review. Renewable and Sustainable Energy Reviews 2007;11:1966-2005.

[2]   Bansal RC, Goyal M. Activated Carbon Asdorption: CRC Press 2005.

[3]   Gratuito MKB, Panyathanmaporn T, Chumnanklang RA, Sirinuntawittaya N, Dutta A. Production of activated carbon from coconut shell: Optimization using response surface methodology. Bioresource Technology 2008;99:4887-95.

[4]   Montgomery. D. Diseño y análisis de experimentos Segunda edición ed: Limusa S.A de C.V 2005.

[5]   Azargohar R, Dalai AK. Production of activated carbon from Luscar char: Experimental and modeling studies. Microporous and Mesoporous Materials 2005;85:219-25.

[6]   Tan IAW, Ahmad AL, Hameed BH. Optimization of preparation conditions for activated carbons from coconut husk using response surface methodology. Chemical Engineering Journal 2008;137:462-70.

[7]   Karacan F, Ozden U, Karacan S. Optimization of manufacturing conditions for activated carbon from Turkish lignite by chemical activation using response surface methodology. Applied Thermal Engineering 2007;27:1212-8.

[8]   Sahu JN, Acharya J, Meikap BC. Optimization of production conditions for activated carbons from Tamarind wood by zinc chloride using response surface methodology. Bioresour Technol 2010;101:1974-82.

[9]   Baçaoui A, Yaacoubi A, Dahbi A, Bennouna C, Phan Tan Luu R, Maldonado-Hodar FJ, Rivera-Utrilla J, Moreno-Castilla C. Optimization of conditions for the preparation of activated carbons from olive-waste cakes. Carbon 2001;39:425-32.

[10]   Rio S, Faur-Brasquet C, Coq LL, Courcoux P, Cloirec PL. Experimental design methodology for the preparation of carbonaceous sorbents from sewage sludge by chemical activation--application to air and water treatments. Chemosphere 2005;58:423-37.

[11]   Nieto-Delgado C, Terrones M, Rangel-Mendez JR. Development of highly microporous activated carbon from the alcoholic beverage industry organic by-products. Biomass and Bioenergy;In Press, Corrected Proof 2010.

[12]   Brunauer S, Emmett PH, Teller E. Adsorption of Gases in Multimolecular Layers. J Am Chem Soc 1938;60:309-19.

[13]   Ahmedna M, Johns MM, Clarke SJ, Marshall WE, Rao RM. Potential of agricultural by-product-based activated carbons for use in raw sugar decolourisation. Journal of the Science of Food and Agriculture 1997;75:117-24.

[14]   Pendyal B, Johns MM, Marshall WE, Ahmedna M, Rao RM. The effect of binders and agricultural by-products on physical and chemical properties of granular activated carbons. Bioresour Technol 1999;68:247-54.

[15]   Ahmedna M, Marshall WE, Rao RM. Surface properties of granular activated carbons from agricultural by-products and their effects on raw sugar decolorization. Bioresour Technol 2000;71:103-12.

[16]   Myers RH, Khuri AI, Carter WH, Jr. Response Surface Methodology: 1966-1988. Technometrics 1989;31:137-57.

[17]   Molina-Sabio M, Rodríguez-Reinoso F. Role of chemical activation in the development of carbon porosity. Colloid Surf A-Physicochem Eng Asp 2004;241:15-25.

[18]   Prahas D, Kartika Y, Indraswati N, Ismadji S. Activated carbon from jackfruit peel waste by H_3PO_4 chemical activation: Pore structure and surface chemistry characterization. Chemical Engineering Journal 2008;140:32-42.

[19]   Jagtoyen M, Derbyshire F. Activated carbons from yellow poplar and white oak by H_3PO_4 activation. Carbon 1998;36:1085-97.

[20]   Jagtoyen M, Derbyshire F. Some considerations of the origins of porosity in carbons from chemically activated wood. Carbon 1993;31:1185-92.

[21]   Jagtoyen M, Thwaites M, Stencel J, McEnaney B, Derbyshire F. Adsorbent carbon synthesis from coals by phosphoric acid activation. Carbon 1992;30:1089-96.

[22]   Ahmadpour A, Do DD. The preparation of active carbons from coal by chemical and physical activation. Carbon 1996;34:471-9.

[23]   Hu Z, Srinivasan MP, Ni Y. Preparation of Mesoporous High-Surface-Area Activated Carbon. Advanced Materials 2000;12:62-5.

[24]   Molina-Sabio M, RodRiguez-Reinoso F, Caturla F, Selles MJ. Porosity in granular carbons activated with phosphoric acid. Carbon 1995;33:1105-13.

[25]   Castro JB, Bonelli PR, Cerrella EG, Cukierman AL. Phosphoric Acid Activation of Agricultural Residues and Bagasse from Sugar Cane: Influence of the Experimental Conditions on Adsorption Characteristics of Activated Carbons. Ind Eng Chem Res 2000;39:4166-72.

[26]   Guo Y, Rockstraw DA. Physical and chemical properties of carbons synthesized from xylan, cellulose, and Kraft lignin by H_3PO_4 activation. Carbon 2006;44:1464-75.

[27]   Cooney DO. Adsorption design for wastewater treatment. Boca Raton, Fl.: Lewis Publishers 1999.

[28]   Solum MS, Pugmire RJ, Jagtoyen M, Derbyshire F. Evolution of carbon structure in chemically activated wood. Carbon 1995;33:1247-54.

[29]   Zawadzki J, Wisniewski M. ^{13}C NMR study of cellulose thermal treatment. J Anal Appl Pyrolysis 2002;62:111-21.

[30]   Puziy AM, Poddubnaya OI, Martínez-Alonso A, Suárez-García F, Tascón JMD. Surface chemistry of phosphorus-containing carbons of lignocellulosic origin. Carbon 2005;43:2857-68.

[31]   Jeong I-J, Kim K-J. An interactive desirability function method to multiresponse optimization. European Journal of Operational Research 2009;195:412-26.

[32]   Engineering Statistics Handbook.Gaithersburg, Md. Austin, Tex.:Croarkin C, Tobias P, Zey C;2001.

[33]   Barton SS, Evans MJB, Halliop E, MacDonald JAF. Acidic and basic sites on the surface of porous carbon. Carbon 1997;35:1361-6.

[34]   Leon y Leon CA, Solar JM, Calemma V, Radovic LR. Evidence for the protonation of basal plane sites on carbon. Carbon 1992;30:797-811.

[35]   Strelko V, Malik DJ, Streat M. Characterisation of the surface of oxidised carbon adsorbents. Carbon 2002;40:95-104.

[36]   Puziy AM, Poddubnaya OI, Gawdzik B, Sobiesiak M, Tsyba MM. Phosphoric acid activation--Functionalization and porosity modification. Applied Surface Science 2007;253:5736-40.

[37]   Pretsch E, Bühlmann P, Affolter C. Structure Determination of Organic Compounds: Tables of Spectral Data: Springer 2004.

[38]   Chen W, Parette R, Zou J, Cannon FS, Dempsey BA. Arsenic removal by iron-modified activated carbon. Water Res 2007;41:1851-8.

[39]   Hristovski KD, Westerhoff PK, Möller T, Sylvester P. Effect of synthesis conditions on nano-iron (hydr)oxide impregnated granulated activated carbon. Chemical Engineering Journal 2009;146:237-43.

[40]   Fierro V, Muñiz G, Gonzalez-Sánchez G, Ballinas ML, Celzard A. Arsenic removal by iron-doped activated carbons prepared by ferric chloride forced hydrolysis. Journal of Hazardous Materials 2009;168:430-7.

[41]   Muñiz G, Fierro V, Celzard A, Furdin G, Gonzalez-Sánchez G, Ballinas ML. Synthesis, characterization and performance in arsenic removal of iron-doped activated carbons prepared by impregnation with Fe(III) and Fe(II). Journal of Hazardous Materials 2009;165:893-902.

[42]   Mezohegyi G, Gonçalves F, Órfão JJM, Fabregat A, Fortuny A, Font J, Bengoa C, Stuber F. Tailored activated carbons as catalysts in biodecolourisation of textile azo dyes. Applied Catalysis B: Environmental 2010;94:179-85.

"Small science

big future:
Nanotechnology "
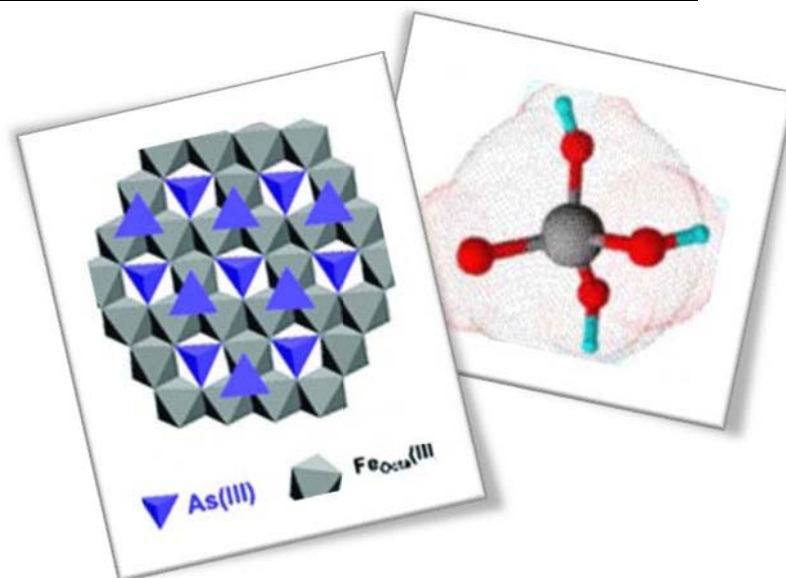
CHAPTER 4

MODIFICATION OF ACTIVATED CARBON WITH IRON OXIDE NANOPARTICLES FOR THE REMOVAL OF ARSENIC FROM WATER

Ground water contamination by arsenic is a severe problem all over the world that can cause several illnesses to people exposed to polluted water even at very low arsenic concentrations. Iron oxides have demonstrated high affinity for the adsorption of arsenic on aqueous solutions, however due to their low mechanical properties, these cannot be used in packed column systems. An alternative is to load iron oxide particles onto the surface of materials often used in adsorption systems. Hence, the aim of this research is to modify activated carbons with iron oxide nanoparticles to generate an adsorbent with high arsenic adsorption capacity. The anchorage methodology was based on the iron hydrolysis, which consists on heating an iron solution to promote the condensation of iron ions until the formation of iron oxide nanoparticles. The surface response methodology was used to evaluate the experimental variables during the hydrolysis process. The studied parameters were: hydrolysis temperature (T: 60-120 °C), hydrolysis time (Ht: 4-16 hours), and the $FeCl_3$ concentration in the hydrolysis solution (C_{Fe}: 0.4-3 mol Fe/L). Both arsenic adsorption capacity and iron content of the modified carbons were the analyzed responses. With the aim to evaluate the effect of the

surface chemistry on the anchorage process, three activated carbons were studied: Filtrasorb 400, commercial activated carbon from Calgon, (F400), and agave bagasse based activated carbon, produced by chemical activation with $ZnCl_2$ (ACZ) or H_3PO_4 (ACP). The iron content of the modified samples ranged from 0.73 to 5.27 %, finding that the anchorage of iron oxide particles was favored by the presence of oxygenated surface groups. The materials containing small particles of iron oxides exhibited an enhanced arsenic adsorption capacity. The production parameters that generate the materials with the highest arsenic adsorption capacity were C_{Fe}=3.05 mol Fe/L, T=96 °C and Ht=56 hours for F400 activated carbon; C_{Fe}=1.16 mol Fe/L, T=110 °C and Ht=6.8 hours for ACZ activated carbon; and C_{Fe}=0.56 mol Fe/L, T=58 °C and Ht=6.8 hours for ACP activated carbon. The optimal materials reported an arsenic adsorption capacity (calculated at an arsenic concentration of 1.5 ppm at equilibrium) of 4.56 mg As/g (F400), 1.18 mg As/g (ACZ) and 0.96 mg As/g (ACP). The adsorption capacity of these materials is similar and in some cases superior to previously reported iron modified carbons, and have the advantage of being modified by a simple methodology.

4.1. INTRODUCTION

Arsenic is a pollutant that can be found in natural waters that have been in contact with geological sources of this element. The incorporation of arsenic in water is mainly by natural weathering, geochemical reactions and soil erosion. Also the arsenic enriched runoffs coming from mining wastes can contribute to increase the arsenic concentration in natural waters. In addition, volcanic emissions, combustion of fossil fuels and some anthropogenic activities also contribute in a minor grade [1, 2]. The main concern of this pollutant is the health implications that can cause at very small concentrations. Arsenic can generate or increase the risk of numerous illnesses such as cancer of skin, lung, bladder, and kidney; pigmentation changes on skin, skin thickening (hyperkeratosis), neurological

disorders, muscular weakness, loss of appetite, and nausea [3, 4]. Because of this, many countries and several international organizations have established concentration limits of arsenic between 50 and 10 ppb for potable water [5]. Different technologies have been proved in order to satisfy these regulations. According with the United States environmental protection agency (USEPA), ion exchange, reverse osmosis, enhanced coagulation/filtration and adsorption have been selected as the best alternatives for the removal of arsenic from water [6]. Among these technologies, adsorption has advantages due to its high removal efficiency, low operation cost and easy operation.

The factor that determines the success of an adsorption system is the affinity between the adsorbent and the molecule to be removed from the stream. Previous studies reported in the literature have shown a high affinity between arsenic and metal oxides/hydroxides in aqueous solution: iron, zirconium, titanium, manganese and aluminum are some of the metal oxides that have proved their efficiency to remove arsenic from water [4, 7, 8]. Due to their high adsorption capacity, high availability and low cost, iron oxides have been widely used on the removal of arsenic from water. However the implementation of iron oxides in adsorption systems is restricted by their poor mechanical properties. An alternative is to load this metal oxide on the surface of granular materials often used in adsorption systems. In this sense activated carbon is an excellent alternative, due to its extensive surface area, mechanical stability and proved efficiency on packed column systems.

The modification of activated carbon with iron oxide particles has been reported in previous works. Some of the methodologies employed are: evaporation of iron salt in presence of activated carbon [9-11]; incipient impregnation at room temperature employing aqueous or organic solutions [12]; precipitation of iron oxide particles under supercritical water conditions [13, 14]; iron precipitation with alkaline solutions [11, 15-17]; and the oxidation/reduction of pre adsorbed iron [18, 19]. A brief description of these methodologies is reported in Table 1.4. The arsenic

adsorption capacity of these materials is competitive and is expected to have success in the treatment of arsenic polluted water, however the majority of the techniques used to anchor iron oxide particles generate bulk agglomerates that can be dissolved when are in contact with water. Also, these agglomerates significantly reduce the surface area and the pore volume of the modified activated carbons. Therefore a methodology to anchor iron nanoparticles onto the activated carbon surface could generate a hybrid material with better performance than the previously reported materials.
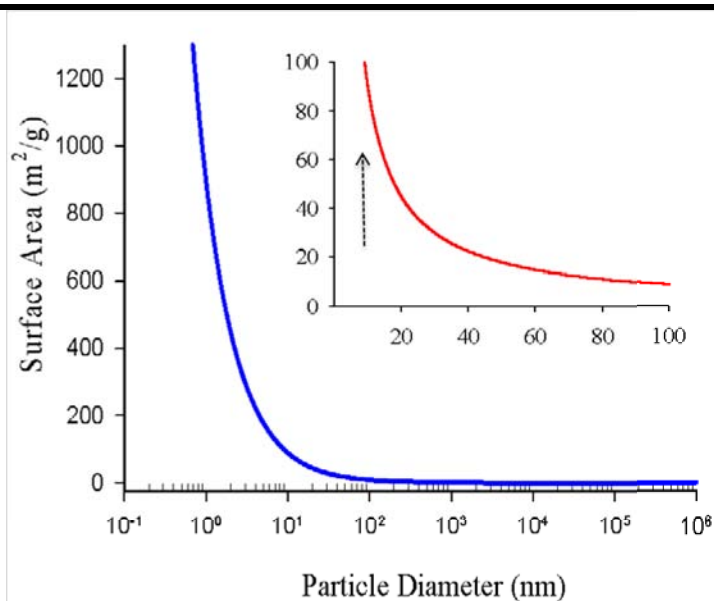
Figure 4.1. Relation between the surface area of the iron particles and their diameter. These data were calculated considering spherical particles and an iron density of 6.7 g/cm^3 (average density between Fe^0 and Fe$_2$O$_3$).

The size of the anchored particles has also a great influence on the arsenic adsorption capacity. Nanoparticles are characterized by having a high reactivity with respect to their bulk equivalent. Recent studies have found that the arsenic removal at the maghemite (γ-Fe$_2$O$_3$) surface remains constant for particles between 300 and 100 nm. However, nanoparticles smaller than 100 nm exhibit enhanced adsorption [20, 21]. This nanoscale effect was also noticed by

Hengzhong et al [22], it was found that particles smaller than 100 nm have high susceptibility to adsorb molecules. This enhanced reactivity presented by nanoparticles is the result of large surface area, and hence, greater density of active sites [23]. Figure 4.1 illustrates the relation between the exposed surface area per gram of particles and the particle diameter. As can be observed, the surface area of the particles remains almost constant for particles with diameter above 100 nm. However, when the particles diameter decreases to less than 100 nm, the surface area per gram of particles rapidly growth (see inset Figure 4.1).

The synthesis of iron oxide nanoparticles is widely reported in the literature [24-26]. However, most of these techniques employ voluminous chemicals such as surfactants, chelating agents and organometallic compounds that have a poor diffusion into the activated carbon pores [24-26]. Therefore, thermal hydrolysis is a methodology that allows the generation of iron oxide nanoparticles without the addition of more chemicals, allowing the synthesis of particles inside the activated carbon pores. The thermal hydrolysis is a simple method for the generation of uniform colloidal metal oxides/hydroxides. This methodology consists in increasing the temperature of a solution that contains the metal cation, this promotes the agglomeration of metal ions until the formation of a solid phase [27]. If the iron hydrolysis is carried out inside the pores of the activated carbon, it is expected that part of the iron particles will be attached to the carbon surface. Recent studies have employed the thermal hydrolysis methodology to anchor iron oxide particles onto the activated carbon surface [28], however, the effect of the production conditions in the arsenic adsorption capacity and the size of the anchored particles have not been studied, being these important features in the adsorption capacity of metal oxides. According with the previous, the objective of the present study is to find the optimal production conditions to anchor iron oxide nanoparticles onto three different activated carbons, employing the thermal hydrolysis methodology, in order to generate a material with competitive arsenic adsorption capacity.

It is to be mention that the first part of this chapter includes the results from the surface response methodology as a first approach to determine the production conditions that allow anchoring iron oxide/hydroxides on each activated carbon: selected samples were analyzed in order to study more in detail the anchorage procedure and the effect of the production conditions. Finally, based on the results obtained in the first experimental design, the production parameters were modified to optimize the anchorage procedure for each activated carbon.

4.1.1 Iron precipitation by thermal hydrolysis
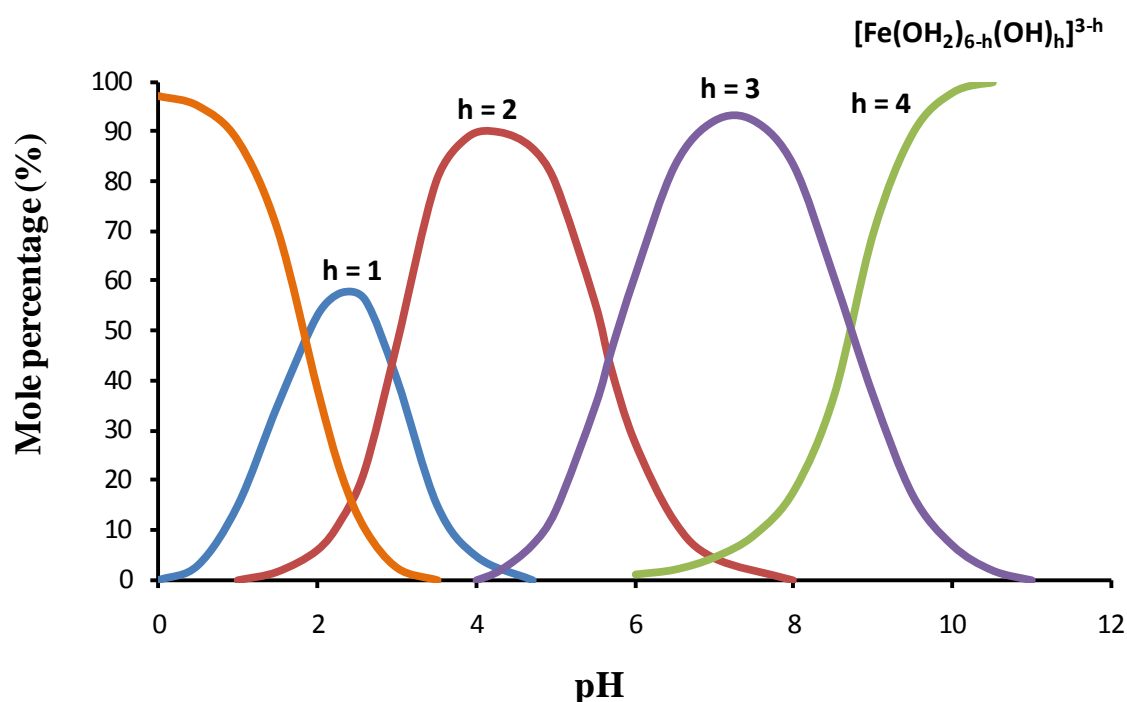
Figure 4.2. Speciation of hexa aquo iron complex of Fe(III) in water solution.

Metal cations in aqueous solution are surrounded by water molecules, generating aquo coordinated complexes that lead to form $[M(OH_2)_n]^{z+}$ species. In aqueous solution, Fe (III) forms hexacoordinated aquo complexes (n=6), whose electric charge is a function of pH (Figure 4.2) [29, 30].

These metal complexes can be hydroxilated by the addition of a base, promoting ligand exchange reactions (Equation 4.1). However, the hydrogen bond network in the liquid ensures fast diffusion paths for the proton and the HO^- ions, so that the reaction may proceeds through a direct attack of the aquo ligand by the hydroxyl group (Equation 4.2)

$$M(OH_2)_n^{Z+}+HO_{aq}^- \rightarrow M(OH)(OH_2)_{n-1}^{(z-1)+}+H_2O \qquad (4.1)$$

$$(4.2)$$
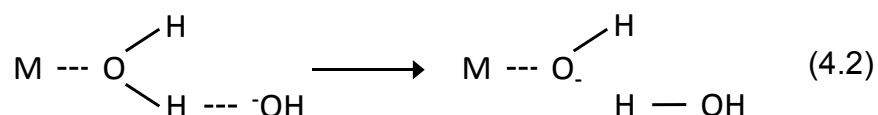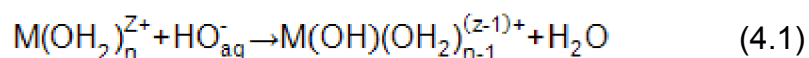
This reaction can proceed until the metal hydroxilated complex acquires a neutral charge (balanced by substitution of aquo ligands by ^-OH groups), then, the repulsion forces between the metal ions disappear, and begin to condense. The kinetics of this neutralization reaction is extremely fast [30], generating an amorphous gel. This unstable gel crystallizes more or less rapidly performing different crystalline phases depending on the acidity of the medium. In such a case the particle size is very heterogeneous by the overlap of nucleation and growth kinetics in the solid phase formation [31].

In contrast when the precipitation of metal oxides is promoted by the increase of temperature (thermal hydrolysis, also called forced hydrolysis) a different crystal formation mechanism occurs. Under thermal hydrolysis the hydroxylation is carried out by the water molecule:

$$M(OH_2)_n^{z+} + hH_2O \rightarrow M(OH)(OH_2)_{n-h}^{(z-h)+} + hH_3O^+ \qquad (4.3)$$
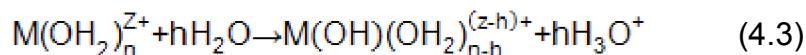
for this reaction [30]

$$\Delta H^o = (75.2 - 9.6z) \text{kJ/mol} \qquad (4.4)$$
$$\Delta S^o = (-148.4 + 73.1z) \text{J/mol} \qquad (4.5)$$

having that the free energy of reaction comprises an enthalpy and entropy contribution:

$$\Delta G^o = \Delta H^o - T\Delta S^o \qquad (4.6)$$

The free energy of the hydrolysis reaction as a function of the cation electric charge at 298 K can be expressed as follow:

$$\Delta G^o_{298} = (119.5 - 31.35z) \text{kJ/mol} \qquad (4.7)$$

where z is the cation electric charge. The reaction is spontaneous ($\Delta G < 0$) for metal ions of electric charge equal or greater than 4. Therefore, at room temperature, tetravalent elements do not exist as purely aquo complexes, even in a strongly acidic medium. For elements with a charge z smaller than 4, ΔG becomes negative only if the temperature is higher than 298K. Therefore it is necessary to heat the solution in order to carry out hydrolysis of Fe(III) cations, since z=3. Iron is characterized by the wide number of iron oxy hydroxides crystals that can be formed. From a thermodynamic point of view, the formation of hematite (α-Fe_2O_3) is the most favored reaction (see Figure 4.3). However, the Gibbs free energy of the iron oxy hydroxide formation is strongly influenced by the iron complex precursor.
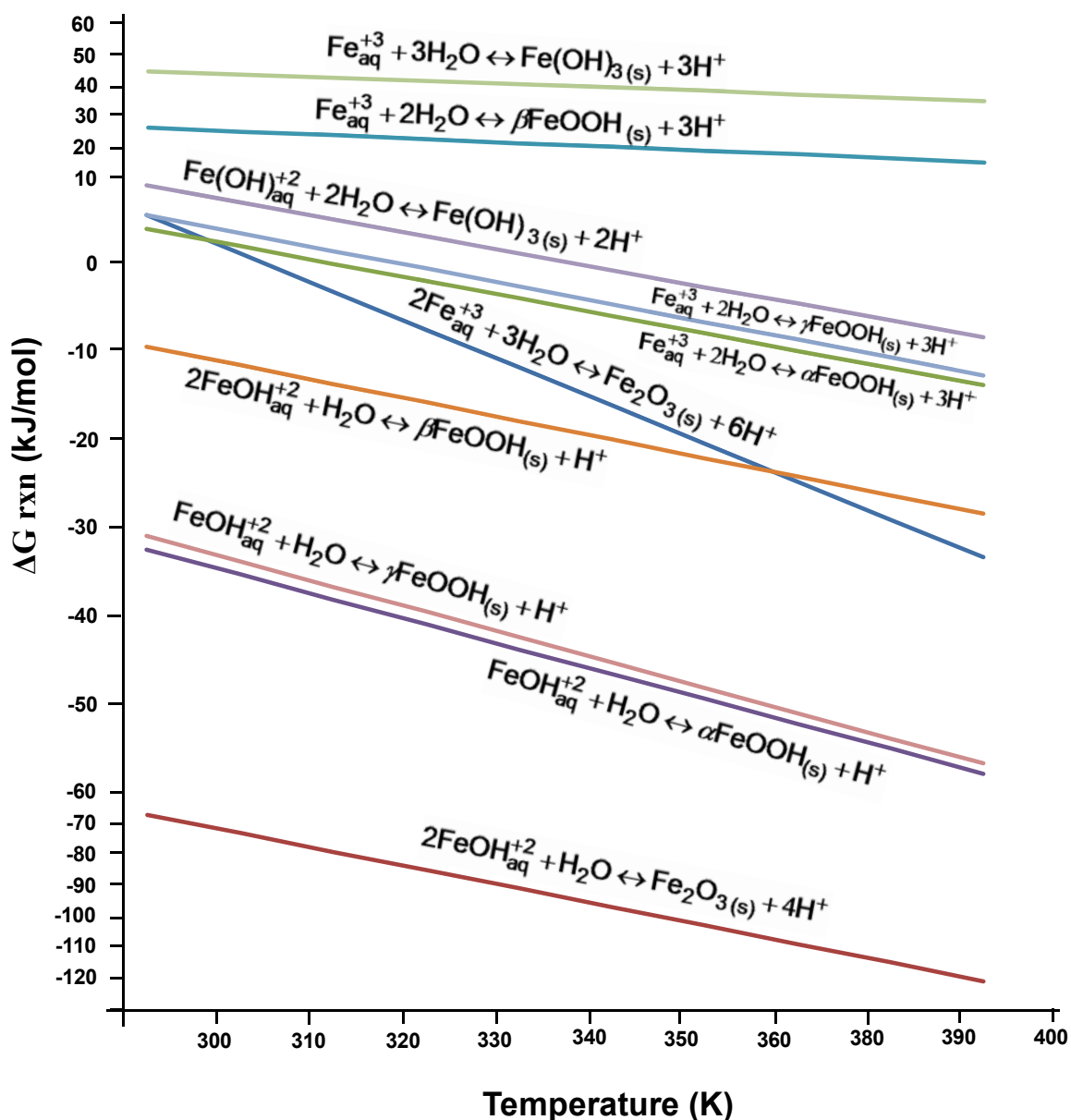
Figure 4.3. Reaction temperature effect onto the Gibbs free energy of iron oxide hydroxide formation from $Fe^{+3}(Fe(H_2O)_6^{+3})$ and $FeOH^{+2}$ $(FeOH(H_2O)_5^{+2})$ iron complexes. The crystalline phases considered are: hematite (Fe_2O_3), gohetite (α- $FeOOH$), akaganeita (β- $FeOOH$), lepidocrocite (γ- $FeOOH$) and ferrhydrite ($FeOOH_{am}$). Linear relations between ΔG and reaction temperature were calculated according to equation 4.8, and thermodynamic data from Cornell et al [32] and Stumm et al [33]. It was supposed that the entropy and enthalpy of reactions are independent of the temperatures (constant specific heat, Cp)

As previously mentioned, the precipitation of metal cations by the addition of a base generates large agglomeration of poorly crystalline iron oxi hydroxides, mainly by the fast kinetic of the hydroxyls in aqueous solution.
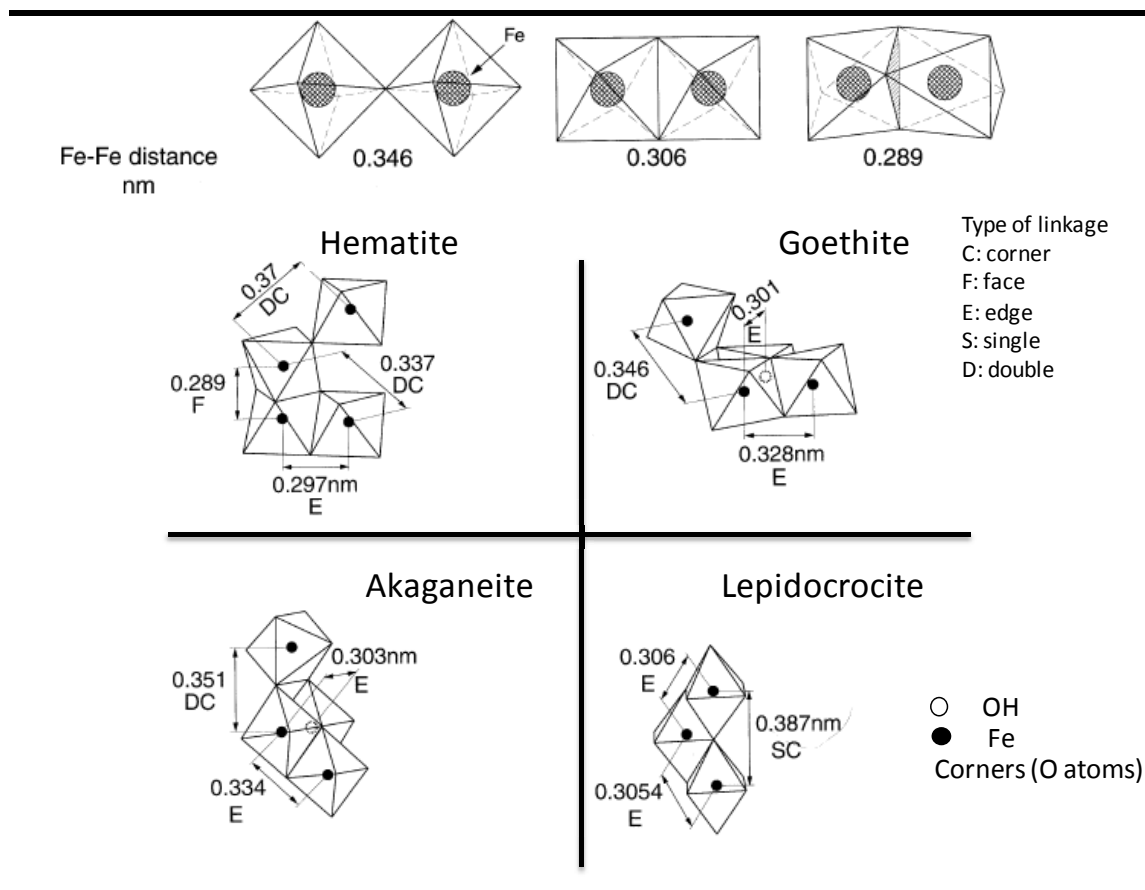
Figure 4.4. Different linkages between octahedic Fe(III) and the basic structural units for hematite, goethite, akaganeitte and lepidocrocite. Modified from Cornell et al [32]

In contrast, when precipitating iron oxi hydroxides by thermal hydrolysis, the slow speed of formation of the hydrolyzed compounds allows decoupling the nucleation and growth steps of the crystal formation, generating narrow particle size distribution [31]. This effect is used to generate iron oxides with a narrow particle size distribution in the nanoscale range, being a practical and inexpensive methodology.

As can be observed in Figure 4.3, there are several iron oxide structures that can be formed under thermal hydrolysis of Fe(III) cations. The common building unit for all Fe hydroxides is the $FeO_3(OH)_3$ octahedron (see Figure 4.4). The spatially arrange of this basic units define the different iron hydroxides. Similary, the iron oxides are conformed by FeO_6 octahedrons (Figure 4.4).

4.2. MATERIALS AND METHODS

4.2.1. Anchorage procedure

The precipitation of iron oxides by thermal hydrolysis of Fe(III) ions in aqueous media depends on several factors, including the iron salt precursor, the iron concentration, pH, the presence of complexing agents, the hydrolysis temperature and the hydrolysis time [34]. In order to study the influence of the production parameters on the particles anchorage onto activated carbon, and hence on the adsorption capacity, different samples were prepared according to the central composite experimental design (CCD). Table 4.1 shows the experimental conditions at which the samples were generated. The variables studied were the iron concentration of the solution in which the hydrolysis took place (C_{Fe}: 0.3 to 3.67 mol/L), hydrolysis time (Ht: 4 to 14 hours) and hydrolysis temperature (T: 70 to 120 ºC). The general procedure followed the next steps: (1) 200 mg of activated carbon of U.S. mesh no. 100/140 (148–105 μm) were placed in contact with 10 mL of $FeCl_3$ solution ($FeCl_3$ $6H_2O$, 97% ACS grade from Fermont) inside a sealed glass container; (2) the mixture was mixed for 24 hours at 25 ºC to allow the diffusion of iron into the pores; (3) thermal hydrolysis was carried out by placing the containers in a preheated furnace at the corresponding temperature and during the selected hydrolysis time, according with the experimental design; (4) after that the samples were rinsed with distilled water until the elimination of all the soluble iron and the iron particles that were not anchored to the carbon surface.

Table 4.1. Experimental design and the responses obtained.

Run	C_{Fe} (mol/L)	T (°C)	Ht (hours)	F400 Q_{As} (mg/g)	F400 Fe %	ACZ Q_{As} (mg/g)	ACZ Fe %	ACP Q_{As} (mg/g)	ACP Fe %
1	1 (-1)	80 (-1)	6 (-1)	3.31	0.73	0.72	1.66	3.27	5.27
2	1 (-1)	110 (+1)	12 (+1)	2.55	1.51	1.31	2.28	1.17	2.99
3	3 (+1)	80 (-1)	12 (+1)	3.34	0.86	1.03	3.84	0.82	2.64
4	3 (+1)	110 (+1)	6 (-1)	3.13	1.12	1.25	4.36	0.81	3.61
5	2 (0)	95 (0)	9 (0)	3.21	1.02	1.06	3.01	1.00	3.01
6	1 (-1)	80 (-1)	12 (+1)	2.81	0.89	0.90	1.72	0.89	2.44
7	1 (-1)	110 (+1)	6 (-1)	2.59	1.05	1.80	1.86	1.23	2.44
8	3 (+1)	80 (-1)	6 (-1)	3.48	0.79	0.73	3.23	0.62	3.12
9	3 (+1)	110 (+1)	12 (+1)	3.16	1.07	1.11	4.63	0.94	3.36
10	2 (0)	95 (0)	9 (0)	3.16	0.98	0.93	3.15	0.87	3.19
11	0.3 (-1.6)	95 (0)	9 (0)	3.20	2.20	0.45	0.92	2.54	2.23
12	3.7 (+1.6)	95 (0)	9 (0)	3.05	1.10	1.05	3.91	0.87	3.13
13	2 (0)	70 (-1.6)	9 (0)	3.55	0.78	0.42	2.42	0.75	2.18
14	2 (0)	120 (+1.6)	9 (0)	3.02	1.23	1.42	4.00	0.92	3.48
15	2 (0)	95 (0)	4 (+1.6)	3.26	0.90	0.73	2.75	0.82	2.97
16	2 (0)	95 (0)	14 (+1.6)	4.44	1.31	1.37	4.12	1.13	3.07
17	2 (0)	95 (0)	9 (0)	3.62	1.07	0.99	3.10	0.89	3.01

C_{Fe}: iron concentration

T: Hydrolysis temperature

Ht: Hydrolysis time

Q_{As}: Arsenic adsorption capacity

Fe%: Iron content of the modified carbons

Finally the modified carbons were dried at 100 ºC for 24 hours. With the aim to study the effect of surface chemistry on the anchorage procedure, three different activated carbon were tested: Filtrasorb 400 activated carbon from Calgon, which is made from bituminous coal under physical activation (F400); agave bagasse based activated carbon produced by chemical activation with $ZnCl_2$ (ACZ) and agave bagasse based activated carbon produced by chemical activation with H_3PO_4 (ACP). The main characteristics of the studied activated carbons are reported in Table 4.2.

Table 4.2. **Activated carbon characteristics.**

Carbon	BET S.A. (m^2/g)	V_{micro} (cm^3/g)	V_{meso} (cm^3/g)	V_{total} (cm^3/g)	Ash (%)[a]	C (%)	O (%)[b]	P (%)	Acid groups (mmol/g)[c]	Basic groups (mmol/g)[c]	pH$_{PZC}$
F400	896	0.340	0.104	0.451	7.1	82.3	9.4	ND	0.23	0.33	8.9
ACP	1058	0.231	0.223	0.488	0.3[a]	69.1	24.6	5.3	1.52	ND	2.7
ACZ	806	0.202	0.052	0.257	0.5	76.8	21.7	ND	2.32	0.05	2.3

ND: No detected

[a] Calculated from the inorganic content of the calcinated sample

[b] By difference, taking into account the ash content (minor components are not included in the table)

4.2.2. Materials characterization

Iron content and single point adsorption experiments were determined for all samples. Iron was determined by atomic absorption spectroscopy (PerkinElmer AAnalyst 400), after acid digestion as follow: approximately 40 mg of activated carbon were mixed with 20 mL of $HNO_3:H_2SO_4$ (5:1) solution (Fermont 70% ACS grade and J.T. Baker 98% ACS grade, respectively); then the mixture was digested by 1 hour at 150 °C in a microwave advanced digestion system (Milestone, Ethos 1); finally, the remaining solution was diluted to 50 mL with deionized water in a volumetric flask and analyzed by absorption spectroscopy at a wavelength of 271.9

nm. Selected samples were evaluated by triplicate to evaluate the accuracy of the method. The standard deviation of the iron content did not exceed 5% of the mean value. The arsenic removal was assessed in batch systems at constant temperature and pH (25 °C and 7, respectively). Temperature was kept constant in an orbital incubator (PRENDO inov6507) and the pH was measured with a glass microelectrode (semi micro electrode Orion 911600, Orion 2-Star Bench top pH Meter). Samples of 25 mg of activated carbon were added to 12 mL of As (V) solution (Na_2HAsO_4 $7H_2O$ 99.995% trace metal basis, Aldrich), prepared from arsenate salt at high concentrations (10 ppm As) in order to obtain adsorption values near to the maximum adsorption capacity. These experiments were stirred at 150 rpm. The solution pH was adjusted daily to pH 7 by adding 0.1 M NaOH and/or 0.1 M HCl until the equilibrium was achieved. After 5 days, the samples were centrifuged and the supernatant was analyzed for arsenic and iron by an inductively coupled plasma spectrometer. The concentration of arsenic adsorbed was calculated by the difference between the initial and residual amounts of arsenic in solution divided by the weight of the adsorbent. The average particle size and the morphology of the anchored particles were determined by direct measurement in scanning electron micrographs (SEM, FEI XL30SFEG) and X-ray diffraction (powder patterns, XRD D8 Advance–Bruker Axs, with Cu Kα radiation λ=1.54060 Å). The diffraction patterns were obtained with a step time of 10 seconds and a step size of 2θ=0.02°. The particle size distribution was determined considering the diameter of 300 particles, measured on diverse micrographs employing the Image J software. The average particle size was obtained from three crystalline peaks using the X-ray diffraction data and the Debye - Scherrer equation:

$$D=\frac{K\lambda}{\beta \cos \Theta} \qquad (4.8)$$

where D is the average particle size in Å, K is a constant near to 1, λ is the wavelength of the Cu Kα radiation, Θ is the diffraction angle and β is the full width

at half maximum intensity of the peak. The quantity of basic and acid groups were determined by neutralization with HCl and NaOH respectively as follow: 10 mL of 0.1M volumetric solution (from J.T. Baker 0.1N ± 1ppm) was mixed with 0.1 g of activated carbon. The mixture was mechanically shaken by 96 hours. Samples were evaluated by triplicate, reporting the average value of the measures. After the equilibration period, an aliquot of the supernatant liquid was then back-titrated by the addition of 25 μL (eppendorf adjustable-volume pipette 10-100 μL, accuracy ±1%) with hydrochloric acid or sodium hydroxide. The chemical groups were calculated by the difference between samples and blank. Finally, the BET surface area and pore size distribution of the selected samples were measured by nitrogen adsorption isotherm at -196 °C employing a Micromeritics ASAP 2020 equipment.

4.2.3. Data analysis

The response surface methodology was employed to determine the optimal production conditions that maximize the arsenic adsorption capacity of the modified carbons. As previously mentioned, the production variables studied are the iron concentration (C_{Fe}), hydrolysis temperature (T) and hydrolysis time (Ht). The properties of the carbon that were analyzed as response variables are the arsenic adsorption capacity (Q_{As}, mg As/g) and the iron content (Fe%). STATISTICA 7.0 was used to conduct the regression analyses, employing the standard deviation, the correlation coefficient and the lack of fit test as statistical parameters to validate the model.

4.3. RESULTS AND DISCUSION

4.3.1. Statistical model analysis

The central composite experimental design employed in this research was selected to calculate the production conditions that produce the activated carbon with the maximum arsenic adsorption capacity. Also, the evolution of the iron content on the

modified carbons was studied. The complete design matrix together with the values of both responses is reported in Table 4.1. These results were analyzed according with the response surface methodology in order to find the coefficients (β) that adequately represent the relation between the production conditions (X: C_{Fe}, Ht and T) and the responses (Y: Q_{As} and Fe%). For both responses, a quadratic model was selected, (Equation 3.2).

$$Y = \beta_0 + \sum_{i=1}^{k} \beta_i X_i + \sum_{i=1}^{k} \beta_i X_i^2 + \sum_{\substack{i=1 \\ i<j}}^{k} \sum_{j=1}^{k} \beta_{ij} X_i X_j \qquad (3.2)$$

The model adequacy was evaluated according with four statistical parameters: test of significance (evaluated by each factor and interactions expressed on equation 3.2), lack of fit test, correlation coefficient and the standard deviation. All the terms included in the final equation (response surface) have a p-value lower than 0.05, which means that the included terms are statistically significant with a confidence level of 95%. Table 4.3 shows the models significance, correlation coefficient and the standard deviation resulting after the statistical analyses of both responses (Q_{As} and Fe%) by the three modified carbons after discarding insignificant terms (terms with p-value > 0.05). The lack of fit test (LOF) describes the variation of the data around the fitted model. If the model does not fit well the data, the p-value of the LOF test will be higher than 0.05 and hence another model (ei: linear, lineal + interactions, pure quadratic) must be employed. The P values for LOF (< 0.05 or near) presented in Table 4.3 show that the selected models adequately represents the data.

The R^2 coefficient gives the proportion of the total variation in the response predicted by the model. R^2 values closer to one are desired to have an accurate prediction of the responses by the model. According with our results the lower value of R^2 was 0.703, which means that at least 70.3 % of the total variation in the responses was attributed to the experimental variables studied. Finally, the

standard deviation was calculated employing the data obtained at the central points of the experimental design (runs 5, 10 and 17, see Table 4.1), because these samples are produced at the same production conditions. As can be observed in Table 4.3 the standard deviation does not exceed 10 % of the mean value by each response.

Table 4.3. **Results of statistical test to validate the models that describe Q_{As} and Fe% as a function of the production conditions.**

Carbon	F-400		ACZ		ACP	
Test / Response	Q_{As}	Fe %	Q_{As}	Fe %	Q_{As}	Fe %
LOF (p-value)	0.0020	0.0287	0.0550	0.0556	0.0265	0.0229
Correlation coefficient (R^2)	0.7030	0.7209	0.7155	0.9762	0.8198	0.7333
Standard deviation [a]	0.024	0.044	0.063	0.070	0.072	0.103

Q_{As}: arsenic adsorption capacity (mg As/g)   [a] Expressed according to the analyzed response

Fe %: Iron content (%)   LOF: Lack of fit test

Table 4.4 reports the calculated regression coefficients (β) after elimination of insignificant terms for both responses (Q_{As} and Fe%) in the three activated carbon tested. These coefficients can be substituted directly in equation 3.2 to predict the response at some specific experimental conditions. Also, this equation can be used to determine the experimental conditions that generate a desired response.

.

Table 4.4. Final regression coefficients in terms of coded and uncoded factors.

Carbon	F-400				ACZ				ACP			
Term / Response	Q_{As}		Fe %		Q_{As}		Fe %		Q_{As}		Fe %	
	UCD	CD	UCD	CD	UCD	CD	UCD	CD	UCD	CD	UCD	CD
Constant	5.08	3.21	-2.26	0.36	-4.43	0.96	1.15	3.09	14.6	0.92	18.3	3.07
C_{fe}	0.02	0.23	-0.62	0.37	0.73	0.06	0.95	**1.99**	-4.27	**-0.91**	-3.26	0.16
C_{fe}^2	-0.11	-0.21	0.17	0.35	-	-	-0.26	-0.51	0.29	0.57	-	-
T	0.01	**-0.35**	0.07	0.05	0.06	**0.55**	-0.02	0.78	-0.10	-0.17	-0.14	0.16
T^2	1E-4	-0.11	1E-3	0.13	-	-	1E-3	0.06	-	-	-	-
Ht	-0.47	0.20	0.09	0.05	0.17	0.13	-0.17	0.54	-0.86	-0.24	-1.15	-0.42
Ht^2	0.02	0.30	-	-	8E-3	0.14	1.2E-3	0.22	-	-	-	-
$T*C_{fe}$	4E-3	0.11	-	-	-7E-3	-0.22	0.01	0.30	0.02	0.52	0.03	0.87
T*Ht	0.02	0.11	-	-	-3E-3	-0.28	1.7E-3	0.10	0.12	0.69	0.06	0.39
$C_{fe}*Ht$	2E-3	0.16	-0.03	**0.53**	-	-	1E-3	9E-3	0.01	0.56	0.01	**0.90**

UCD: coefficients based on uncoded terms

CD: coefficients based on coded terms

Terms in bold denote the production variable

 with high impact in the response

C_{Fe}: $FeCl_3$ concentration

T: Hydrolysis temperature

Ht: Hydrolysis time

Q_{As}: Arsenic adsorption capacity

Fe%: Iron content of the modified carbons

On the other hand, the reported coefficients in Table 4.4 (coded values) can be used as a measurement of the effect of each factor. The terms in bold denote the production variables that had high impact in the evaluated response. Accordingly, the Fe% in the carbons is more influenced by the iron concentration of the hydrolysis solution (C_{Fe}). For iron modified ACP activated carbon (ACP-Fe) and iron modified F400 activated carbon (F400-Fe) the hydrolysis time (Ht) has a considerable influence, since the interaction term C_{Fe}*Ht has the highest effect. For the three carbons, the variables previously mentioned display a positive effect, which means that a high C_{Fe} promotes the anchorage of iron particles onto the carbon surface. This results can be explained as follow: the precipitation of iron by thermal hydrolysis is leaded by the addition of metal ions. Previous studies have demonstrated that once the nucleus is formed, the addition reaction is fast, and is controlled by the diffusion of metal ions [31]. At high iron concentration, the number of molecules that can diffuse to precipitate on the carbon surface is greater than at low iron concentration. This can be the reason why the iron concentration is the factor that controls the iron content of the modified carbons.

On the other hand, hydrolysis temperature (T) is the production variable that most influences the arsenic adsorption capacity of the iron modified ACZ activated carbons (ACZ-Fe). In contrast the ACP-Fe carbons are more influenced by the iron concentration. The arsenic removal by the modified activated carbons depends on size and availability of the iron oxides. In this sense it is expected that high hydrolysis temperatures for ACZ carbons and low iron concentrations for ACP carbons favor the anchorage of iron nanoparticles. For modified F400 activated carbon there is not a predominant variable that influences Q_{As}: the effect of each term has a similar value. Further characterization of the anchored particles to the carbon surface is needed in order to generate a correlation between the production variables and the arsenic adsorption capacity

4.3.2. Effect of production conditions on the carbons iron content

Figure 4.5 shows the response surfaces that describe the evolution of iron loaded onto the carbons regarding the hydrolysis conditions: contour plots are also included for each graph. As it can be observed in Figure 4.5 A and B the iron content of F400-Fe carbons slightly increased as T increased. On the other hand the iron content of the carbon follows a parabolic tendency in relation to C_{Fe}, being the extreme values (low and high C_{Fe}) the conditions at which the iron content of the carbons increased. On the other hand, as can be seen in Figure 4.5 C and D, C_{Fe} is the production variable that dominated the loading of iron for ACZ-Fe carbons. Also, it can be seen that T has effect just at high C_{Fe}. Finally, the iron content of the ACP-Fe samples increased as both production variables, C_{Fe} and T, increased (Figure 4.5 E and F).

Figure 4.5 also shows that the iron content of ACZ-Fe and ACP-Fe carbons was superior to the iron content of F400-Fe activated carbons. The iron content of ACZ-Fe carbons ranged from 0.92 to 4.63 %, from 2.18 to 5.27 % for ACP-Fe carbons and from 0.73 to 2.2 % for F400-Fe activated carbons. The main difference between the carbon samples used in this research is the surface chemistry. F400 activated carbon is a slightly basic carbon with low content of oxygenated surface groups (5.9 mmol O / g Carbon). On the other hand, ACZ and ACP carbons are acid carbons with a considerable amount of oxygenated surface groups (13.6 and 15.4 mmol O / g Carbon, respectively). These results suggest that the oxygenated surface groups promote the anchorage of iron onto the carbons surface. It can be explained as a function of the reaction mechanism by which the iron oxides are formed under thermal hydrolysis.
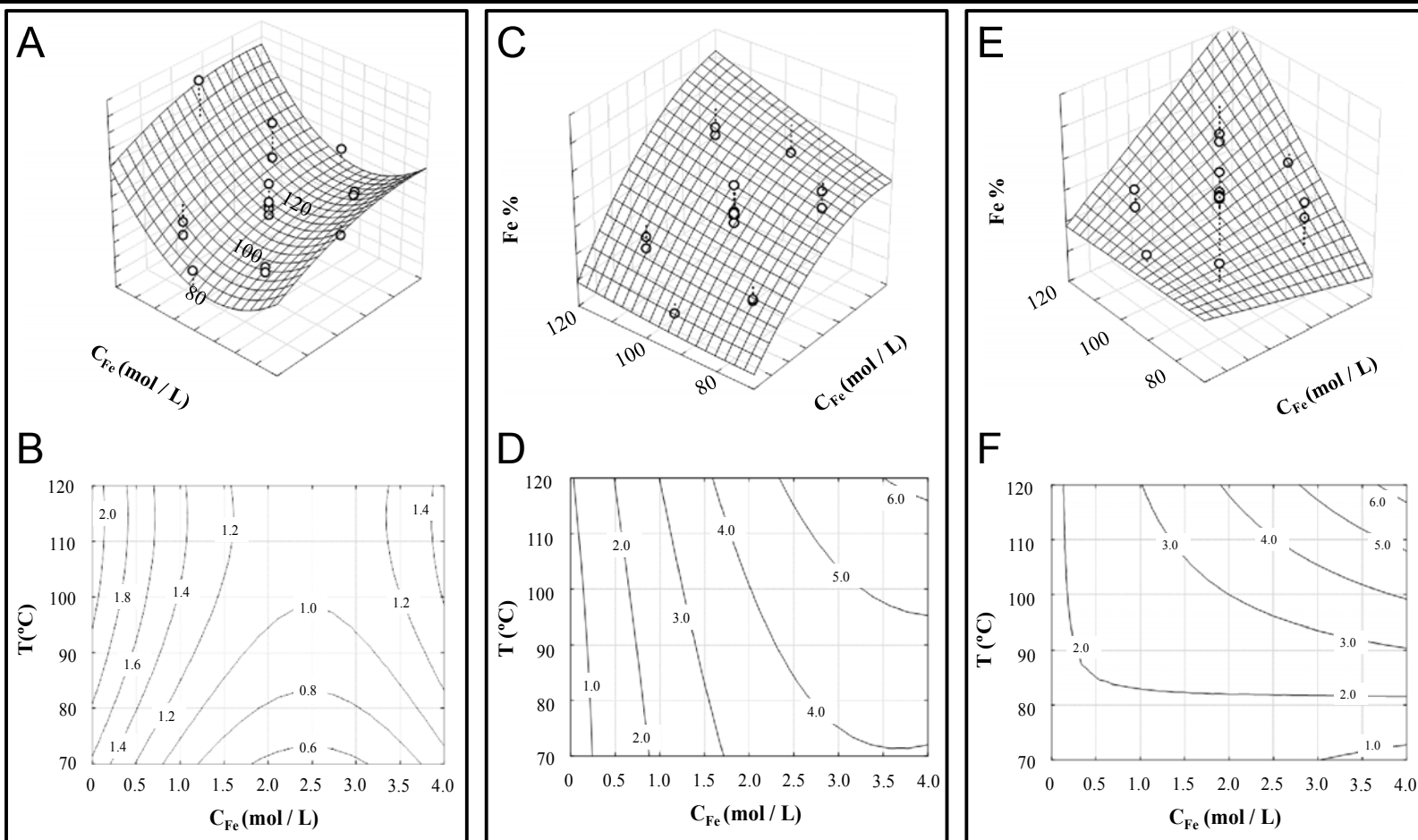
Figure 4.5. Surface responses and contour plots that show the effect of iron concentration (C_{Fe}) and hydrolysis temperature (T) in the iron content (Fe %) of the modified activated carbons:F400 (A and B); ACZ (C and D);and ACP (E and F). The hydrolysis time was kept constant at the optimal value: 4 hours for F400 and 14 hours for ACP and ACZ carbons.

As previously mentioned, the formation of the iron oxide crystals by the thermal hydrolysis is leaded by the neutralization of the metal aquo complex by water molecules (equation 4.3).
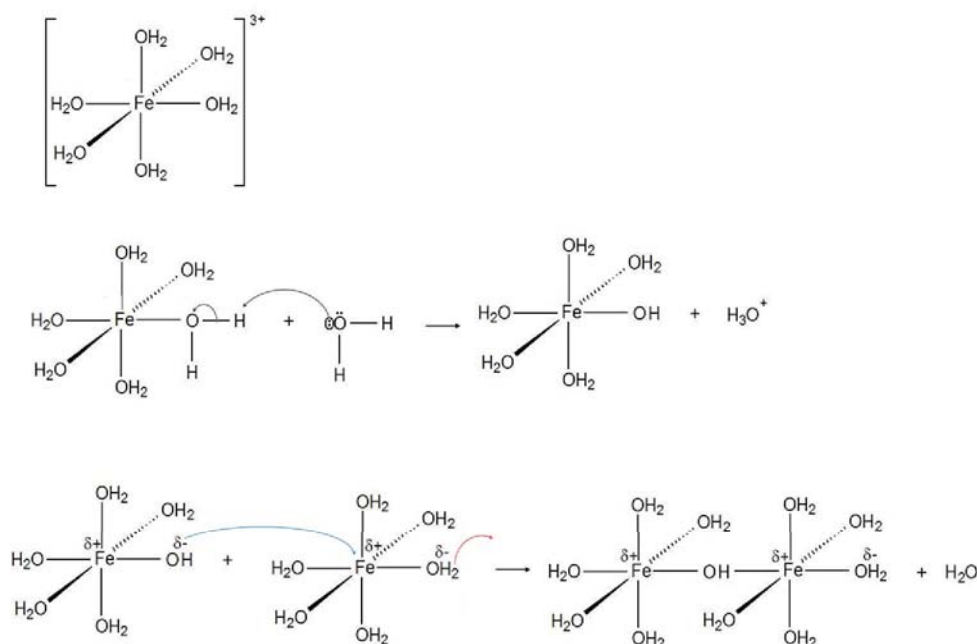
Figure 4.6. Mechanism of the condensation reacionts (A) Chemical structure of Fe(III) in aqueous solution, performing hexa-aquo complexes. (B) Initiation: deprotonation mechanism of hexa-aquo iron complexes. (C) Propagation: olation mechanis by which iron complexes begin to condense.

This is the first step in the so called condensation reaction of crystal formation (Figure 4.6 B) [35]. Once the $[Fe(OH)(OH_2)_5]^{2+}$ is formed, the hydroxo ligand can acts as a nucleophile that can react with other aquo complex eliminating an aquo ligand and performing an hydroxo bridge between the metal cations. This reaction is often called "olation" by the formation of an "ol" bridge between the metal cations (Figure 4.6 C). As the oxo bridge is more stable than the hydroxo ligand, furher deprotonation can occur to generate the oxo bond characteristic of the condensed

metal oxides. Finally, the condensation of hydroxylated complexes ends as soon as the conditions allowing nucleophilic substitution are no longer present. Because condensation causes water elimination, the change in composition of the reaction product modify its average electronegativity, causing chare redistribution within its structure and, therefore, a change in the reactivity of the functional groups. Hence, OH ligands in the crystal agglomerations may lose their nucleophilic character and cations may lose their electrophilic character [32].
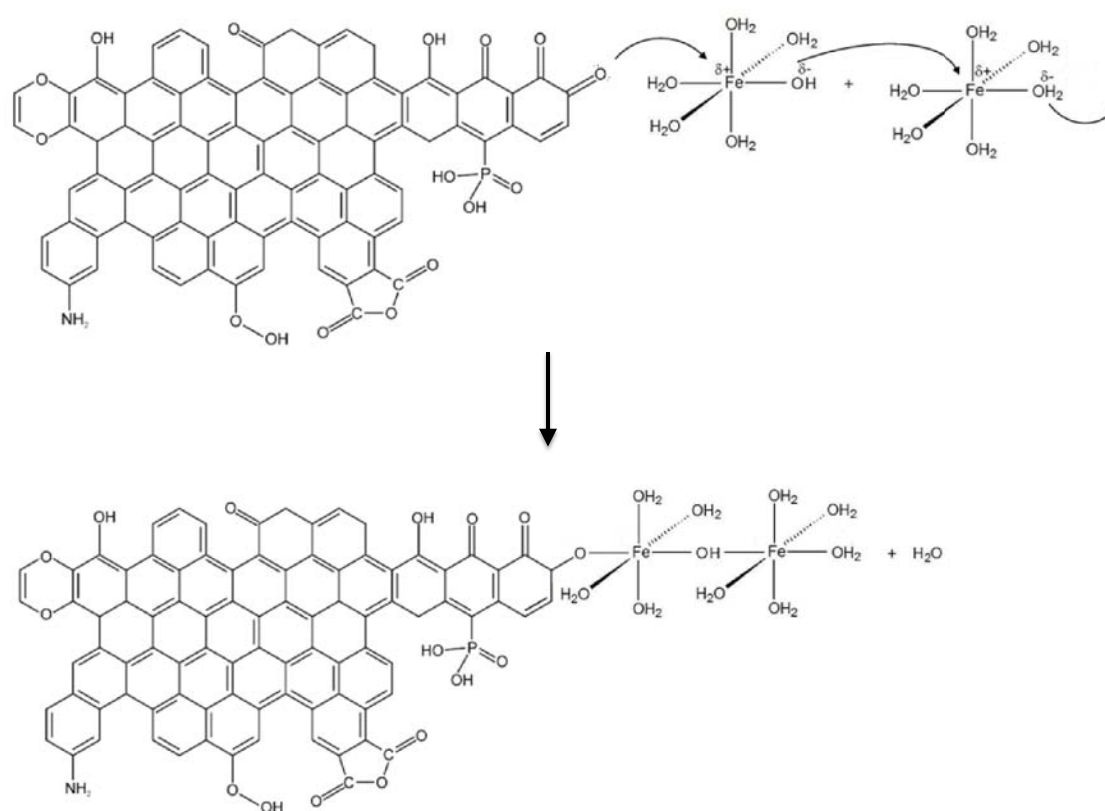
Figure 4.7. Proposed mechanism of the iron hydrolysis in presence of activated carbon. The oxygenated surface groups promote the water elimination and the later agglomeration of iron clusters.

The hydrolysis reaction is initiated by (OH) groups, generated during the deprotonation of $[Fe(OH_2)_6]^{+3}$ complexes. When the thermal hydrolysis is carried

out in the presence of activated carbon, we propose that the oxygenated surface groups can be part of the hydrolysis reactions. The delocalized electrons in the graphite structure and mostly the free electrons found in the oxygenated surface groups of activated carbon can act as a nucleophilic specie, and hence initiate the hydrolysis mechanism (Figure 4.7). This could generate a covalent bond between the carbon surface and the iron particle, allowing the anchorage of iron particles. Also, previous modifications have demonstrated that the oxidation of activated carbon before impregnation allows loading a greater amount of iron onto the carbon surface [11, 19, 28, 36].

4.3.3. Arsenic adsorption capacity

Figure 4.8 shows the response surfaces and the contour plots for the arsenic adsorption capacity of the modified carbons. The average Q_{As} for the modified samples is 3.23 mg As/g C, 1.02 mg As/g C and 1.15 mg As/g C for F400-Fe, ACZ-Fe and ACP-Fe carbons, respectively. Considering the iron content of these samples, these results were unexpected, since the carbon with less iron content (F400-Fe activated carbon) exhibits the highest arsenic adsorption capacity. In order to explain these results, adsorption capacities of untreated activated carbons were determined. These analyses showed that ACZ and ACP carbons do not have any affinity for arsenic, however F400 activated carbon showed a considerable arsenic adsorption capacity (1.3 mg As/g C). This behavior can be explained by the high ash content of this carbon (7.1%), which can interact with arsenic to be removed from the aqueous solution. It is well known that arsenic anions adsorb onto hydroxilated surfaces by the formation of inner sphere complexes [4, 37-40]. Most of the transition metal oxides generate an hydroxilated surface when they are in contact with water. This effect is attributed to the reaction between hydroxyl ions or water molecules with the surface metal atoms. This reaction is promoted because the surface metal atoms are unsaturated, hence this unoccupied orbitals can acts as a Lewis acid, that can acts with Lewis bases such as hydroxyl ions or water [32].
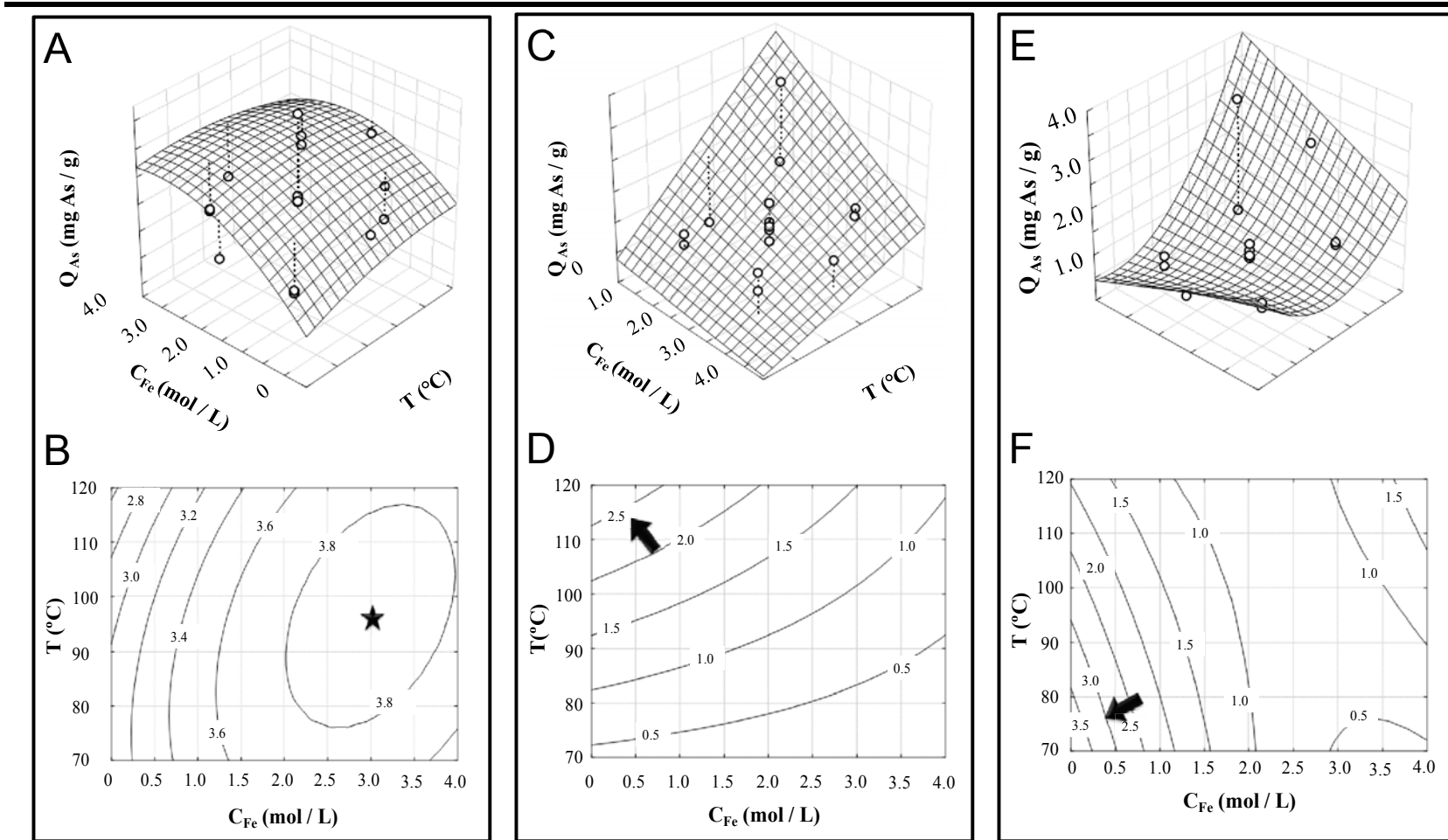
Figure 4.8. Surface responses that show the effect of iron concentration (C_{Fe}) and hydrolysis temperature (T) on the arsenic adsorption capacity (Q_{As}) of the modified activated carbons: F400 (A and B); ACZ (C and D);and ACP (E and F). The hydrolysis time was kept constant at the optimal value: 4 hours for F400 and 14 hours for ACP and ACZ carbons.

Therefore, the metal oxides that compose the ash content of F400 activated carbon can have affinity by arsenic oxo anions, removing it from the aqueous solution. This results agree with previous studies, that have found that coconut shell based carbons and bituminous carbons with high ash content (3.0 to 5.5 %) have a considerable arsenic adsorption capacity, (2.4 to 4.91 mg As/g C) [41]. Even considering the fact that the raw F400 activated carbon has a considerable arsenic adsorption capacity, the performance of the modified one can not be compared with the ACP and ACZ carbons based on iron content. The iron loaded onto ACP-Fe and ACZ-Fe samples is greater compared with the contained in F400-Fe carbons, however, this extra iron do not increase Q_{As}. It is probable that part of the iron loaded onto the ACP-Fe and ACZ-Fe was not available for arsenic removal. To illustrate this effect Figure 4.9 shows the arsenic adsorption capacity per gram of iron of all the samples generated by the three activated carbons tested. As it can be observed Q_{As} per gram of iron, follows the same tendency for the three modified carbons: as the iron content increased, the removal of arsenic per gram of iron decreased. The surface area (BET) of selected samples is also reported in Figure 4.9. As can be observed, the surface area of ACZ-Fe and F400-Fe carbons decreased for samples with high Fe%. According with the pore size distribution of raw ACZ and F400 carbons (see Table 4.2), most of the pore volume of these carbons (around 75%) are within micropores (pores with diameter < 2nm). The narrow pores contained in these carbons can be easily blocked by iron particles, decreasing their surface area. Thus, the decrease of arsenic removal is because part of the iron particles remain inside the blocked pores. Different results were observed for ACP-Fe samples: the surface area of these modified carbons decreased about 100 m^2/g in comparison with the raw ACP activated carbons. In this case it is assume that the surface area did not decrease because ACP activated carbon has a well developed mesoporous structure (see Table 4.2) at which the iron oxide particles can be supported without causing a considerable blockage of pores.
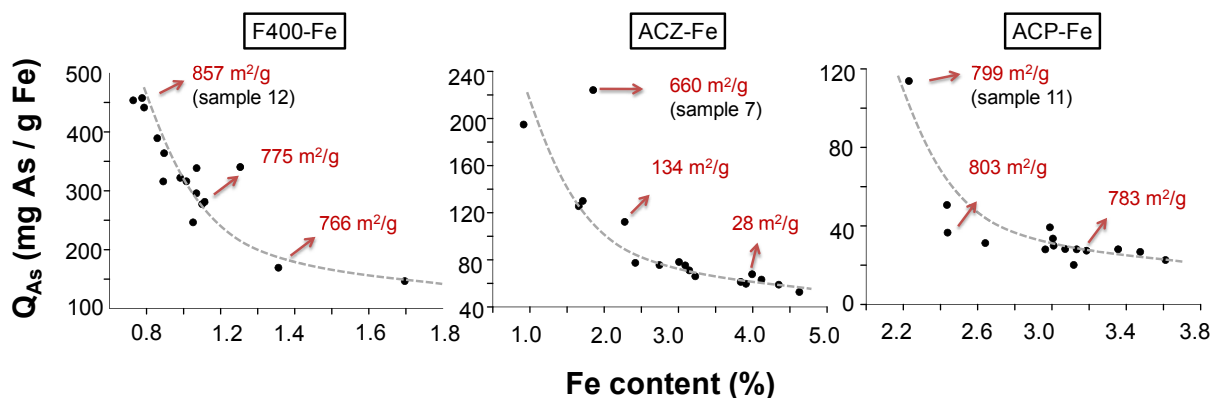
Figure 4.9. Relation between arsenic adsorption capacities per gram of iron, regarding the total iron concentration on the activated carbon.

On the other hand, if we compare Q_{As} per gram of iron (Figure 4.9) we can see that it is higher for F400-Fe activated carbons (ranged from 146 to 457 mg As/g Fe). Q_{As} per gram of iron for ACZ-Fe carbons ranged from 52 to 224 mg As/g Fe; and for ACP-Fe carbons ranged from 113 to 22 mg As/g Fe. This effect could be related to the particle size of iron oxide/hydroxides. As stated above, the removal of arsenic by iron oxides can vary according with the accessibility of the preloaded iron, but also, it can vary with the particle size of the iron oxide particles. Therefore it is expected that materials with high Q_{As} per gram of iron present small iron particles. In order to clarify these speculations, the size of the iron oxide particles of samples with high Q_{As} per gram of iron (samples 12, 7 and 11 for F400-Fe, ACZ-Fe and ACP-Fe carbons, respectively) were studied in detail by scanning electron microscopy and X ray diffraction. Figure 4.10 shows the scanning electron micrographs of these samples.
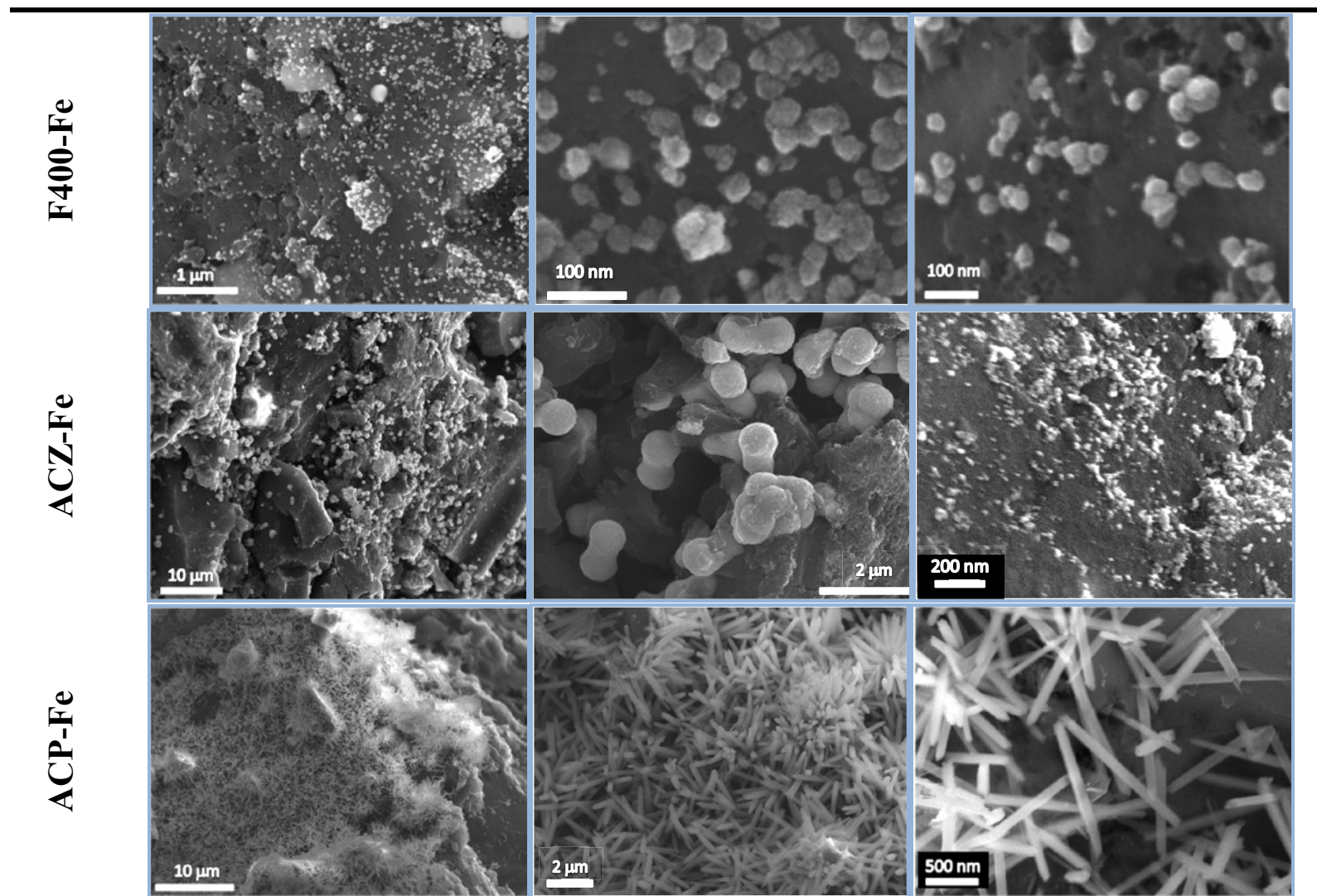
Figure 4.10. Scaning electron micrographs of selected samples. F400-Fe (sample 12); ACZ-Fe (sample 7);and ACP-Fe (sample 11).

As can be observed in Figure 4.10, the morphology and size of the iron particles differ for each material. F400-Fe activated carbon has spherical particles widely distributed on its surface. The micrographs for ACZ-Fe carbon reveals spherical and "peanut shape" iron particles with different diameters. Spherical particles have diameter below 100 nm (see Figure 4.10), since peanut shape particles have diameter up to 1 μm. Finally, ACP-Fe sample showed a very different crystal structure consisting on acicular shape iron oxide particles widely distributed all over the carbon surface. XRD analyses of these samples were performed in order to calculate the mean particle size and the crystalline structure of the iron oxide/hydroxide anchored onto the activated carbon surface. The American Mineralogist Crystal Structure Database (AMCSD) and MINDAT database (http://www.mindat.org) were employed to identify the crystal structure of the iron oxide particles anchored onto the activated carbons [42]. Figure 4.11 shows the XRD patterns of the modified activated carbons. The peaks that appear at 2θ around 24°, 33°, 36°, 50°, 54°, 62° and 64° in the diffraction pattern of ACZ-Fe and F400-Fe samples correspond to hematite crystals. Also peaks at 2θ around 69° and 27° in the ACZ-Fe, ACP-Fe and F400-Fe can be associated to the presence of Akaganeite (β-FeO (OH Cl)) iron hydroxide crystals.

XRD analyses were employed to calculate the mean particle size of the iron oxide/hydroxide particles, founding that F400-Fe carbon has an average particle size of 43.3 ± 2 nm. In contrast the average diameter of iron oxides on ACZ-Fe and ACP-Fe activated carbons were higher: the analyses showed an average particle size of 149.9±6 nm and 280 nm, respectively. In this sense the F400-Fe carbons have a higher arsenic removal since the loaded iron particles are smaller than the ones in the ACZ-Fe and ACP-Fe activated carbons.

Particularly, hematite and akaganeite are the only cystall anchored onto the activated carbon surface. According with the thermodynamic calculation of the iron oxide hydroxides formation (Figure 4.3) hematite is the crystal most favored. Also, the Gibbs free energy of these reactions is favored as the reaction temperature

increase. However this values just provide a guide to what compound may form under any particular condition, but because the kinetic of transformation of Fe oxides are often slow, meta stable phases are frequently observed and may exist over long period of time [32].
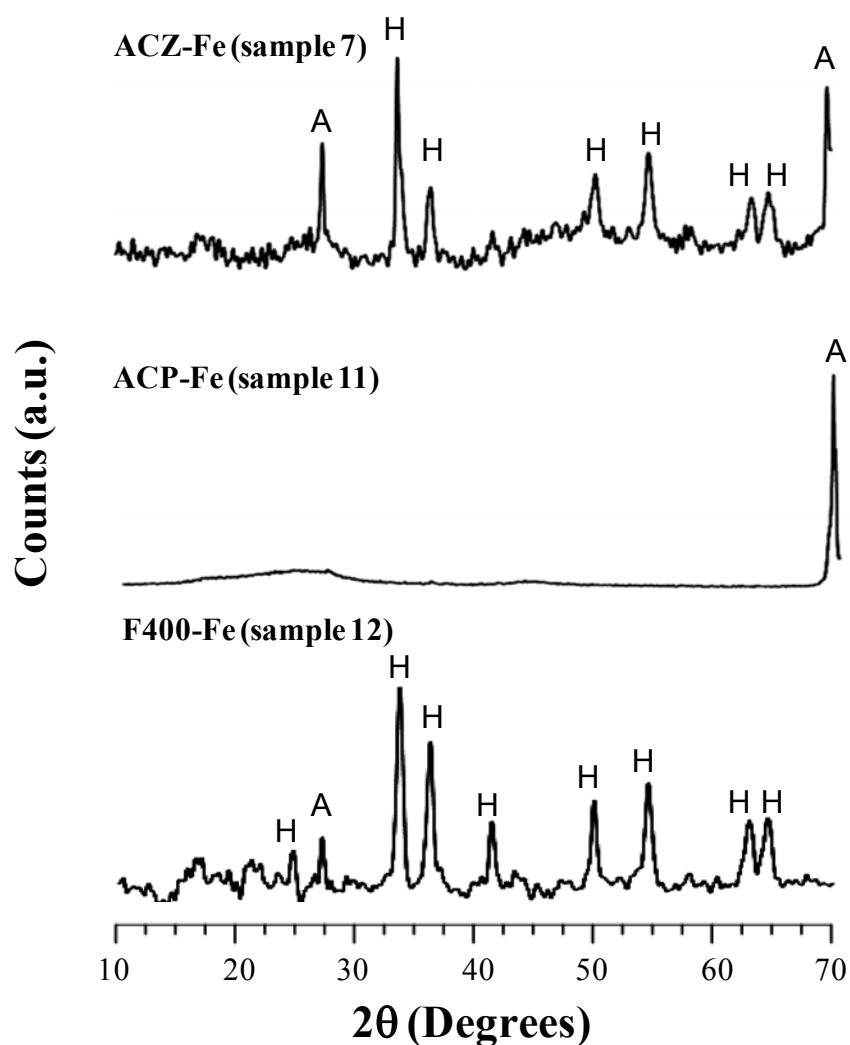
Figure 4.11. X Ray diffraction patterns of iron modified activated carbons. Labels indicate the crystal structure as follow: H: hematite (Fe_2O_3); and A: akaganeite (β-$FeO(OH\ Cl)$).

Regarding to the production conditions, the main difference between the production conditions of the samples that appear in Figure 4.10 are the concentration of $FeCl_3$ (3.7 M for F400 activated carbon, 1 M for ACZ activated carbon and 0.3 M for ACP activated carbon). This parameter conditions solution pH of our system. During the development of this research, the solution pH was not studied, hence this parameters was a function of the ions in solution. $FeCl_3$ in aqueous solution dissolve to form Fe^{+3} and Cl^- ions (equation 4.10). The solution pH is determined by the reactions that occur between the ions in solution and water molecules. Chloride ions do not react with water, since it is the conjugate base of a strong acid (HCl) and hence it remains as Cl^- ion. In contrast, ferric ions react with water to perform hydroxo complexes (equation 4.11). Once the hydroxilated comlex is formed, it can also react with water molecules (equation 4.12).

$$FeCl_{3(s)} \rightarrow Fe^{3+}_{(aq)} + 3Cl^-_{(aq)} \qquad (4.10)$$

$$Fe^{3+}_{(aq)} + H_2O \leftrightarrow FeOH^{2+}_{(aq)} + H^+ \qquad (4.11)$$

$$FeOH^{2+}_{(aq)} + H_2O \leftrightarrow Fe(OH)^+_{2(aq)} + H^+ \qquad (4.12)$$
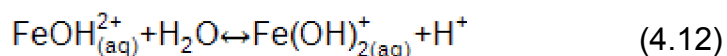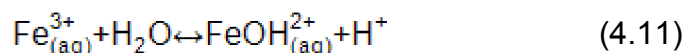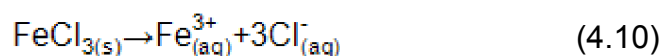
These hydrolysis reactions release protons to the media, decreasing the solution pH. Taking into account the $FeCl_3$ concentrations employed in the experiments (0.3 to 3.7 M) and the equilibrium constant of the hydrolysis of the iron ion of all the possible hydroxilated complexes [33], the solution pH ranged from 0.68 to 1.45. According with the speciation diagrams (Figure 4.2) the predominant species are Fe^{3+} and $Fe(OH)^{2+}$, hence, the formation of the iron oxides could proceed by the thermal hydrolysis of both species. According with the Gibbs free energy of the iron oxide hydroxides formation (Figure 4.3), hematite formation is the most favored reaction when the solid is formed from $Fe(OH)^{2+}$ ions at 95°C (368 K). However, if the reaction proceed from Fe^{3+} ions, akaganeite crystals are the iron hydroxide

most favored. This results agree with the XRD results, corroborate the presence of both crystalline structures in the ACP and ACZ samples.

The reason why the particles on F400-Fe carbons are smaller than the ones on ACZ-Fe and ACP-Fe is not totally clear. As previously mentioned, the deposit of iron onto the carbon surface begins with the formation of a nucleus. After that, the iron particle growths, influenced by factors such as hydrolysis temperature and the concentration of the hydrolysis solution. The oxygen content of the carbons (see Table 4.1) evidences that the surface groups can acts as nuclei former and favors the formation of iron particles on samples ACZ-Fe and ACP-Fe and hence the iron oxides can reach high particle diameters. Also the crystalline structure of the iron particles can influence the arsenic adsorption capacity. As observed in Figure 4.10 and Figure 4.11 crystalline structures of the iron particles vary according with the production conditions and the type of activated carbon. Iron oxides have the characteristic to form diverse crystalline structures. According with Cornell et al [32], the morphology of the crystal is governed by the rate at which the different faces growth and depends on a number of factors: the arrangements of the ions in the crystal, the driving force of the crystal formation (chemical potential), and the growth environment (solvent, presence of foreign ions). Thermodynamically, the most stable iron oxide species are hematite (Fe_2O_3) and goethite (FeOOH). Under hydrothermal conditions at high temperatures (>70° C), high concentrations of iron and low pH, the precipitation of iron as hematite crystals is promoted. However, if the hydrolysis solution contain chloride ions, both akaganeite and hematite crystals can be formed [32]. Also, although the crystalline structure of an iron oxide is well defined, the shape of the particle can vary according with the growing of some specific crystalline face. This generates a variety of morphologies (also called habits) that can influence the arsenic adsorption capacity.

The latest is consistent with the findings in this investigation, since hematite and akaganeite are the crystalline structures present on the modified activated carbons produced in this research. According with the diffraction patterns of F400-Fe

sample (Figure 4.10), it can be seen that this material has mainly hematite crystals and a small amount of akaganeite.

This is because this carbon was synthesized at high iron concentrations (C_{Fe}=3.5 M), condition that, as reported, favored hematite formation. On the other hand ACZ-Fe sample has both crystalline species (hematite and akaganeite), with a considerable high amount of akaganeite crystals. This could be related to the iron concentration employed to modify this carbon, since was relatively low (C_{Fe}=1 M), which promotes the formation of akaganeite. Also, it is possible that during the washing and drying of the modified carbons part of the akaganenite was transformed to hematite by means of chloride elimination and dehydration reactions

Finally, according with the diffraction pattern of ACP-Fe sample, the anchored iron oxides correspond only to akaganeite crystals. This effect could be attributed to the low concentration of iron in the hydrolysis solution (for sample 11 C_{Fe} was 0.3 M,) since this conditions favors the formation of this crystalline phase. Also to the surface chemistry of the ACP activated carbon can influence the formation of acicular shape particles. Previous studies about the formation of monodispersive particles by iron hydrolysis have found that the addition of a small amount of phosphate ions leads the formation of acicular shape β-FeOOH [27, 43, 44]. Hence the phosphate groups in the surface of ACP activated carbon can influence this iron oxide morphology at low iron oxide concentrations.

In this section Q_{As} expressed per gram of iron was useful to emphasize the importance of the iron oxides/hydroxides particles size and their availability to adsorb arsenic. However, for practical purposes, the material to be used in real applications will be the one that has the highest Q_{As} per gram of carbon. According with the shape of the surface responses reported in Figure 4.8, it is expected that the arsenic adsorption capacity of the modified activated carbons can be enhanced by modifying the production parameter in the direction that the surface response growths (marked with an arrow in Figure 4.8). In this sense, the following sections

are focused on the production conditions optimization in order to generate materials with the highest Q_{As} possible per gram of carbon.

4.3.4. Optimization

An advantage of employing the response surface methodology is that the effect of each production parameter, regarding the measured response, can be determinated. In this sense we can modify the production conditions to get a desired response. In this case we want to find the production conditions at which the iron modified activated carbons have the maximum arsenic adsorption capacity. As can be seen in Figure 4.8, the variations of Q_{As} are hardly influenced by the kind of activated carbon employed and hence the optimal anchorage conditions should be different for each activated carbon. In this section the optimization of the production conditions were carried out evaluating each carbon separately, based on the results of the first experimental design.

4.3.4.1. F400 activated carbon

From the response surface and contour curves presented in Figure 4.8 A and B, the optimum production conditions can be observed: C_{Fe}=3.05, T=96 °C and Ht=14 hours. It is worth noticing that, the hydrolysis time of 14 hours is the boundary value of this production variable in the first experimental design. In this sense it is expected that the arsenic adsorption capacity of this modified carbon increases when increasing the hydrolysis time. With the aim to explore this possibility, 5 samples were prepared at the optimal C_{Fe} and T, and at higher hydrolysis times than 14 hours. Q_{As} and Fe% of these samples are given in Figure 4.12. As predicted by the response surface, the arsenic adsorption capacity increased with hydrolysis time, reaching its maximum value at a hydrolysis time of 56 hours, obtaining an arsenic adsorption capacity of 4.27 mg As/g C. This increase in Q_{As} is attributed to the anchorage of new particles in the carbon surface, increasing slightly the iron content of the modified carbons (Figure 4.12). However at Ht higher than 56 hours the Q_{As} decreased. This could be related to the

agglomeration of iron oxide particles. Something to remark is that the surface area did not exhibit an appreciable change when Ht was increased: the surface area of the carbon produced at 56 hours of hydrolysis time decreased just 42 m^2/g compared to the one processed for 14 hours.
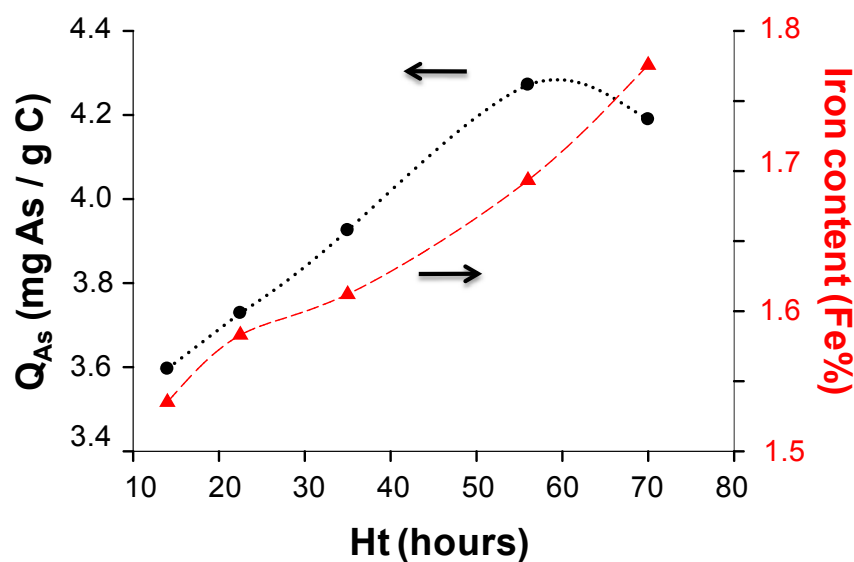
Figure 4.12. Evaluation of hydrolysis time (Ht) on the arsenic adsorption capacity (Q_{As}) (left axis) and the iron content (right axis) of F400-Fe activated carbon. C_{Fe} and T were kept constant at 3.05 mol/L and 96 °C, respectively.

4.3.4.2. ACZ activated carbon

According with the results given in Figure 4.8C and D, Q_{As} of ACZ-Fe carbons increased with the hydrolysis temperature. In contrast, the iron concentration of the hydrolysis solutions had a negative effect on the arsenic adsorption capacity because it decreased as C_{Fe} increased. Regarding the hydrolysis time, 6.8 hours was the time at which the arsenic adsorption capacity gets its maximum value. Taking this into account, the production conditions that maximize Q_{As} of ACZ activated carbon are a temperature above 110 °C, low iron concentration and a hydrolysis time of 6.8 hours. However, at temperatures higher than 110 °C, the pressure inside the vessel increased, opening the seal of the container used.

Because of this, the only variable that could be studied in order to increase Q_{As} was C_{Fe}.
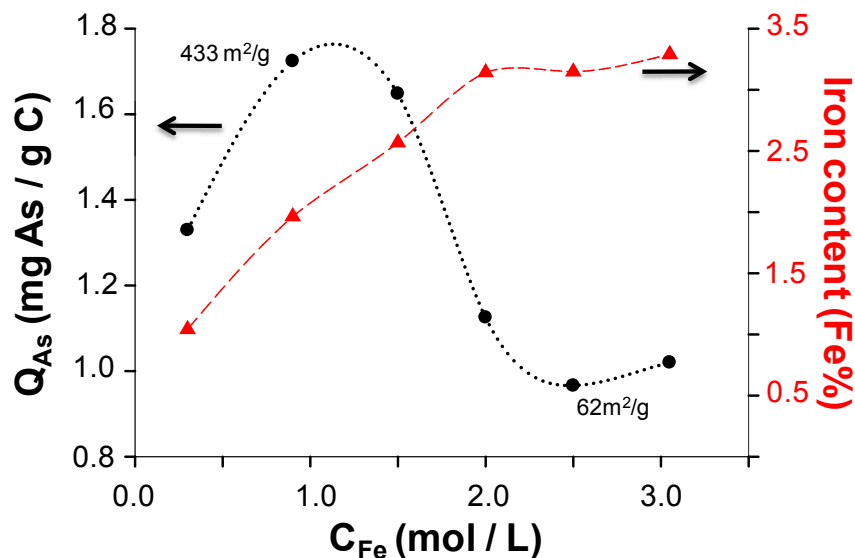
Figure 4.13. Evaluation of Iron concentration (C_{Fe}) on the arsenic adsorption capacity (Q_{As}) (left axis) and the iron content (right axis) of ACZ-Fe activated carbon. Hydrolysis time and hydrolysis temperature were kept constant at 6.8 hours and 110 °C, respectively.

Similar to what was done for F400 carbons, 6 samples were prepared at the optimal hydrolysis time (6.8 hours) and at the chosen hydrolysis temperature (110 °C), varying the iron concentration in the hydrolysis solution. The arsenic adsorption capacity and the iron content of the generated materials are reported in Figure 4.13. As predicted by the first experimental design, Figure 4.13 shows that low C_{Fe} favored the arsenic adsorption capacity by the ACZ modified carbons. The maximum arsenic adsorption capacity was 1.72 mg As/g C, at an iron concentration of 0.9 mol Fe/L. Following the dotted line that connects the experimental data in Figure 4.13 it can be assume that the optimal C_{Fe} is 1.16 mol/L. ACZ activated carbon was modified at the optimal C_{Fe} value, generating a

carbon with an arsenic adsorption capacity of 1.75±0.18 mg As/g C and an iron content of 1.34±0.08 Fe%.

Table 4.5. **Experimental design and the responses obtained.**

Run	Production conditions (Coded levels)			Q $_{As}$ (mg / g)	Fe %
	C_{Fe} (mol/L)	T (°C)	Ht (hours)		
1	0.4 (-1)	40 (-1)	6 (-1)	0.84	1.42
2	0.4 (-1)	40 (-1)	9 (+1)	0.59	1.41
3	0.4 (-1)	60 (+1)	6 (-1)	1.01	1.66
4	0.4 (-1)	60 (+1)	9 (+1)	0.87	1.46
5	1.0 (+1)	40 (-1)	6 (-1)	0.56	1.56
6	1.0 (+1)	40 (-1)	9 (+1)	0.74	1.39
7	1.0 (+1)	60 (+1)	6 (-1)	0.77	1.64
8	1.0 (+1)	60 (+1)	9 (+1)	0.74	1.40
9	0.2 (-1.6)	50 (0)	7.5 (0)	0.98	1.24
10	1.2 (+1.6)	50 (0)	7.5 (0)	0.75	1.60
11	0.7 (0)	33.2 (-1.6)	7.5 (0)	0.75	1.31
12	0.7 (0)	66.8 (+1.6)	7.5 (0)	1.07	1.51
13	0.7 (0)	50 (0)	5 (+1.6)	1.01	1.57
14	0.7 (0)	50 (0)	10 (+1.6)	0.86	1.32
15	0.7 (0)	50 (0)	7.5 (0)	1.05	1.25
16	0.7 (0)	50 (0)	7.5 (0)	1.10	1.30
17	0.7 (0)	50 (0)	7.5 (0)	1.03	1.27

4.3.4.3. ACP carbon

Figure 4.8 E and F indicates that the production conditions at which the ACP-Fe carbons increased their arsenic adsorption capacity are those at low hydrolysis temperature and low iron concentration and short hydrolysis time. Because of this, a second experimental design was performed in order to find the experimental conditions that increase the arsenic adsorption capacity of this activated carbon. A central composite experimental design was employed, redefining the production

variables to lower values than those established in the first experimental design. The experimental conditions and the analyzed responses are given in Table 4.5.

Similar to what was done for the previous analysis, iron content and the arsenic adsorption capacity was analyzed, generating the surface plots reported in Figure 4.14. As expected, the iron content of the samples is lower than the obtained on the previous design. In this second experimental design the iron content ranged from 1.24 to 1.66 Fe%. Similar to the F400-Fe samples, the shape of the response surface of the iron content (Figure 4.14A) showed the minimum value that can be reached with ACP carbons. On the other hand, the arsenic adsorption capacity ranged from 0.56 to 1.11 mg As/g C. The production conditions that generated the material with the highest arsenic adsorption capacity (Q_{As}=1.11 mg As/g) were C_{Fe}=0.56 mol Fe/L, T=58 °C and Ht=6.8 hours. The BET surface area were not significantly affected by the presence of iron oxide particles in the modified materials, since the surface area of the virgin activated carbon was 1058 m^2/g, and the one for the modified activated carbons was 902 m^2/g.

Something to remark is that the maximum arsenic adsorption capacity found by this experimental design was similar to the average value obtained on the previous experimental design, but lowers than the arsenic adsorption capacity of sample 1 and sample 11 of the first experimental design (referred as experimental run 1 and 11 in Table 4.1). The reason why these samples have an unexpected adsorption capacity compared with the rest of the samples is related to the morphology of the iron loaded onto the carbon samples. As can be observed in Figure 4.10C, the morphology of the iron loaded on sample 11 of the first experimental design has a particular acicular shape. These iron oxide particles increased the surface area of the modified samples from 1058 m^2/g to 1234 m^2/g. Because of the increment in surface area caused by the iron oxide particles, the arsenic adsorption capacity also increased compared with the rest of the samples (ACZ-Fe and ACP-Fe) that had spherical particles.
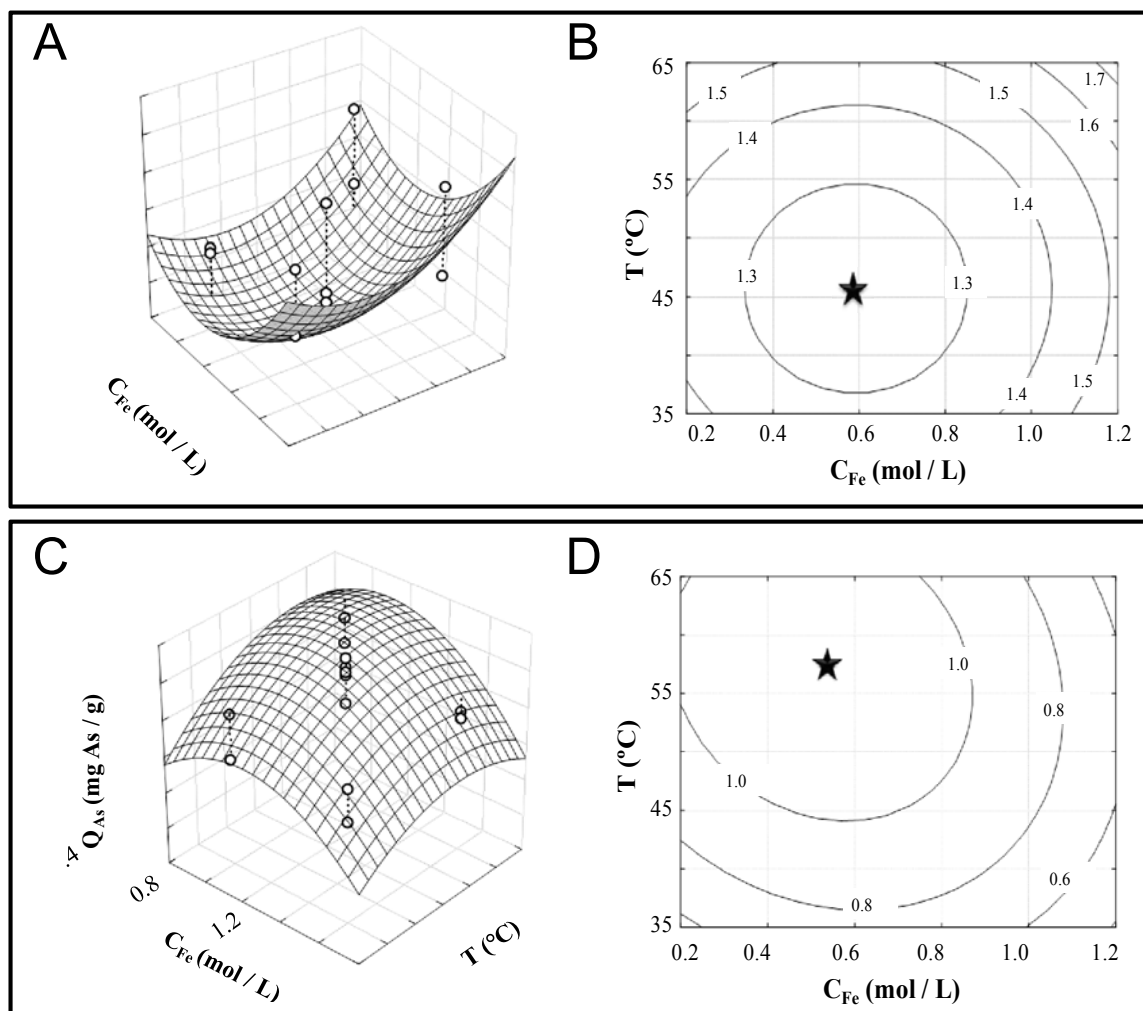
Figure 4.14: Surface response and contour plots for iron content (Fe%, A and B) and arsenic adsorption capacity (Q_{As}, C and D) for ACP modified samples according with the experimental design reported in Table 4.5.

However, a considerable amount of iron oxide particles was detected in the batch adsorption experiments (7.3 % of the total iron preloaded onto the carbon), which is attributed to the release of acicular iron oxide particles. The release of the acicular particles can be caused by the collision of carbon granules during batch adsorption experiments, since the samples were stirred until the adsorption

equilibrium was reached. Scanning electron micrographs of the modified carbons before and after adsorption experiments confirmed these findings (Figure 4.15).
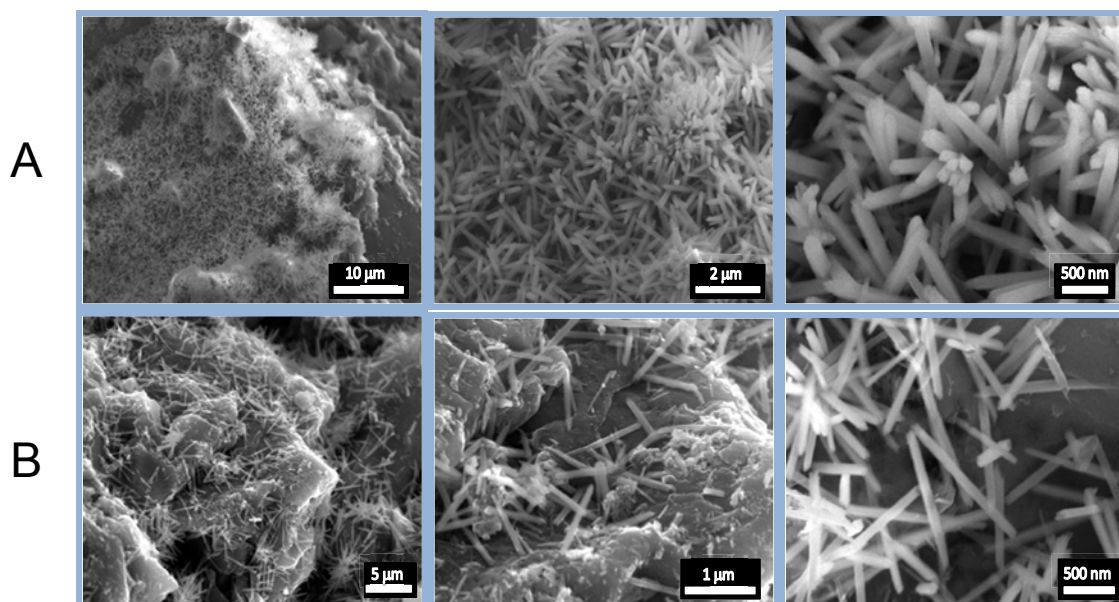
Figure 4.15. Scanning electron micrographs of ACP-Fe carbon (sample 11) before (A) and after (B) arsenic adsorption.

Hence, even when the adsorption capacity of carbons with acicular shape particles is higher than the rest of the ACP-Fe carbons, their application in aqueous streams is limited by the release of iron. However, due to their high arsenic adsorption capacity, the evaluation of this material in a packed column system is needed in order to determine its applicability.

4.3.5. Characterization of the optimum materials

4.3.5.1 Powder X-ray diffraction (XRD)

Figure 4.16 shows XRD results of raw activated carbons and modified carbons produced at optimal conditions. As can be observed, the three carbons employed in this research have two broad peaks around $2\theta=23°$ and $2\theta=43°$ that are characteristic of amorphous structures of activated carbon. These peaks are

related to the graphite-like microcrystallites randomly oriented, corresponding to graphite (002) and graphite (100) planes. Additionally to these peaks, F400 activated carbon has other peaks (marked in Figure 4.16) that could be related to small amounts of inorganic salts such as hematite goethite, alumina or silica, however due to the low intensity of these peaks it is difficult to be conclusive.
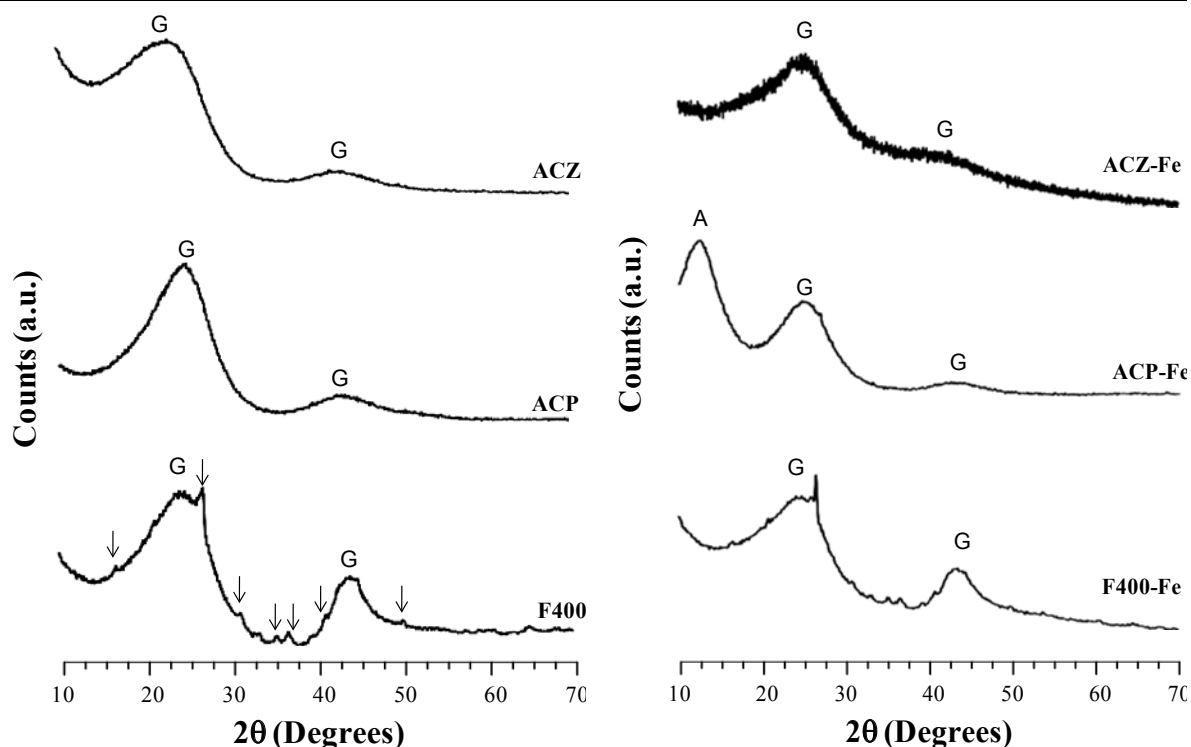
Figure 4.16. X Ray diffraction patterns of virgin (left) and iron modified (right) activated carbons. Labels indicate the crystal structure: G: graphite (C) and A: akaganeite (β-FeO(Cl,OH)).

For ACZ-Fe activated carbon no difference could be observed between the XRD patterns of raw and iron doped activated carbons, suggesting either that the deposited iron oxides are amorphous or that the particles are too small to diffract. Similar results were obtained by F400-Fe activate carbon, since the XRD pattern of the modified carbon do not change considerably. The small peaks presented in the pristine F400 activated carbon remains after the impregnation of the iron oxide particles, with a slight size decrement, which can be related with the partial

dissolution of these salts. However, the diffraction patterns don not exhibit some information about the iron oxide particles anchored onto the activated carbon surface despite the iron content of the F400 activated carbon increase from 0.34 to 1.45%. Finally, ACP-Fe activated carbon showed a broad peak centered at $2\theta=12.5°$, which can correspond to akaganeite crystals. Due to the broadest of the peak, it is expected that the akaganeite particles were poorly crystalline and with a particle size below 100 nm. Because the XRD patterns of the modified activated carbons do not exhibit the crystalline peaks of the anchored iron oxides, the calculation of the mean particle size was determined by SEM observations.

4.3.5.2 Scanning electron microscopy (SEM)

The iron modified activated carbons were analyzed by scanning electron microscopy, in order to examine the particle size and distribution of the iron oxides anchored onto the modified activated carbons. It is worthy to notice that the activated carbon granules were partially milled before the SEM observations in order to get images of the internal carbon granules. Selected micrographs of the three modified activated carbons are included in Figure 4.17. According with the SEM observations the majority of the iron oxide particles anchored onto F400-Fe activated carbon appear as agglomerates (marked with arrows in Figure 4.17) of very small spherical particles, with diameter from 2 to 10 nm. These particles are mainly located in the activated carbon dislocations, where it is expected that unsaturated carbon atoms are more reactive. However, particles with greater diameters were also observed, ranging between 6 and 58 nm (Figure 4.17 bottom micrographs) being observed mainly on the external part of the activated carbon granule.

Different results were observed for ACP-Fe activated carbon: it was possible to observe two kinds of iron oxide. On one hand, iron oxide spherical particles with a diameter between 4 and 15 nm with a mean particle size distribution of 8±2 nm (micrographs on the top of Figure 4.18).
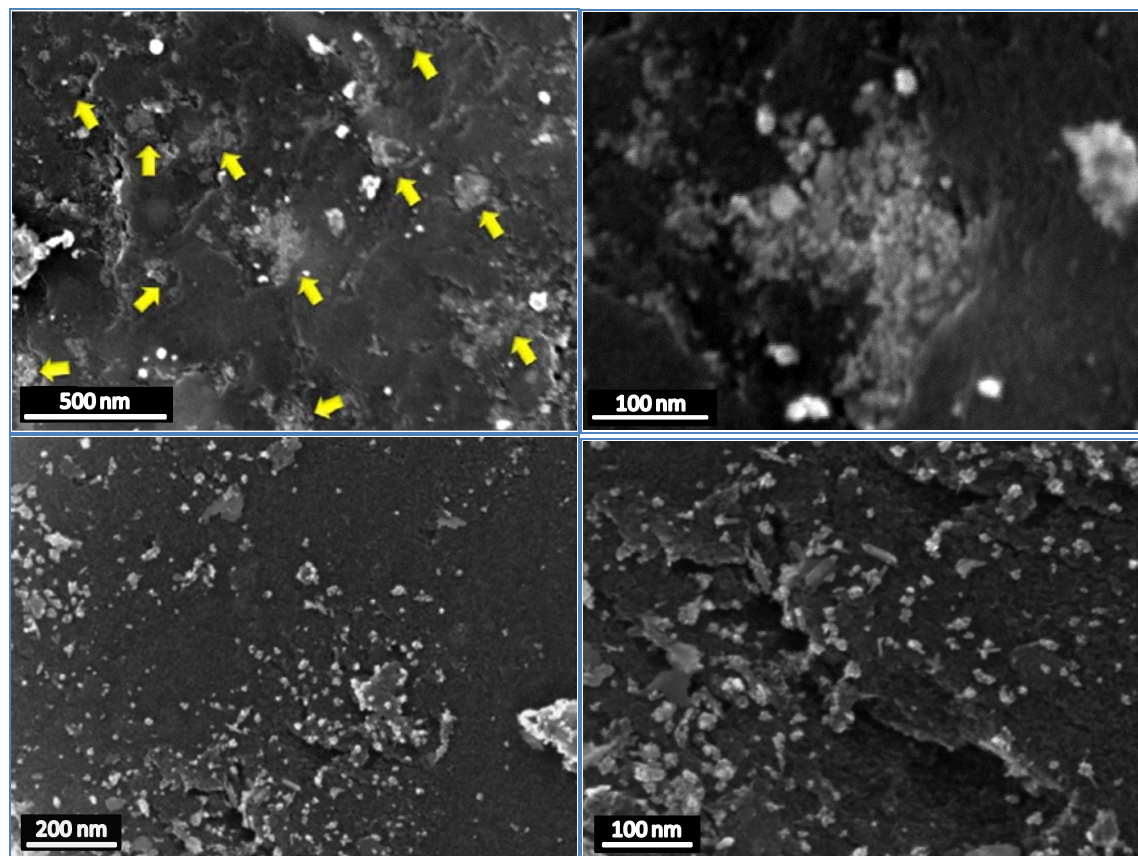
Figure 4.17. Scanning electron micrographs of F400-Fe activated carbon modified under the optimal production conditions.

These particles are similar to the ones observed on F400-Fe activated carbon, but the diameter of the particles onto the ACP-Fe surface is slightly bigger and the distribution is not as wide as on the F400-Fe activated carbon. On the other hand, amorphous agglomerates of iron oxide nanoparticles were also observed (micrographs on the bottom of Figure 4.18). Elemental analysis carried out by energy dispersive x-ray analysis (EDX) showed a considerable amount of iron and chloride in areas that contain these particles, hence it could be concluded that this particles correspond the akaganeite crystals, that are the responsible of the broad peak observed in the XRD analysis. The presence of these different iron oxide

morphologies onto the carbon surface is not totally clear. It can be speculated that this effect could be related to the presence of different amounts of phosphate groups on the carbon surface: in zones with small amounts of phosphate groups spherical particles (that was found in F400-Fe activated carbon also) are formed; in contrast, zones with high amount of phosphate groups linked to the activated carbon surface, can promote the formation of akaganetite crystals and hence, different morphologies.
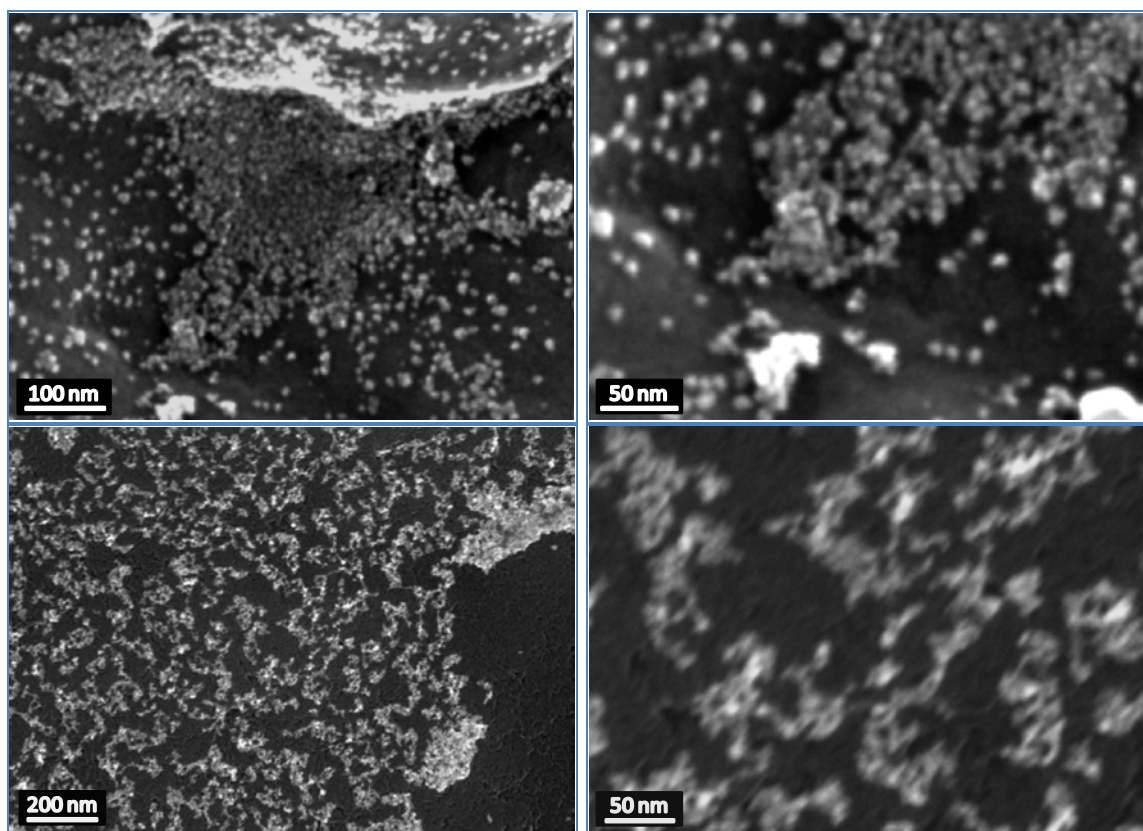
Figure 4.18. Scanning electron micrographs of ACP-Fe activated carbon modified under the optimal production conditions.

Also, during the analysis of ACZ-Fe activated carbon it was possible to detect two iron oxide morphologies: Semi spherical shape iron oxide particles (micrographs at top of Figure 4.19), that according with the SEM observation, are present with less frequency on the activated carbon surface. In this case, the spherical particles

have a bigger particle diameter to the ones observed in F400-Fe and ACP-Fe activated carbons, since their diameter ranged from 15 to 36 nm with an average particle size of 20±6 nm. And on the other hand, it was possible to observe amorphous agglomerates (micrographs at top of Figure 4.19), widely distributed on the activated carbon surface.
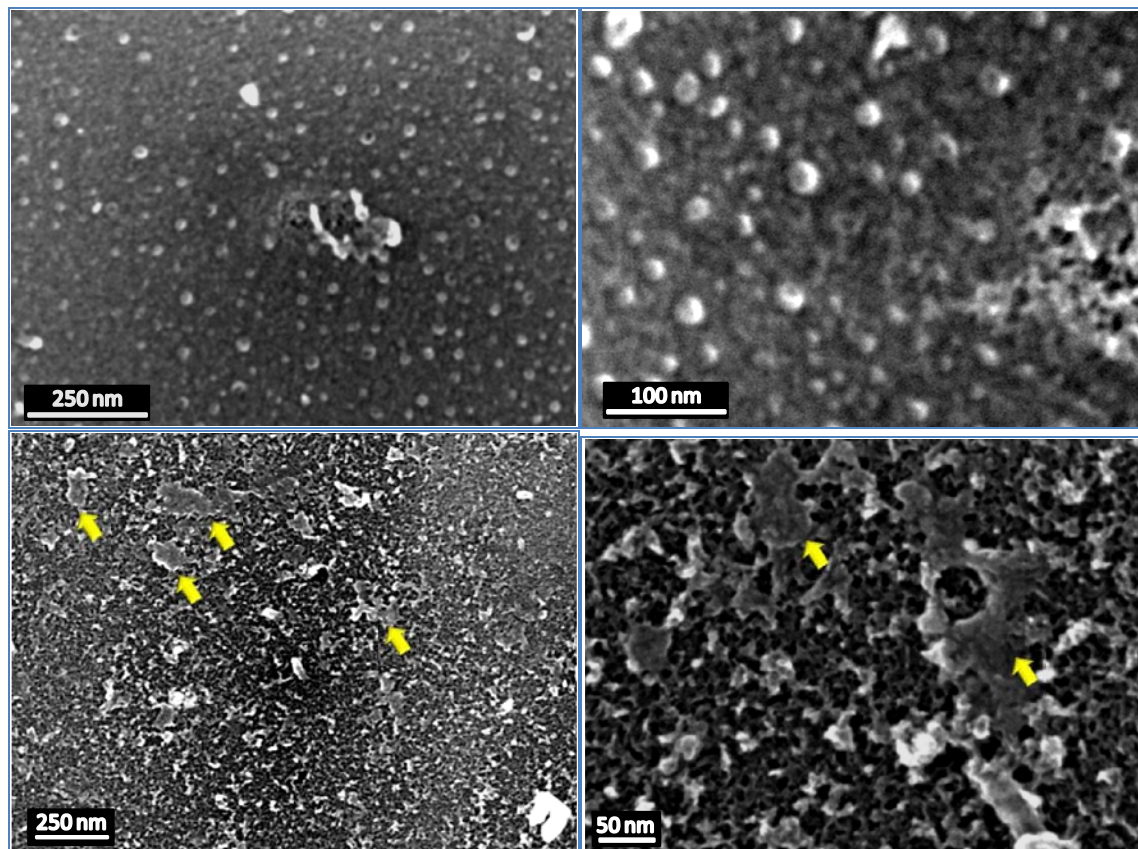
Figure 4.19. Scanning electron micrographs of ACZ-Fe activated carbon modified under the optimal production conditions.

According to the shape of these agglomerations, it is expected that these iron oxides correspond to ferrihydrite, characterized by their poor ordered structure (see Figure 4.19). Previous studies have reported that the nucleation of hematite iron oxide takes place in ferrihydrite aggregates after an aging time at room temperature (see Figure 4.20), this because the aggregation appears to facilitate

the hematite crystallization [32]. As previously found, the crystalline structure that is preferentially formed during the thermal hydrolysis is hematite for ACZ and F400 activated carbons, as was observed in the XRD analysis of the samples generated in the first experimental design (see Figure 4.11) Then, it is expected that the short hydrolysis time employed to modify ACZ-Fe activated carbons (6.8 hours) does not allow the completilly transformation of the amorphous ferrihydrite into hematite crystals, generating the agglomerates observed in Figure 4.19.
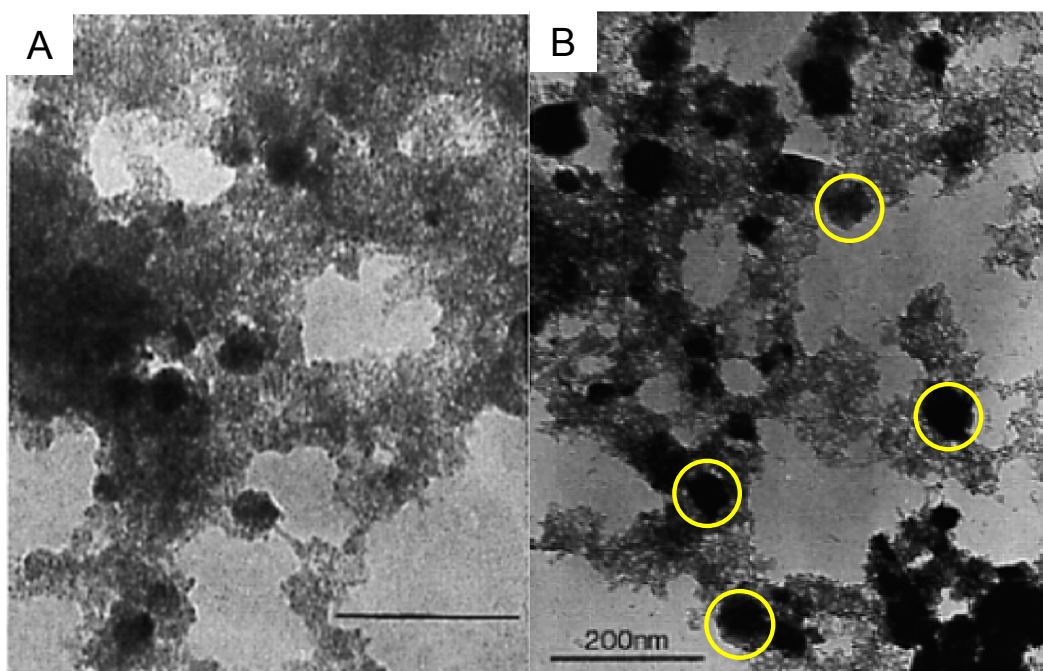
Figure 4.20. Transmission electron micrograph documenting the transformation of ferrihydrite to hematite iron oxide after a considerable aging time. A: initial ferrihydrite sample. B: micrographs that show a considerable reduction of ferrihydrite and the formation of hematite crystals, (circle marked). Image reproduced from Cornell et al. [32]

4.3.5.3 Surface area and pore size distribution

Nitrogen adsorption/desorption isotherms for the virgin and modified activated carbons at optimal production conditions were measured. From these data, BET surface area and pore size distribution (DFT calculations) were determined. The

surface area of raw materials decreased after their modification with iron oxide / hydroxide particles: from 1058 to 942 m^2/g for ACP-Fe activated carbon; from 896 to 839 m^2/g for F400-Fe activated carbon; and from 896 to 433m^2/g for ACZ-Fe activated carbon. In the same way the pore volume of modified carbons was lower than the pristine materials, as can be observed in Figure 4.21. F400 activated carbon concentrates most of its pore volume in pores with diameter between 5 and 12 Å, with a considerable amount of pores with diameter of 6 Å. After the modification of this carbon with iron oxide/hydroxide particles the total pore volume decrease from 0.471 cm^3/g to 0.387 cm^3/g (17.0%), lossing 4.75% and 31.1% of the initial microporous and mesoporous volume, respectively. As can bee seen in Figure 4.21, the principal peak presented at 6 Å of pore width in the incremental pore volume of the virgin F400 activated carbon is displaced to lower pore diameters. The reason of this pore width reduction is not totally clear; assuming that this difference is not due to an experimental error, this reduction could be related to some chloride or ferric ions remaining in the microporous structure, since the atomic radius of chloride and ferric ions is 1.7 Å and 0.63 Å, respectively. Another reason for the reduction of the pore size of F400-Fe activated carbon could be related to some iron oxide particle anchored onto micropores. However, these are too large according with the particles found during the SEM analysis (see Figure 4.17) On the other hand the pore volume contained in micropores wider than 6 Å remains similar to the pristine activated carbon.

Cumulative

Incremental

Pore volume (cm³/g)

Pore width (Å)

F400

ACP

ACZ
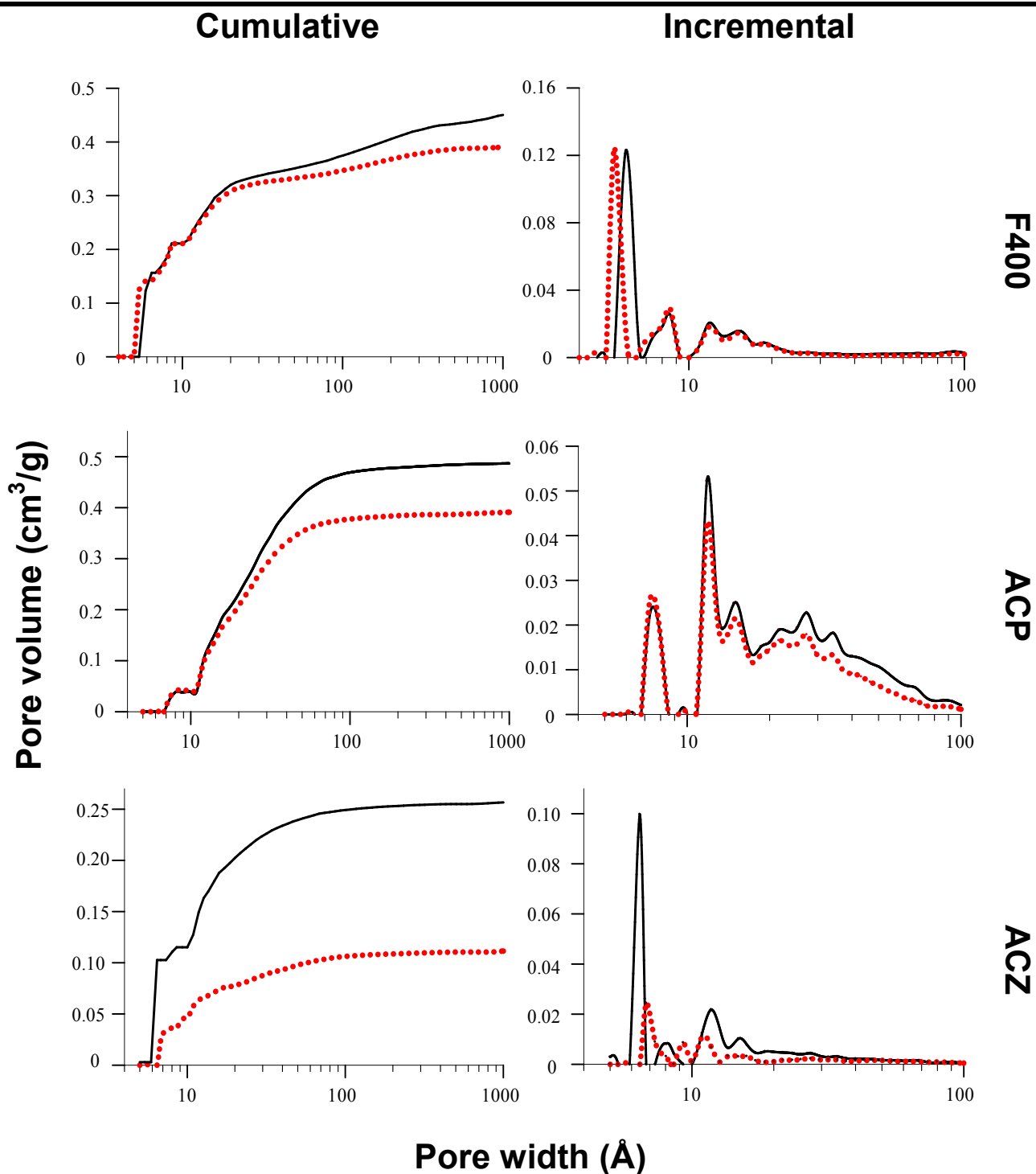
Figure 4.21. Pose size distribution of the virgin (solid line) and iron modified carbons (dotted line) synthesized at the optimal production conditions.

Most of the decrement in pore volume of the F400-Fe activated carbon is presented in the mesopore structure. To illustrate this change, Figure 4.22A show the distribution of mesoporous volume of F400 and F400-Fe activated carbons. As can be seen, the mesopore structure of F400-Fe activated carbon has similar shape to the F400 activated carbon but with low pore volume, which means that the iron oxide particles are dispersed inside the mesopores of the activated carbon, without blocking pores. This assumption is supported by the particle size of the F400-Fe activated carbon (see Figure 4.17): the particle size ranged from 20 to 100 Å.

On the other hand, ACP activated carbon has a wide pore size distribution, containing pores with diameter that ranges from 7 Å to 100 Å (Figure 4.21). This pore structure is suitable to be modified with iron oxide particles, since in comparison with narrow distributions, this porous structure facilitates the diffusion of Fe ions through the pores during the hydrolysis, avoiding the blockage of pores and hence the diminish of the activated carbon surface area. Comparing the pore structure of the raw ACP activated carbon with the ACP-Fe activated carbon, it can seen a decrement of pore volume presented mainly in the mesoporous range. The total pore volume decreased from 0.488 cm^3/g to 0.394 cm^3/g (19.3%): the micropore volume decrease 10.3% of the initial micropore volume, being the pores with diameter superior to 10 Å the most affected. On the other hand, the mesopore volume decreased 29.1% of the initial volume. Similar to the reported for F400-Fe activated carbon, the pore structure of the pristine ACP and the modified ACP-Fe activated carbons is similar, which means that the iron oxide particles are dispersed inside the mesopores of the activated carbon, without blocking the pores entrance (see Figure 4.22B). These results agree with the SEM observations, since the diameter of the iron oxide particles ranged from 40 to 150 Å (see Figure 4.18).
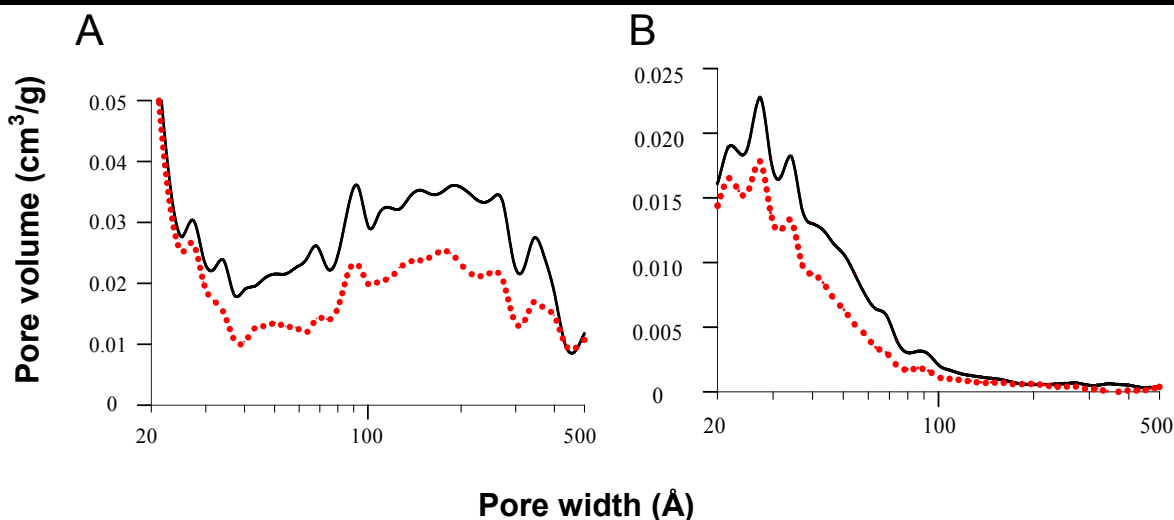
Figure 4.22. Pose size distribution in the mesopores range of the virgin (solid line) and iron modified carbons (dotted line) synthesized at the optimal production conditions. A: F400 activated carbon, and B: ACP activated carbon.

Finally, ACZ activated carbon has a pore size distribution similar to the F400 activated carbon: the majority of its pore volume is concentrated in pores with diameters between 6 Å and 12 Å (Figure 4.18) being the micropore volume 80 % of the total pore volume of ACZ activated carbon. This narrow pore size distribution presented in ACZ activated carbon is easily blocked by the iron oxides anchored onto the activated carbon surface, since the particles have a diameter that ranges from 150 to 360 Å. In this case the pore structure of the modified activated carbon is very different to that of the ACZ activated carbons, which means that the iron oxide particles are blocking pores in the modified activated carbon. This can be seen in Figure 4.19, where ferrihydrite agglomerates are blocking the pores entrance. After the modification of this activated carbon with iron oxide/ hydroxide particles at the optimal conditions, the total pore volume decreased from 0.257 to 0.117 cm^3/g (54.5%), with a decrement of 61.6% of the microporous volume and a 37.8% of the mesoporous volume. With these results it can be conclude that a well developed mesopore structure is needed in order to avoid the blockage of the pores by iron oxide particles.

4.3.5.4. Adsorption isotherms

Figure 4.23 shows the As (V) adsorption isotherms of the modified materials generated at the optimal experimental conditions. The adsorption isotherms of the virgin activated carbons were also evaluated. The ACZ and ACP activated carbons did not exhibit affinity for arsenic, being their arsenic adsorption capacity less that 0.01 mg As/g. In contrast F400 activated carbon exhibited a considerable arsenic adsorption capacity, therefore its adsorption isotherm is also reported in Figure 4.23. The data were best fitted by the Freundlich isotherm model; the isotherm parameters and the main characteristics of the generated materials are reported in Table 4.6. F400-Fe carbon was the material that had the higher arsenic adsorption capacity within the entire range of arsenic concentration studied. The adsorption capacity of the F400 activated carbon doubled after its modification (for example at 1.5 ppm of arsenic).
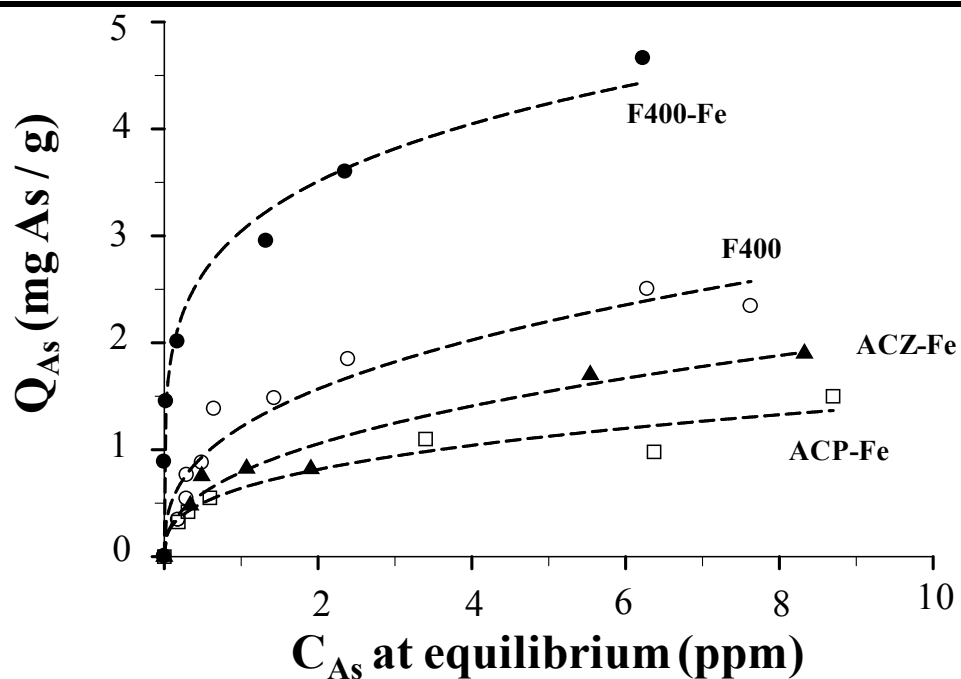
Figure 4.23. Adsorption isotherms of iron modified carbons and F400 virgin carbon. The iron modified activated carbons reported in this graph were produced at the optimal production conditions. Isotherms obtained at 25 °C and pH = 7

Table 4.6. **Main characteristics and adsorption isotherms parameters according with the Freundlich isotherm of the modified carbons generated at the optimal production conditions.**

Sample	BET S.A. (m^2/g)	pH$_{PZC}$*	Iron content (%)	K$_f$	1/n	R
F400	896	8.94	0.34	1.211	0.371	0.971
F400-Fe	904	8.62	1.45	3.040	0.206	0.990
ACZ-Fe	433	3.07	1.34	0.788	0.418	0.984
ACP-Fe	902	3.59	1.65	0.638	0.352	0.971

pH$_{PZC}$: Point zero electric charge pH   n: Freundlich isotherm constant (dimensionless)

R:correlation coefficient   Kf: Freundlich isotherm constant (L$^{1/h}$/ mg^{1-1h} g^{-1})

From the shape of the adsorption isotherm of F400-Fe, it can be seen that this carbon exhibits a high affinity for arsenic at low arsenic concentrations. This is a desired characteristic in materials that want to be used for treatment of water polluted with arsenic, since most of the arsenic-contaminated areas do not exceed a concentration of 1.5 ppm of arsenic [45]. On the other hand the arsenic adsorption capacity of ACP-Fe and ACZ-Fe activated carbons, calculated at 1.5 ppm of As at equilibrium, was 0.96 and 1.18 mg As/g C respectively. As discussed before, the reasons of the superior arsenic adsorption capacity of F400-Fe activated carbon over ACP-Fe and ACZ-Fe carbons are the availability and particle size of the iron oxides loaded onto this carbon. However, comparing the characteristics of the iron modified activated carbons we can speculate that their pH$_{PZC}$ could play an important role on the arsenic adsorption capacity. The arsenic adsorption experiments were carried out at pH=7. Taking into account the pH$_{PZC}$ of the modified carbons (Table 4.6), the net electric charge of ACP-Fe and ACZ-Fe at pH 7 is negative. In contrast, it is expected that the electric charge of F400-Fe at

pH 7 was slightly positive because this pH is below its pH_{PZC}. Arsenate predominates as mono or divalent anion at pH 7, therefore, the oxygenated groups of ACZ-Fe and ACP-Fe carbons can repel these anionic species, decreasing the arsenic adsorption capacity. Finally, comparing our results with previously modified activated carbons (Table 1.4), our materials have similar and in some cases superior adsorption capacities than other iron modified carbons.

4.4. CONCLUSIONS

This study has demonstrated that thermal hydrolysis is an excellent method to anchor iron nanoparticles onto granular activated carbon. The production conditions that generate materials with high arsenic adsorption capacity depend on the type of carbon employed. The presence of oxygenated surface groups onto the carbon surface promotes the anchorage of iron oxide particles, since carbons with high oxygen content (ACP and ACZ carbons) have higher iron content. However, according with our results there is not a direct relationship between iron content and arsenic adsorption capacity, since factors as availability of iron to adsorb arsenic and the particle size of iron oxides are parameters that strongly influence the arsenic removal. By mean of the surface response methodology, it is possible to determine the optimal experimental conditions to anchorage iron oxide particles onto carbon materials. The optimal conditions to anchor iron particles for F400 activated carbons are: C_{Fe}=3.05 mol Fe/L, T=96 °C and Ht=56 hours; for ACZ activated carbons are: C_{Fe}=1.16 mol Fe/L, T=110 °C and Ht=6.8 hours; and C_{Fe}=0.56 mol Fe/L. T=58 °C and Ht=6.8 hours for ACP activated carbons. The surface area decrease is insignificant for ACP and F400 modified carbons (less that 10 % of its initial surface area), however for ACZ carbon, the surface area decreases considerably (from 846 m^2/g to 433 m^2/g). The arsenic adsorption capacity measured at pH 7, 25°C and 1ppm of arsenic concentration at equilibrium is 3.25 mg As/g, 1.45 mg As/g and 1.65mg As/g for F400-Fe, ACZ-Fe and ACP-Fe

respectively, being this values in some cases superior to previously reported modified activated carbons.

4.5. REFERENCES

[1]   Morin G, Calas G. Arsenic in Soils, Mine Tailings, and Former Industrial Sites. ELEMENTS 2006;April 1, 2006;2:97-101.

[2]   O'Day PA. Chemistry and Mineralogy of Arsenic. ELEMENTS 2006;April 1, 2006;2:77-83.

[3]   Ghosh P, Banerjee M, Giri AK, Ray K. Toxicogenomics of arsenic: Classical ideas and recent advances. Mutation Research/Reviews in Mutation Research;2008/10//;659:293-301.

[4]   Mohan D, Pittman JCU. Arsenic removal from water/wastewater using adsorbents--A critical review. Journal of Hazardous Materials 2007;142:1-53.

[5]   World Health Organization. Guidelines for drinking-water quality. First addendum to third edition, volume 1, Recommendations. Geneva: World Health Organization 2006.

[6]   Agency EP. Treatments technologies for arsenic removal. 2005.

[7]   Pena ME, Korfiatis GP, Patel M, Lippincott L, Meng X. Adsorption of As(V) and As(III) by nanocrystalline titanium dioxide. Water Research 2005;39:2327-37.

[8]   Gupta K, Biswas K, Ghosh UC. Nanostructure Iron(III)â�’Zirconium(IV) Binary Mixed Oxide: Synthesis, Characterization, and Physicochemical Aspects of Arsenic(III) Sorption from the Aqueous Solution. Industrial & Engineering Chemistry Research 2008;47:9903-12.

[9]   Castro CS, Guerreiro MC, Oliveira LCA, Gonçalves M, Anastácio AS, Nazzaro M. Iron oxide dispersed over activated carbon: Support influence on

the oxidation of the model molecule methylene blue. Applied Catalysis A: General 2009;367:53-8.

[10] Jang M, Chen W, Cannon FS. Preloading Hydrous Ferric Oxide into Granular Activated Carbon for Arsenic Removal. Environmental Science & Technology 2008;42:3369-74.

[11] Chen W, Parette R, Zou J, Cannon FS, Dempsey BA. Arsenic removal by iron-modified activated carbon. Water Research 2007;41:1851-8.

[12] Rey A, Faraldos M, Casas JA, Zazo JA, Bahamonde A, Rodríguez JJ. Catalytic wet peroxide oxidation of phenol over Fe/AC catalysts: Influence of iron precursor and activated carbon surface. Applied Catalysis B: Environmental 2009;86:69-77.

[13] Xu C, Teja AS. Supercritical water synthesis and deposition of iron oxide ([alpha]-Fe2O3) nanoparticles in activated carbon. The Journal of Supercritical Fluids 2006;39:135-41.

[14] Xu C, Teja AS. Characteristics of iron oxide/activated carbon nanocomposites prepared using supercritical water. Applied Catalysis A: General 2008;348:251-6.

[15] Zhang QL, Lin YC, Chen X, Gao NY. A method for preparing ferric activated carbon composites adsorbents to remove arsenic from drinking water. Journal of Hazardous Materials 2007;148:671-8.

[16] Mondal P, Balomajumder C, Mohanty B. A laboratory study for the treatment of arsenic, iron, and manganese bearing ground water using Fe3+ impregnated activated carbon: Effects of shaking time, pH and temperature. Journal of Hazardous Materials 2007;144:420-6.

[17] Mondal P, Majumder CB, Mohanty B. Effects of adsorbent dose, its particle size and initial arsenic concentration on the removal of arsenic, iron and manganese from simulated ground water by Fe3+ impregnated activated carbon. Journal of Hazardous Materials 2008;150:695-702.

[18] Zhu H, Jia Y, Wu X, Wang H. Removal of arsenic from water by supported nano zero-valent iron on activated carbon. Journal of Hazardous Materials 2009;172:1591-6.

[19] Gu Z, Fang J, Deng B. Preparation and Evaluation of GAC-Based Iron-Containing Adsorbents for Arsenic Removal. Environmental Science & Technology 2005;39:3833-43.

[20] Auffan M, Rose J, Proux O, Borschneck D, Masion A, Chaurand P, Hazemann J-L, Chaneac C, Jolivet J-P, Wiesner MR, Van Geen A, Bottero J-Y. Enhanced Adsorption of Arsenic onto Maghemites Nanoparticles: As(III) as a Probe of the Surface Structure and Heterogeneity. Langmuir 2008;24:3215-22.

[21] S. Yean LC, C.T. Yavuz, J.T. Mayo, W.W. Yu, A.T. Kan, V.L. Colvin, M.B. Tomson. Effect of magnetite particle size on adsorption and desorption of arsenite and arsenate Journal of Materials Research 2005;December;20:3255-64.

[22] Zhang H, Penn RL, Hamers RJ, Banfield JF. Enhanced Adsorption of Molecules on Surfaces of Nanocrystalline Particles. The Journal of Physical Chemistry B 1999;103:4656-62.

[23] Tratnyek PG, Johnson RL. Nanotechnologies for environmental cleanup. Nano Today 2006;1:44-8.

[24] Dale LH. Synthesis, Properties, and Applications of Iron Nanoparticles. Small 2005;1:482-501.

[25] Wu W, He Q, Jiang C. Magnetic Iron Oxide Nanoparticles: Synthesis and Surface Functionalization Strategies. Nanoscale Research Letters 2008;3:397-415.

[26] Tavakoli A, Sohrabi M, Kargari A. A review of methods for synthesis of nanostructured metals with emphasis on iron compounds. Chemical Papers 2007;61:151-70.

[27] Matijevic E. Production of Monodispersed Colloidal Particles. Annual Review of Materials Science 1985;15:483-516.

[28] Fierro V, Muñiz G, Gonzalez-Sánchez G, Ballinas ML, Celzard A. Arsenic removal by iron-doped activated carbons prepared by ferric chloride forced hydrolysis. J Hazard Mater 2009;168:430-7.

[29] Jean-Pierre Jolivet CCaET. Iron oxide chemistry. From molecular clusters to extended solid networks. Chemical Communications 2004;5:481 - 7.

[30] Baes CF, Mesmer RE. The hydrolysis of cations. New York: Wiley 1976.

[31] Jean-Pierre Jolivet MH, Jacques Livage, Eric Bescher. Metal Oxide Chemistry and Synthesis, From Solution to Solid State. West Sussex: John Wiley and Sons Ltd 2000.

[32] Cornell RM, Schwertmann U. The iron oxides : structure, properties, reactions, occurences and uses. 2nd, completely rev. and extended ed. Weinheim [Cambridge]: Wiley-VCH 2003.

[33] Aquatic chemistry chemical equilibria and rates in natural waters.New York:Stumm W, Morgan JJ, NetLibrary Inc.;1996.

[34] Music S, Krehula S, Popovic S, Skoko Z. Some factors influencing forced hydrolysis of FeCl3 solutions. Materials Letters 2003;57:1096-102.

[35] Hench LL, West JK. Chemical processing of advanced materials. New York: J. Wiley & Sons 1992.

[36] Hristovski KD, Westerhoff PK, Möller T, Sylvester P. Effect of synthesis conditions on nano-iron (hydr)oxide impregnated granulated activated carbon. Chemical Engineering Journal 2009;146:237-43.

[37] Farquhar ML, Charnock JM, Livens FR, Vaughan DJ. Mechanisms of Arsenic Uptake from Aqueous Solution by Interaction with Goethite, Lepidocrocite, Mackinawite, and Pyrite:â€‰ An X-ray Absorption Spectroscopy Study. Environmental Science & Technology 2002;36:1757-62.

[38] Goldberg S, Johnston CT. Mechanisms of Arsenic Adsorption on Amorphous Oxides Evaluated Using Macroscopic Measurements, Vibrational Spectroscopy, and Surface Complexation Modeling. Journal of Colloid and Interface Science 2001;234:204-16.

[39] Guo X, Du Y, Chen F, Park H-S, Xie Y. Mechanism of removal of arsenic by bead cellulose loaded with iron oxyhydroxide ([beta]-FeOOH): EXAFS study. Journal of Colloid and Interface Science 2007;314:427-33.

[40] Manceau A. The mechanism of anion adsorption on iron oxides: Evidence for the bonding of arsenate tetrahedra on free Fe(O, OH)6 edges. Geochimica et Cosmochimica Acta 1995;59:3647-53.

[41] Lorenzen L, van Deventer JSJ, Landi WM. Factors affecting the mechanism of the adsorption of arsenic species on activated carbon. Minerals Engineering;1995/5//;8:557-69.

[42] Downs RT, Hall-Wallace M. The American Mineralogist crystal structure database. American Mineralogist 2003;January 1, 2003;88:247-50.

[43] Matijevic E. Preparation and properties of uniform size colloids. Chemistry of Materials 1993;5:412-26.

[44] Ozaki M, Kratohvil S, Matijevic E. Formation of monodispersed spindle-type hematite particles. Journal of Colloid and Interface Science 1984;102:146-51.

[45] Smedley PL, Kinniburgh DG. A review of the source, behaviour and distribution of arsenic in natural waters. Applied Geochemistry 2002;17:517-68.

"The aim of a discussion should not be victory, but progress. "
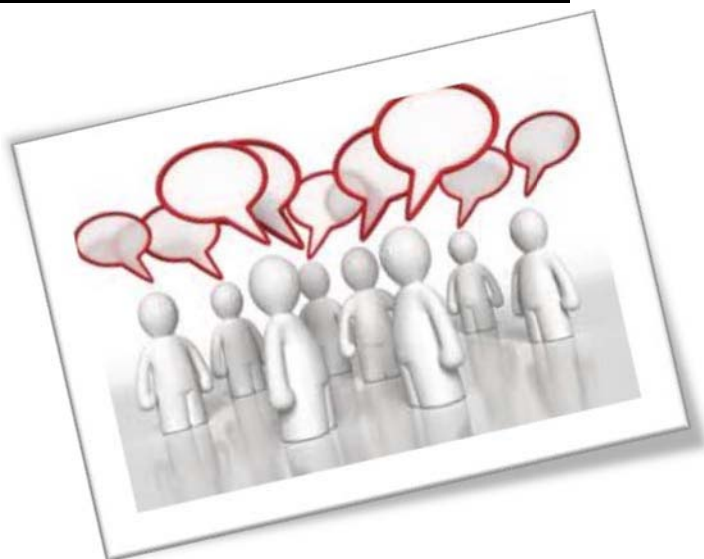
CHAPTER 5

GENERAL DISCUSSION

Activated carbon is a versatile adsorbent that can efficiently remove several compounds from aqueous and gas phase. These activated carbon characteristics are mainly due to its extensive surface area contained in its intricate pore structure. In this sense, the methodologies to produce activated carbon are focused on the generation of pores into the precursor by means of activation processes. According with the results exposed in chapter 2, the carbonization of agave bagasse perform pores all along the bagasse fiber with diameters from 3 to 10 μm (see Figure 2.4). The in-situ characterization of the carbonization process of agave bagasse fibers employing an environmental scanning electron microscope (ESEM) demonstrated that the generation of this macroporous structure is related to the volatilization of the most labile structures of the agave bagasse fibers (Appendix A). However, the surface area of the carbonized fibers did not increase significantly. For large the surface area of carbonized fibers, it is necessary to introduce pores with diameters below 50 nm. There are two strategies to achieve

this objective: 1) carbonizing the precursor under an oxidizing atmosphere or 2) incorporating an activating agent in the precursor before carbonization. The first strategy is often used when mineral carbon (anthracite, bituminous, lignite, etc) is used as a precursor where most of the carbon is structured as graphite sheets. The oxidizing gases volatiles part of the carbon structure, developing pore structure. However when a lignocellulosic material is used as an activated carbon precursor, this strategy does not produce good results since the majority of the carbon is consumed during the carbonization process. The preferred strategy involves the incorporation of inorganic salts or acids before the carbonization process in order to avoid the volatilization of carbon and hence, generating a carbon structure. In this research two activating agents were tested: $ZnCl_2$ and H_3PO_4. The incorporation of these chemicals modified the thermal degradation of the agave bagasse as can be observed in the TG-DTG diagrams (see Figure 2.1) where the maximum weight loss occurred at lower temperatures than the presented by the unimpregnated agave bagasse. Previous studies have found that both activating agents catalyze the dehydrating reactions that begins to degrade the biopolymers that compose the lignocellosic materials (see Figure 2.2 and Figure 2.3). Hence the carbon structure begins to consolidate, forming random structures. Also, during the thermal treatment a fluid phase composed by low molecular weight biopolymers and molten activating agent is formed. About 300 °C a rapid evolution of gases emerged through the molten phase, generating a new porous structure all along the fibers (Appendix A). Finally the obtained carbon is rinsed, removing the residual activating agent, generating in this way the micropore structure that gives to the activated carbon its extended surface area.

According with the results included in chapter 3, it was possible to control the physical properties (surface area and hardness) of the activated carbon obtained from agave bagasse. The production conditions that controled the surface area of the generated activated carbons are the concentration of activating agent and the activation temperature. As previously mentioned, activating agents promote

several reactions that generate the porous structure of carbons, however the rate and the intensity of these reactions depend on the activation temperature.

When $ZnCl_2$ is employed as activating agent, activation temperatures up to 350 °C and moderate concentration of activating agent (up to 0.5 g $ZnCl_2$/g bagasse) are needed to generate carbons with surface area similar to the one presented by commercial activated carbons (800 m^2/g, see Figure 3.4). If the concentration of activating agent increases up to 1.5 g $ZnCl_2$/g bagasse, the generated activated carbon can reach surface areas as high as 2000 m^2/g. This mainly by the large number of pores formed after the removal of the activating agent. However, the materials generated at high impregnation ratios (R > 1.5 g $ZnCl_2$/g bagasse) have poor mechanical properties. The weakening of the activated carbons produced at high concentration of activating agent can be attributed to the thinning of pore walls, caused by the high concentration of activating agent. The pores of $ZnCl_2$ activated carbons are mainly in the microporous range (pores with diameter below 2 nm width). Finally, this carbon has a high oxygen content, which gives to it an acidic character (pH_{PZC} from 1.8 to 3.2) in aqueous solution. According with the characteristics of this agave bagasse based activated carbon (high surface area and high oxygen content), it is expected that this material will be an excellent adsorbent to remove metal cations from water.

Also, H_3PO_4 was successfully implemented to produce activated carbon from agave bagasse. Similarly to $ZnCl_2$, H_3PO_4 catalyzed dehydrating reactions that consolidate the carbon structure. However these reactions seem to begin before the thermal treatment, since a considerable degradation of the agave bagasse fibers was observed during the impregnation of the agave bagasse with H_3PO_4. This effect is reflected on the surface area of the treated materials since generated carbons at low activation temperatures (230 °C) have a considerable surface area (388 m^2/g). Chemical analyses of the generated carbons with H_3PO_4 showed that part of the remaining phosphoric acid in the carbon structure was attached by C–O–P linkages to the carbon matrix. This phosphate bridges promote the expansion of the carbon structure, developing the activated carbon porosity. The activated

carbons obtained have good mechanical properties, because H_3PO_4 acts as a binder of carbon fragments formed during the activation process, giving attrition resistance to the final products. However, increasing the impregnation ratio (up to 2 g H_3PO_4 / g agave bagasse) caused a decrement of the surface area and hardness of the activated carbon (see Figure 3.3). This observation is probably due to the contraction of the pore structure caused by the thermal breakdown of phosphate esters at high concentration of activating agent and high activation temperatures (up to 500 °C). The surface area of the H_3PO_4 activated carbons is considerably lower that the carbons obtained with $ZnCl_2$. It could be related to the expansion of pores due to reactions between the precursor and the phosphoric acid that generate mesopores. Finally the presence of phosphate groups in the activated carbon surface could enhance the removal of metal cations from aqueous solutions due to the high stability of metal-phosphate complexes.

As a second part of this research, the modification of the previously synthesized activated carbons with iron oxide / hydroxide nanoparticles was proposed. This modification had the aim to increase the arsenic adsorption capacity of these carbonaceous materials. The implemented methodology was based on thermal hydrolysis which consists in the precipitation of iron oxides / hydroxides by the heating of an aqueous solution that contains iron cations. This methodology has demonstrated to be an efficient method to synthesize iron oxide nanoparticles. Our results reveal that the quantity of iron anchored onto the carbon surface is highly influenced by the surface chemistry of the modified carbons. Under the same experimental conditions, the maximum quantity of iron that could be anchored onto the surface of an activated carbon with low oxygen content (9 %) was 2.2 %. In contrast, carbons with high oxygen content (from 20 to 25 %) can reach an iron content as high as 5.3 % (see Table 4.1). These results suggest that the oxygenated surface groups (hydroxyl, carbonyl, ketones, etc) can act as an initiator of crystals growth during the thermal hydrolysis of iron. The formation of a crystalline structure of iron in aqueous solution requires the hydrolysis of iron- hexa aquo cations $[Fe(OH_2)_6]^{+3}$, by means of a process that can be considered as an

inorganic polymerization. The key factor that governs the formation of iron oxides is the initiation of the polymerization and the rate at which monomer or dimer iron species diffuse until reaching the iron particle and to being incorporated in the iron oxide nucleus. The polymerization is induced by the addition of a base or by heating the solution, which deprotonates the aquo ligands of the iron complexes. Once the aquo ligands are deprotonated, a dipole is formed in the iron complex, which leads to a nuceophilic addition with another iron complex. The subsequent addition of metal ions by the elimination of water molecules form the crystalline iron oxide structure. When the iron hydrolysis is carried out inside the pores of the activated carbon, the surface groups can take part in the hydrolysis reactions. Oxygenated surface groups have free electrons that can promote nucleophilic reactions, initiating the condensation of iron complexes onto the carbon surface.

Analyzing the arsenic adsorption capacities of the iron modified carbons, it was found that carbons with low iron content have the highest arsenic adsorption capacities. This effect can be explained as follows: the arsenic removal by modified carbons is due to the iron oxide particles anchored onto the carbon surface and hence their size and availability will determine the arsenic adsorption capacity of these materials. According with our results, activated carbons with high iron content showed a considerable decrement of their surface area, which means that part of the iron oxide remained inside blocked pores, been inaccessible for arsenic adsorption. Also the particle size of the iron oxides loaded onto the carbon had a great influence in the arsenic adsorption capacity. The surface area of metal oxide nanoparticles is greater than the large particles (see Figure 4.1) which causes that iron oxide nanoparticles have more reactive sites and hence superior arsenic adsorption capacity.

By means of the experimental design, it was possible to determine the optimal experimental conditions that allow anchoring iron oxide nanoparticles onto activated carbons. These optimal conditions are different for each carbon, because the pore structure and the surface chemistry influence the anchorage procedure.

The majority of the pore volume of ACZ activated carbons is contained in pores with diameter below 2 nm and because of this, these are easily blocked. To avoid this, a low concentration of iron in the hydrolysis process is needed. Similarly, ACP activated carbons require moderate impregnation conditions to avoid the agglomeration of iron oxide particles. Despite F400 activated carbon has the majority of its pore volume in pores with diameters below 2 nm, the impregnation conditions needed to anchor iron particles are relatively high (C_{Fe}=3 M, T=95 °C and Ht=56 hours). This could be related to the surface chemistry of F400 activated carbon, since this carbon have less oxygenated surface groups.

"Finally, in conclusion let me say…."

CHAPTER 6

GENERAL CONCLUSIONS

6.1 CONCLUSIONS

According with our results it is possible to use organic wastes from the mescal industry to produce high quality activated carbons, which is an alternative to treat these residues and at the same time generate a value-added product of great demand worldwide. The resulting activated carbons are essentially microporous, however it is possible to increase the mesoporous pore volume in the activated carbons by modifying the production conditions and the quantity of activating agent employed.

After a statistical analysis, it was possible to identify the factors that mainly influence the hardness and surface area of the activated carbons produced from agave bagasse. The concentration of activating agent is the factor that principally affects both responses regardless of the activating agent employed. The response surfaces obtained for each experimental design can be used as a useful tool in the production of activated carbon from agave bagasse in order to predict the physical properties of the activated carbons at specific production conditions or in order to

establish the production conditions that meet certain quality parameters. Both activating agents demonstrated to be effective to produce activated carbon from agave bagasse, however, the developed characteristics hardly depend on the activating agent employed, since $ZnCl_2$ impregnated samples develop higher surface area than those produced with H_3PO_4. Also, it was possible to determine the experimental conditions that yield the best of both responses. Part of the oxygen present on the precursor remains after the activation process and thus the generated carbons have a low point of zero electric charge. Also, H_3PO_4 incorporates phosphorus in the activated carbons structure.

According with the results reported by the iron modified activated carbons, the thermal hydrolysis is an excellent method to anchor highly dispersed iron nanoparticles onto granular activated carbons. The production conditions that generate materials with high arsenic adsorption capacity depend on the type of carbon employed. Oxygenated surface groups promote the anchorage of iron particles on the carbon surface. However, the iron oxide particles size on these carbons growth rapidly, generating agglomeration of iron particles that block the pores of the modified activated carbons. According with our results there is not a direct relationship between iron content and arsenic adsorption capacity, since such factors as availability of iron to adsorb arsenic and the particle size of iron oxides are parameters that strongly influence the arsenic removal. The crystalline structure of the iron particles loaded onto the activated carbons depends on the production conditions: high hydrolysis temperatures and high $FeCl_3$ concentration generate hematite crystals onto the carbon surface, and low $FeCl_3$ concentrations favor the generation of akaganeite iron hydroxide. Finally, activated carbons with a well developed mesoporous structure are easier to modify with iron nanoparticles than microporous carbons. This because microporous carbons are easily blocked by the iron loaded onto the carbon. Also, a moderate concentration of oxygenated surface groups is preferred in order to control more easily the iron oxide particle size anchored on the surface of activated carbons.

6.2 FUTURE WORK

This research contributed to establish the production conditions to produce activated carbon from agave bagasse by chemical activation with $ZnCl_2$ and H_3PO_4. However there are other activation strategies that can be employed to produce activated carbon from agave bagasse. Because chemical activation is the most suitable methodology to produce activated carbons from lignocellulosic materials, activating agents such as alkyl oxides can be tested.

Also the formation of monoliths with a mixture of milled agave bagasse and alkyl oxides could be a good possibility to produce carbons with superior surface area and defined particle size.

In this research it was possible to produce activated carbons with surface area as high as 2000 m^2/g. However, these materials exhibit low mechanical properties. An alternative that could be evaluated is the formation of granules from powder activated carbon by mixing this material with some commercial binder. This could generate granular materials with high surface area that can be used in packed column systems.

One of the main concerns about chemical activation is the environmental implications of the spent activating agent. In this study, the recovery of activating agent was evaluated, founding a high recovery of $ZnCl_2$. A detailed study of the recovery and reuse of the spent activating agent must be carried out in order to generate an activation process that does not generate hazardous residues.

The activated carbons generated from agave bagasse have similar physical and chemical properties than commercial activated carbons. According with the chemical composition of the obtained materials it is expected that these will be excellent adsorbents of metal cations from aqueous solutions. The evaluation of

the removal of metal cations such as cadmium, zinc and lead can complete the characterization of these activated carbons.

Thermal hydrolysis was a good methodology to anchor iron particles onto the carbon surface, but there are some aspects to improve. The effect of iron concentration, hydrolysis time and hydrolysis temperature were evaluated on this research, however parameters such as initial pH, relative pressure in the hydrolysis vessel, aging time of the iron particles (after hydrolysis), and the ionic strength of the iron solution are parameters that could influence the size and the crystalline structure of the loaded particles onto the activated carbons.

The iron modified carbons generated at the optimal production conditions do not release iron to the solution in batch experiment. These could be attributed to some interaction between the carbon surface and the iron particles. Our results suggest that oxygenated groups promote the anchorage of iron particles. However the characterization of samples with techniques such as X-ray photoelectron spectroscopy, Mossbauer spectroscopy and transmission electron microscopy is needed in order to establish the interaction between carbon and the anchored iron particles.

Analyzing the iron modified activated carbons, it was possible to detect diverse iron particles of different morphologies anchored to the activated carbon surface: spherical, peanut and acicular. A detailed microscopic and crystallographic study of the samples generated during this research is needed in order to determine the factors that influence the formation of these particles.

According with the results reported in chapter 4 of this thesis, the pore structure has a great influence on the anchorage of iron oxide particles onto activated carbon, being the carbons with a wide pore size distribution the most suitable materials. In this sense it could be interesting to study the anchorage of iron oxide particles onto activated carbons with different surface chemistry but similar pore structure in order to eliminate diffusion effects in activated carbons with a narrow pore size distribution.

The evaluation of arsenic adsorption by the iron oxide modified materials was measured under batch experiments with synthetic water at constant pH and temperature at relatively high arsenic concentrations. In order to complete the adsorption characteristics of these modified activated carbons, experiments that evaluate the effect of solution pH, adsorption temperature and adsorption in the presence of other anions at typically founded arsenic concentration (below 1.5 ppm) are needed.

The evaluation of the arsenic adsorption under dynamic systems (packed columns) is needed in order to determine the application feasibility of these carbons in the treatment of arsenic polluted water.

6.3 LIST OF PUBLICATIONS

6.3.1 Conference proceedings

César Nieto-Delgado, Mauricio Terrones and José-René Rangel-Mendez "*Activated carbon surface groups influence on the anchorage of iron nanoparticles and their contribution to their arsenic adsorption from water*" on the annual world conference on carbon. Carbon 2010. American Carbon Society, Clemson University, USA. July 2010 (Oral presentation)

César Nieto-Delgado, Mauricio Terrones and José-René Rangel-Mendez "*Iron doped granular activated carbon for Arsenic removal from water: method to anchor iron nanoparticles* " on the 2th Young Water Professional Conference, Juriquilla, México. April 2010 (Oral presentation). This work was awarded with an "**Honorable mention**" as one of the best oral presentation of the conference.

C. Nieto-Delgado, M. Terrones and J.R. Rangel-Mendez "*In situ transformation of agave bagasse into activated carbon using an environmental scanning electron microscope*" on the annual world conference on carbon. Carbon 2009. European Carbon Association Biarritz, France. June 2009 (Oral presentation)

C. Nieto-Delgado, M. Terrones and J.R. Rangel-Mendez "*Production of activated carbon from agave salmiana bagasse: optimization of surface area and hardness by using the response surface methodology*" on the annual world conference on carbon. Carbon 2009. European Carbon Association Biarritz, France. June 2009 (Poster presentation)

C. Nieto-Delgado, J.R. Rangel-Mendez* and M. Terrones "*Agave bagasse as a precursor to produce highly microporous activated carbons*" on the annual world conference on carbon. Carbon 2008. Science Council of Japan and The Carbon Society of Japan. Nagano Japan. July 2008 (Oral presentation). This work was

awarded with the "**Japanese Carbon Award for Students**" provided to students who submit an excellent paper to Carbon conference 2008.

6.3.2 Research papers

Development of highly microporous activated carbon from the alcoholic beverage industry organic by-products. C. Nieto-Delgado, M. Terrones and J.R. Rangel-Mendez. Journal of Biomass and Bioenergy Biomass and Bioenergy, In Press, Corrected Proof, Available online 1 September 2010

Production of activated carbon from agave salmiana bagasse: surface area and hardness optimization by using the response surface methodology. C. Nieto-Delgado and J.R. Rangel-Mendez (submitted to Journal of Hazardous Materials)

Iron doped granular activated carbon for Arsenic removal from water: method to anchor iron nanoparticles. C. Nieto-Delgado and J.R. Rangel-Mendez (Publication in preparation)

In situ transformation of agave bagasse into activated carbon using an environmental scanning electron microscope. C. Nieto-Delgado, M. Terrones and J.R. Rangel-Mendez (Publication in preparation)

6.4 ATTENDANCE TO CONFERENCES

Mexico – Canada International Symposium on Advanced Technologies for the Treatment of Drinking Water and Waste Water. Celaya Guanajuato Mexico, March 29-30, 2007.

Ion Exchange and Arsenic Remediation from Drinking Water Workshop, San Luis Potosí, SLP, México. August 2007.

Carbon conference 2008, organized by the Science Council of Japan and The Carbon Society of Japan. Nagano Japan. July 2008.

Carbon conference 2009, organized by the European Carbon Association Biarritz, France. June 2009.

Tratamiento Anaerobio y Post-Tratamiento de Aguas Residuales Domésticas, San Luis Potosí, SLP, México. Febrero 2010.

Second Young Water Professional Conference, organized by the international water association, Juriquilla, México. April 2010.

Carbon conference 2010, organized by the American Carbon Society, Clemson University, USA. July 2010.

APPENDIX A

IN SITU TRANSFORMATION OF AGAVE BAGASSE INTO ACTIVATED CARBON BY USING AN ENVIRONMENTAL SCANNING ELECTRON MICROSCOPE

The activation process of chemically treated agave bagasse was monitored and analyzed in detailed in real time during the production of activated carbon by using an environmental scanning electron microscope (ESEM). The agave bagasse was produced by chemical activation with $ZnCl_2$: the effect of the activating agent concentration was studied. The heating rate and the activation temperature were controlled with a heating stage able to operate up to 1000 °C. Energy dispersion X-ray analysis (EDX) was also employed to distinguish the chemical composition of the material during the different carbonization stages. Raw bagasse samples exhibit a very low porosity, but at lower concentration of activating agent (weight ratio below 0.5 g $ZnCl_2$ per gram of agave bagasse) under heating, of up to 250 ºC honey comb macroporous structure was obtained. The diameter of these parallel channels along the fibers is between 10 and 20 μm, and the thickness of the walls is from 3 to 5 μm. At higher temperature than 600 ºC, the pore structure of the activated carbon collapses due to combustion of the material. At weight ratio above 1.5 g $ZnCl_2$ per gram of agave bagasse, the formation of a fluid phase has been observed at temperature higher than 260ºC: the images show

first the melting of the impregnated sample and later the formation of a new blister structure generated by the gas release from internal reactions.

A.1 INTRODUCTION

The activated carbon production is one of the most studied processes in carbon science. These studies are of great interest because the large application of this adsorbent material worldwide. According with the production methodology, the activation process has been classified as chemical or physical activation. Also the combination of both methodologies has been successfully applied demonstrating that there are a lot of possibilities to produce high quality activated carbon [1-3]. Although the physical and chemical activation method has been used to produce activated carbons form many years, the mechanism is not totally clear. Several studies have demonstrated that the activation step is a complex process that depends of the activation methodology and the nature of the precursor [4-6]. Particularity, in studies regarding the chemical activation of lignocelluloses materials have reported an unusual modification of their morphology, such as a "molten plastic state" formed during the activation process [7-9], but almost no research has been focused on their characterization. Recently, agave bagasse has been proposed as a new precursor to produce activated carbon [10] by chemical activation, using $ZnCl_2$ or H_3PO_4 as activating agent: this research identified interesting modification of the bagasse fiber morphology, both when carbonized and in the activation process. In the study reported herein, the same process was used to produce activated carbons from agave bagasse using an environmental scanning electron microscope (ESEM) to examine the microstructural changes accompanying carbonization and/or activation of the solid material in real time. The varieties of electron microscopes are suitable for studying not only the morphologies of materials but also the changes in these materials under different conditions. Such experimental tests are commonly known as in situ techniques, which depend on the type of microscope and the space available in its analysis

chamber. Several types of in situ experiments can be performed such as: mechanical deformation tests, heating or cooling experiments, electron irradiation, the application of electric or magnetic fields and also the application of different ambient atmospheres [11]. The ESEM is a modified scanning electron microscope (SEM) that offers new applications and advantages over the conventional SEM. The ESEM is able to image uncoated and hydrated samples by means of a differential pumping system and gaseous secondary electron detector. These differential pumping systems also allows relatively high pressures of the chamber in comparison with conventional SEM, with a variety of gases as water vapor, inert gases or also oxygen [12]. All these characteristics allow to develop similar experiments to those conducted in laboratory and hence to get more information about the studied process.

The main objective of this research was to investigate the activation process of both $ZnCl_2$ impregnated and raw agave bagasse samples in an ESEM, to study the mechanisms of carbon activation as well as to clarify the processes that develop a molten phase that has been previously reported in literature.

A.2 MATERIALS AND METHODS

Agave bagasse fibers collected from a local distillery from San Luis Potosi, Mexico, were employed without any pretreatment. Selected samples were handled carefully to avoid the splitting of the main structure and to obtain small blocks of vertically aligned fibers. These blocks were weighted and mixed with the appropriate amount of $ZnCl_2$ to weight ratio (R) of 0.5 and 1 (R= weight of $ZnCl_2$ / weight of bagasse). To homogeneously incorporate the activating agent to the agave bagasse, enough deionized water was added and the mixture was equilibrated 24 hours. After that the mixture was heated up to 60 ºC until dryness.

The work described in this manuscript was carried out by using a FEI Quanta 200 Environmental SEM, equipped with a tungsten filament, a gaseous secondary

electron detector (GSED) and a heating stage. In all cases the accelerating voltage used was 15 kV, the magnification was set to 600X, and the heating rate was 10 ºC/min. It should be noted that ESEM experiments were carried out at 190 Pa of total pressure rather than at atmospheric pressure, usually used in laboratory and in industrial practices. Micrographs were taken throughout the heating process to characterize the carbonaceous material.

A.3 RESULTS AND DISCUSSION

A.3.1 Raw agave bagasse

The agave bagasse fiber appear as a solid fiber without any apparent pore structure at room temperature. After the heating started, no distinct difference in the structure could be appreciated until 275 ºC. The only change in structure was the decrease of the fiber diameter, mainly by dehydration of the fiber. At temperature higher than 300 ºC, a slowly formation of macropores was observed. This combustion performance demonstrated the heterogeneity of the agave bagasse fibers. Agave bagasse comes from the residual fibers remaining after cooked agave heads are shredded and milled with the aim of extracting the soluble sugars that are subsequently used to produce tequila or mescal. From a physiological point of view, the bagasse fibers are the rind and fibrovascular bundles (Figure A.1A), dispersed throughout the interior of the agave head, which serve to bearing and store nutrients for the plant [13]. These fibers are constituted primarily of axially-elongated cells formed by primary and secondary cell walls (Figure A.2B). Chemically, these structures are composed by three polymers: cellulose, hemicellulose and lignin. Lignin has been found in the middle lamella that connects the cell walls of the fibers in adjacent lignified tissues. The rest of the wall layers, including the secondary wall, have also some lignin content but these are mainly made up of cellulose (and hemicellulose) [14, 15]. Different studies about the thermal degradation of lignocellulose materials have found that lignin has the

highest temperature of degradation (280-500 ºC) compared with cellulose (240 – 350 ºC) and hemicellulose (200-260 ºC) [16]. These particular arrangement of the axial cells in the agave bagasse fibers, together with the outer part of the cell wall are mainly constituted by the less volatile biopolymer (lignin), which is why a macroporous structure is developed during the thermal treatment (Figure A.1). Something to remark is the temperature at which the physical change of the agave bagasse fiber began (275ºC) that matched with the temperature of degradation of the byopolimers (240 – 280 ºC).
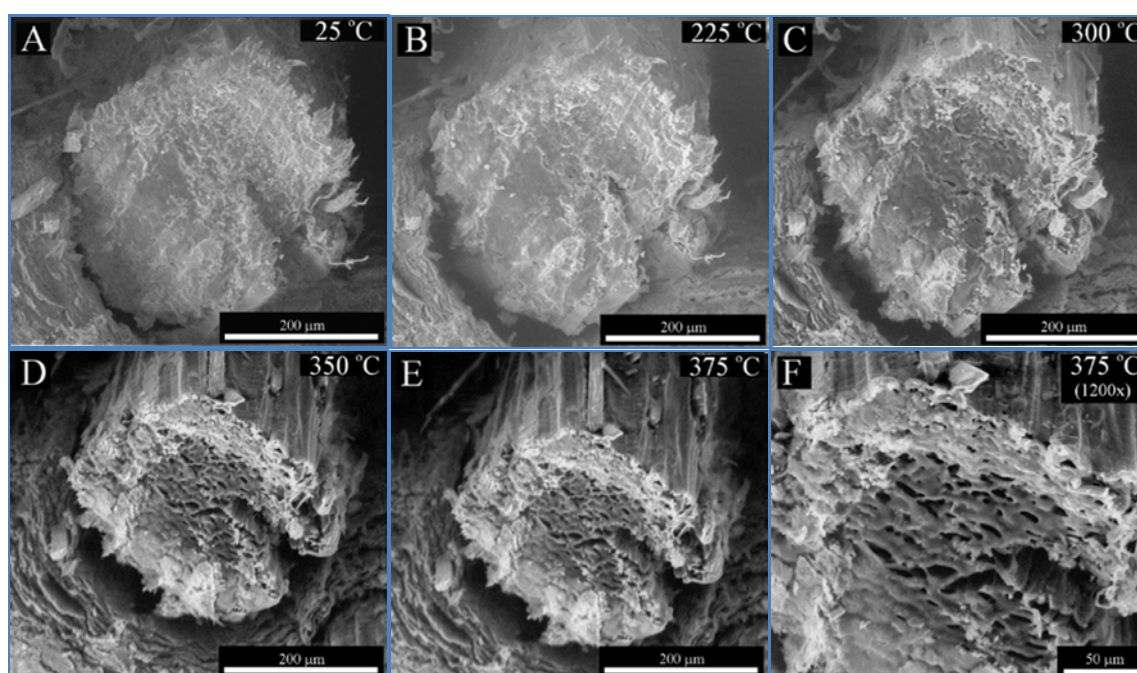
Figure A.1. Snapshots of the carbonization process of raw agave bagasse. The heating rate was 10 ºC/min; the chamber pressure was set to 190 Pa under air atmosphere. The temperature at which the micrographs were taken appears in the up right side of each image.

Even when a macroporous structure was developed, due to the gasification of the more volatile tissue of the agave bagasse fibers, the surface area of the carbonized samples consists of just few square meters per gram (about 3 m^2/g). This indicates that during the carbonization process none microporous structure

was developed even at high carbonization temperatures (600 °C). These results evidence the need of using activating agents to develop surface area during the activation process.
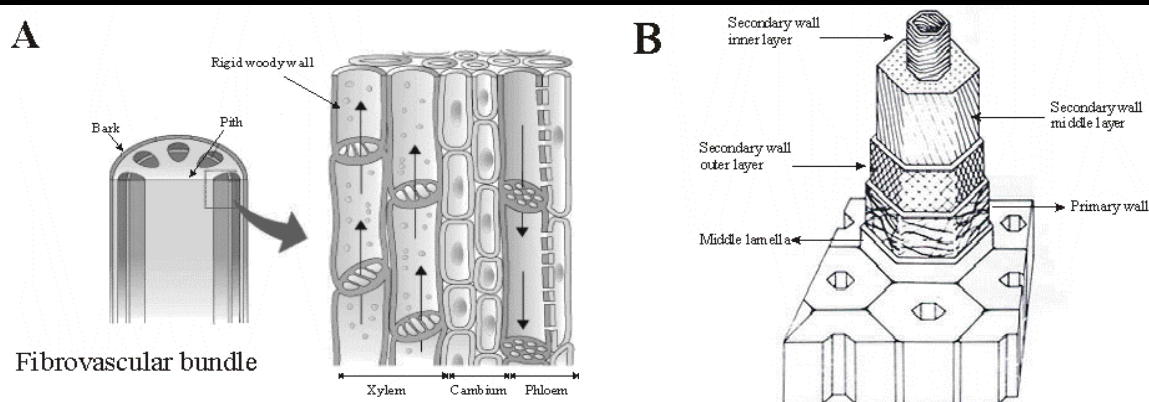
Figure A.2. Morphological structure of the agave bagasse fiber. A: schematic composition of the agave bagasse fiber composed by different tissue that serves as conducting and reserve system. B: different structures forming the cell wall in lignocelluloses materials from Dey et al [14]).

A.3.2 ZnCl₂ Impregnated agave bagasse

Figure A.3 shows micrographs taken at different times to follow the microestructural changes of $ZnCl_2$ impregnated agave during heating at 10 °C/min. At room temperature the fiber exhibits similar macroporous structure similar to the carbonized fiber. This effect could be attributed to the thermal treatment applied when evaporating water during the impregnation step. The physical change was minimum until 250 °C. After this temperature a rapid change began; the agave bagasse fiber looked as if it had melted. These changes toke place near of the melting point of $ZnCl_2$ salt, which is 290 °C. Something to remark is that the experiment was carry out inside a chamber with lower pressure than atmospheric, which could caused a decrease of the melting temperature of $ZnCl_2$. Different authors have reported the correlation between the melting point of the salt used as activating agent and the pore development in the carbon, founding that below the melting point of the salt, the surface area of the char does not increase much. The

latest because reactions between carbon and the activating agent that form pores had not yet taken place although the salt had melted and penetrated into the char [4, 5].
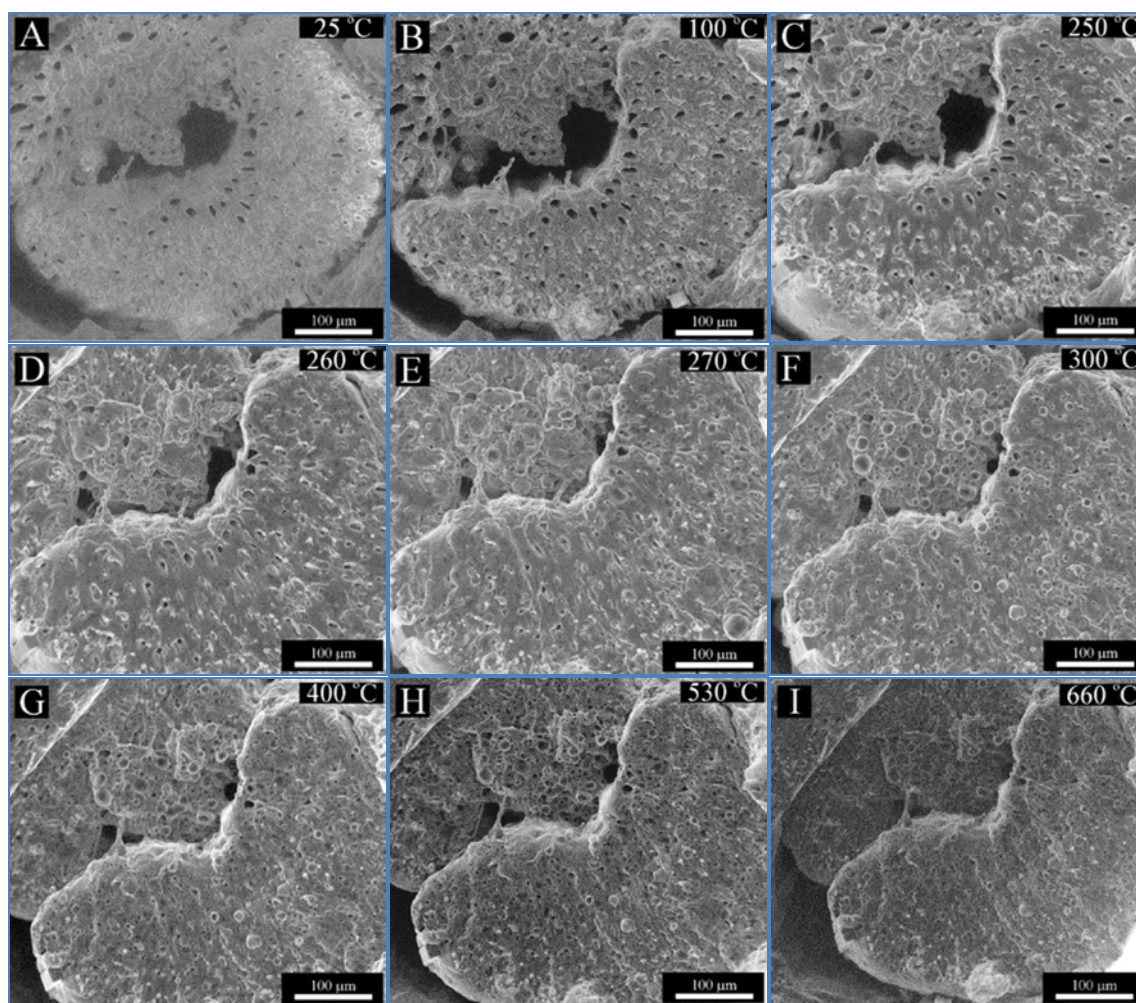
Figure A.3. Snapshots of the activation process of the agave bagasse fiber impregnated with $ZnCl_2$ (R=1). The heating rate was 10 ºC/min; the chamber pressure was set to 190 Pa under air atmosphere. The temperature at which the micrographs were taken appears in the up right side of each image.

As it can be observed on Figure A.3D, once the salt was melted, it began to interact with the fiber, and promoted a complex depolymerization mechanism evolving dehydration, cyclization, condensation, and heterolytic cleavage reactions

[8]. This depolymerization promoted the formation of some light compounds that may be released as gas, but if the generate biopolymer chain is of a size that does not allow its volatilization, this will remain as a condensed phase. These biopolymer chains together with the melted $ZnCl_2$ can be the components of the melted phase that was observed in the ESEM images (Figure A.4D and E). At high temperatures, a kind of blister structure was observed in the melted phase due to gas release, once the macropore channels were obstructed by the melted phase, which contains bubbles with a tiny hole (diameter around 2 μm) in the center of these, where generated gases emerge (Figure A.4). These kind of structures not only appear in the transversal zone of the fiber but also all along the outer side of the fiber.
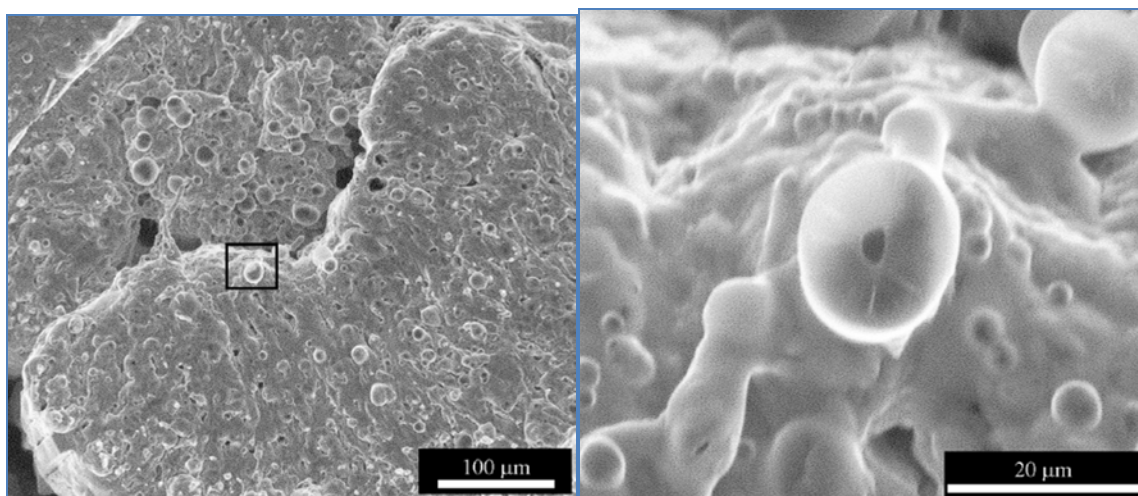
Figure A.4. Micrographs of an impregnated agave bagasse fiber at 380 ºC; right image shows higher magnifications of the selected area.

The resolution of the ESEM does not allow to examine the microporous structure, however later observations of activated samples, after the washing step to remove all the remaining activating agent, demonstrated that a porous structure was developed inside the fiber, apparently created by both the release of gases and

elimination of activating agent (Figure A.5). At a temperature around 500 ºC, a considerable number of macropores was introduced (Figure A.3H).
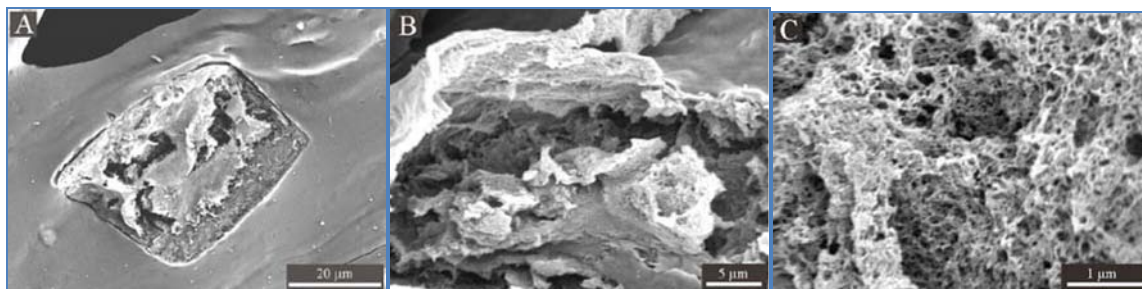
Figure A.5. Micrographs of a washed agave bagasse fiber after the activation step at 350 ºC.

A.4. CONCLUSIONS

According with the ESEM images the mechanism to generate microporous structures can be hypothized as follows: the impregnated agave bagasse fiber does not have any change until the melting point of $ZnCl_2$ (290 ºC). Once the salt is melted, this penetrates into the biological structures of the lignocellulosic material and promotes different kind of reactions that dehydrate the material, degrade the biopolymers chains, and generate aromatic carbon rings that modify the physical characteristics of the biopolymer. These modifications help melting the agave bagasse fiber. This observation is associated with the onset of "rubbery flow" of biopolymers caused by slippage of the shorter chains, carrying out the formation of a "plastic phase" that covers the initial macroporous structure. While the macroporous structure is blocked the generated gases require an exit to vent, that causes the formation of blisters from which gases come out. The released gases perform a pathway that after cooling forms part of the internal pore structure, greatly contributing to the high surface area of activated carbons. These new structures within the generated pores could be one of the main reasons for which micropores are introduced inside activated carbons during chemical activation.

A.5. SUPPORTING INFORMATION

Two movies that contain the evolution of the morphological changes of the raw and $ZnCl_2$ impregnated agave bagasse were created. Both files are found in the included CD.

A.6 REFERENCES

[1]   Rodriguez-Reinoso F, Molina-Sabio M. Activated carbons from lignocellulosic materials by chemical and/or physical activation: an overview. Carbon. 1992;30(7):1111-8.

[2]   Hu Z, Srinivasan MP, Ni Y. Novel activation process for preparing highly microporous and mesoporous activated carbons. Carbon. 2001;39(6):877-86.

[3]   Hussein MZB, Rahman MBBA, Yahaya AHJ, Hin T-YY, Ahmad N. Oil Palm Trunk as a Raw Material for Activated Carbon Production. Journal of Porous Materials. 2001;8(4):327-34.

[4]   Lillo-Ródenas MA, Juan-Juan J, Cazorla-Amorós D, Linares-Solano A. About reactions occurring during chemical activation with hydroxides. Carbon. 2004;42(7):1371-5.

[5]   Evans MJB, Halliop E, MacDonald JAF. The production of chemically-activated carbon. Carbon. 1999;37(2):269-74.

[6]   Molina-Sabio M, Rodríguez-Reinoso F. Role of chemical activation in the development of carbon porosity. Colloids and Surfaces A: Physicochemical and Engineering Aspects. 2004;241(1-3):15-25.

[7]   Evans RJ, Milne TA. Molecular characterization of the pyrolysis of biomass. 1. Fundamentals. Energy & Fuels. 1987;1(2):123-37.

[8]   Varhegyi G, Antal MJ, Szekely T, Till F, Jakab E, Szabo P. Simultaneous thermogravimetric-mass spectrometric studies of the thermal decomposition of biopolymers. 2. Sugarcane bagasse in the presence and absence of catalysts. Energy & Fuels. 1988;2(3):273-7.

[9]   Tsai W, Chang C, Lee S, Wang S. Thermogravimetric Analysis of Corn Cob Impregnated With Zinc Chloride for Preparation of Activated Carbon. J Therm Anal Calorim. 2000;63(2):351-7.

[10]   C. Nieto-Delgado MT, J.R. Rangel-Mendez. Agave bagasse as a precursor to produce highly microporous activated carbons. *2008 International Conference on Carbon, World Conference on Carbon*. Nagano, Japan: Organizing committee of CARBON'08 2008.

[11]   In Situ Microscopy. *Electron Microscopy of Polymers* 2008:145-59.

[12]   Scanning Electron Microscopy (SEM). *Electron Microscopy of Polymers* 2008:87-120.

[13]   Iniguez-Covarrubias G, Lange SE, Rowell RM. Utilization of byproducts from the tequila industry: part 1: agave bagasse as a raw material for animal feeding and fiberboard production. Bioresour Technol. 2001;77(1):25-32.

[14]   Harborne PMDaJB, ed. Plant Biochemistry. United Kingdom: Academic press 1997.

[15]   Butterfield B. The structure of wood: form and function. *Primary Wood Processing* 2006:1-22.

[16]   Mohan D, Pittman CU, Steele PH. Pyrolysis of Wood/Biomass for Bio-oil: A Critical Review. Energy & Fuels. 2006;20(3):848-89.